UNIVERSITY OF LEEDS

Abrupt climate changes during the last ice age: a study of millennial-scale variability in climate simulations

Yvan Malo Romé

Submitted in accordance with the requirements for the degree of
Doctor of Philosophy

The University of Leeds

Faculty of Environment

School of Earth and Environment

The 9th of January 2024

Intellectual Property

The candidate confirms that the work submitted is his own, except where work which has formed part of jointly authored publications has been included. The contribution of the candidate and the other authors to this work has been explicitly indicated below. The candidate confirms that appropriate credit has been given within the thesis where reference has been made to the work of others.

The work in Chapter 2 of this thesis has been published in Palaeoceanography as follows: Yvan M. Romé, Ruza F. Ivanovic, Lauren J. Gregoire, Sam Sherriff-Tadano, Paul J. Valdes. Millennial-Scale Climate Oscillations Triggered by Deglacial Meltwater Discharge in Last Glacial Maximum Simulations, Paleoceanography and Paleoclimatology, 37, 10, e2022PA004451, https://doi.org/10.1029/2022PA004451, 2022. YMR designed the main project, ran the simulations, conducted the analysis and wrote the paper. RFI and LJG provided core guidance. SST provided the technical expertise on the discussion and the comparison to proxy records. PJV provided the model expertise and the base simulations and input files.

The work in Chapter 3 of this thesis is ready to be submitted to Climate Dynamics, with the authorship of Yvan M. Romé, Ruza F. Ivanovic, Lauren J. Gregoire, Didier Swingedouw, Sam Sherriff-Tadano and Reyk Börner with the provisional title: "Simulated glacial millennial-scale climate variability driven by a coupled inter-basin salt oscillator". YMR designed the main project, ran the simulations, conducted the analysis and prepared the manuscript. RFI and LJG provided core guidance. DS and SST provided feedback and expertise on the mechanism and the discussion. RB contributed to the framing and the theoretical discussion. We acknowledge the contribution of Paul Valdes (University of Bristol) and Edward Armstrong (University of Helsinki), who designed and provided expertise on the salinity tendency diagnostic tool.

The work in Chapter 4 of this thesis is awaiting review by the coauthors before submission to Climate of the Past, with the authorship of Yvan M. Romé, Ruza F. Ivanovic, Lauren J. Gregoire, Brooke Snoll, Oliver G. Pollard and Jacob Perez, with the provisional title: "Last deglaciation simulations sensitivity to the choice of ice sheets reconstructions and meltwater discharge pattern". YMR designed the main project, ran the simulations,

conducted the analysis and prepared the manuscript. RFI and LJG provided core guidance. Brooke Snoll provided the dataset and advice for the model-data comparison. OGP provided code and advice for the analysis of meltwater thresholds. JP provided code and expertise for the atmospheric circulation analysis.

Signed 

Acknowledgements

First of all, I would like to thank my two supervisors, Ruza Ivanovic and Lauren Gregoire, for all the support, feedback, and inspiration over the years. You have always remained positive and encouraging and made the whole PhD experience a wonderful experience despite the difficult circumstances. I also wanted to thank Chuncheng Guo, Kerim Nisancioglu and Janne Repschläger for all the training and advice they gave me in the first years of my PhD. Finally, thank you to Chris Smith for agreeing to join the project in the last two months to help with the writing.

This thesis is the result of all the fantastic collaborators I have been fortunate enough to work with: Sam Sherriff-Tadano, Paul Valdes, Didier Swingedouw, Reyk Börner, Oliver Pollard, Brooke Snoll and Jacob Perez. I would also like to recognise the incredible help of the CEMAC team in Leeds, and in particular Richard Rigby and Julia Tindall, for all the computational support they have provided.

The four years of the PhD have been unforgettable thanks to all the great people I have met at the University. Thank you to Oliver, Brooke, Sam, Richard, Violet, Niall, Suzie, Paloma, Will and all the members of the Climate-Ice and PCC groups over the years, and to the 11.06 office for the fun, supportive and sometimes chaotic working environment.

I would have never been able to complete this PhD without my friends and housemates in France and in the UK, and I would like to thank them all. Thanks to my Mum, Dad, Josselin, Briac and Maurice the cat for being a fun and supportive family. And finally, thank you to Lizzie for your flawless positivity and kindness that got me through the PhD.

This project was funded by the Natural Environment Research Council (NERC) Panorama Doctoral Training Partnership (DTP) under grant NE/S007458/1.

Abstract

Simulating the climate is more important than it has ever been if we want to foresee the disruptions of global climate change. Climate simulations are, however, limited by our lack of understanding of the tipping points of the climate systems. Such tipping points have been crossed the last deglaciation, between 19 and 11.7 thousand years before present, whose chain of events recalls the demise of the modern ice sheets. Deglacial abrupt climate changes are linked to complete reorganisations of Atlantic Meridional Overturning Circulation (AMOC) by the effect of the freshwater released by the melting ice sheets. The AMOC can shift between several modes, but the precise drivers and consequences of these shifts are still to be established.

To investigate this problem, I produced a new set of simulations from a general circulation model displaying millennial-scale variability that resembles the abrupt climate change sequence of the last glacial period and the last deglaciation. Under the right balance of magnitude and location of the freshwater forcing field derived from the ice sheet melting history, the North Atlantic climate experiences a pseudo-oscillating behaviour with a periodicity of around 1500 years and Greenland temperature changes of about 10°C. I proposed a mechanism to explain the millennial-scale variability in these simulations based on a slow global salt oscillator and abrupt North Atlantic convection component coupled by modifications in the AMOC regime. This mechanism is key to understanding what combination of boundary conditions and forcings can lead to millennial-scale variability in glacial simulations, and this theory was applied to new last glacial maximum simulations forced with deglacial meltwater history using two different ice sheet reconstructions.

The choice of the ice sheet reconstruction can modify the processes at stake in North Atlantic abrupt climate shifts. In particular, this mechanism relies on an abrupt recovery of deep water formation in the Nordic Sea that is obtained only when Eurasian ice sheet katabatic winds are strong enough. The uncertainties around the ice sheet reconstructions and their associated meltwater discharge are still preventing the exact reproduction of the chain of events of the last deglaciation, but this study provides a new way to understand the window of parameters where millennial-scale variability in a more systematic way to trigger them in climate simulations.

Contents

List of Figures

List of Tables

Abbreviations

AABW AntArctic Bottom Waters

AMOC Atlantic Meridional Overturning Circulation

AOGCMs Atmosphere-Ocean General Circulation Models

BRIDGE Bristol Research Initiative for the Dynamic Global Environment

CMIP Coupled Model Intercomparison Project

COM Centre Of Mass

D-O Dansgaard-Oeschger

GCMs General Circulation Models

GI Greenland Interstadial

GIN Greenland-Iceland-Nordic

GIS Greenland-Iceland-Scotland

GS Greenland Stadial

H Heinrich

HadCM3 Hadley Centre Climate Model 3

HS1 Heinrich Stadial 1

IPCC Intergovernmental Panel on Climate Change

IRD Ice-Rafted Debris

ITCZ Intertropical Convergence Zone

ka thousand years

ka BP thousand years before present

LGM Last Glacial Maximum

MIS Marine Isototope Stages

MIS3 Marine Isototope Stage 3

MLD Mixed Layer Depth

MOSES2 Met Office Surface Exchange Scheme 2

MWP1a Meltwater Pulse 1a

NADW North Atlantic Deep Waters

PMIP Paleoclimate Modelling Intercomparison Project

ppb parts per billion

ppm parts per million

PSD Power Spectral Density

SPG Subpolar Gyre

SST Sea Surface Temperature

TRIFFID Top-down Representation of Interactive Foliage and Flora including Dynamics

Chapter 1

Introduction and Literature review

1.1 Literature review

1.1.1 Climate variability, abrupt climate changes and tipping points

Climate is the long-term average of the chaotic and short-term meteorological events. **Climate variability** is observed when the climate system observes a deviation from its long-term mean at time-scales shorter than geological processes. A review of climate change and variability through Earth's history was written by Ruddiman (2001). Over the last 60 million years, different types of climate variability were based on reconstructions of temperature and CO_2 concentrations changes plotted in Figure 1.1. During the Eocene (∼55 to ∼34 million years before present), the climate was generally warmer because of higher greenhouse gas concentrations. CO_2 levels may have reached 2000 parts per million (ppm) (Beerling and Royer, 2011) resulting in global mean surface temperatures up to 16°C higher than the preindustrial period (1850 - 1900 Inglis et al., 2020). The increase in CO_2 was linked to changes in geo-chemical properties of the ocean and the atmosphere, and volcanic activity (Svensen et al., 2004). During the past ten million years, the global temperature gradually cooled down under the influence of tectonic changes affecting the atmospheric CO_2 draw-down through weathering fluxes and the ocean circulation (Ruddiman, 2001). Ice sheets formed at the poles as the Earth entered its most recent ice age 2.6 million years before present. The Earth's orbit follows three cycles: changes in eccentricity, describing the shape of the orbit, have a periodicity of ∼100,000 years; changes in obliquity, related to the angle between the rotation axis and the orbit plane, have a periodicity of ∼41,000 years; changes in precession, influencing the contrast between seasons, have a periodicity of ∼26,000 years. Glacial-Interglacial cycles emerged during the Pliocene (∼5.4 to ∼2.6 million years before present), and were greatly amplified during the mid-Pliocestocene Transition around 3 million years ago and through the Quaternary (∼2.5 million years before present). The glacial periods were triggered by the changes in eccentricity and a combination of changes in the obliquity and the precession determines the intensity of the glacial and interglacial periods (Jouzel et al., 2007).

Within the last glacial period, dated between 115 and 11.7 thousand years before present (ka BP), **millennial-scale variability** dominated the climate records. This mode of variability was observed in ice cores (Jouzel et al., 2007; Wolff et al., 2010), marine sediments (Lisiecki and Raymo, 2005, see Section 1.2.2) and speleotherms (Cheng et al., 2016). At this time scale, the complex interplay of the ocean, ice sheets and atmosphere led to some of the most dramatic climate changes observed in climate records: these are called **abrupt climate changes**. A view of climate variability during the last glacial period is given in Figure 1.2. The two main forms of millennial-scale variability are the **Dansgaard-Oeschger events** and the **Heinrich events**.

Dansgaard-Oeschger (D-O) events (Dansgaard et al., 1993) are cyclical transitions between cold *stadial* climates and warm *interstadial* climates that happened during the last

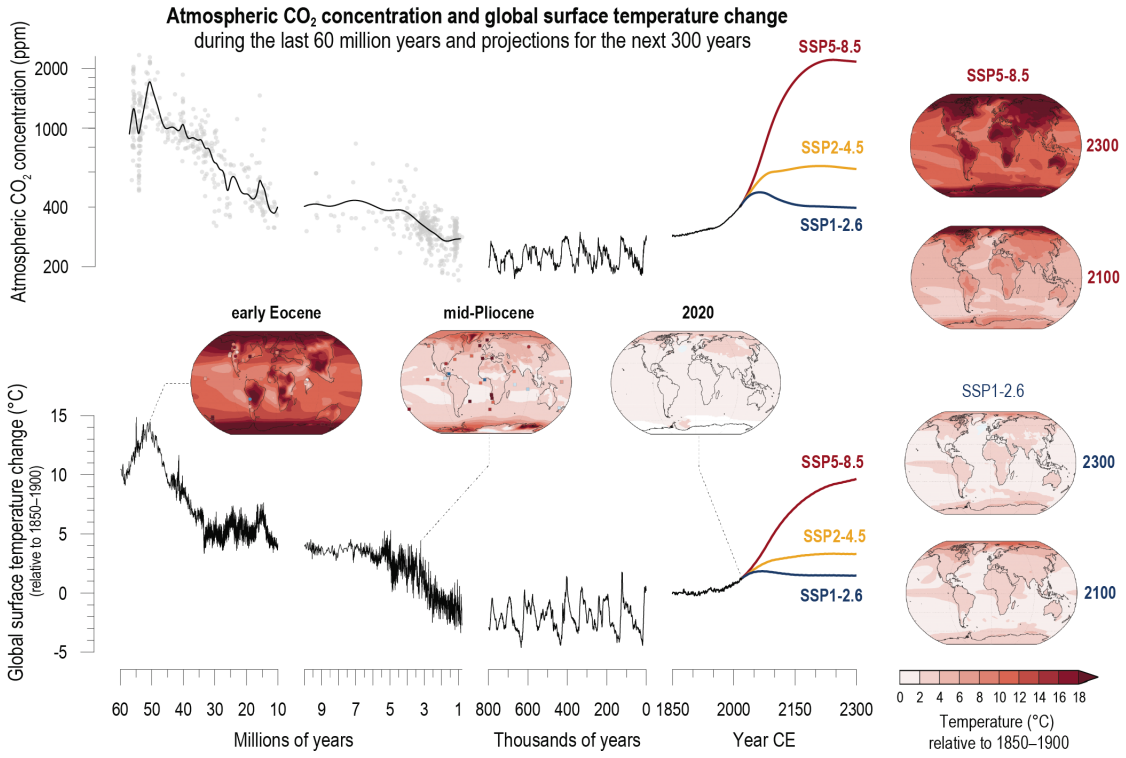

Figure 1.1: **Climate variability of the last 60 million years**. As observed in records of global surface temperature and CO_2 concentrations, and future climate projections. Figure TS.1 in IPCC (2023b).

glacial period. They were particularly frequent during Marine Isototope Stage 3 (MIS3), between ∼57 ka BP to ∼26 ka BP. First observed in Greenland ice cores, (Bond et al., 1993), D-O events had an extensive impact on the North Atlantic climate (Shackleton et al., 2000; Pedro et al., 2022). Their influence can be felt on many climate components at different locations, such as Southern Hemisphere temperatures (Blunier and Brook, 2001; Jouzel et al., 2007), ocean circulation (Burckel et al., 2015; Henry et al., 2016), Northern Hemisphere sea ice extent (Dokken et al., 2013) or East Asian monsoon (Cheng et al., 2016). Early studies argued that D-O cycles occurred with a periodicity of around 1500 years (Schulz, 2002; Rahmstorf, 2003). It is now believed that D-O cycles are more irregular and can last between 400 and 2,600 years (Wolff et al., 2010). A typical D-O cycle is composed of a cold and relatively stable **stadial** phase, followed by an abrupt warming to a warm **insterstadial** phase, returning to stadial conditions in first a slow and then an abrupt cooling phase (Thomas et al., 2009). Nonetheless, there are significant variations amongst D-O cycles and the *stadial* and *interstadial* states can have very different durations from one cycle to another (Lohmann and Ditlevsen, 2019). D-O transitions can increase the Greenland temperatures by up to $16.5°C$ (Kindler et al., 2014; Buizert et al., 2014; Martin et al., 2023), with warming rates of about $1°C$ per decade for about a hundred years (Lohmann and Ditlevsen, 2019). The end of the warming phase can be marked by an overshoot phase in the North Atlantic (Dokken et al., 2013) when the subsurface heat accumulated under the perennial sea ice is released abruptly (Rasmussen and Thomsen, 2004; Marcott et al., 2011). The existence of the slow cooling phase implies that the magnitude of the abrupt cooling phases is generally smaller than the warming phases, but the abrupt cooling rates can reach similar values to the abrupt warming rates. There is an antiphasing of the Greenland and Antarctica temperatures (i.e. the Antarctica temperatures are at a maximum when Greenland temperatures are at a minimum and vice versa) – called the bipolar see-saw phenomenon and described in Stocker (1998) and Stocker and Johnsen (2003). The existence of this bipolar see-saw is evidence of the key role played by changes in the Atlantic Meridional Overturning Circulation (AMOC), as hypothesised by Rahmstorf (2002) and Clark et al. (2002).

With the increased ice volume stored in ice sheets in glacial conditions, periods of intense iceberg calving have regularly been recorded by Ice-Rafted Debris (IRD) in the Southern, Pacific and North Atlantic oceans during the last glacial period (Ehrmann et al., 1991; Wolf and Thiede, 1991; Rea et al., 1995). The peaks in the IRD records are called **Heinrich Events** (Heinrich, 1988). During Heinrich events, the geochemical signature of IRD indicates that their main provenance was the Laurentide ice sheet (Hemming, 2004). After calving, the icebergs were transported by surface currents into the North Atlantic where they melted, depositing most of their sediments between 40° N and 55° N in the Ruddiman belt (Ruddiman, 1977). Iceberg melting in the North Atlantic accounts for around $0.04Sv$ ($1Sv$ equals $10^6 m^3/s$) freshwater discharge over 500 years (Roberts et al., 2014a).

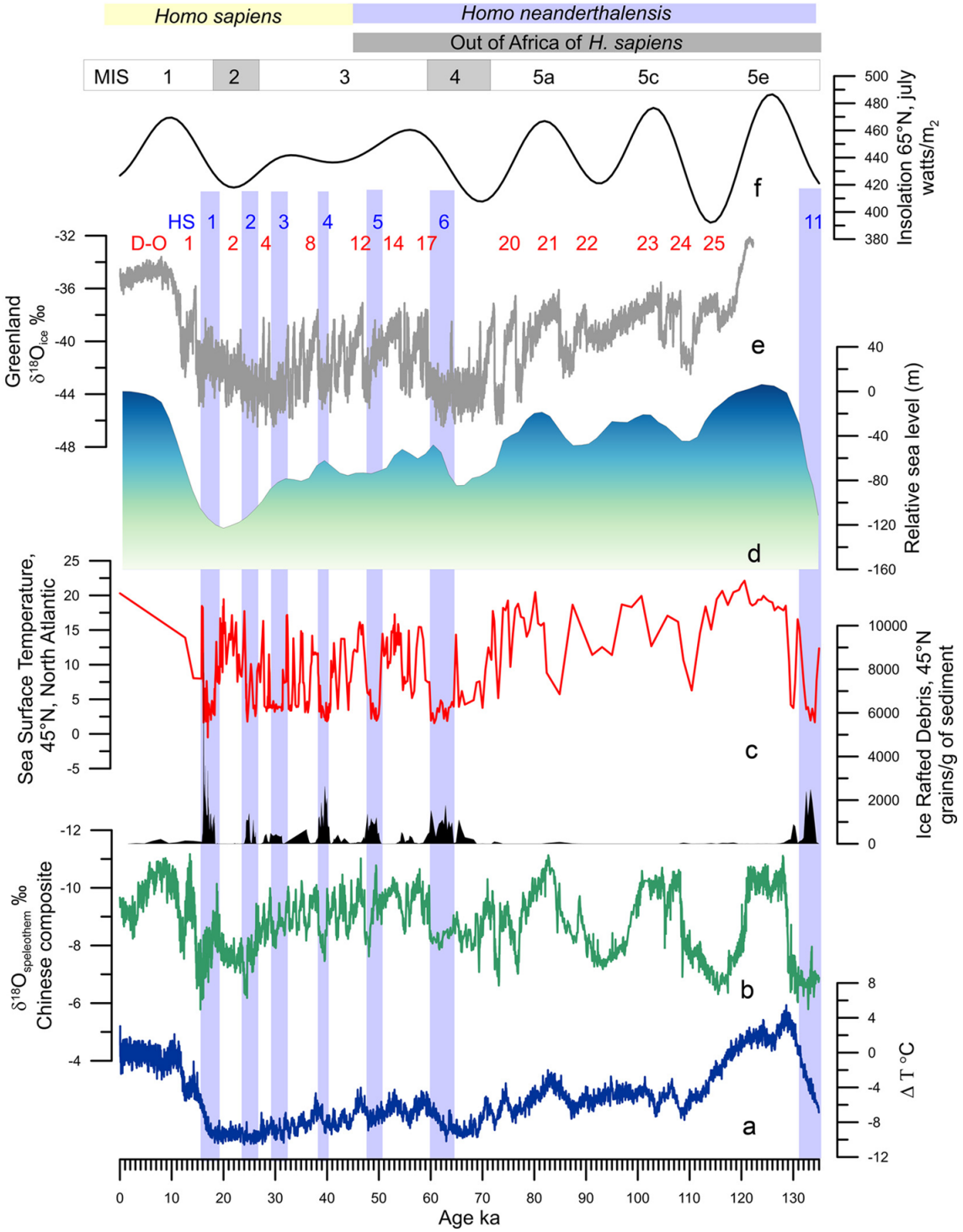

Figure 1.2: **Millennial-scale climatic variability of the last glacial cycle**. *a.* Antarctic temperature anomalies (Jouzel et al., 2007). *b.* Composite Chinese speleotherm record (Cheng et al., 2016). *c.* Ice-rafted debris and *d.* Sea surface temperatures reconstructed foraminifera assemblages of core MD04-2845 (45° N, 5° W Sánchez Goñi, 2020). *d.* Relative sea-level changes (Waelbroeck et al., 2002). *e.* Greenland ice core $\delta^{18}O$ (Rasmussen et al., 2014). *f.* Insolation variations in July at 65° N (Berger and Loutre, 1991). Taken from Sánchez Goñi (2020).

However, some cores also recorded significant activity coming from the Eurasian (Grousset et al., 1993; Gwiazda et al., 1996) and the British-Irish ice sheets (Scourse et al., 2009). Heinrich events are observed during (and not prior to) stadials called **Heinrich stadials** (Barker et al., 2015). The classical theory states that orbital precession (Heinrich, 1988) triggered Heinrich events, and they have been linked since to different feedback between atmosphere and ice sheet mass balance (Wunsch, 2006; Alvarez-Solas et al., 2019), ocean circulation (Wang and Mysak, 2006), ice shelves (Hulbe et al., 2004; Alvarez-Solas et al., 2013) and sea ice (MacAyeal, 1993; González and Dupont, 2009; Bassis et al., 2017).

Since the Holocene (11.700 ka BP to year 1850), millennial-scale variability is not as dominant in climate records and measurements (Khider et al., 2014; Hébert et al., 2022). Centennial scale events have also been observed, but their effect remains moderate compared to the millennial-scale variability of the last glacial period. The Little Ice Age spanned between the 14^{th} and the 19^{th} centuries, when global temperature dropped by up to $0.5°C$ in response to solar and volcanic activity and a weakening of the subpolar gyre (Eddy, 1976; Miller et al., 2012; Moreno-Chamarro et al., 2017). Following the Little Ice Age, Thornalley et al. (2018) observed a weakening of the AMOC over the past 150 years. Generally, the most recent climate observations are dominated by decadal and sub-decadal variability such as the El Niño Southern Oscillation, the Atlantic Multi-decadal Variability and the North Atlantic Oscillations – reviews are provided by IPCC (2023a) and Hernández et al. (2020).

Since the year 1900, the global mean temperature have increased by $\sim 1°C$ and the CO_2 concentrations by $\sim 130ppm$ (IPCC, 2023b). If no action is taken, temperature increase could reach up to $5.7°C$ and CO_2 concentrations could exceed $1000ppm$ by the end of the century (IPCC, 2023b). The rates of climate change observed in the past hundred years do not have any equivalent in the known climate history. Nonetheless, studying past climate changes can improve our confidence in projecting future climate changes (Tierney et al., 2020a). For instance, the mid-Pliocene (∼3.3 to 3 million years ago) provides an analogy to the current levels of CO_2 (Haywood et al., 2016), and the early Eocene (∼55 to 50 million years ago) a view of the climate response to extreme CO_2 increase (Lunt et al., 2012). The mechanisms behind the last glacial period's millennial-scale variability could be crucial in relation to the concept of tipping points, one of the most uncertain and potentially dramatic consequences of climate change. A tipping point is crossed when the forcing reaches a certain threshold that triggers abrupt and irreversible climate changes (Lenton et al., 2008; Armstrong McKay et al., 2022). Such tipping points have been crossed during the last glacial period. At this period, ice sheet retreat was hypothesised to reach up to hundreds of meters per day (Batchelor et al., 2023) during abrupt climate warmings, almost ten times higher than the modern rates calculated from satellite observations (Milillo et al., 2022).

The collapse of the AMOC has been identified as one of the tipping points that would have

the most dramatic impact on the climate (Lenton et al., 2019). Such collapse would result in local temperature changes of 4 to $10°C$ in the North Atlantic in about 50 years (Vellinga and Wood, 2002; Armstrong McKay et al., 2022). Recent studies have argued that early warnings for a tipping point (Lenton, 2011) were identified by performing statistical analysis on fingerprints of the AMOC – in this case, changes of Sea Surface Temperature (SST) by Ditlevsen and Ditlevsen (2023), Boers (2021) and Caesar et al. (2018), and Atlantic multi-decadal variability by Michel et al. (2022). The validity of this protocol remains contested (Alexander-Turner et al., 2018; Kilbourne et al., 2022), and similar conclusions are still to be reached with other methods. In measurements of North Atlantic circulation (Frajka-Williams et al., 2019; Danabasoglu et al., 2021), the initial hypothesis of a decline of the AMOC since 2004 presented by Smeed et al. (2014) has been attributed to interannual variability (Jackson et al., 2022; Latif et al., 2022), and the measurements of the overturning circulation strength were deemed too short to derive any statistically significant conclusion (Lobelle et al., 2020). In climate models, the response of the AMOC to future climate change is more contrasted. Climate models of the Coupled Model Intercomparison Project (CMIP) Phase 6, or CMIP6, tend to simulate more AMOC shift before 2100 than CMIP5 models (Gong et al., 2022), but the spread of model responses is still consequent (Bellomo et al., 2021). Nonetheless, these conclusions might be biased, as it has been suggested that AMOC is too stable in climate models (Liu et al., 2017), and that most of the simulations do not include meltwater discharge (Lohmann and Ditlevsen, 2021).

1.1.2 The Atlantic Meridional Overturning Circulation

The previous section stresses the central role of the AMOC in past and future climate changes. The AMOC is the Atlantic branch of a global network of ocean currents called the global overturning circulation (Broecker, 1997; Kuhlbrodt et al., 2007). In modern days, the global overturning circulation is composed of three meridional circulations: the AMOC, the Pacific meridional overturning circulation, and the Indian Ocean deep meridional overturning circulation, connected by the Antarctica circumpolar current (Vallis, 2016). The meridional overturning circulation is defined as the integral of meridional velocities along the section of a basin following equation 1.1 (e.g. Frajka-Williams et al., 2019).

$$\Psi(y,z) = \int_0^z \int_{x_{west}}^{x_{east}} v(x,y,z')\,dxdz' \tag{1.1}$$

With x_{east} and x_{west} the zonal boundaries of the basin at the latitude y and $v(x,y,z)$ the meridional ocean velocity. This definition indicates that the overturning circulation represents the average northwards motion of the water at a certain latitude. It does not imply that every water parcel at this latitude will follow the same direction, a confusion that has become frequent following the introduction of the conveyor belt concept by Broecker

(1991). Bower et al. (2009) designed an experiment where they released 55 sounds in the Labrador Sea, and only four of them followed the expected path of the AMOC. This motivated the community to move away from the over-simplified conveyor belt theory to consider overturning circulations in their entire complexity (Wunsch, 2010; Lozier et al., 2019).

The AMOC is driven by buoyancy fluxes and surface winds (Jackson et al., 2022). Both the density and wind components are necessary to observe an overturning circulation and thermohaline circulation (Jeffreys, 1925) is now considered an obsolete term (Munk and Wunsch, 1998; Kuhlbrodt et al., 2007). The buoyancy fluxes are responsible for the Gulf Stream and the North Atlantic Current where light surface waters are transported from the Tropics into the North Atlantic (Xu et al., 2018). As they reach high latitudes, they lose heat to the atmosphere and become denser. This increase in upper density is even more substantial when light freshwater is present at the surface. When the water column stratification passes a threshold, deep convection can be activated along continental slopes and marine ridges (Sayol et al., 2019). The winds influence ocean circulation through Ekman transport, where surface and subsurface waters move perpendicularly to the winds, and geostrophic currents, where waters follow the pressure gradients (Jackson et al., 2022). Winds create surface currents that are responsible for the upwelling and sinking regions in the ocean (Toggweiler and Samuels, 1998). The regions where the upper cell of the AMOC sinks in the North Atlantic to create the North Atlantic Deep Waters (NADW) are called the deep water formation sites (Schmittner et al., 2007). When the water sinks, the conservation of mass imposes a return flow that creates a deep southwards current to the Southern Ocean. There, the water is mixed with other deep water sources and is upwelled to the surface. It can then either be recirculated at the surface of the different basins, or, if it is mixed with brine rejection, sink to create the dense AntArctic Bottom Waters (AABW) that spread over the ocean floor of the Atlantic Ocean (Orsi et al., 1999; Talley, 2013). The turnover time of this system is typically estimated between 500 and 1500 years (Broecker and Peng, 1982; Tachikawa et al., 2003). A schematic of the AMOC is given in Figure 1.3.

Direct observations of the AMOC have been made since the start of the 21^{st} century (Frajka-Williams et al., 2019) by mooring arrays to measure water velocity across the entire water column. The RAPID array located at 26.5° N estimated the strength of the AMOC to be around $17Sv$, accounting for a northwards heat transport of around $1.25PW$ into the North Atlantic (McCarthy et al., 2015). This transport was confirmed by atmospheric observations and is about four times smaller than the energy transported by the atmospheric circulation (Seager et al., 2002; Trenberth et al., 2019). This transport of heat has a strong local effect on the climate of the North-East Atlantic, and can drive temperature changes by up to $8°C$ in the Nordic Seas (Vellinga and Wood, 2002; Ferreira et al., 2018). The ONSAP array, located across the Labrador Sea and the Greenland-

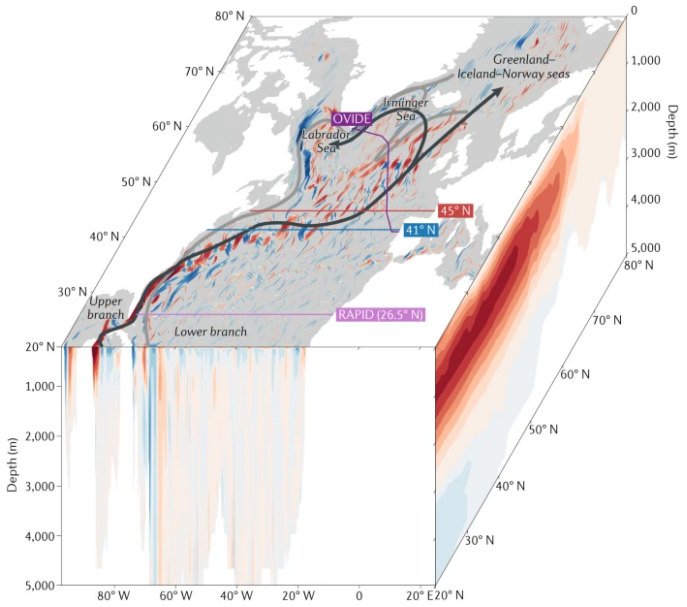

Figure 1.3: **Schematic of the Atlantic Meridional Overturning Circulation**. The surface currents are indicated in black, and the return deep currents are indicated in grey. In the surface panel, sinking is plotted in red and upwelling is indicated in blue. The right-hand panel shows the zonally integrated meridional circulation. Red colours indicate a clockwise motion, and blue colours an anti-clockwise motion. Taken from Jackson et al. (2022).

Iceland-Scotland (GIS) ridge, has been used to observe deep water formation in the North Atlantic (Lozier et al., 2019). In modern oceans, the deep water formation sites are observed mainly in the Iceland and Irminger Seas (Lherminier et al., 2010; Petit et al., 2020), but also exist in the Nordic Seas (Isachsen et al., 2007) and the Labrador Sea (Yashayaev, 2007), where the densest waters are formed (Ferreira et al., 2018; Jackson et al., 2022). There is an ongoing question on whether the Labrador Sea deep water formation actively contributes to the variability of the AMOC (Lozier et al., 2019). Overall, the deep water formation site observations are broadly consistent with model simulations (Jackson and Petit, 2022).

The overturning circulation has changed throughout Earth's history and has influenced the climates of the past (Ferreira et al., 2018). The AMOC is believed to have been a persistent feature during the Quaternary (Raymo et al., 2004). However, the shape of the AMOC in the last glacial period was very likely different from the modern one, and more frequent and dramatic variability of the AMOC was recorded during the last glacial period (Lynch-Stieglitz, 2017). To obtain information about the ocean circulation of the Quaternary, the community relies on several tracers (Frank, 2002; Lynch-Stieglitz, 2003). A quick review is given in Section 1.2.2. The interpretation of these tracers can be a topic of debate, and even time slices with abundant data, such as the Last Glacial Maximum, 21,000 years ago, are still disputed. For example, the reconstruction of the

AMOC during Heinrich Stadial 1, between 17.8 ka BP and 14.6 ka BP, can be interpreted as an overturning circulation collapsed (McManus et al., 2004), weakened (Bradtmiller et al., 2014) or still active (Repschläger et al., 2021) depending on the proxy used and the location of the cores. Combining multiple sources of proxy reconstructions and climate simulations is a good way to constrain the AMOC reconstructions. Such studies have been used, for example, to determine that during the last glacial maximum (∼21 ka BP), the upper cell of the AMOC was probably shallower and weaker but not completely collapsed (Muglia and Schmittner, 2021; Pöppelmeier et al., 2023).

The ocean circulation proxy reconstructions demonstrate that the AMOC can remain in specific states for a prolonged time, and mathematical studies concluded that the AMOC should exist in more than one stable mode, leading to the **multi-modal AMOC regime** theory. This concept has been demonstrated in theoretical models (Stommel, 1961; Weijer et al., 2019), observations (Broecker et al., 1985; Böhm et al., 2015) and climate models (Manabe and Stouffer, 1988). The modes were defined in Böhm et al. (2015) and reproduced in Figure 1.4. The **warm AMOC** mode is the mode observed in present conditions, where the upper cell of the AMOC is fast flowing and reaches the Nordic Seas, and NADW can sink down to 5000 meters in the North Atlantic. The **cold AMOC mode** is observed when the deep water formation region shifts southwards and the upper cell of the AMOC becomes weaker and shallower, leading to an expansion of the AABW. The **off AMOC mode** is obtained when the AMOC has collapsed and no longer reaches the North Atlantic, cooling the temperatures across the region. The multi-modality of the AMOC has been linked to abrupt climate changes during the last glacial period (Clark et al., 2002). Yet, it is still misunderstood, and the mechanism behind switches between different AMOC modes is still largely unknown, resulting in discrepancies between the models (Stouffer et al., 2006) and the reconstructions (Muglia and Schmittner, 2015). Finally, the multi-modal AMOC regime theory was formulated from mathematical models that may underestimate the complexity of the real world, and there is a growing scepticism that the AMOC has ever been completely off during the last glacial period (Oppo et al., 2015; Repschläger et al., 2015, 2021).

1.1.3 The last glacial period and the last deglaciation

In Section 1.1.1, it was discussed that the millennial-scale variability was dominant during the **last glacial period**, and the switches between AMOC modes introduced in Section 1.1.2 are key to understanding the chain of events of this period. The last glacial period is the most recent glacial cycle of the last ice age. Both hemispheres were subject to cold temperatures, (N.G.R.I.P, 2004; Jouzel et al., 2007; Veres et al., 2013), with cooling relative to the pre-industrial temperatures as low as $20°C$ in Greenland and over $10°C$ in Antarctica (Buizert et al., 2021; Martin et al., 2023). Large ice sheets stretched over Greenland, North America (the Laurentide and Cordilleran ice sheets), Scandinavia (the

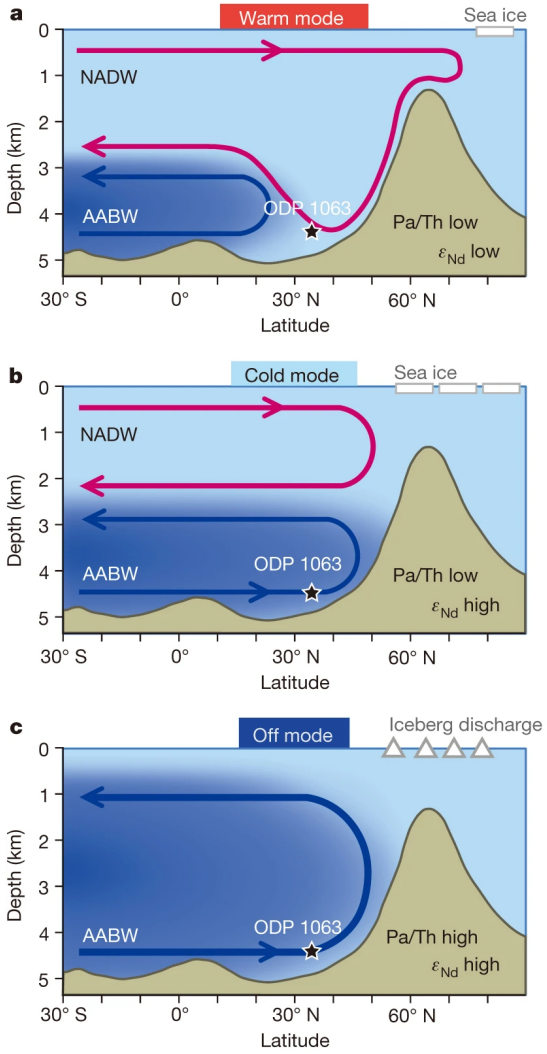

Figure 1.4: **The multi-modal AMOC regime theory**. Taken from Böhm et al. (2015). The water mass, circulation, depth, the sea ice and the iceberg discharges indicates the typical observations for a mode and do not fit a particular cycle. Pa/Th and ε_{Nd} are ocean tracers described in Section 1.2.2. ODP 1063 indicates the location of the site analysed in Böhm et al. (2015).

Fennoscandian ice sheet), the British Isles (the British-Irish ice sheet) and Antarctica (Hughes et al., 2016; Batchelor et al., 2019; Gowan et al., 2021). The last Glacial period can be split into four stages corresponding to coherent levels of $\delta^{18}O$ in benthic sediment cores (see Section 1.2.2) – these periods are called the Marine Isototope Stages (MIS) (Lisiecki and Raymo, 2005; Lisiecki and Stern, 2016). MIS3, stretching from ∼57 ka BP to ∼26 ka BP (Andel, 2002; Huber et al., 2006; Van Meerbeeck et al., 2009), was a relatively mild glacial stage where the most frequent occurrence of Dansgaard-Oeschger variability was observed (Wolff et al., 2010). MIS2, between ∼26 ka BP and ∼11.7 ka BP corresponds to the colder last glacial maximum followed by the terminations of the glacial period called the last deglaciation. The last deglaciation is remarkable for the variety of climate disruptions witnessed in a short amount of geological time, and its proximity to our age makes it one of the best-studied times in climate history.

The last deglaciation sets off from the **Last Glacial Maximum (LGM)**, around 21 ka BP. The last glacial maximum is defined by a minimum in sea level records and stable cold climate in the North Atlantic (Peltier and Fairbanks, 2006; Clark et al., 2009; Lambeck et al., 2014), corresponding to a maximum extent of the Northern Hemisphere ice sheet (Peltier et al., 2015; Abe-Ouchi et al., 2015; Hughes et al., 2016; Batchelor et al., 2019; Gowan et al., 2021). At the last glacial maximum, evidence suggests that the sea level was around 115 meters lower than the present levels (Simms et al., 2019). The sea level records indicate discrepancies in the times when the Northern Hemisphere ice sheets reached their maximum extent, a period of consistently low global sea levels can be identified between 26.5 ka BP and 19 ka BP, and the date of 21 ka BP is commonly used as the most representative date for the Last Glacial Maximum (Clark et al., 2009). Lower greenhouse gas concentrations (Loulergue et al., 2008; Schilt et al., 2010; Bereiter et al., 2015) and higher dust concentrations (Lambert et al., 2015) provided a negative radiative forcing that resulted in colder temperatures than pre-industrial values. The global mean surface air temperature was colder than modern conditions by $4°C$ to $6°C$ (Annan and Hargreaves, 2013; Tierney et al., 2020b) with temperature decreases of as much as $17°C$ in Greenland (Buizert et al., 2018). The global mean sea surface temperature was colder than modern conditions by $1.7°C$ to $3.2°C$. In the North Atlantic, the average cooling was around $3°C$, reaching as low as $10°C$ at high latitude, and the Southern Ocean was colder by $\sim 1.5°C$ (Waelbroeck et al., 2009; Tierney et al., 2020b; Paul et al., 2021). The AMOC was probably weak and shallow but not completely collapsed (Repschläger et al., 2021; Pöppelmeier et al., 2023). At this time, the deep water formation sites were similar to what they are in modern oceanography (Lynch-Stieglitz et al., 2007; Howe et al., 2016; Ferreira et al., 2018), including convection in the Nordic Seas (Larkin et al., 2022).

The transition from the last glacial maximum to the **last deglaciation** was triggered by an increase in summer insolation (Hays et al., 1976). The last deglaciation (19 ka BP to 11.7 ka BP) (Clark et al., 2012), corresponds to the period when the Earth gradually

warmed towards the Holocene (Jouzel et al., 2007; Buizert et al., 2014). Following the increase of summer insolation (Berger and Loutre, 1991) and greenhouse gas concentrations (Loulergue et al., 2008; Schilt et al., 2010; Bereiter et al., 2015), the summer temperatures increased (Abe-Ouchi et al., 2013; Gregoire et al., 2015) and melted the large ice sheets of the last glacial maximum, first in the Northern Hemisphere (Clark et al., 2012; Tarasov et al., 2012; Lambeck et al., 2014) and then in the Southern Hemisphere (Briggs et al., 2014; Argus et al., 2014). This resulted in a loss of around 130 meters of sea level equivalent of ice in less than ten thousand years (Peltier and Fairbanks, 2006; Lambeck et al., 2014; Nakada et al., 2016) and produced additional feedback on global mean temperature through a reduction in surface albedo. Overlying the long-term warming trend of the deglaciation, the last deglaciation also exhibited more abrupt events that can be attributed to millennial-scale variability. A summary of the background conditions and climate changes of the last deglaciation is given in Figure 1.5.

Heinrich Stadial 1 (HS1), between 17.8 ka BP and 14.6 ka BP (Rasmussen et al., 2014; Martin et al., 2023), started after the end of the last glacial maximum and constituted a series of contradictory events both from a spatial and temporal point of view (Denton et al., 2006; Roche et al., 2011). The temperatures were expected to increase globally following the orbital forcing, but only the Southern Hemisphere followed this trend (Parrenin et al., 2007). Instead, surface atmosphere and sea temperatures remained cold (Bard et al., 2000; Buizert et al., 2014; Pedro et al., 2022). Meltwater discharge from the melting ice sheet probably led to a slowed down AMOC during Heinrich stadial 1 (McManus et al., 2004; Bradtmiller et al., 2014; Ng et al., 2018), although active deep water formation sites in the North Atlantic rule out a complete shut down (Repschläger et al., 2021). As a result, the freshwater release is believed to have been the main driver of change in the early Heinrich Stadial 1 (Zaragosi et al., 2001; Toucanne et al., 2015; Peck et al., 2006) especially since meltwater could be directly routed to deep water formation sites (Condron and Winsor, 2012). At the end of this stage, a peak in ice-rafted debris was recorded during Heinrich event 1 around 16.8 ka BP (Hemming, 2004). It is unlikely that Heinrich event 1 contributed to the meltwater discharge that drove Heinrich stadial 1 as it is consistently dated at the end of the period (Hall et al., 2006; Stanford et al., 2011; Stern and Lisiecki, 2013; Hodell et al., 2017). It may, however, have provided positive feedback to prolong the weakening of the AMOC (Alvarez-Solas et al., 2010; Barker et al., 2015). The iceberg discharged during Heinrich event 1 comes predominantly from the Laurentide ice sheet (Hemming, 2004), but signals from both the Laurentide and Eurasian ice sheets were also recorded (Scourse et al., 2009; Bigg et al., 2012).

After Heinrich event 1, an abrupt transition into a warm interstadial state (Liu et al., 2009) was triggered. This transition, labelled **Bølling–Allerød Warming** (abbreviated Bølling Warming), started at 14.7 ka BP (Severinghaus and Brook, 1999). In Greenland ice cores, the temperature changes reached $14°C$ in 200 years (Steffensen et al., 2008; Buizert

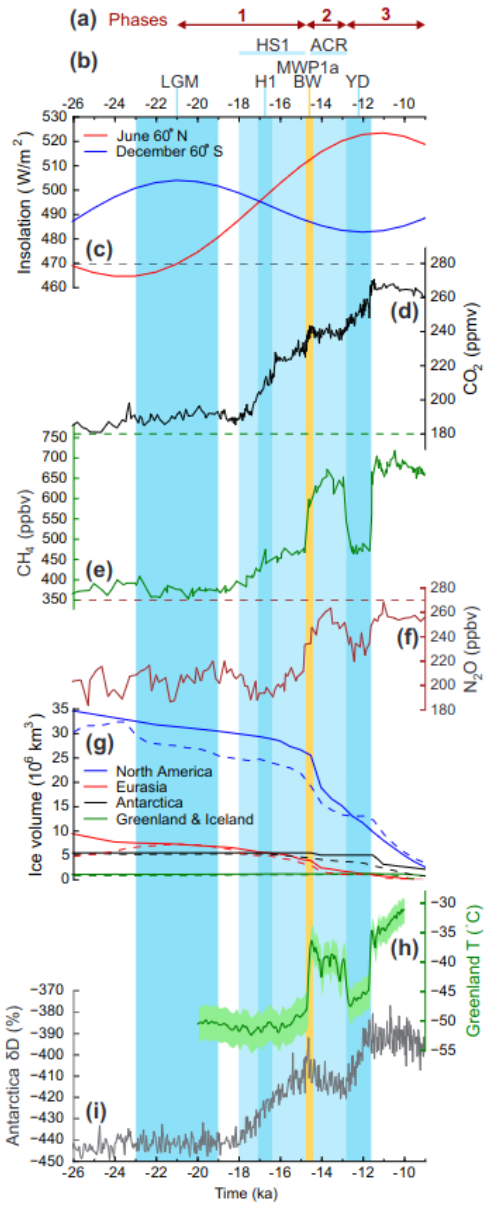

Figure 1.5: **The last deglaciation: forcings and events**. Taken from Ivanovic et al. (2016). *a.* Phases of the PMIP protocol core experiments. *b.* Climate events and periods. *c.* June insolation at 60° N (red line) and December insolation at 60° S (blue line) from Berger (1978). *d.* Atmospheric carbon dioxide concentration in Antarctica from Bereiter et al. (2015). *e.* Atmospheric methane concentration in Antarctica from Loulergue et al. (2008). *f.* Atmospheric nitrous oxide concentration in Antarctica from Schilt et al. (2010). Dashed lines show pre-industrial levels in panels *c,d,e*. *g.* Volume of the ice sheets according to ICE6G-C ice sheet reconstruction (solid lines, Argus et al. (2014); Peltier et al. (2015)) and GLAC-1D ice sheet reconstruction (dashed lines, Tarasov and Peltier (2002); Tarasov et al. (2012); Briggs et al. (2014)). *h.* Greenland temperature reconstruction from Buizert et al. (2014). *i.* Antarctica δD from Jouzel et al. (2007).

et al., 2014; Martin et al., 2023) and triggered significant ice volume loss in the following millennia. An abrupt sea level rise caused by the melting of ice sheets was observed during this period and called **Meltwater Pulse 1a (MWP1a)**, between 14.7 ka BP to 14.3 ka BP (Deschamps et al., 2012). The primary source of this meltwater discharge is believed to have been the saddle collapse of the Laurentide and the Cordilleran ice sheets (Gregoire et al., 2012), with additional contributions from Antarctica (Peltier, 2005; Argus et al., 2014; Briggs et al., 2014) and the other Northern Hemisphere ice sheets (Tarasov et al., 2012). The warming triggered a phase of Antarctic temperature decrease, the Antarctic cold reversal ($\sim$ 14.5 ka BP to $\sim$ 12.8 ka BP Jouzel et al., 2007) in a mechanism that recalls the bipolar see-saw (Stocker, 1998; Menviel et al., 2011). After the warm phase that followed the Bølling Warming, an abrupt cooling phase was recorded in the Greenland and Antarctica ice cores and called the **Younger Dryas** (12.9 ka BP – 11.7 ka BP Murton et al., 2010; Liu et al., 2012). The climate changes of the Younger Dryas were mostly constrained to the Northern hemisphere (Shakun et al., 2012), and even in the North Atlantic it is difficult to see a geographically consistent signal in temperatures (Clark et al., 2012; Shakun et al., 2012) and ocean circulation (Ng et al., 2018) records. A drop in methane concentrations (Loulergue et al., 2008) and, to a lower extent, nitrous oxide concentration (Schilt et al., 2010) was observed, but the carbon dioxide continued to increase during this period (Bereiter et al., 2015). A change in the source of moisture was also hypothesised to have contributed to $\delta^{18}O$ records fluctuations (Liu et al., 2012). This event was the final major climate change of the last deglaciation that continued its warming towards Holocene temperatures as the radiative forcing reached a maximum from 11.7 ka BP (Severinghaus et al., 1998; Clark et al., 2012). This warming was only briefly interrupted by another meltwater discharge event called the **8.2ka event** where freshwater discharged in the Labrador Sea weakened the AMOC (Born and Levermann, 2010; You et al., 2023) and led to a $3°C$ cooling in Greenland for 160 years (Morrill et al., 2013; Matero et al., 2017).

The relative timing the last deglaciation chain of events is now reaching a consensus (Clark et al., 2012). On the other hand, the mechanisms behind the deglacial climate changes are still a highly debated topic. **Transient simulations** of the last deglaciation in climate models have been used as a tool for exploring these processes for decades (Liu et al., 2009; Roche et al., 2011; Menviel et al., 2011). A Paleoclimate Modelling Intercomparison Project (PMIP) international working group was created to coordinate the efforts by providing a protocol for simulating climate changes of the last deglaciation written by Ivanovic et al. (2016). The simulations covering the early part of the last deglaciation were analysed by Snoll et al. (2023) where the "meltwater paradox" is highlighted. The "meltwater paradox" is that simulations of the last deglaciation that reproduces the most accurate abrupt climate changes of the last deglaciation are driven by meltwater fluxes that are not compatible with reconstructed changes in ice sheets, but simulations that

use realistic data-constrained freshwater flux produces changes incompatible with climate proxy records. For instance, Kapsch et al. (2022) and Snoll et al. (2023) have computed the meltwater discharge from changes in ice volume but they have not been able to produce the abrupt climate changes at the expected timing. Liu et al. (2009) and He et al. (2021), on the other hand, adjusted the meltwater discharge to produce simulations of the last deglaciation that are a good fit to the records in terms of timing and amplitude of change. The resulting meltwater fluxes do not match the patterns derived from ice sheet reconstructions and require a shutdown of the discharge during HS1, which is difficult to explain from records. Obase and Abe-Ouchi (2019) also simulated the right timing for the Bolling-Allerod Warming with relatively weak freshwater discharge and meltwater discharge during Heinrich Stadial 1. They managed this by starting from a cold AMOC mode at the LGM but, therefore, did not capture the AMOC slowdown of Heinrich stadial 1 and used freshwater fluxes that were effectively weaker than the ice sheet-derived meltwater flux.

Geological data of past ice sheet evolution has well documented the patterns and timing of ice sheet retreat (e.g. Hughes et al., 2016; Batchelor et al., 2019; Gowan et al., 2021). The ice thickness, however, remains hard to figure and is only constrained via relative sea level records via the highly uncertain modelling of the Glacial Isostatic Adjustment of the solid earth (Pollard et al., 2023). The meltwater flux is a derivative of ice thickness changes and, thus, even more difficult to constrain. Very few studies have attempted to reconstruct meltwater flux through geochemical tracers (Toucanne et al., 2015; Wickert, 2016), and suffer from large uncertainties and insufficient coverage in the data. The uncertainty around the volume of the ice sheets during the last delgaciation is also reflected in the last deglaciation "missing ice" problem (Clark and Tarasov, 2014; Gowan et al., 2021): there is a mismatch between the sea level equivalent of the LGM ($\sim 130m$ higher than present day) and the sea level increase observed at the last deglaciation ($\sim 115m$) (Gebbie et al., 2019). The presence of a Siberian ice sheet has been one of the hypotheses to explain this inconsistency (Clark and Tarasov, 2014). The PMIP4 last deglaciation protocol provides the option of using three ice sheet reconstructions: PMIP3 (Abe-Ouchi et al., 2015), ICE6G-C (shortened ICE6G, Argus et al., 2014; Peltier et al., 2015) and GLAC-1D (Tarasov and Peltier, 2002; Tarasov et al., 2012; Briggs et al., 2014; Ivanovic et al., 2016). Only ICE6G and GLAC-1D will be used in this thesis and a comparison of the two ice sheets during the deglaciation made by Ivanovic et al. (2016) is given in Figure 1.6. ICE6G was designed so that the total ice volume and the local ice thickness fit the sea level records and global isostatic rebound measurements as accurately as possible. GLAC-1D is formed by the assemblage of different ice sheet reconstructions combining glaciological models and multi-ensemble runs constrained by the reconstructed ice sheet extents. GLAC-1D has a 100-year temporal resolution, and ICE6G has a 500-year time resolution over the last deglaciation period. Finally, the two ice sheets reconstructions use

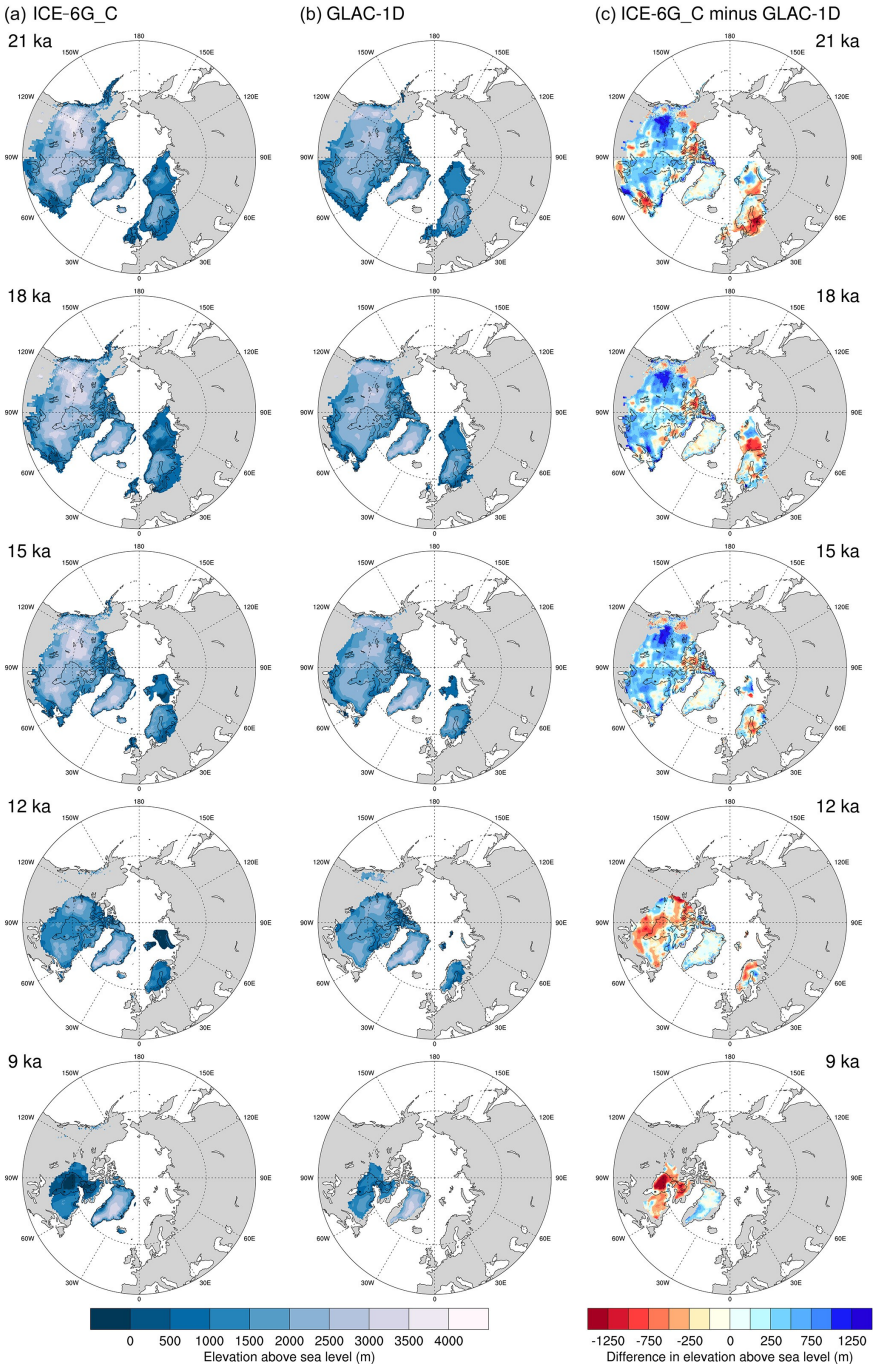

Figure 1.6: **Comparison of the ice sheet reconstructions over the last deglaciation.** Taken from Ivanovic et al. (2016). Northern Hemisphere ice sheet elevation at 21, 18, 15, 12 and 9 ka BP for *a.* the ICE-6G reconstruction and *b.* the GLAC-1D reconstruction and *c.* the ICE6G - GLAC-1D anomalies. The ice sheet elevation was plotted where the ice fraction was over 0.5.

the ice extent same constraints for the North American ice sheet (Dyke, 2004), but not for the Eurasian ice sheet where ICE6G uses the DATED database (Gyllencreutz et al., 2007) whereas GLAC-1D relies on the updated DATED-1 database (Hughes et al., 2016).

The ice sheet reconstruction used in the climate models can yield significantly different simulations of the last deglaciation (Kapsch et al., 2022; Bouttes et al., 2023). For instance, Bouttes et al. (2023) obtained the Antarctic Cold Reversal only with ICE6G ice sheets and Kapsch et al. (2022) the Younger Dryas only with GLAC-1D ice sheets. These differences are due to the fact that the ice sheet can modify the albedo and radiative balance (Roberts and Valdes, 2017), winds and gyres (Montoya et al., 2011; Roberts et al., 2014b; Madonna et al., 2017), the atmospheric circulation (Izumi et al., 2023) and the sea level pressure (Pausata et al., 2011) around them. The main impact of the choice of the ice sheet reconstruction comes from the meltwater discharge, although this is one of the least well-constrained (Bethke et al., 2012). Ivanovic et al. (2018a) showed that the right input of freshwater can trigger climate changes that match paleo records but that the role of the Eurasian ice sheet melt is often overlooked and results in the use of unrealistically large fluxes from the North American ice sheet.

1.1.4 Modelling millennial-scale variability

The multi-modality of the AMOC has been at the centre of the hypotheses to explain millennial-scale variability mechanisms (Broecker et al., 1990; Clark et al., 2002). The two-box ocean model imagined by Stommel (1961) provides the basis of most of these hypotheses. In his paper, Stommel (1961) shows in a simple representation of the Atlantic basin that convection in two interconnected reservoirs can exist in two stable regimes of overturning circulation. In his influential **salt oscillator** theory, Broecker et al. (1990) offered an explanation for the shifts between the different AMOC modes: when the AMOC is weak, salt is accumulated in the Atlantic by evaporation and increases the surface density, leading to the reactivation of the North Atlantic vertical convection; when the AMOC is strong, the salt is exported out of the Atlantic by the overturning circulation and the surface density decreases, leading to the deactivation of the North Atlantic deep water formation sites. This mechanism is sometimes referred to as the salt advection feedback (Drijfhout et al., 2011). Various studies (Rahmstorf, 1996; Huisman et al., 2010; Drijfhout et al., 2011) have argued that this mechanism depends on the sign of the salt export by the meridional overturning circulation out of the Atlantic. The role of the ice sheets, introduced by Broecker et al. (1990), is also a topic of discussion as ice sheets can either amplify the oscillations (e.g. Boers et al., 2018) or prevent them (e.g. Gregory et al., 2003).

The question of the excitation of the oscillator is also highly debated. It was initially believed that a strong freshwater discharge was necessary to trigger a shift between different modes of the AMOC (Paillard and Labeyrie, 1994; Vidal et al., 1997). In order to repro-

duce this perturbation, 'hosing experiments' were performed with complex Atmosphere-Ocean General Circulation Models (AOGCMs) (Kageyama et al., 2010, 2013b). In its most classical form, a 'hosing experiment' consists of a uniform freshwater flux between $0.1Sv$ and $0.4Sv$ released between latitudes 40° N - 50° N, or in some cases 60° N - 80° N, in the North Atlantic (e.g Manabe and Stouffer, 1997; Ganopolski and Rahmstorf, 2001; Stouffer et al., 2006; Renold et al., 2010; Cheng et al., 2011; Menviel et al., 2014; Brown and Galbraith, 2016). This method has proven successful to induce AMOC mode shifts in General Circulation Models (GCMs). However, it requires unrealistic freshwater fluxes that largely overestimate the expected values attained during the last glacial period (Roberts et al., 2014a; Bradtmiller et al., 2014). The AMOC is very sensitive to the location of the freshwater release (Roche et al., 2010), but even focusing the discharge in more accurate regions is not sufficient to trigger abrupt climate change with realistic freshwater fluxes (Snoll et al., 2023). Freshwater hosing simulations have also been used as a periodic forcing in the context of the stochastic resonance theory (Alley et al., 2001; Ganopolski and Rahmstorf, 2002; Cimatoribus et al., 2013). In this case, the salt oscillator acts as a relaxation oscillator and internal ocean variability amplifies the initial periodic freshwater forcing at its resonance frequency. The freshwater discharge of Heinrich events can reach $0.08Sv$ (Roberts et al., 2014a) and could be a way to trigger such stochastic resonance (Schulz et al., 2002; Timmermann et al., 2003). Finally, freshwater hosing experiments have been used to explore the hysteresis cycle of the response of the AMOC to external forcing (Rahmstorf, 1996; Hofmann and Rahmstorf, 2009). The mode switches are indeed highly dependent on the AMOC history, and there is an asymmetry in the amount of freshwater needed to trigger stadial-to-interstadial and interstadial-to-stadial transitions.

Freshwater forcing is not always required to trigger millennial-scale variability. Welander (1982) showed with a simple mixed layer model that spontaneous oscillations can occur in the water column at deep water formation sites, and Cessi (1996) linked the mixed layer oscillator to surface freshwater fluxes. This model does not take into account the advective processes of the overturning circulation, and Colin de Verdière (2007) proposed a framework to couple Stommel (1961)'s box oscillations to Welander (1982)'s convective oscillations. At last, Winton (1993) introduced a new idea for vertical instability called deep-decoupling oscillations, where the presence or not of a strong halocline at North Atlantic deep water formation sites deactivates or reactivates the overturning circulation. In the past decade, general circulation models have managed to overcome the belief that they were too stable (Hofmann and Rahmstorf, 2009; Valdes, 2011) and were lacking key physical processes (Clement and Peterson, 2008) to simulate spontaneous millennial-scale variability. Abrupt climate changes with amplitude and duration matching the Greenland ice cores records were obtained spontaneously or using climate forcings with a wide range of models and experimental designs (e.g. Peltier and Vettoretti, 2014; Brown and Galbraith, 2016; Klockmann et al., 2018; Kuniyoshi et al., 2022; Armstrong et al., 2022). An example

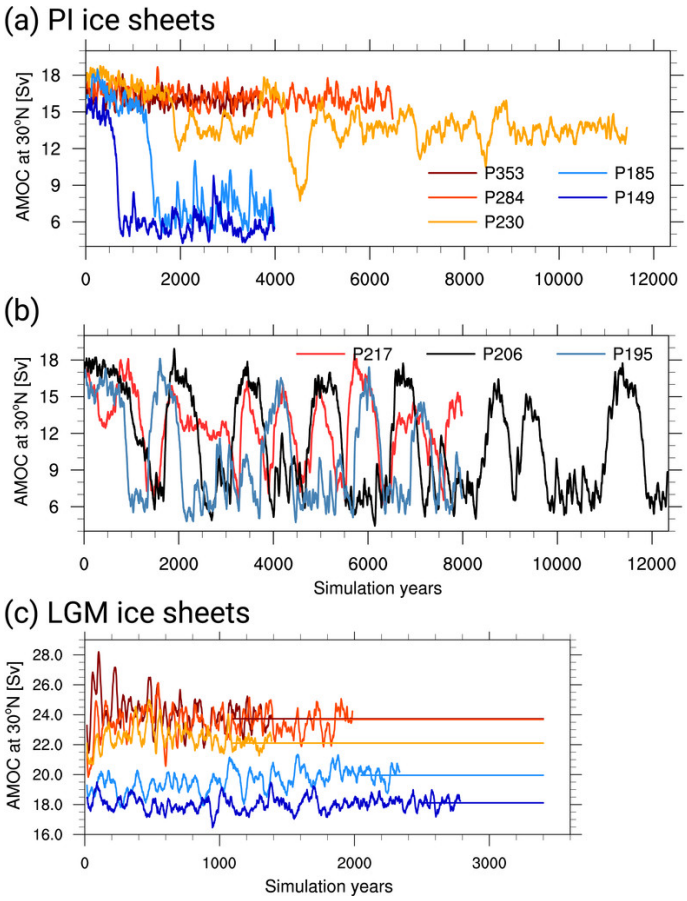

Figure 1.7: **Millennial-scale variability in a GCM.** Maximum overturning circulation at 30° N in the Atlantic ocean for simulations described in Klockmann et al. (2018). PXXX indicates the CO_2 concentration of $XXXppm$. *a.* Non-oscillating simulations obtained with pre-industrial ice sheets. **b.** Oscillating simulations obtained with pre-industrial ice sheets. *c.* Non-oscillating simulations obtained with LGM ice sheets, in this case the PMIP3 LGM ice sheets (Abe-Ouchi et al., 2015).

of pseudo-oscillating cycles obtained by Klockmann et al. (2018) is given in Figure 1.7.

The mechanisms observed in state-of-the-art General Circulation Models that display spontaneous oscillations in glacial conditions are varied but compatible with the theoretical studies. Vettoretti and Peltier (2018) explained the periodical climate changes in CESM1 of Peltier and Vettoretti (2014) by a salt oscillator driven by instabilities in North Atlantic sea ice and convection. The salt oscillator is also at the centre of Armstrong et al. (2022)'s theory, only this time it is winds and meridional density gradients that destabilise the North Atlantic convection. The role of the Subpolar Gyre (SPG) is the cornerstone of Li and Born (2019)'s theory and its influence was also observed in Klockmann et al. (2018). Klockmann et al. (2020) argue that in MPI-ESM wind-driven feedback, similar to the Kleppin et al. (2015) theory, or density-driven feedback, similar to the Montoya et al. (2011) theory, between the AMOC and the SPG can result in positive and negative cou-

pling, respectively. Kuniyoshi et al. (2022) also observes the effect of the subpolar gyre in MIROC-ESM, but in their case, the mechanism is heat-driven rather than salinity-driven. The thermal effect was equally observed by Brown and Galbraith (2016), and such control of the oscillations was already widely discussed in several studies (Marcott et al., 2011; Oka et al., 2012; Dokken et al., 2013; Oka et al., 2021).

The research community has attempted to answer the question of the uniqueness of the physical mechanism behind abrupt climate changes (Malmierca-Vallet et al., 2022), but such a unique mechanism, if it exists, remains unclear. This question extends to the millennial-scale variability outside of the last glacial period and centennial-scale variability (Dijkstra and Ghil, 2005) observed at different time periods (Kessler et al., 2020) and with different periodicity (Jiang et al., 2021; Mehling et al., 2022). Comprehensive reviews of the millennial-scale physical processes at play during the last glacial period are given in Li and Born (2019) and Menviel et al. (2020). These reviews, however, tend to focus on the North Atlantic. The Southern and Indian Oceans have been identified as key regions to understand the salt and heat import into the North Atlantic (Knorr and Lohmann, 2003; Banderas et al., 2015; Buizert and Schmittner, 2015; Thompson et al., 2019; Oka et al., 2021; Nuber et al., 2023), and therefore need to be included in the processes considered. Finally, it feels counter-intuitive that in some studies, pre-industrial conditions were more favourable to the existence of millennial-scale variability than glacial conditions (e.g. Brown and Galbraith, 2016; Klockmann et al., 2018)). Following Barker and Knorr (2021)'s definition, the window of opportunity is the ensemble of boundary conditions and forcing where abrupt climate transitions can occur. In this thesis, I will sometimes refer to the inputs of the climate models (i.e. boundary conditions and climate forcing) as the parameters, and the ensemble of configuration as the parameter space. They are not to be confounded with the model parametrisation that was not considered in this study. Climate model studies have demonstrated that the location of the window of opportunity is very sensitive to changes in ice sheet extent and geometry (Zhang et al., 2014; Brown and Galbraith, 2016; Klockmann et al., 2018), CO_2 concentrations (Brown and Galbraith, 2016; Zhang et al., 2017; Klockmann et al., 2018; Vettoretti et al., 2022) and solar insolation (Zhang et al., 2021; Kuniyoshi et al., 2022).

1.2 Tools and techniques

1.2.1 General circulation models - HadCM3

Climate records inform scientists about the Earth's past conditions and help to shape theories about its evolution. In order to validate these theories and to explore the physical processes in detail, climate models need to be used. There are many different types of climate models, from simple physical models used to replicate a specific physical process to complex geochemical models tracking the evolution of chemical tracers. When looking

at the general evolution of past climate, the use of general circulation models, and in particular coupled atmosphere-ocean GCMs, is favoured. AOGCMs are the result of the coupling of an atmosphere model and an ocean model, independently resolving the dynamical primitive equations at each grid cell in response to boundary conditions and climate forcings. Sub-grid scale processes, such as turbulent diffusion, precipitation, cloud dynamics or heat exchange, are parameterised. The coupling between the Atmosphere and the Ocean models is done by synchronising the surface temperatures and fluxes at regular time steps. Additional models can be coupled to an AOGCM in order to account for different components of the climate system.

The simulations run for this thesis all use the Hadley Centre Climate Model 3 (HadCM3) general circulation model. More specifically, they are using the BRIDGE Bristol Research Initiative for the Dynamic Global Environment (BRIDGE) version of the model atmosphere-ocean general circulation model described by Valdes et al. (2017). The Atmosphere model has a horizontal resolution of $2.5° \times 3.75°$ and 19 vertical levels, and therefore a 96 x 73 x 19 atmosphere grid, described by Pope et al. (2000). The Ocean model has a horizontal resolution of $1.25° \times 1.25°$ over 20 depth levels, and therefore a 288 x 144 ocean grid, described by Gordon et al. (2000). The ocean model is a rigid-lid model, which means that the land-sea mask and the ocean volume are not modified by the model, and the exchange of waters between the different components is modelled by changes in the salinity and temperature fields of the different water masses. The atmosphere model is run every 30 minutes and the Ocean model every hour, and the two components are coupled to each other every simulation day. The sea ice component uses a simple thermodynamical model in HadCM3 and sea ice cover is calculated by assuming a freezing point of $-1.8°C$ and constant ice salinity (Cattle et al., 1997). There are no ocean points in the Gibraltar Strait and heat and salt exchanges between the Atlantic and Mediterranean Sea are parametrised by a diffusive pipe (Ivanovic et al., 2014). Ice sheets are prescribed by modifying the orography and the albedo of land points. Atmosphere-land water and energy fluxes are calculated using the Met Office Surface Exchange Scheme 2 (MOSES2) land surface model (Cox et al., 1999) fully coupled to the Top-down Representation of Interactive Foliage and Flora including Dynamics (TRIFFID) vegetation model (Cox, 2001).

HadCM3 has been used for more than 20 years in various contexts. It was first intended to study historical climate change (Stott et al., 2000) and has been part of the CMIP3 multi-model ensemble used for the third and fourth Intergovernmental Panel on Climate Change (IPCC) Assessment (Reichler and Kim, 2008). Because of its good performance, it was still used in the CMIP5 ensemble almost 15 years after its creation (Taylor et al., 2012), before being superseded by HadGEM2. Today, HadCM3 continues to be used to simulate palaeo-climates because it is a robust General Circulation Model that has been successfully applied to simulate a range of past cold and warm climates, with an optimum balance of

resolution and speed to perform multi-millennial simulations (Valdes et al., 2017). On the University of Leeds Advanced Research Computing ARC4 supercomputer, it can produce up to 60 model days per day on 20 or 24 cores. It is part of the PMIP4 models and has been used in simulations of the Eocene (Lunt et al., 2012), and the Pliocene (Haywood et al., 2016). Armstrong et al. (2019) produced a set of HadCM3 simulations covering the last glacial period, and HadCM3 has been regularly used to simulate the abrupt climate changes of the Early Holocene, 8200 years ago (Matero et al., 2017) the last deglaciation (Snoll et al., 2022) and the last glacial period (Armstrong et al., 2022). Most recently, HadCM3 was used to perform LGM simulations (Kageyama et al., 2021) using the latest PMIP4 protocol (Kageyama et al., 2017) and with both the ICE6G and the GLAC-1D ice sheet reconstructions (e.g. Izumi et al., 2023).

1.2.2 Proxy reconstructions in Palaeoclimatology

The evidence of past glacial changes is contained in Earth's geological archives. Direct measurements of the past climate are rare and do not extend much further than a few centuries (e.g. Hassan, 1981). When no direct measurements are available, the scientific community has to rely on indirect measurements of the climatic conditions called **proxy records**. There exist many different proxies for different variables, geological times and geographical location (Ruddiman, 2001; Cronin, 2010). This section provides a quick review of the proxy records relevant to this thesis.

Stable isotopes in ice cores

Ice cores from Greenland and Antarctica provide some of the most valuable information about the Northern and Southern Hemisphere climate over the past 110,000 and 800,000 years, respectively. They are collected in large international ice coring campaigns where long and continuous cores are drilled from the surface to the bottom of the ice sheet. This thesis will mostly use the records from two specific programs, the NGRIP (N.G.R.I.P, 2004) site in Greenland and the EPICA (Jouzel et al., 2007) program in Antarctica, but many more projects exist. Ice cores have been used for direct measurements of greenhouse gases from fossil air bubbles trapped in ice cores (Loulergue et al., 2008; Schilt et al., 2010; Bereiter et al., 2015), and for indirect measurements of past temperatures.

Temperature reconstruction can be obtained by analysing the chemical composition of the ice cores with stable isotope ratios (Jouzel, 1999). This method lies in the fact that changes in climatic conditions can modify the abundance ratio of different stable isotopes of the same element. The oxygen isotope ratio $\delta^{18}O$ has widely been used as a proxy for temperatures. The most common oxygen isotope is the ^{16}O, representing 99.8% of the total amount on the planet, while the other 0.2% is mostly formed of the ^{18}O isotope. The different components of the climate system have different ways of storing and exchanging these two isotopes, and the exchange rates depend on the background climate,

especially temperature. The climate changes will, therefore, modify the ratio between the two isotopes, which can be calculated as $\delta^{18}O$ following equation 1.2.

$$\delta^{18}O = \frac{^{18}O/^{16}O - (^{18}O/^{16}O)_{standard}}{(^{18}O/^{16}O)_{standard}} * 1000 \tag{1.2}$$

With $^{18}O/^{16}O)_{standard} = 8‰$. The snow that precipitates over ice sheets tends to have a lighter $\delta^{18}O$ if the temperature over the ice sheet and/or from the source of the precipitation is cooler, and a heavier $\delta^{18}O$ if the temperature over the ice sheet and/or from the source of the precipitation is warmer. The temperature influence on $\delta^{18}O$ is robust in Greenland and Antarctica (Dansgaard et al., 1993; Grootes, 1993). In Antarctica, because of its clearer signal than in the Greenland ice cores, scientists prefer to rely on the deuterium ratio δD that measures the abundance of ^{2}H compared to ^{1}H (Jouzel et al., 2007). More precisely, the deuterium excess is used to account for both the $\delta^{18}O$ and the δD following the equation 1.3.

$$d = \delta D - 8 * \delta^{18}O \tag{1.3}$$

These two isotopes can track the past local air temperature over the ice cores but are also impacted by the sea surface temperatures and moisture in the source regions of the precipitation, as well as the winds and precipitation patterns of the ice sheets. More recent reconstructions, like Buizert et al. (2014), combined multiple sources of $\delta^{18}O$ data to other proxy records and climate simulations to reduce the uncertainty in the temperature reconstructions. Ice cores can only be used to estimate the atmosphere temperatures at the poles, and regional atmospheric temperatures need to be reconstructed differently. The land temperatures can be calculated from inland precipitation through changes in the stable oxygen ratio in speleotherms (e.g. Cheng et al., 2016) and in lakes sediments (Cronin, 2010), or using pollen records (e.g. Waelbroeck et al., 2009).

Proxies for ocean temperatures

Stable isotope ratios can also be used in ocean sediment records. Foraminiferas use oxygen to form their calcite shell, or test, and the oxygen isotopic ratio of the shell deposited in the depth of the ocean mirrors the isotopic composition of the environment where it was formed. Benthic foraminifera $\delta^{18}O$ have been used, for instance, to create the marine stacks of Lisiecki and Raymo (2005) used to define the marine isotope stages. To get more accurate measurements of the temperature, however, this method is not the preferred option as changes in oceanic $\delta^{18}O$ are mainly controlled by the ice volume of continental ice sheets (Shackleton, 1967). The ice volume influence dominates the temperature effect in glacial periods when a lot of ^{18}O depleted waters are stored on land, and the global oceans are saturated in ^{16}O.

Planktic and benthic foraminifera can be used in other ways to estimate the surface and deep ocean temperatures, respectively. The most common way is the use of the Mg/Ca ratio. This ratio measures the occurrence of the substitution of the calcium atom in the foraminifer's $CaCO_3$ test by an atom of magnesium. Water temperatures mainly drive the substitution process and can, therefore, be used as an ocean temperature proxy (Nürnberg et al., 1996). Both the Mg/Ca and the $\delta^{18}O$ are nonetheless limited by strong measurement bias. First, these measurements are influenced by local salinity, which is a difficult variable to derive from proxy records. Second, the deposition process can be affected by ocean currents and disruptions of the ocean floor. Finally, the seasonality - different species bloom at different times of the year - and the depth - different species live at different depths - of the foraminifera used for the measurements have to be considered.

In order to prevent the misinterpretation of the temperature measurements obtained from these two techniques, additional proxies can be used. $U^{k'}_{37}$ is a biomarker of the alkenones saturation in algae due to a process dependent on temperatures (Prahl and Wakeham, 1987). TEX_{86} links variation in membrane lipids of marine micro-organisms to changes in the sea surface temperatures (Schouten et al., 2002). Finally, foraminifera assemblage counts the relative abundance of different species to indicate the water conditions at the time when they were deposited (Kucera et al., 2005). This technique is also one of the only ways to observe the movement of sea ice, as the distribution of foraminifera changes in Arctic conditions (Carstens et al., 1997), which is very difficult to reconstruct from any other proxy records. In the end, the use of one or another of these metrics depends on what data is available in the sediment cores, and the most accurate temperature estimations are obtained when different methods are cross-checked.

Reconstructing the ocean circulation

The complex dynamics of the ocean and the heterogeneity of the different water masses means that no proxy records exist that can give direct information on the strength of the overturning circulation. Instead, geochemical tracers transported through the global ocean have been used to infer changes in ocean circulation (Lynch-Stieglitz, 2017). The oceanic productivity is estimated by the $\delta^{13}C$, the ratio between the two carbon isotopes ^{13}C and ^{12}C. The ventilation can be derived from the radiocarbon age $\Delta^{14}C$, derived from measuring the radioactive isotope of Carbon fixed by planktons at the surface and used to estimate the time since the last contact of a water mass with the surface (Dentith et al., 2019a). Different geochemical proxies, such as Cd/Ca, can map the nutrient availability of nutrients in a water mass. ε_{Nd} in the North Atlantic records the signature of water masses and can be interpreted to infer changes in AMOC (Jeandel et al., 2007; Robinson et al., 2021).

The most commonly used tracer for circulation change is the protactinium/thorium ratio $^{231}Pa/^{230}Th$ (Robinson et al., 2019). Both Protactinium and Thorium are radioactive

elements issued from the decay of Uranium in the water column. These two elements are transported by the water before being buried in sediments. ^{230}Th is lighter and easier to transport than ^{231}Pa. In the case of a weak circulation in the basin, only ^{230}Th is evacuated and $^{231}Pa/^{230}Th$ becomes high. In the case of a strong circulation, both components are transported out of the basin efficiently, and the $^{231}Pa/^{230}Th$ gets closer to its production ratio of about 0.093. However, the scavenging of these two elements is in-homogeneous in different basins and requires precise information about the water mass composition and history. This led to significant discrepancies in its estimation within the same basins (Burckel et al., 2016), and motivated the use of multiple sources of $^{231}Pa/^{230}Th$ (Ng et al., 2018).

Chronological dating of proxy records

A significant source of uncertainty in proxy reconstructions is the dating of climate records. Some proxy records, like tree rings, speleotherms and coral reefs, can provide direct evidence of the age of measurements through annual layer counting (Cronin, 2010). Up to ∼41 ka BP, annual layer counting is also possible in ice cores (Svensson et al., 2008), which makes them one of the best-constrained climate records with a temporal resolution of ∼100 years over MIS3 (Barbante et al., 2006; Veres et al., 2013). In case sediments accumulate rapidly on the ocean floor, precise dating of sediments cores up to a temporal resolution of a decade is possible, as is the case in the Cariaco Basin off Venezuela (Peterson and Haug, 2006). In most cases, however, the precise dates of the records cannot be directly estimated, and the age model, linking the data points to an estimated age, should be estimated indirectly. The rate of decay of radioactive elements, such as ^{14}C, over the last 12,000 years, and $^{234}U/^{230}Th$, between 120 ka BP and 12 ka BP, are regularly used to constrain the age of the records. Remarkable layers in the cores can also be matched to well-identified events, such as volcanic eruptions and tephra layers (Larsen and Eiríksson, 2008). Otherwise, the records should be correlated with well-dated ice cores (N.G.R.I.P, 2004), marine $\delta^{18}O$ stacks (Lisiecki and Raymo, 2005) or speleotherms (Cheng et al., 2016) reconstructions.

1.3 Thesis objective and research questions

This thesis aims to address the following objective:

To investigate the mechanism that caused millennial-scale variability during the last deglaciation using a general circulation model forced with different ice sheet reconstructions.

To answer this question, this thesis presents new glacial HadCM3 simulations that display millennial-scale variability when forced with specific combinations of boundary conditions, in this case the ice sheet extent and elevation, and climate forcings, in this case the ice sheet meltwater discharge. These simulations were run with a comprehensive set of outputs to enable a thorough analysis of the processes at stake during abrupt climate changes. Two ice-sheet reconstructions, ICE6G and GLAC-1D, were used to assess the sensitivity of the model to changes in forcings and background conditions. The main objective can be broken down into the three following questions:

- **RQ1** - What are the mechanisms behind millennial-scale variability during the last glacial period?
- **RQ2** - What is the influence of the ice sheet geometry and the meltwater discharge history on the occurrence and characteristics of millennial-scale variability?
- **RQ3** - How did the transient evolution of ice sheet meltwater discharge influence the occurrence of millennial-scale variability during the last deglaciation and the last glacial period?

RQ1 - What are the mechanisms behind millennial-scale variability during glacial periods?

Millennial-scale variability mechanisms have been explored in theoretical models (e.g. Broecker et al., 1990), general circulation models (e.g. Vettoretti et al., 2022) and from proxy reconstruction (e.g. Pedro et al., 2022), but no mechanisms have so far gained general acceptance. The variety of conditions in which such variability has been observed questions the uniqueness of such a mechanism. There are nonetheless consistent features commonly associated with millennial-scale variability across all events: abrupt temperature changes in Greenland by $\sim 10°C$ (Kindler et al., 2014), an anti-phased and weaker signal in Antarctica temperatures (Stocker, 1998), cycle duration between 500 and 4,500 years (Thomas et al., 2009), shifts in AMOC modes (Clark et al., 2002) and global reorganisation of the atmospheric circulation (Peterson and Haug, 2006).

To get a deeper understanding of millennial-scale variability, it needs to be reproduced and studied from climate simulations. Simple box models have managed to produce abrupt climate shifts following Broecker et al. (1990)'s salt oscillator theory based on Stommel

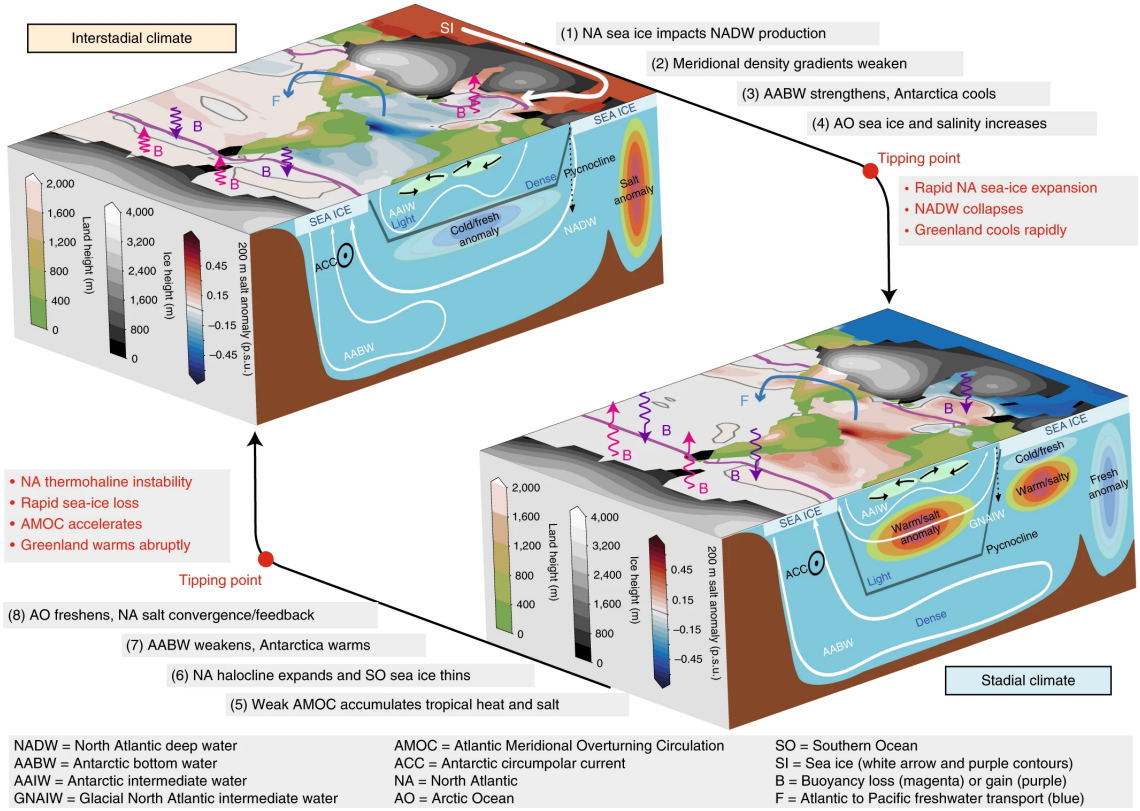

Figure 1.8: **A mechanism for millennial-scale variability**. Taken from (Vettoretti et al., 2022).

(1961)'s multi-stable Atlantic model. The first occurrence of such variability in a complex climate model was obtained by Ganopolski and Rahmstorf (2001) through the stochastic resonance theory. It took more than a decade before Peltier and Vettoretti (2014) managed to simulate spontaneous oscillations in general circulation models. Since then, multiple groups have reported such behaviour and proposed mechanisms (Malmierca-Vallet et al., 2023), such as Vettoretti et al. (2022)'s reproduced in Figure 1.8.

Armstrong et al. (2022) have recently succeeded in simulating millennial-scale variability with the HadCM3 climate model from a single time slice during MIS3 in a series of snapshot simulations of the last glacial period. The mechanism they identified relies on Broecker et al. (1990)'s salt oscillator modulated by meridional density gradients and wind forcing in the North Atlantic. This offers a unique opportunity to compare two mechanisms for abrupt climate change for two different configurations of the same model. Particular attention will be paid to understanding the role of the salt oscillator as a driver or a response to North Atlantic climate changes, using a comprehensive set of salinity fluxes diagnostics. The analysis of the mechanism will be expanded by comparing the new oscillating simulations not only to the simulations that did not manage to obtain millennial-scale variability in this thesis, but also to the existing mechanism theories published in the literature.

RQ2 - What is the influence of the ice sheet geometry and the meltwater discharge history on the occurrence and characteristics of millennial-scale variability

The concept of the window of opportunity is key to understanding the sensitivity of millennial-scale variability in climate models to modifications in boundary conditions and forcings. Barker and Knorr (2021) defines the window of opportunity as the region of the parameter space (including climate forcing) which gives rise to more frequent and larger amplitude millennial-scale climate variability – see Figure 1.9. The parameters refer to all the components that can be modified in climate simulations, and the parameter space is the ensemble of the parameter configurations. The parameters that are the most likely to affect the millennial-scale variability are the orbital parameters, the greenhouse gas concentrations, the ice sheet layout for the boundary conditions and the freshwater discharge for the climate forcings. Within the last glacial period, the orbital parameters variations are relatively well constrained in their timings and magnitudes (Berger, 1978), and the greenhouse gas records still hold uncertainty in terms of timing, but are well constrained in terms of magnitude (Berger, 1978; Loulergue et al., 2008; Schilt et al., 2010; Bereiter et al., 2015). Their effect on millennial-scale variability have been thoroughly investigated and sweet spots were identified in several studies with different GCMs (e.g. Brown and Galbraith, 2016; Klockmann et al., 2018; Vettoretti et al., 2022).

On the other hand, the past ice-sheet extent and elevation constraints are still lagging, and its impact on climate simulations is still to be understood. The ice sheet extent and topography can modify the radiative balance (Roberts and Valdes, 2017), the winds (Montoya et al., 2011; Roberts et al., 2014b; Madonna et al., 2017) and the atmospheric circulation (Izumi et al., 2023) around them. During the last glacial period, this modified the climate background and moved the location of the window of opportunity (i.e. the necessary forcing to trigger abrupt climate change). For instance, Brown and Galbraith (2016) and Klockmann et al. (2018) only managed to simulate abrupt climate changes using pre-industrial ice sheets, because glacial ice sheets tended to stabilise the North Atlantic deep water formation in their simulations. Ice sheet geometries during the last glacial period have been reconstructed with different methods producing significantly different evolutions (Tarasov et al., 2012; Peltier et al., 2015; Gowan et al., 2021), and their consequences on climate simulations need to be assessed.

The effect of the freshwater released from the melting of ice sheets has been clearly identified as the main driver behind AMOC mode shifts, but its understanding is still in its early days (Bethke et al., 2012). The constraints of the meltwater discharged during the last glacial period are lacking and the location and magnitude of the forcing have varied significantly between modelling studies (Stouffer et al., 2006; Kageyama et al., 2010, 2013b; Snoll et al., 2023). To tackle this gap, Ivanovic et al. (2017) created a protocol to derive meltwater discharge from changes in ice sheet elevation. This protocol was used

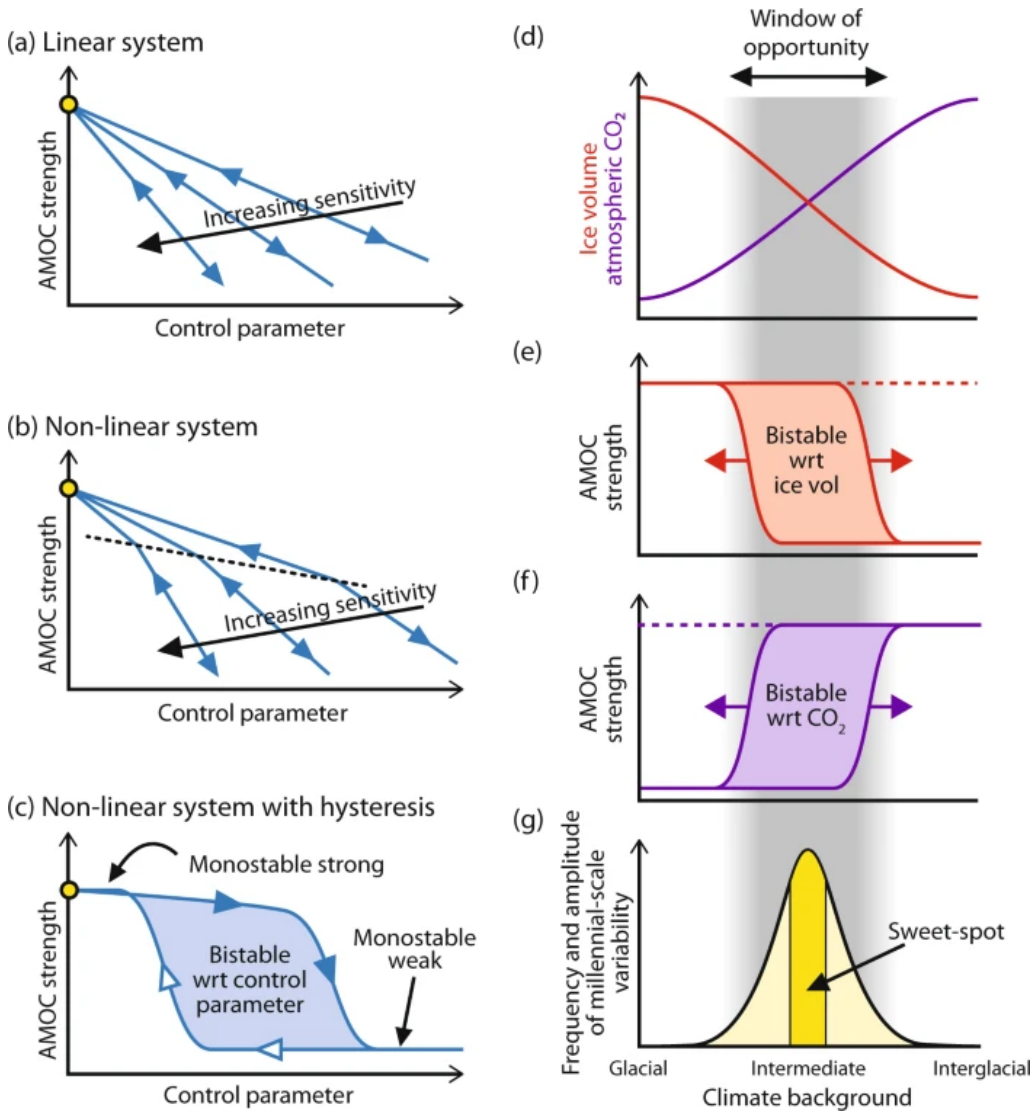

Figure 1.9: **The window of opportunity.** The window of opportunity concept and associated vocabulary, defined by (Barker and Knorr, 2021).

in HadCM3 simulations (Matero et al., 2017; Ivanovic et al., 2018a) and showed promising results in that it managed to trigger abrupt climate changes with realistic meltwater fluxes. Kapsch et al. (2022) and Bouttes et al. (2023) used a similar method in deglacial simulations testing two different ice sheet reconstructions. However, to my knowledge, no study has isolated the effect of the ice sheet topography and meltwater discharge during the last deglaciation. The HadCM3 simulations created for this thesis allow a detailed analysis of the effect of various meltwater discharge patterns in two different boundary conditions corresponding to two ice sheet reconstructions.

RQ3 - How did the transient evolution of ice sheet meltwater discharge influence the occurrence of millennial-scale variability during the last deglaciation and the last glacial period?

Despite the quality and the number of proxy reconstructions for the last deglaciation (Clark et al., 2002), no climate simulation of the period have succeeded in replicating the chain of events of this period (Snoll et al., 2023). The main challenge in last deglaciation simulations is to get the timing and the magnitude of the Bølling Warming and Younger Dryas transitions right. Obase and Abe-Ouchi (2019) were arguably the closest as they triggered the Bølling Warming with the correct timing and relatively little meltwater fluxes. They managed to do so by starting from a prolonged cold AMOC state. This finding revives the debate on the interpretation of overturning circulation tracers during the last deglaciation (Repschläger et al., 2021). Because they have a direct impact on the AMOC, the ice sheet layout and the meltwater discharge are here again a primary source of uncertainty when running simulations of the period (Kapsch et al., 2022; Bouttes et al., 2023) – see Figure 1.10.

Last deglaciation climate change events have been commonly associated with last glacial period millennial-scale variability, and the Bølling Warming is sometimes referred to as the most recent D-O event (Wolff et al., 2010). However, there is no evidence that D-O events and deglacial transitions are two occurrences of the same phenomenon, and other hypotheses have been put forward to explain the variations in $\delta^{18}O$ records during the last deglaciation (Liu et al., 2012). The simulations of this thesis are perfectly fitted to answer this question by conducting a process-based analysis of the chain of events of the last deglaciation as well as the last glacial period D-O sequence.

Finally, the interest in palaeo abrupt climate changes was reinforced by the debate about future tipping points. So far, modern-day climate simulations have struggled to produce consistent conclusions in the AMOC response to future climate changes (Bellomo et al., 2021). Understanding the last glacial period millennial-scale variability can inform the interpretation of early climate warnings for AMOC collapse (Ditlevsen and Ditlevsen, 2023).

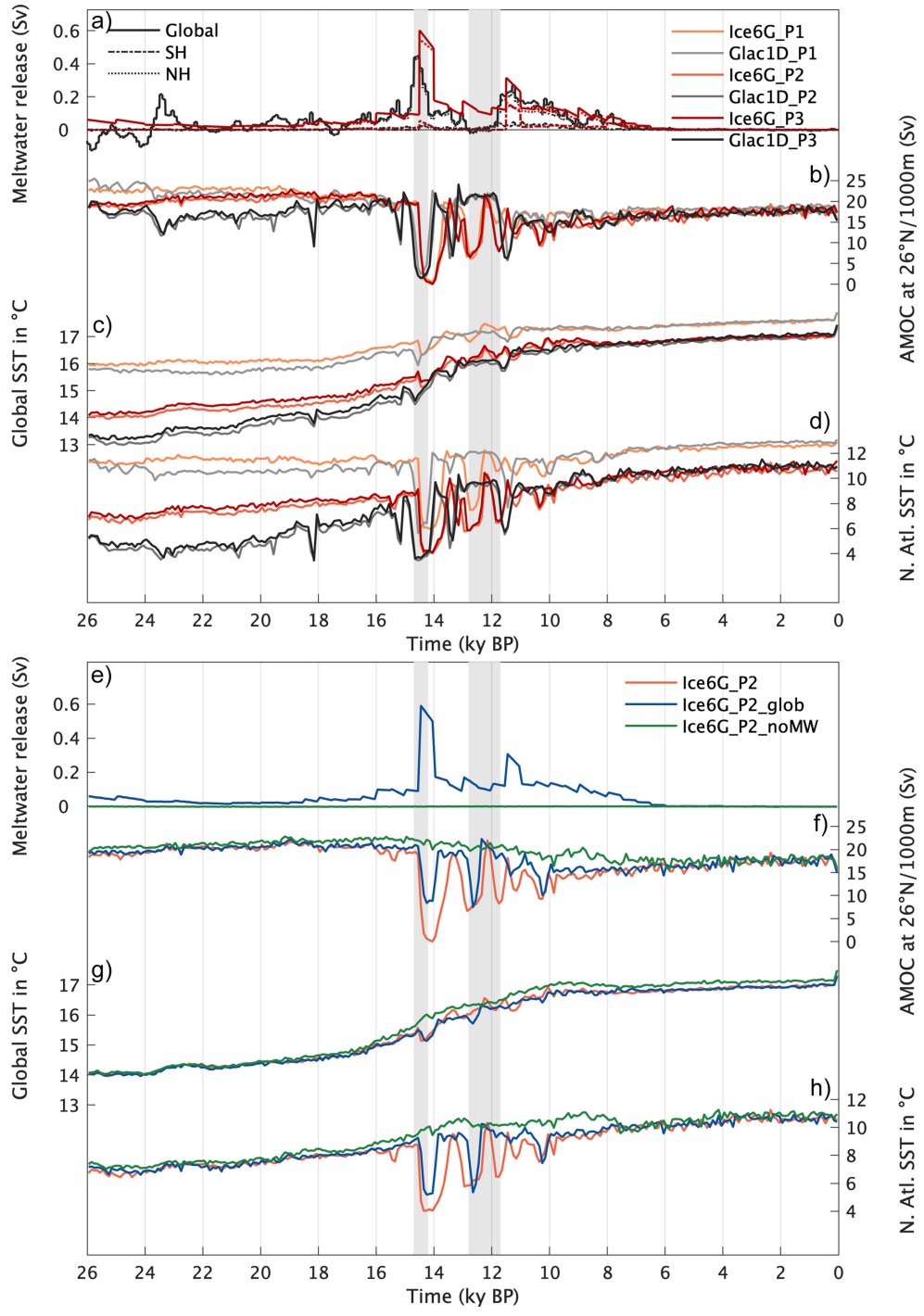

Figure 1.10: **Transient simulations of the last deglaciation.** Transient model response to different ice-sheet boundary conditions and implementations of meltwater release for the simulations presented in (Kapsch et al., 2022). PX indicates different configurations of the model. Vertical shadings mark approximate timings of the Bølling-Allerød (left) and Younger Dryas (right).

Research approach and thesis workflow

The objectives identified in the three research questions can be achieved following the six research objectives presented in Table 1.1.

The research questions and objectives are addressed in the results chapters 2, 3 and 4 and the discussion chapter 5. The results chapters have either been published (Romé et al., 2022) or are about to be submitted (Chapter 3 and Chapter 4) to peer-reviewed journals. They have been written in the style of academic publication, including individual abstracts, introductions, methods and supplementary information for every publication. Chapter 5 reviews how the three results chapters tackled the research objectives and provide answers to the research questions.

Chapter 2, *Millennial-Scale Climate Oscillations Triggered by Deglacial Meltwater Discharge in Last Glacial Maximum Simulations*, primarily addresses RQ2, and provides the tools to answer RQ1 and parts of the answer to RQ3. This Chapter presents a new set of last glacial maximum simulations displaying millennial-scale variability (*RO1*) when forced with the right combined magnitude and distribution of freshwater discharge obtained from the ice sheet reconstruction melting history during the early last deglaciation (*RO2*). The content of this Chapter was published in Romé et al. (2022), and was replicated with only editorial modifications to the text and the figures to fit the formatting of the thesis. It includes contributions from Ruza F. Ivanovic, Lauren J. Gregoire, Sam Sherriff-Tadano and Paul J. Valdes.

Chapter 3, *Simulated glacial millennial-scale variability driven by a coupled inter-basin salt oscillator*, primarily addresses RQ1 by investigating the mechanism of the millennial-scale variability simulated in Chapter 2 (*RO2*). Additionally, it tackles RQ2 by explaining mechanistically why some of the simulations described in Chapter 2 do not oscillate. The mechanism is reviewed on the non-oscillating simulations and other mechanisms in the existing literature to highlight its applications and limitations (*RO3*). This Chapter was designed to be submitted to Climate Dynamics and includes contributions from Ruza F. Ivanovic, Lauren J. Gregoire, Didier Swingedouw, Sam Sherriff-Tadano and Reyk Börner.

Chapter 4, *Last deglaciation simulations sensitivity to the choice of ice sheets reconstructions and meltwater discharge pattern*, addresses RQ2 and RQ3 by exploring the effect of time-evolving meltwater discharge patterns with two different ice sheet topography (*RO4*) to simulate the abrupt climate changes of the last deglaciation (*RO5*). It analyses the results using the mechanisms identified in Chapter 3 (*RO3*) and evaluates their relevance to the D-O sequence of the last glacial period (*RO6*). This Chapter was designed to be submitted to Climate of the Past. It includes contributions from Ruza F. Ivanovic, Lauren J. Gregoire, Brooke Snoll, Oliver G. Pollard and Jacob Perez.

The Discussion Chapter 5 concludes on the different research questions of Section 1.3 by

Table 1.1: **Research objectives.** Research objectives and their corresponding research questions and thesis chapter.

Research objective	Research questions	Chapter
RO1 - Simulate millennial-scale variability in HadCM3	RQ1, RQ2, RQ3	2
RO2 - Identify the mechanism behind millennial-scale variability in HadCM3	RQ1	3
RO3 - Define the conditions for the validity of the millennial-scale variability mechanism	RQ1, RQ3	3, 4
RO4 - Explore the sensitivity of millennial-scale variability occurrence to ice sheets layout and meltwater discharge	RQ2	2, 4
RO5 - Simulate abrupt climate changes that resemble the last deglaciation chain of events with time-evolving meltwater simulations	RQ3	4
RO6 - Compare the simulated millennial-scale variability to past and future abrupt climate changes	RQ3	4, 5

recalling the gaps identified in Chapter 1 and using the material produced in Chapter 2, 3 and 4. It also presents the limitations of this thesis, its relevance in future climate predictions (*RO6*) and the potential avenues for future work.

Chapter 2

Millennial-scale climate oscillations triggered by deglacial meltwater discharge in last glacial maximum simulations

Abstract

Our limited understanding of millennial-scale variability in the context of the last glacial period can be explained by the lack of a reliable modelling framework to study abrupt climate changes under realistic glacial backgrounds. In this article, we describe a new set of long-run last glacial maximum experiments where such climate shifts were triggered by different snapshots of ice-sheet meltwater derived from the early stages of the last deglaciation. Depending on the location and the magnitude of the forcing, we observe three distinct dynamical regimes and highlight a subtle window of opportunity where the climate can sustain oscillations between cold and warm modes. We identify the Eurasian Arctic and Nordic Seas regions as being most sensitive to meltwater discharge in the context of switching to a cold mode, compared to freshwater fluxes from the Laurentide ice sheets. These cold climates follow a consistent pattern in temperature, sea ice and convection, and are largely independent from freshwater release as a result of effective AMOC collapse. Warm modes, on the other hand, show more complexity in their response to the regional pattern of the meltwater input, and within them, we observe significant differences linked to the reorganisation of deep water formation sites and the subpolar gyre. Broadly, the main characteristics of the oscillations, obtained under full-glacial conditions with ice-sheet reconstruction derived meltwater patterns, share similar characteristics with $\delta^{18}O$ records of the last glacial period, although our experiment design prevents detailed conclusions from being drawn on whether these represent actual Dansgaard-Oeschger events.

2.1 Introduction

The last glacial period was characterised by strong millennial-scale variability (e.g. Bigg and Wadley, 2001; Wolff et al., 2010; Fletcher et al., 2010), observed through the occurrence of sharp and dramatic shifts in climate state. The best example of such abrupt changes are Dansgaard-Oeschger events (D-O events; Dansgaard et al., 1993). They consist of transitions between cold stadial and warm interstadial climate conditions that occur in cycles as long as six hundred to a few thousand years. Dansgaard-Oeschger events were first identified in $\delta^{18}O$ records of Greenland ice cores (Bond et al., 1993) before also being observed in Antarctica (Blunier and Brook, 2001; Voelker, 2002). Since their discovery, they have been identified in a wide range of different parts of the Earth system, both marine (e.g. Shackleton et al., 2000; Wolff et al., 2010; Dokken et al., 2013; Henry et al., 2016) and terrestrial (e.g. Sánchez Goñi et al., 2000; Wang et al., 2001, 2007; Margari et al., 2009; Stockhecke et al., 2016), and can be linked to meridional shifts of the Intertropical Convergence Zone (ITCZ) (Peterson and Haug, 2006).

During decades of study, numerous hypotheses have been put forward to understand the underlying mechanisms behind D-O events (a comprehensive list can be found in Li and Born (2019)), and, more generally, millennial scale variability. Despite this effort, a consistent and comprehensive theory is yet to be firmly established. Nonetheless, at the crossroads of all theories lies the crucial role of the Atlantic Meridional Overturning Circulation (AMOC Rahmstorf, 2002; Burckel et al., 2015; Henry et al., 2016). A modification of the thermohaline circulation affects heat and salt redistribution between the tropics and the poles, and consequently has a global-scale impact on the climate (Clark et al., 2002; Rahmstorf, 2002). There is substantial evidence that the AMOC has existed in other configurations (or 'modes') than the one we observe at present times (e.g. Böhm et al., 2015), and that AMOC may thus have the capacity to exist in multiple stable states, as predicted theoretically (Stommel, 1961) and supported by early observations (Broecker et al., 1985) and climate models (Manabe and Stouffer, 1988). We believe that uncovering the causes of AMOC modes switches would result in greatly improving our understanding of abrupt climate changes.

The AMOC can be disrupted by freshwater release events in the North Atlantic-Arctic region. They have the power to target vital points of the thermohaline circulation by affecting the ocean density profile at North Atlantic Deep Water (NADW) formation sites (Broecker et al., 1985; Paillard and Labeyrie, 1994; Vidal et al., 1997). In models, freshwater hosing experiments have been widely used to force abrupt climate transitions (e.g. Manabe and Stouffer, 1997; Ganopolski and Rahmstorf, 2001; Kageyama et al., 2010) and observe hysteresis cycles (e.g. Schmittner et al., 2002). They also highlighted the large sensitivity of the climate to the strength and the location of the release, especially in the Greenland-Iceland-Nordic (GIN) Seas (Smith and Gregory, 2009; Roche et al., 2010).

Consequently, it is valuable to explore the different sources of freshwater that had the potential to lead to millennial-scale variability.

Iceberg surges during Heinrich (H) events (Heinrich, 1988) recorded by Ice-Rafted Debris (IRD) in the North Atlantic (Hemming, 2004), were first candidates to be held responsible for initiating stadial climates. It is now widely accepted that H events are not at the origin of D-O events, they are triggered within stadial states (Barker et al., 2015) and are not recorded at every D-O occurrence (Lynch-Stieglitz, 2017). Instead, we can conceive of them as a likely response to the earlier climate-ocean perturbation or even a positive feedback mechanism for perpetuating/amplifying stadial climates (Ivanovic et al., 2018a). Meltwater released from the long term decline of ice sheets was another significant source of freshwater during the last glacial period (Gregoire et al., 2012), although only a few studies have investigated the influence of such 'background' melt (e.g. Matero et al., 2017; Ivanovic et al., 2018a; Kapsch et al., 2022), probably because it requires precise constraints on the ice sheet geometry and history of melt/growth (Bethke et al., 2012). Holding the most complete records of ice sheet evolution, both in terms of spatial and temporal resolution, (e.g. Dyke, 2004; Hughes et al., 2016; Briggs et al., 2014; Bradwell et al., 2021), the last deglaciation, and especially its early phase between $\sim$ 21–16 ka BP (thousand years before present) offers the perfect setting to assess the ability of the early phase of continental deglaciation (i.e. the long-term background melt from disintegrating ice sheets) to generate millennial-scale variability in glacial conditions.

The last deglaciation initiated from the Last Glacial Maximum (LGM; $\sim$ 21 ka BP Clark et al., 2009), which is the time when the Northern Hemisphere ice sheets shaped during the preceding glacial period reached their maximum extent (Batchelor et al., 2019). The upper cell of the AMOC was likely shallower, but it is not known whether it was stronger or weaker than present day (Gebbie, 2014; Lynch-Stieglitz, 2017; Muglia and Schmittner, 2021). A steady increase in Northern Hemisphere summer insolation (Berger, 1978) triggered the long-term demise of the Laurentide and Eurasian ice sheets, with rising concentrations of atmospheric CO_2 positively reinforcing the deglaciation (Gregoire et al., 2015). However, while Southern Hemisphere temperatures gradually rose (Parrenin et al., 2007), the climate in the North remained cold for several thousand years; a period known as Heinrich Stadial 1 ($\sim$18–15 ka BP Denton et al., 2006; Roche et al., 2011; Ng et al., 2018). The most recent of Heinrich events, H1 (Hemming, 2004; Stanford et al., 2011), began some two thousand years after the onset of Heinrich Stadial 1 (Stern and Lisiecki, 2013; Hodell et al., 2017). In the years of deglaciation that followed the LGM, several millennial scale events were observed (Weber et al., 2014). Two episodes are particularly relevant to our study: the sudden Bølling Warming ($\sim$ 14.5–13 ka BP Severinghaus and Brook, 1999) concurrent with an intensification of the AMOC (Ng et al., 2018; Du et al., 2020), and the ensuing Younger Dryas, when Northern Hemisphere climate abruptly returned to a stadial state with glacial re-advance ($\sim$ 13–12 ka; Murton et al., 2010; Liu

et al., 2012). While not formally identified as D-O events, similarities in climate and ocean evolution between these last deglaciation events and D-O oscillations have prompted others to at least draw analogies between them, and to speculate on whether they have a common cause (e.g. Obase and Abe-Ouchi, 2019).

Simulating climate oscillations in glacial conditions has proven to be very challenging, and even more so during the LGM. This is because of the strong feedback between the large ice sheets and wind stress, deep water formation and energy balance (Oka et al., 2012; Ullman et al., 2014; Beghin et al., 2015; Roberts and Valdes, 2017), which act to intensify, or at least stabilise, the AMOC (Oka et al., 2012; Klockmann et al., 2016; Sherriff-Tadano et al., 2018). Most models from both the Paleoclimate Modelling Intercomparison Project Phase 3 (PMIP3; Muglia and Schmittner, 2015) and Phase 4 (PMIP4; Kageyama et al., 2021) tend to simulate a deeper and stronger NADW than inferred from palaeo records, which could explain why few modelling studies have observed millennial scale variability in glacial background (e.g. Klockmann et al., 2018). In order to trigger abrupt climate transitions, freshwater hosing experiments have historically needed to overestimate fluxes as reviewed by Kageyama et al. (2010) (e.g. Liu et al., 2009; Menviel et al., 2011), and have not succeeded in simulating abrupt changes when using 'realistic' fluxes (Bethke et al., 2012; Gregoire et al., 2012; Snoll et al., 2022). Obase and Abe-Ouchi (2019) have arguably come the closest to overcoming this meltwater 'paradox' by simulating the Bølling Warming even with some deglacial meltwater forcing. However, even they require a significantly lower than likely freshwater discharge from the deglaciating ice sheets (e.g. Peltier et al., 2015).

The dispute over what could feasibly cause abrupt climate changes not directly driven by freshwater fluxes led the community to start actively searching for oscillating behaviours in their models. At the same time, the criticism that simulations integrated for only a few hundred or a thousand years should not be considered to have a steady-state or 'spun-up' ocean circulation began to gain traction (Marzocchi and Jansen, 2017; Dentith et al., 2019b), prompting modellers to run long simulations with higher-order climate models — made possible by the increase of computational power — in order to examine long-term drifts. It is therefore probably not a coincidence that more and more coupled Atmosphere-Ocean General Circulation Models (AOGCMs) have reported observing AMOC mode oscillations in recent years (e.g. Peltier and Vettoretti, 2014; Brown and Galbraith, 2016; Klockmann et al., 2018; Sherriff-Tadano and Abe-Ouchi, 2020). They have been achieved under a range of different freshwater hosing scenarios (e.g. Cheng et al., 2011), atmospheric CO_2 concentrations (e.g. Zhang et al., 2017) and ice sheet geometries (e.g. Klockmann et al., 2018), although, to our knowledge, only Peltier and Vettoretti (2014) and Kuniyoshi et al. (2022) managed to obtain AMOC oscillations under glacial conditions.

To sum-up the combined results from these studies, there seems to exist a window of opportunity (Barker and Knorr, 2021; Vettoretti et al., 2022) in each model's inputs (parameter

values, boundary conditions and forcings) and background climates where oscillations can establish and sustain (e.g. Peltier and Vettoretti, 2014; Brown and Galbraith, 2016; Klockmann et al., 2018). The ice sheets' layout in particular has a strong influence on the local and global climate, including on the atmospheric circulation (Löfverström et al., 2014; Roberts et al., 2014b; Sherriff-Tadano et al., 2021), the gyres (Gregoire et al., 2018), the energy balance (Roberts and Valdes, 2017) and freshwater fluxes (Matero et al., 2017). As a result, the new generation of better constrained and more detailed ice sheet reconstructions such as ICE-6G_C (Peltier et al., 2015; Argus et al., 2014) and GLAC-1D (Tarasov and Peltier, 2002; Tarasov et al., 2012; Briggs et al., 2014; Ivanovic et al., 2016) may prove to be decisive in whether or not the 'right' conditions for triggering abrupt climate changes are obtained.

In this chapter, we present our contribution to this initiative in the form of a new set of LGM simulations forced with deglacial meltwater. Inspired by an initial experiment that showed millennial-scale variability under a transient meltwater forcing, we designed our simulations with fixed meltwater inputs in order to be able to describe the oscillations in detail and evaluate the sensitivity of the oscillatory behaviour to meltwater patterns. These inputs were derived from snapshots of the early deglaciation meltwater history (specifically, between 21.5 and 17.8 ka BP) calculated from GLAC-1D ice sheet reconstruction.

Depending on the freshwater pattern, we observe three different dynamical regimes, including regular and self-sustained climate oscillations. The oscillations are characterised by switches between strong, shallow glacial AMOC and near- or completely- collapsed AMOC modes, a Greenland surface cooling/warming of $\sim 10°C$, and a periodicity of about 1.5 thousand years (ka). The cold/warm modes resemble, but should not be considered too strictly to be stadial/interstadial states, due to the use of a quasi-ideal experimental set-up. The oscillating regime can be sustained for about 10,000 years (the maximum length of the experiments). These are, to our knowledge, the first general circulation model simulations to use ice sheet reconstruction-derived distributions of meltwater to produce strong AMOC oscillations under glacial maximum climate conditions, and to investigate the sensitivity of the oscillations to patterns of meltwater discharged to the ocean.

The non-oscillating regimes inform us of the pre-requisite conditions for passing through the oscillating window. Here, we describe the various simulations in detail, their oscillatory or non-oscillatory climate/ocean states, and the different Earth system components involved in the abrupt events. We conclude with a discussion on the relevance of our simulations in the context of known past abrupt climate changes. The design introduced in this study allows us to undertake a relatively systematic set of sensitivity tests of the impact of realistic freshwater distributions (albeit for unrealistic lengths of time) on ocean circulation, with the multi-millennial integrations enabling us to explore the long-term effect of each pattern.

2.2 Methods

2.2.1 The model

The simulations introduced in this article were completed using the BRIDGE (Bristol Research Initiative for the Dynamic Global Environment group) version of the HadCM3 atmosphere-ocean general circulation model (GCM Valdes et al., 2017). This GCM consists of a 19 layers × 2.5° × 3.75° atmosphere model more completely described by Pope et al. (2000), coupled every simulation day with a 20 layers (up to 5,500m deep) × 1.25° × 1.25° ocean model, described by Gordon et al. (2000) (Bryan and Cox, 1972; Fofonoff and Millard Jr, 1983; Fofonoff, 1985). This version of HadCM3 includes the MOSES 2.1 land model (Cox et al., 1999), and the TRIFFID dynamic vegetation model (Cox, 2001). HadCM3 has been tested in many different scenarios (IPCC, 2014; Reichler and Kim, 2008), and was optimised for running multi-millennial simulations (Valdes et al., 2017).

2.2.2 Experimental design

The LGM simulation that makes up the base climate state for all simulations presented here was created following the PMIP4 protocol for 21 ka BP (Kageyama et al., 2017) using the GLAC-1D ice sheet reconstruction (Tarasov and Peltier, 2002; Tarasov et al., 2012; Briggs et al., 2014; Ivanovic et al., 2016); see Section 2.9 and Figure 2.9 (Bereiter et al., 2015; Loulergue et al., 2008; Schilt et al., 2010). This new HadCM3 LGM simulation was initialised from a chain of existing multi-millennial HadCM3 PMIP3 LGM simulations, which were started from multi-millennial continuations of earlier HadCM3 LGM simulations (Davies-Barnard et al., 2017), giving a pre-PMIP4 LGM spin-up of several thousand years. The new PMIP4 GLAC-1D set-up was integrated for 3,500 years, and the end of this final spin-up phase provides the initial condition for all simulations presented here. We continued the LGM simulation for a further 4,000 years in parallel with our other experiments to provide a reference climate state (*CTRL*) for comparison to the other simulations. There are small, steady drifts in the ocean over the run (Figure 2.10), but the signal of the trends are dwarfed in comparison to the changes of interest described below, and little is gained for this study by extending *CTRL* further. The starting year of *CTRL* is defined as year 0.

GLAC-1D has rarely been used for LGM simulations compared to the other ice sheet reconstructions (Kageyama et al., 2021) such as ICE-6G_C (Peltier et al., 2015) and the PMIP3 ice sheet (Abe-Ouchi et al., 2015). It was preferred for this study because compared to the alternative reconstructions, it includes more recent constraints on the Eurasian ice sheets provided by the DATED-1 project (Hughes et al., 2016), a region that could be crucial for accurately capturing the early deglacial climate history (Ivanovic et al., 2018a). A transient meltwater history was derived from GLAC-1D's representation of the deglaciation (Section 2.10). We decided against using the transient meltwater flux, because the added

Table 2.1: **Experiments summary.** All experiments were designed with LGM boundary conditions, using the LGM GLAC-1D ice sheet extent and associated geographies. Entries in the *Category* and global mean *Salinity Target (PSU)* columns are explained in Sections 2.4 and 2.2.2, respectively.

Simulation	Meltwater (Total flux)	Integration length	Category	Salinity Target (PSU)
CTRL	None	4,000 years	reference	35.8334
21.5k	21.5 ka ($0.039Sv$)	4,000 years	warm	35.834
21k	21 ka ($0.054Sv$)	4,000 years	warm	35.8334
20.7k	20.7 ka ($0.084Sv$)	10,000 years	oscillating	35.8225
19.4k	19.4 ka ($0.106Sv$)	10,000 years	oscillating	35.7901
18.2k	18.2 ka ($0.109Sv$)	10,000 years	cold	35.7348
17.8k	17.8 ka ($0084Sv$)	10,000 years	oscillating	35.7125

complexity introduced by the temporal variability and possible ocean 'memory' of the preceding [uncertain] meltwater history would have convoluted the physical interpretation of our results. Instead, we examined the triggering of abrupt climate changes using a simpler approach; by selecting six different, fixed-forcing scenarios (our 'snapshots'), that allow us to investigate the sensitivity of the glacial ocean and surface climate to early deglacial freshwater inputs (Figure 2.1*a*).

The snapshots were identified for their ability to collectively capture a broad range of possible situations that may have led to changes in ocean circulation and surface climate. The six scenarios correspond to different modes of discharge and are named after the period they were extracted from (see Figure 2.1*a*); see Figure 2.1*c* for the spatial distribution of the fluxes. The *21.5k*, *21k* and *20.7k* snapshots were chosen for being close to the LGM, sharing a similar distribution, but with different rates of meltwater discharge. The *19.4k* snapshot hosts a strong Labrador Sea/North Eastern American coast/Gulf of Mexico discharge (shortened to 'North American' discharge hereafter), but has a relatively small meltwater flux to the Arctic. Conversely, *18.2k* and *17.8k* have high Arctic and low North Atlantic discharge, with *18.2k* having the most freshwater entering the Arctic. These six snapshots of the deglacial meltwater history were used as forcing for six new equilibrium-type (i.e. constant-forcing) simulations, started from year 0. The meltwater was discharged into the surface layer of the ocean and kept constant throughout the runs. A justification is given in Section 2.10 (Quadfasel et al., 1990; Roche et al., 2007).

Table 2.1 presents a summary of all experiments. The difference between any of them is the prescribed ice sheet meltwater (or absence of it, in *CTRL*).

The idea of having a continuous fixed meltwater discharge for thousands of years is unrealistic by nature. However, in the most extreme scenario (*18.2k*), the total forcing corresponds to a sea level rise of 102 m in 10,000 years, which, for context, is still less than what has been reconstructed for the whole of the last deglaciation (Lambeck et al., 2014).

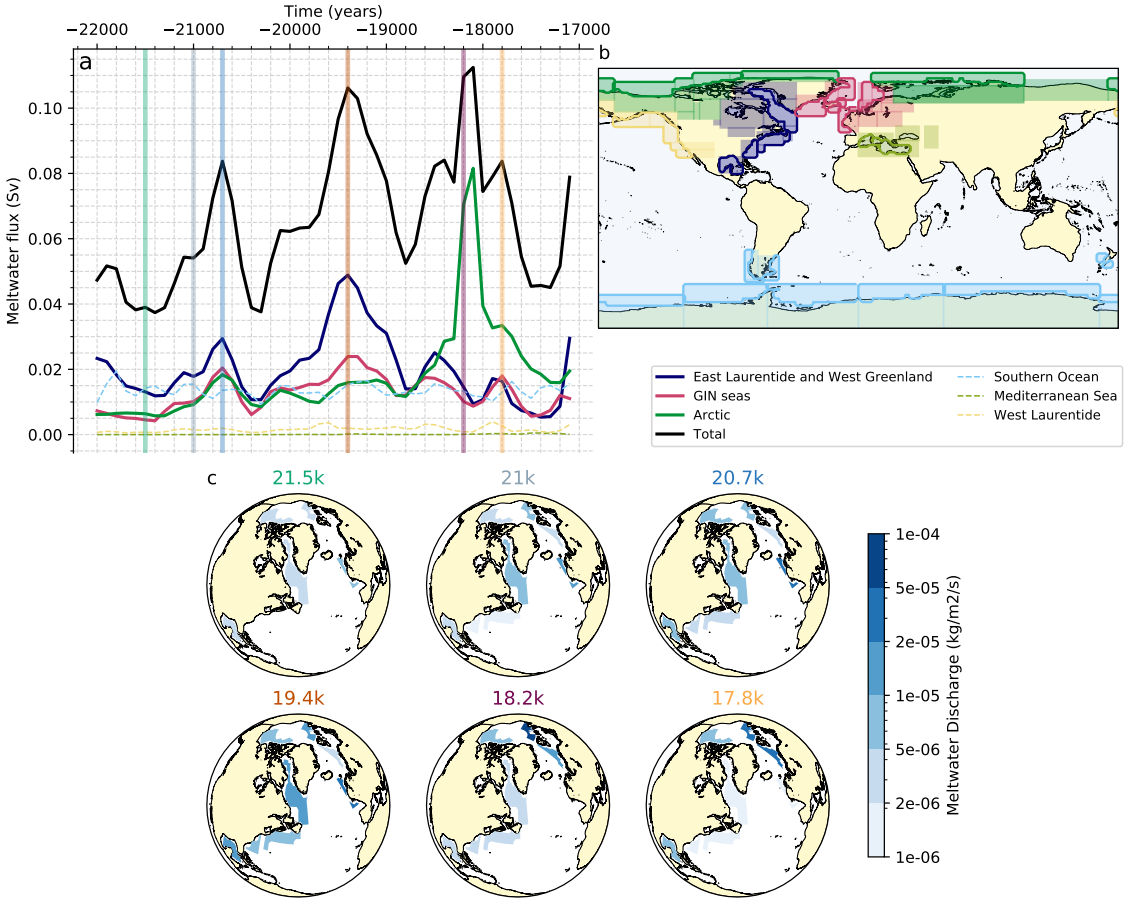

Figure 2.1: **Meltwater discharge protocol.** *a.* Meltwater discharge history over the early deglaciation and its distribution over the main regions defined in panel *b*. This plot incorporates the 200-years smoothing described in Section 2.10. Vertical bars represent the time steps chosen for calculating each constant meltwater-forcing snapshot (see Section 2.2.2, and Table 2.1). Regions of low discharge are plotted in dotted lines. *b.* Map of ice meltwater collection and spreading areas. Each individual box corresponds to a freshwater collection area, redistributed to the corresponding spreading areas (within the same box) indicated by the bold contours. Six main regions were defined for the presented analysis, as labelled on the right (colours). Note that these regions do not correspond to individual regions but rather to clusters of spreading areas. The colour coding matches panel *a*. *c.* Ice sheet meltwater discharge snapshot used for each perturbed meltwater simulation. The names and colours of the simulations correspond to the snapshot time on panel *b*. The colour coding of each simulation matches figures in the following figures. Please note the logarithmic scale.

The fixed global flux, between 0.039 and $0.109Sv$, is of the same order of magnitude as the mean global discharge in Ivanovic et al. (2018a) – $\sim 0.05Sv$, derived from ICE-6G ice sheet reconstruction (Peltier et al., 2015). It is also lower than the mean estimations of previous Heinrich Stadial 1 transient simulations (e.g. Liu et al., 2009; Menviel et al., 2011). It therefore remains appropriate to consider our results in light of glacial and deglacial variability in order to understand the effect of the forcing, though we are careful to highlight that they are not transient simulations of deglacial meltwater neither do they correspond to any specific meltwater discharge event. To avoid long-term drifts in mean ocean salinity caused by the long freshwater forcing, we impose a constant global mean salinity target (following the *VFLUX* method of Dentith et al. (2019b)) commensurate with the starting condition for each 'snapshot' (Table 2.1). The salinity target conserves water in relation to terrestrial ice volume (applied as relative to the present day) and thus, in the context of these simulations, counteracts global freshening by removing the excess water as a very small proportion of freshwater from every ocean grid cell at every ocean model timestep (one hour). This approach is in keeping with the snapshot/equilibrium experimental design whilst still allowing the ocean to 'feel' the surface forcing. See Section 2.11 for details.

Most simulations were run for 10,000 years; long enough to characterise their climate behaviours. However, like *CTRL*, two simulations (*21.5k* and *20.7k*), were terminated after 4,000 years. At this point, little was changing in those simulations, and since no further time series were required for the analysis, we opted to conserve the computing resource.

Some simulations experienced numerical instability after a few thousand years observed through a stream function runaway off the coast of the Philippines. This quirk was resolved by smoothing the bathymetry in the region of the instability and restarting the run a few years before the instability arose. More information, including the detail of the smoothing algorithm and its very minor impact on the climate response, is given in Section 2.12.

2.2.3 Characterising oscillations and defining warm/cold-mode composites

All experiments apart from *CTRL* show some kind of alternation between weaker and stronger AMOC phases, or 'modes'. Changes in the AMOC are correlated to increases and decreases in NGRIP temperatures (North Greenland Ice Core Project, 42.32° W, 75.01° N) and so we will also refer to these phases as 'cold' and 'warm' modes, respectively. We do not use the terms *stadial* and *interstadial* to describe the cold and warm states because of the complicated connotations associated with these terms, but they may be thought of in such a light.

In order to characterise oscillations in the simulations, we applied a filtering algorithm

and Fourier analysis to derive the spectrum of the temperature time series at the location of NGRIP, see Section 2.13 for details. If there is a peak in the spectrum, then oscillations can be defined and described, and we apply a Butterworth low-pass filter to screen-out the frequencies lower than the millennial-scale variability of interest.

We also found it useful, in our analysis, to examine characteristics common to all warm and cold modes in the suite of simulations. Thus, to build a composite of the two modes from the time series of results, we defined quantitative boundaries bespoke to each simulation (it proved ineffective to adopt a consistent definition for all simulations because of their differences). Points below the weak limits (in AMOC strength/NGRIP temperature) were added to the composite cold mode and points above the strong limits were added to the warm modes. This approach is described in Section 2.14, where we demonstrate that the choice of how to define the composite modes does not significantly impact the results, and that to manually set up the weak and strong limits was an easy and robust method to build the composite states.

2.3 A new weak, shallow AMOC LGM simulation

The *CTRL* run replicates and continues the HadCM3-GLAC-1D LGM simulation presented in Kageyama et al. (2021). The global mean surface temperature is $6.6°C$ colder than Pre-Industrial (PI). Compared to other PMIP4 simulations, this simulation is in the coolest range, almost $2°C$ below the average mean temperature, and is colder than any PMIP3 simulations analysed by Kageyama et al. (2021), yet close to the current estimate from global temperature reconstructions ($\sim 6.1°C \pm 0.4°C$ cooler than PI in Tierney et al. (2020b), $\sim 7.0 \pm 1.0°C$ cooler than PI in Osman et al. (2021). The global mean ocean surface temperature was cooler by $3.4°C$, which is significantly cooler than the $\sim 1.7 \pm 0.1°C$ cooler than PI inferred by Paul et al. (2021), but again is a good match to the reconstruction by Tierney et al. (2020b) ($\sim 3.1 \pm 0.3°C$ cooler than PI). Contrary to most PMIP4 models, HadCM3 produces an AMOC that is both shallower and weaker in a full-glacial background compared to its pre-industrial state, although AMOC is still vigorous with a maximum strength of $20Sv$ at 30° N. We also note that the simulation gets slightly cooler when using GLAC-1D compared to ICE-6G_C (Ivanovic et al., 2018a), despite similar values for the maximum overturning circulation.

A summary of the *CTRL* equilibrium North Atlantic climate is shown by Figure 2.2. The thermohaline circulation is fuelled by intense convection in the northeast Atlantic, with deep water formation sites, indicated by the Mixed Layer Depth (MLD) , located primarily south of Iceland and west of the British Isles (Figure 2.2*b*). This creates a corridor in the eastern part of the Atlantic where warm waters can transit to high latitudes, while the western part of the ocean gets covered by winter sea ice and observes a much cooler climate (Figure 2.2*c*). The winter sea ice layer extends towards the East of the North Atlantic

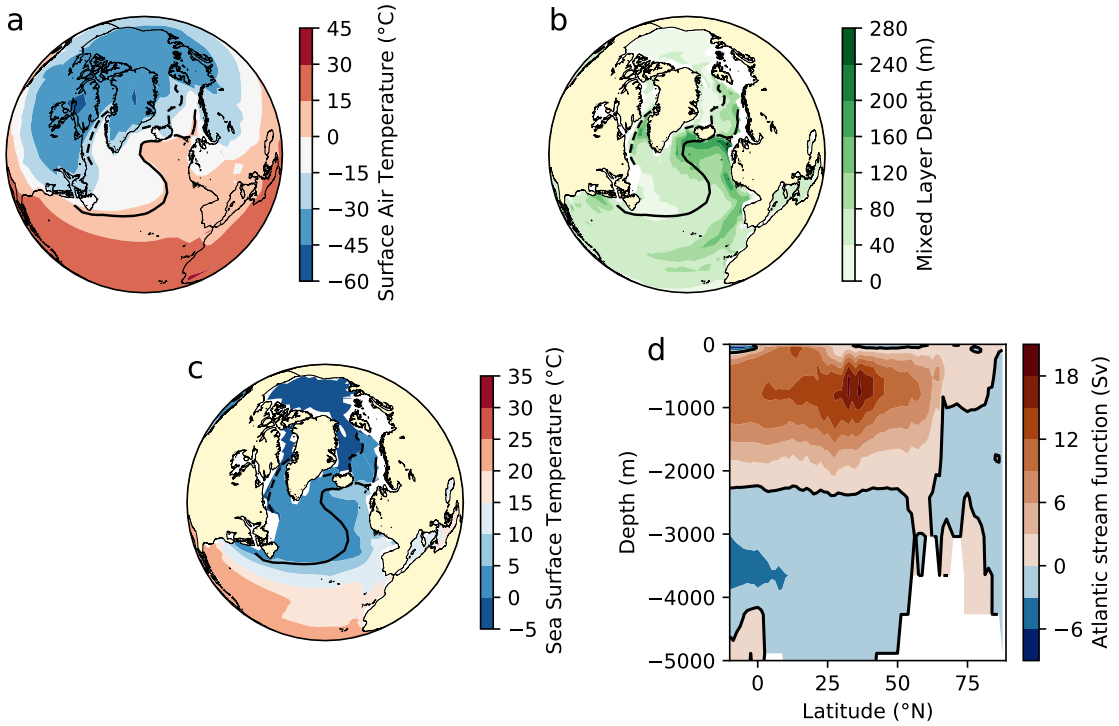

Figure 2.2: **Control climate state.** Mean annual conditions between simulation years 3900 and 4000 for *CTRL* over the North Atlantic. *a.* Surface air temperature. *b.* Mixed layer depth. *c.* Sea surface temperature. *d.* Meridional overturning stream function in the Atlantic basin. Dashed/solid lines indicate the September/March 50% sea-ice extent.

basin, creating a strong North-South gradient in atmospheric temperature in this region (Figure 2.2*a*). This is slightly more extensive than what is predicted in Tierney et al. (2020b) but matches the general layout, including a sea-ice free Iceland Basin. The Arctic Ocean is covered in sea ice all year long. Dense waters sink in the Labrador Sea when the sea ice is less extensive in this region in late autumn. For information, Figure 2.2 was reproduced for the Southern Ocean in Figure 2.11.

2.4 Climate response to the meltwater perturbations

We observe significant differences in the climate response of the six meltwater experiments (Figure 2.3), best encapsulated by the evolution of the AMOC index. For this study, we define the AMOC index as the maximal value of the overturning circulation in the Atlantic ocean at 26.5° N. This index corresponds to the modern RAPID-array AMOC measurement grid (Smeed et al., 2014; Frajka-Williams et al., 2019) and has been regularly used in palaeo-studies (e.g. Guo et al., 2019). For context, the interannual variability is in a range of $\pm 2Sv$, which fits what has been estimated by measurements between April 2004–February 2017 (Frajka-Williams et al., 2019), although the relatively short period of measurements makes it hard to give a robust conclusion.

The meltwater simulations can be assigned to three different regimes, according to the AMOC index (Figure 2.3*b*). In the first regime, simulations *21.5k* and *21k* returned to the reference state after a short cooling event during the initial years of the forcing, when the ocean adjusts to the introduction of the weak meltwater fluxes. This AMOC decline lasted for approximately 500 years, with the index weakening by as much as $5Sv$ for *21k* and $1.5Sv$ for *21.5k* approximately halfway through this initial cooling. While *21.5k* hardly recorded a change of polar temperatures (Figure 2.3*c*), the drop in *21k* AMOC strength drives up to $5°C$ cooling over Greenland. Neither simulation shows a strong response over Antarctica (Figure 2.3*d*). Accordingly, *21.5k* and *21k* will be referred to as *warm simulations* (note that with an LGM baseline climate, this term is relative).

In a second regime of its own, the AMOC in *18.2k* almost entirely collapsed as soon as meltwater was discharged, causing Northern Hemisphere cooling and a significant shift southward of the ITCZ (Figure 2.3*e*). Short recovery episodes occur at irregular intervals through the 10,000 years of the simulation, but they cannot be sustained for longer than a few hundred years. This simulation will be labelled a *cold simulation*.

Finally, through Fourier analysis (Figure 2.4*c*; Section 2.2.3) we identify three *oscillating simulations* (*20.7k*, *19.4k* and *17.8k*). They switch to a cold state at the onset of the run and continue in a quasi-oscillating regime between cold (near collapsed AMOC, similar to *18.2k*) and warm modes (equivalent or stronger AMOC with respect to *CTRL*). The three *oscillating simulations* behave in a similar way and will be described in more detail in the following sections.

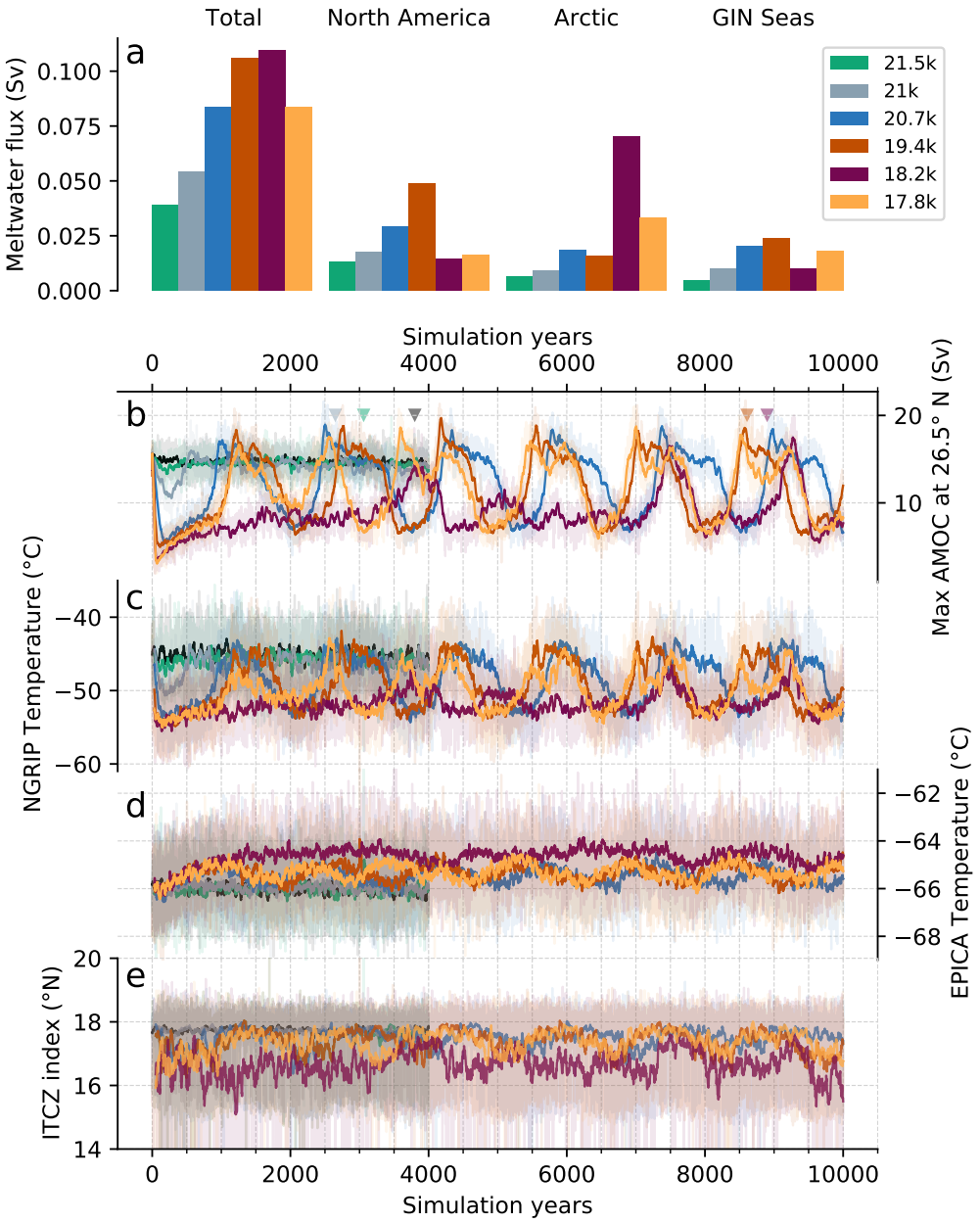

Figure 2.3: **Snapshot simulations evolution.** *a.* Snapshot experiments' total meltwater discharge and distributions, summarised (the three main regions are defined in Figure 2.1b. *b.* AMOC index (max Atlantic overturning circulation at 26.5° N). *c.* Greenland Surface Air Temperatures at NGRIP (42.32° W, 75.01° N). *d.* Antarctica Surface Air Temperatures at EPICA Dome C (Concordia Station of the European Project for Ice Coring in Antarctica, 123.21° E, 75.06° S). *e.* Intertropical Conversion Zone index (corresponding to the simulated mean Northern extent of the equatorial rain belt, defined in Section 2.15, inspired by Braconnot et al. (2007) and Singarayer et al. (2017)). Solid lines represent the 30-years running mean and transparent envelopes represent inter-annual variability, except for panel *e*, where the solid line is the 50-year running mean for ease of readability. Arrows indicate the date of the application of localised bathymetric-smoothing (see Section 2.12) for *21k*, *21.5k*, *CTRL*, *19.4k* and *20.7k* (left to right).

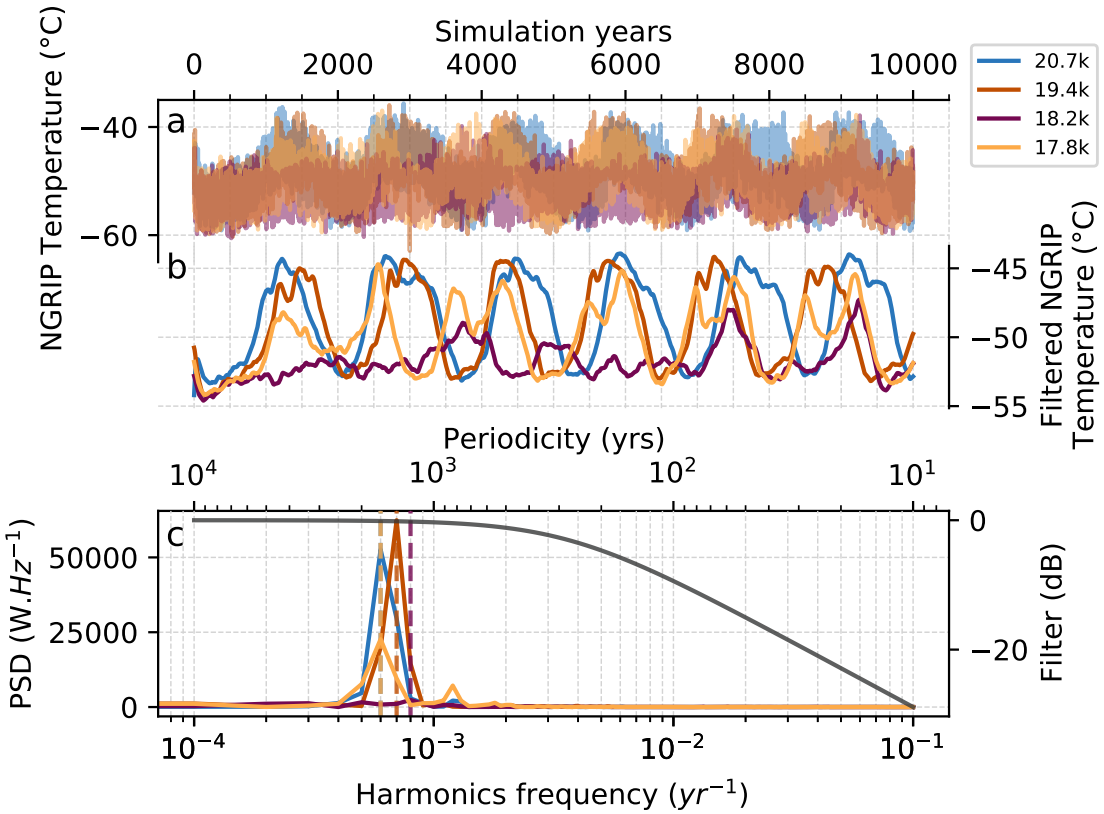

Figure 2.4: **Spectral analysis of the oscillating and cold simulations.** Spectral analysis of simulated surface air temperature through time above NGRIP (42.32° W, 75.01° N). *a.* Unfiltered signal for *oscillating* and *cold* simulations. *b.* Filtered response, using first class low-pass Butterworth filter. *c.* Power Spectral density (PSD, left hand scale) of the unfiltered signal. Dotted lines indicate the dominant frequency/period for each simulation. Grey line in panel *c* shows the bode diagram of the low-pass filter. Simulations *21.5k* and *21k* are not shown as their Fourier analysis was not conclusive. A zoom over the millenial-scale variability frequency band is provided in Figure 2.12.

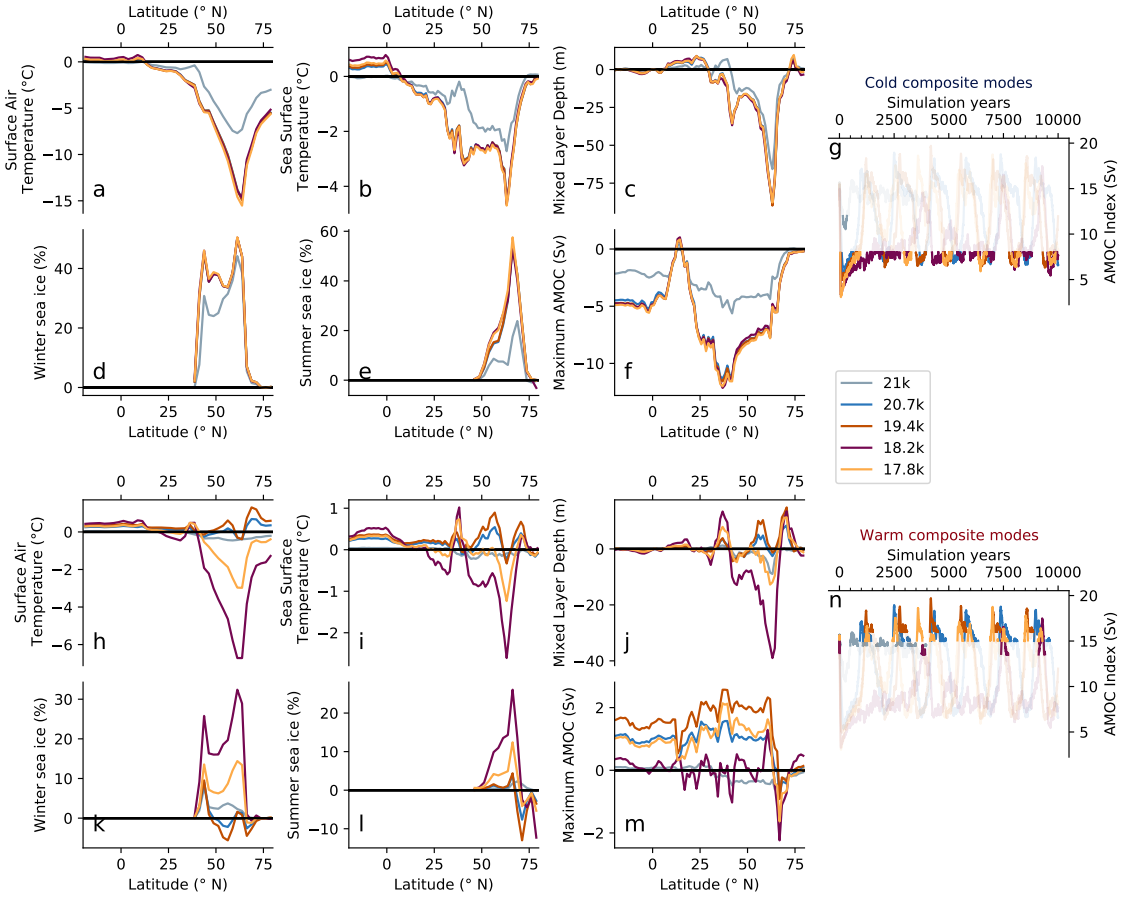

Figure 2.5: **Zonal means on composite modes.** Composite cold and warm modes' mean zonal anomalies between the meltwater simulations and the reference state in the Atlantic (70° W – 10° E). For cold modes (top), panels show the zonally averaged *a.* surface air temperature, *b.* sea surface temperature, *c.* mixed layer depth, *d.* winter sea ice concentration, *e.* summer sea ice and *f.* maximum overturning circulation flow over the water column. For warm modes (bottom), panels show the zonally averaged *h.* surface air temperature, *i.* sea surface temperature, *j.* mixed layer depth, *k.* winter sea ice concentration, *l.* summer sea ice and *m.* maximum overturning circulation flow over the water column. For orientation, an AMOC time series highlighting the periods contributing to the composite cold and warm modes is shown by panels *g* and *n*, respectively. The warm and cold modes of *21.5k* and the warm mode of *21k* were excluded.

The *oscillating* and *warm* simulations show a clear distinction between an initial transient state and a steady state. The transient states correspond to the adjustment of the model to the sudden introduction of meltwater. In the *warm* simulations, the transient state is seen in the initial drop, lasting $\sim$ 500 years. In the oscillating simulations, the transient state is manifested by an irregular first oscillation, lasting $\sim$ 1500 years. We cannot determine such distinction in the *cold* simulation.

During the cold modes (Figure 2.5, top), we observe strong consistency between the *oscillating simulations* and the *cold simulation*, to the point where it becomes almost impossible to distinguish between them. These experiments show a maximum in atmospheric and oceanic cooling around 60° N (Figure 2.5*a*,*b*), where sea ice cover is now present both in winter and summer after the deep water formation sites vanished (Figure 2.5*c*–*e*). A second peak of winter sea ice is noticeable around 40° N, but is not as clear in summer sea ice nor mixed layer depth. This second peak corresponds to the closing of the warm water corridor off the western coast of Europe and the spread of winter sea ice in this region. It is around these latitudes that we observe a maximal reduction of the AMOC by up to $14Sv$ (Figure 2.5*f*). Because of the loss of convection at high latitudes, the upper cell of the AMOC largely dwindles north and south of 20° N. *21k* follows a similar pattern during the transient state. The soft decline of the AMOC is consistent with a shift southward of the convection sites, most likely resulting from a slightly cooler North Atlantic climate (Figure 2.5*c*–*f*). We observe a clear reduction of sea surface temperature by as much as $2°C$ and of surface air temperature by up to $7.5°C$ at high latitudes (Figure 2.5*a*,*b*,*f*). It is remarkable that *21k*'s winter sea ice expansion and mixed layer depth shallowing are comparable to the *oscillating* and *cold* simulations, demonstrating an increased seasonality compared to the reference *CTRL* state (Figure 2.5*c*–*d*). *21.5k* is omitted from this analysis (see Section 2.14).

We do not observe such consistency between simulations during their warm modes (Figure 2.5, bottom). They all show a significant recovery from the cold modes, but it is impossible to underline a single common behaviour. For example, despite a couple of periodic recovery phases of the AMOC in *18.2k* (around 3,500, 7,000 and 9,000 years into the run; Figure 2.3*b*), the warm modes remain in a relatively cold-climate state (Figure 2.5 *h*–*i*). At 60° N, sea surface temperatures are down by $2°C$ and surface air temperatures drop by $6.5°C$ compared to *CTRL*. Shallower mixed layer depths around the same latitude indicate that Iceland/Irminger Basin and Labrador Sea convection sites are still greatly disrupted (Figure 2.5*j*). This keeps the sea ice edge far south in both summer and winter (Figure 2.5*k*–*l*). Amongst the *oscillating simulations*, the AMOC index is stronger than in *CTRL* (Figure 2.5*m*), increasing by as much as $2Sv$ in the subpolar region. However, for the most part, these simulations also show disparities in key climate descriptors, at least in terms of amplitude of the anomalies. Surface temperatures and sea ice extent in *18.2k* and *17.8k* bear the closest resemblance across this subset of simulations, whereas

temperatures and sea ice extent in *20.7k* and *19.4k* indicate a slightly warmer climate (Figure 2.5*h*, *i*, *j*, *l*) despite there being stronger ocean convection in *17.8k* (Figure 2.5*j*). The oscillating simulations all show an increase in winter sea ice around 40° N compared to *CTRL*, corresponding to the narrowing of the warm water corridor along the coast of western Europe (Figure 2.5*k*). In summary, none of the simulations exactly returned to the *CTRL* reference climate during their respective warm modes, indicating significant regional legacy induced by the imposed meltwater patterns. We did not include the warm modes of the *warm* simulations as they would be indistinguishable from *CTRL* with this method.

2.5 Influence of the meltwater discharge

Abrupt climate changes are triggered by constant meltwater discharge in our simulations. Yet, we observe a strong non-linearity between the climate response and the location and the influx of freshwater (Figure 2.3). For instance, despite a similar total influx of about $0.1Sv$, *19.4k* is tipped into an *oscillating* regime while *18.2k* ends up in a *cold* regime. On the other hand, *20.7k* and *19.4k* display similar oscillating dynamics even though the total flux is around 20% weaker in *20.7k* than *19.4k*. All of this hints at the importance of differences in the meltwater discharge pattern. Whilst the spatial distribution of freshwater forcing is comparable between *21k* and *20.7k*, only *20.7k* manages to generate oscillations. It demonstrates that not only the spatial distribution of the freshwater flux is an important control on the oceanic response, but that there is also a sweet spot in the perturbation conditions where the forcing needs to be strong enough to trigger a switch to stadial states, but not so strong that it (semi-)permanently suppresses a recovery as in *18.2k*.

A threshold is reached in the cold climate modes, when the climate cools so far that it becomes insensitive to further meltwater discharge (Figure 2.5). Independent of the forcing, all simulations produce a similar spatial pattern in temperature, sea ice and deep water formation layout during the weak phases, but only when the surface atmosphere cools by as much as $15°C$ does the climate cross a tipping point where the cold phases can be sustained for a few hundred years. This corresponds to the vanishing of all oceanic convection north of 40° N (Figure 2.5*c*), resulting in an almost collapsed AMOC (up to $12Sv$ weaker) in the North Atlantic (Figure 2.5*f*). When all the deep water formation sites have vanished, the response becomes decoupled from the forcing and only smaller regional effects can be induced. This phenomenon resonates with the conclusion of Smith and Gregory (2009).

The effect of regional patterns of discharge on the climate response can be tracked by creating a composite of warm modes mixed layer depth and sea surface salinity (Figure 2.13). It shows clearly distinct results between the simulations with prevalent North American meltwater inputs (*20.7k*, *19.4k*) and the simulations dominated by Arctic discharge (*18.2k*,

17.8k). The *warm* simulations (*21.5k*, *21k*) show almost no signal.

The effect of Arctic/GIN Seas discharge is decisive for triggering the shift from warm to cold AMOC states and leads to the strongest modification of the warm modes (Figure 2.5). This could be the result of two factors. First, meltwater released from the Northern Eurasian ice-sheet leads to large salinity modifications by up to $8PSU$ in the Arctic (Figure 2.13 *k–l*), which can massively disrupt the meridional salinity gradient. Second, meltwater is released relatively close to the main deep water formation sites in the GIN seas and in the Irminger/Iceland Basins, which it can reach by following the Greenland currents without having been significantly mixed with saltier warmer and saltier waters (Born and Levermann, 2010). Meltwater entering the GIN Seas should play a similar role, but the relatively low discharge in this area in our simulations makes it hard to conclude with certainty.

On the other hand, meltwater released off the northeast coast of North America has a weaker impact. Simulation *19.4k* has greater discharge in the region and similar fluxes to the Arctic and GIN Seas compared to *20.7k*. However, this increase in North Atlantic meltwater does not drive any significant ocean or climate response. From Figure 2.13 *i–j*, we infer that North American meltwater discharge is quickly dispersed. It has a direct effect on closing the Labrador Sea deep water formation site, but because this site is easily shut down in our simulations this does not impact significantly the AMOC. Because the water has to transit all around the subpolar gyre to target the more crucial sites in the eastern North Atlantic, the water will be mixed with tropical waters, weakening the forcing. The increased sensitivity to Arctic discharge compared to North American discharge in our simulations ties in with the conclusions of Roche et al. (2010) and Condron and Winsor (2012).

The existence of a sweet spot in the rate and location of meltwater discharge to the ocean for triggering climate transitions also depends on the background climate. Understanding the conditions leading to the creation of such a window of opportunity (Barker and Knorr, 2021) where abrupt climate changes can arise has been widely discussed (e.g. Brown and Galbraith, 2016; Zhang et al., 2017; Klockmann et al., 2018). Among the parameters likely to influence it, the choice of ice sheet reconstruction seems key, even more so in our simulations, as we rely on it both for the background climate state and for the meltwater forcing scenarios. In previous HadCM3-family deglaciation studies (e.g. Ivanovic et al., 2018a; Gregoire et al., 2012), different ice sheets reconstructions did not yield as significant climate transitions, in spite of having a comparable baseline climate state (Kageyama et al., 2021) and magnitude of forcing. Other variables are also considered. Klockmann et al. (2018) and Zhang et al. (2017) only observed abrupt climate transitions under certain CO_2 concentrations. Model paramterisation is also crucial, as for instance Peltier and Vettoretti (2014) managed to obtain oscillations by changing the vertical mixing coefficient. Precisely what about this particular reference state provides such a compliant framework

for simulating AMOC oscillations may form the basis of future study.

2.6 Bimodal warm states linked to reorganisation of deep water formation and subpolar gyre layout

Intriguingly, the *oscillating simulations* frequently undergo a double warm peak during times of strong AMOC (Figure 2.4*b*). This is particularly clear in the late cycles of *17.8k* (i.e. after 3,000 years), where the first peak in each warm phase is slightly cooler than the second. It indicates two distinct climate states separated by a cooling and then warming transition that is lower in amplitude than the cold-AMOC to warm-AMOC mode shift and which do not resemble the classical two-stage recovery hypothesis described by Renold et al. (2010) and Cheng et al. (2011). Changes in sites of deep water formation and the SubPolar Gyre (SPG) have been at the centre of recent studies of abrupt climate and ocean circulation changes (Li and Born, 2019; Klockmann et al., 2020) and could shed some light on this warm-mode transition stage. Hence, we next examine the relationship between the AMOC index, the longitude of the Centre Of Mass (COM) of the Mixed Layer Depth (MLD) and different physical indicators. The centre of mass does not indicate the actual location of the deep-water formation sites but should be seen as a tool to visualise the changes in the convection layout.

There is a linear relationship of roughly $1°C.Sv^{-1}$ between the AMOC index and the temperature at NGRIP (Figure 2.6*a*), demonstrating once again that AMOC index and NGRIP temperatures are interchangeable when it comes to identifying climate modes in our simulations. The intensity of the convection sites follow a similar trend (Figure 2.6*b*), with roughly a 10 metre increase of the maximum mixed layer depth in the North Atlantic for each degree of warming over Greenland. Both these relationships remain consistent irrespective of the specific warm modes that the *oscillating simulations* are in. However, for equivalent maximum AMOC strengths, the location of the deep water formation sites and the geometry of the subpolar gyre are clearly distinct between the two different warm modes. This is manifested in the ESPG index and latitude of the SPG COM, which split into two branches for high AMOC indices (Figure 2.6*c–d*). To further describe this phenomenon, we examine the different convection layouts in Figure 2.7. Two warm modes can be distinguished, each showing different deep water formation activity in the GIN and the Irminger seas. We use the peaks in their respective time series (Figure 2.7*b–c*) to build a composite mean of the MLD over the three modes (Figure 2.7*d–f*). The analysis was performed on *17.8k* as it shows the clearest distinction between the two warm modes.

We follow the dynamics of the warm mode shifts by tracking the arrows in Figure 2.6, omitting in this analysis the initial spin-up period corresponding to values falling outside of the cycles (for example, the first 300 years in *20.7k*). Starting from a *cold* mode, the recovery of the AMOC is first fuelled by convection in the GIN Seas, with very little signal

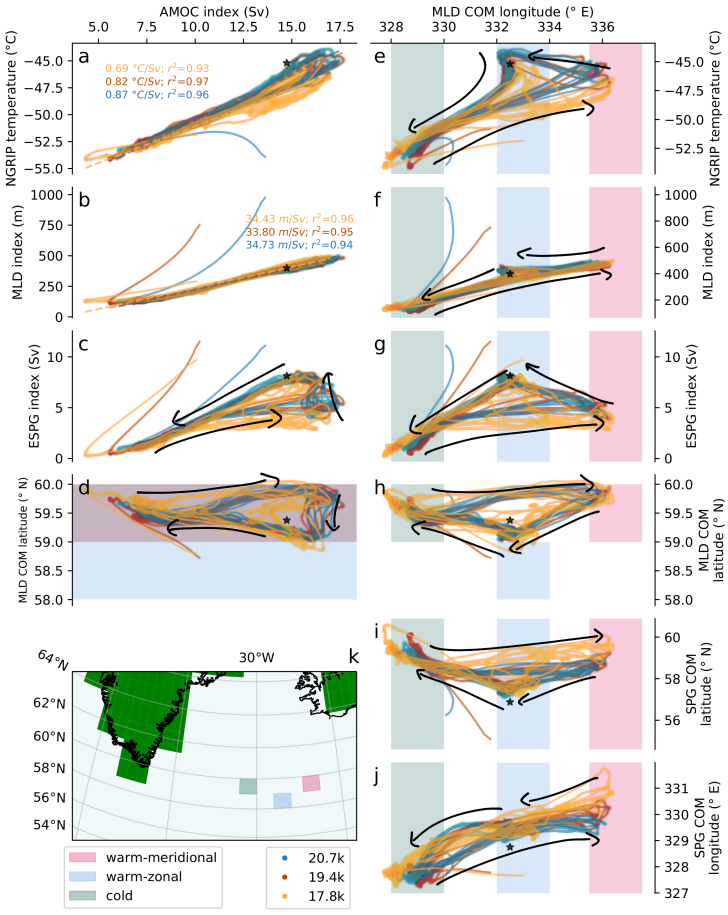

Figure 2.6: **Phase space of the oscillating simulations.** Phase plot of the three *oscillating simulations* showing the relationship between the maximal value of the overturning circulation in the Atlantic ocean at 26.5° N (AMOC index) and *a.* surface air temperature at NGRIP (42.32° W, 75.01° N), *b.* the maximum mixed layer depth in the Northern Hemisphere Atlantic (MLD index), *c.* the mean barotropic stream function in Eastern North Atlantic (ESPG index - see Klockmann et al. (2020) and Figure 2.14 for zones definition), *d.* the latitude of the centre of mass of the mixed layer depth (MLD COM latitude); and between the longitude of the centre of mass of the mixed layer depth (MLD COM longitude) and *e.* the temperature at NGRIP, *f.* the MLD index, *g.* the ESPG index, *h.* MLD COM latitude, *i.* the latitude of the centre of mass of the barotropic stream function in the subpolar region (SPG COM latitude) and *j.* the longitude of the centre of mass of the barotropic stream function in the subpolar region (SPG COM longitude). The calculation of the centre of mass is detailed in Section 2.16. Colour shading indicates the location of the main areas of activity of the centre of mass of the mixed layer depth during the different modes, as plotted on panel *k.* Arrows indicate the direction of flow (through time) over the phase space; from green (cold) to blue (warm-meridional) to red (warm-zonal) modes. All time series were filtered following the algorithm presented in Section 2.13 and a 30-year running mean line is shown here, for readability. The black stars indicate the mean annual values calculated from the last 100-years of *CTRL*.

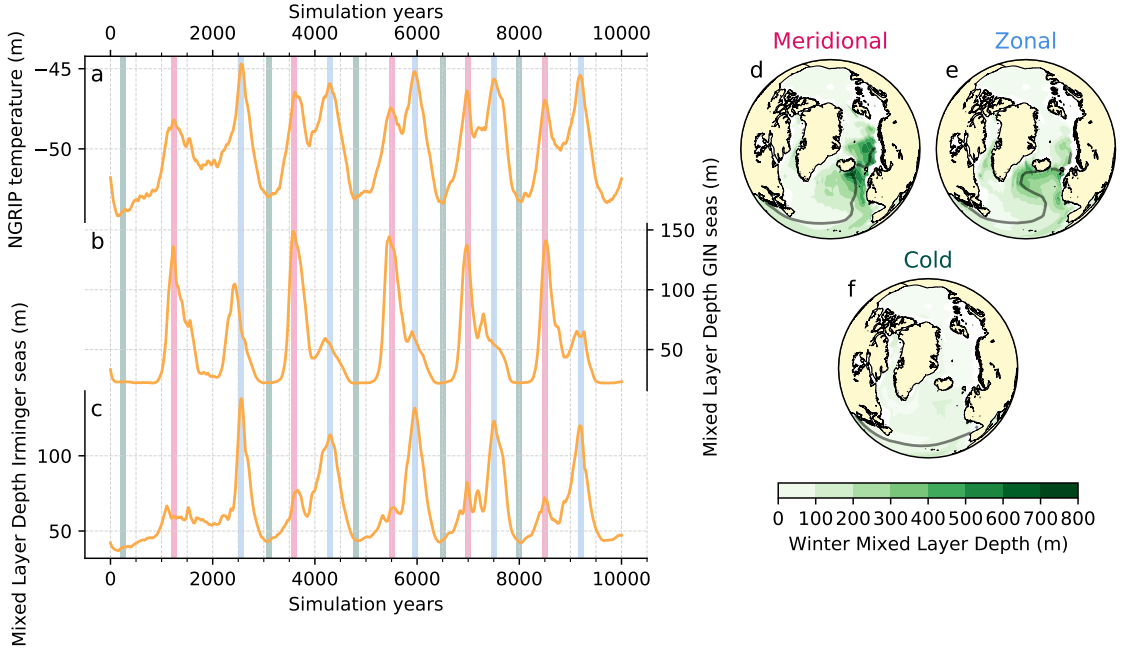

Figure 2.7: **Deep water formation sites in the *17.8k* simulation.** *a.* maximum Atlantic overturning circulation at 26° N. *b.* Mixed Layer Depth in the GIN seas (see Figure 2.14). *c.* Mixed Layer Depth in the Irminger Sea (see Figure 2.14). The meridional, zonal and cold modes were identified from the time series (pink, blue and green vertical bands, respectively, in panels *a*–*c*). Winter Composite mean of the Mixed layer depth is plotted for the meridional mode (panel *d*), the zonal mode (panel *e*) and the cold mode (panel *f*). Solid lines indicate the contour for 50% winter sea-ice concentration.

in the Irminger basin, which is covered in sea ice in Winter (Figure 2.7*f*). This results in a shift eastwards and northwards of the centre of mass of the convection sites, as indicated by a deeper mixed layer (Figure 2.6*h*). Although situated in an area of intense sea ice formation, the Labrador Sea deep water formation site is not always reactivated during this mode. As a result, the subpolar gyre, which is initially weak and contracted during the *cold* phase, gets slightly stronger and extends eastwards (Figure 2.6*g*, *i*, *j*), entering the *warm-meridional* mode (so labelled for the disposition of the deep water formation sites during this phase). After sustaining a *warm-meridional* state for a few hundred years, the deep water formation layout is disrupted again to return to a state that resembles *CTRL* (comparing Figure 2.2 to Figure 2.7*d*), with convection occurring primarily in the Iceland/Irminger basin and the resumption of Labrador Sea deep water formation (Figure 2.7*e*). The convection is distributed over a larger region and consequently the MLD index slightly dwindles. Conversely, the subpolar gyre intensifies, and moves southward and westward (Figure 2.6*i–j*). We call this state the *warm-zonal* phase.

Interestingly, we also observe short episodes of AMOC overshoot occurring immediately after the transition from *cold* to *warm-meridional* modes. The overshoots only exist at the onset of *warm-meridional modes* and are associated with stronger convection in the GIN Seas (Figure 2.7*b*).

Overall, these two *warm* states of strong AMOC are different from the two modes described by Cheng et al. (2011), where there is a transfer of deep water formation across the Atlantic from the the Labrador Sea to the GIN Seas, the latter associated with an AMOC overshoot. In all three of *oscillating* simulations, a relatively strong convection is maintained throughout both warm phases of the cycle, with permanent activity in the Iceland Basin and a transfer of deep water formation sites from the GIN seas to the Irminger Sea.

2.7 A good example of Dansgaard-Oeschger events?

At first glance, the *oscillating simulations* resemble some recorded D-O events. From a purely descriptive point of view, presented in Table 2.2, we observe a periodicity (defined as the inverse of the dominant frequency in Figure 2.4) of between 1,540 and 1,930 years (the *18.2k* simulation has a periodicity of 1,290 years, but strictly we do not define this as an *oscillating* simulation). In terms of the duration of D-O cycles, this simulated periodicity is close to the range approximated from palaeo records (about 1,500 years) during times of regular occurrence (Thomas et al., 2009; Lohmann and Ditlevsen, 2019). As an example, we compared our simulated cycles with D-O 9-11, which occurred between 44 ka BP and 40 ka BP (Figure 2.8) and look the most like our *oscillating* simulations. In Table 2.2, we also compiled the main characteristics of oscillating simulations from three other models (Peltier and Vettoretti, 2014; Klockmann et al., 2020; Kuniyoshi et al., 2022).

The information were extracted from the text and/or estimated from the plots when it was possible. Note that biases in the comparison may arise from the different resolution of the models (e.g. both CESM1 and MPI-ESM have higher spatial atmospheric resolution over Greenland compared to HadCM3) as well as from the definition of NGRIP temperatures (e.g. whether a smaller of larger area is used) and the filtering methods. The duration of the oscillations is also very similar to the simulated events of Klockmann et al. (2020) and Kuniyoshi et al. (2022), but two to three times longer than Peltier and Vettoretti (2014). As already discussed, *18.2k* does not qualify as an *oscillating* simulation due to its *cold* characteristics (Section 2.4). Yet, in Figure 2.4, we observe two smaller peaks identified by the frequency analysis algorithm, one at $\sim$1,300 years and one at $\sim$3,500 years, which also correspond to typical D-O values (e.g. Kindler et al., 2014).

The temperature ranges between warm and cold climate/AMOC modes are similar, with changes of about $10°C$ recorded (Huber et al., 2006; Kindler et al., 2014) and simulated (this study) at NGRIP. From the other model studies cited in this study, only Peltier and Vettoretti (2014) obtained a similar amplitude of Greenland temperature change. Both Klockmann et al. (2020) and Kuniyoshi et al. (2022) observed smaller transitions similar more to the $6°C$ amplitude of *18.2k* oscillations, but still within the lower range of reconstructed D-O events. The sea ice extent extends down to the Iberian margin in winter, which is what is consistent with what is observed during some Heinrich stadials (Voelker and de Abreu, 2011).

Notwithstanding some similarities with recorded D-O events, because all simulations were realised in a maximum glacial background (specifically, the LGM), the analogy between these simulations and D-O events is not straight forward. The comparison between our simulation and other occurrences of D-O events than D-O 9-11 is often inconclusive. This is all the more true as we can also identify significant discrepancies between the model results and observations. For example, the simulated cycles do not match exactly the typical shapes of D-O events (Lohmann and Ditlevsen, 2019); an abrupt warming followed by a slow cooling over a few hundred to a few thousand years within the warm phase followed by a sharper cooling to finish off the cycle. Our simulations displayed a gradual transition between the cold modes to the warm modes, and the strong-AMOC phases were maintained rather steadily for $\sim$500 years before undergoing a slow cooling into the weak-AMOC phase of the cycle (Table 2.2). The warming and cooling rates are less sharp than palaeo-records suggest, with a typical rate of $3°C$ temperature change per 100 years, about 10 times slower than indicated in Lohmann and Ditlevsen (2019). It has to be noted that despite a potential damping of the warming and cooling rates due to the filtering, the duration of filtered signals matched the unfiltered ones well, indicating that our conclusion on the shape of the simulated cycles are not an artefact of the analytical method. Kuniyoshi et al. (2022) similarly produced an oscillating ocean/climate with warming rates not exceeding $6°C.100yrs^{-1}$, in contrast to the ten times faster warming

Table 2.2: **Oscillating simulations metrics.** Typical oscillation descriptors for the *oscillating* and *cold* simulations defined from the filtered NGRIP temperature time series (Figure 2.4) and compared to simulations from Peltier and Vettoretti (2014), Klockmann et al. (2020) and Kuniyoshi et al. (2022). Periodicity was identified using the analysis presented in Figure 2.4*c*. Amplitude was defined as the difference between the warmest and coldest point of the filtered NGRIP temperature time series Figure 2.4*b*. Warming and cooling rates were defined as the maximum and minimum of the derivative of the filtered NGRIP temperatures time series, respectively. Descriptors of the simulations performed by Peltier and Vettoretti (2014) were estimated from Figure 1 by Vettoretti and Peltier (2018). Descriptors of the simulations performed by Klockmann et al. (2020) were taken from their main text. Descriptors of the simulations performed by Kuniyoshi et al. (2022) were taken from experiment P270 and estimated from Figure 3 by Kuniyoshi et al. (2022).

Simulation	Periodicity (ka)	Amplitude ($^{\circ}C$C)	Warming rate ($^{\circ}C.100yrs^{-1}$)	Cooling rate ($^{\circ}C.100yrs^{-1}$)
20.7k	1.54	10.9	4.94	-3.98
19.4k	1.93	8.92	5.19	-3.72
18.2k	1.29	5.90	2.84	-3.57
17.8k	1.67	7.65	4.17	-5.28
Peltier and Vettoretti (2014)	~ 0.8	~ 10	~ 50	$\sim$ -5
Klockmann et al. (2020)	1.5 to 2.0	5 to 6	25 to 50	-5 to -35
Kuniyoshi et al. (2022)	~ 1.5	~ 6	~ 6	$\sim$ -6

rates simulated by Peltier and Vettoretti (2014) and Klockmann et al. (2020) (their cooling rates overlap with ours).

We observe an asynchronicity between the North Atlantic and Antarctica signal. This asynchronicity recalls the bipolar see-saw phenomenon described in (Stocker, 1998; Stocker and Johnsen, 2003). The Antarctica temperatures seem to lead the Greenland temperatures by 200-500 years in both the warming and cooling phases in Figure 2.8*a–b*, although it is difficult to identify a clear pattern. This does not fit the classical estimation (Antarctica lags the Greenland signal by $\sim$ 150 years in Svensson et al. (2020)) and challenges once again the resemblance of our oscillations to D-O events. At last, it is possible that the periodicity observed is an artefact of the model when forced with constant sustained freshwater. By using a dynamical freshwater release pattern, we would be able to conclude on the comparability of these oscillations to actual palaeo-records.

Presently, we cannot categorically conclude whether or not our oscillations relate to D-O events. Differences in the shape of real and simulated D-O cycles may be explained by the quasi-idealised nature of our experiment design, specifically, the glacial maximum and fixed nature of our climate model boundary conditions/forcings (set to 21 ka, PMIP4 LGM protocol with GLAC-1D ice sheet plus the respective meltwater scenarios from the early deglaciation in GLAC-1D). The framework for our simulations was designed to simplify the identification of different behaviours in response to early deglacial meltwater forcing, mainly inspired by the hypotheses formed in conclusion to earlier work by Ivanovic et al. (2018a). It provides a solid and systematic foundation for further work to study the mechanisms at play in the climate simulations presented here. However, this framework may interfere with or block some of the complex dynamics of D-O events and damp the abrupt climate changes. We indeed observe the sharpest cooling events at the onset of each simulation, indicating that the initial reorganisation of deep water formation sites in response to a change in freshwater forcing may lead to the strongest and fastest climate disruption. Also, our setup does not include feedbacks between ice sheet melt and temperature changes, which could influence the periodicity of amplitude of changes (Gregoire et al., 2016; Ivanovic et al., 2017). We therefore speculate that implementing a transient meltwater pattern consistent with what is known about past ice sheets during times of abrupt climate change could be a good way to better account for the dynamical interactions and abrupt reorganisations of the earth system, but ultimately, transient coupled climate-ice sheet simulations are needed to fully unlock the challenge of understanding D-O cycles and abrupt deglaical climate change. Finally, the discrepancies between observed D-O cycles and our simulations may also be related to weaknesses in the climate model itself. This version of HadCM3 seems to be unable to capture the fast physics component that has been observed in Vettoretti and Peltier (2018), and this may be related to the representation of ocean vertical diffusion (Peltier and Vettoretti, 2014).

Furthermore, and specifically to address D-O cycles, we also need to be able to reproduce

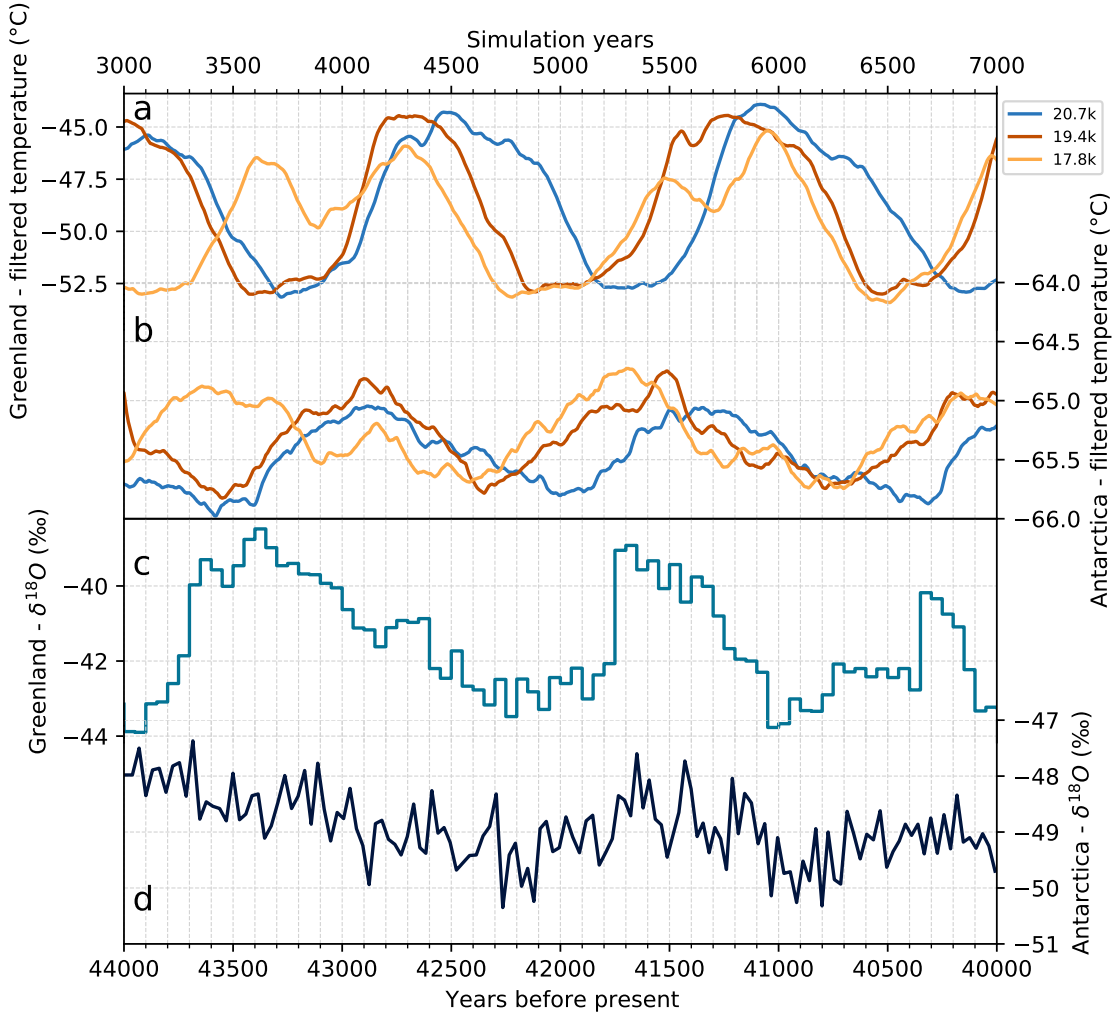

Figure 2.8: **Comparison to ice core records and bipolar see-saw.** Temporally filtered signals of simulated surface air temperature over *a.* Greenland (NGRIP; 42.32° W, 75.01° N) and *b.* Antarctica (EPICA Dome C; 123.21° E, 75.06° S) for simulation years 3,000 to 7,000. *c.* NGRIP and *d.* EDML (Dronning Maud Land; 0.04° E, 75.00° S) $\delta^{18}O$ records between years 40,000 and 44,000 before present showing D-O events 11, 10 and 9, from N.G.R.I.P (2004) and Barbante et al. (2006), respectively.

the phenomenon of oscillating weak-strong AMOC modes outside of a glacial maximum background. Marine Isotope Stage 3 (MIS3, 29–57 ka BP Lisiecki and Raymo, 2005), as depicted in Figure 2.8*c–d* for comparison to our results, has been often considered an appropriate candidate for such studies. Stadial conditions then were warmer than at the LGM, and it contains the most regular occurrences of D-O events recorded. Currently, one major challenge for setting off such a suite of simulations is that our oscillations are triggered by meltwater discharge, with a strong dependency on nuanced differences in the rate and location of freshwater inputs to the ocean. Thus, robust and detailed constraints on ice sheet extent are necessary to design an appropriate model experiment.

Apart from Heinrich stadials, MIS3 was not a time when ice sheet melting is thought to have been particularly strong, and there is likely to have been a lower meltwater flux than in our *oscillating simulations* (Hughes et al., 2016; Batchelor et al., 2019). However, D-O 15-17 are believed to have been associated with changes of ice sheet extent (Lambeck, 2004), and because their shape remarkably resembles the observed oscillatory cycles of our simulations (Barbante et al., 2006; Rasmussen et al., 2016; Erhardt et al., 2019), they could be good candidates for being triggered by relatively low-levels of Northern Hemisphere ice sheet melt; it is possible that a weaker glacial climate state had a more sensitive ocean to smaller meltwater fluxes than our LGM-based simulations. However, the further back in time we go, the less constrained ice sheet extent (and geometry more broadly) and our model boundary conditions become, which again poses a practical limitation for how well such a climate model experiment could be designed to explore the detail of real past events. We think, therefore, that it is essential to obtain a deeper understanding of the physical mechanisms at stake during the climate oscillation before investigating further the relationship between our simulations and observed D-O cycles.

2.8 Conclusion

Using snapshots of the meltwater discharge derived from the GLAC-1D ice sheet history of the early last deglaciation, we produced a set of oscillating simulations in the HadCM3 climate model under glacial maximum (PMIP4 LGM) conditions. Switching regularly between cold and warm modes, this behaviour can only be attained in a narrow range of circumstances: if the freshwater forcing is too strong and/or applied in a particularly sensitive part of the ocean, the climate cannot fully recover to a warm mode and stays cold for the majority of the simulation. On the other hand, if the forcing is too weak, the transition to a cold mode is incomplete and the system rebounds to stay permanently in a warm state.

Understanding what can be defined as a ‘weak’ or ‘strong’ freshwater flux is not straightforward, as the response to the forcing is non-linear. All simulations are in the range of plausible magnitudes for meltwater discharge over the last deglaciation — although

the scenarios are made quasi-idealised by sustaining a constant meltwater discharge over thousands of years rather than following the transient history — but differ significantly in terms of total amplitude, and the geographical distribution of the freshwater fluxes. We observe that meltwater released in regions close to the main convection sites, namely the Nordic Seas and the Irminger/Iceland Basins, is the most effective at disrupting the AMOC. One possible inference from this finding is that in spite of being smaller in size compared to the North American ice sheet, Eurasian ice sheet demise punches above its weight in having the potential to trigger abrupt climate changes over the last deglaciation. Conversely, Laurentide ice sheet meltwater is required to be much more substantial to produce similar disruptions to Atlantic Ocean circulation and climate. The impact of the initial climate and ocean state on our results must also be considered. The cold interstadial state obtained with GLAC-1D ice sheets, with a relatively weak AMOC, convection concentrated around Iceland and extensive sea ice in the Western North Atlantic, creates a background that may favour the triggering of abrupt climate changes from Eurasian ice sheet melting.

When reaching a cold mode in our simulations, the ocean and climate response to meltwater forcing becomes decoupled from the direct influence of freshwater input at high latitudes. Because the AMOC is collapsed in these states, and the susceptible North Atlantic deep water formation sites vanished, meltwater perturbations will not propagate any longer, producing only smaller, regional perturbations. Cold modes correspond to an extreme cooling of the North Atlantic, and especially over former convection regions, with winter sea ice stretching down to Spain. We note a strong consistency in the climate change pattern of all simulations irrespective of whether they belong to the *oscillating*, *cold*, or, to a lesser extent, *warm* regimes. This is not true for the warm modes, where the response is very dependent on the meltwater forcing scenario. We observe a range of different AMOC responses, from overshooting to damping, and the resulting climate is very different for each of the simulations. In particular, the simulations dominated by Arctic discharge never manage to completely return to the reference (*CTRL*) state. We also observe a two-phase, bi-modal warm condition in the *oscillating* simulations, with shifts between deep water-formation sites from a more meridional distribution (with primary convection situated in the Nordic Seas) to a more zonal configuration comparable to *CTRL*. Resumption of Labrador Sea convection is inconsistent, sometimes being short lived and intense and sometimes being wholly absent, and in these glacial simulations, its connection to the upper cell of the overturning circulation is tenuous.

In summary, while we cannot conclusively determine that the oscillations we simulate are comparable to D-O events, there are resemblances that make such a comparison inviting. D-O events were rarely observed in full-glacial climates and are not believed to be directly forced by changes in ice sheet meltwater discharge. Still, the oscillating simulations presented here offer a valuable framework to analyse further the mechanisms behind

the millennial-scale variability in glacial backgrounds. Intriguingly, they provide a set of insightful simulations that are so far unique in that relatively small influxes of freshwater trigger self-sustaining AMOC and Greenland temperature oscillations from glacial *maximum* conditions with a very large LGM North American ice sheet. Finally, the presented simulations pave the way for further study of ice sheet meltwater as a *trigger*, but not a direct *driver*, of abrupt climate changes within the last deglaciation.

Chapter 2 - Supplementary Information

The supplementary information includes

1. Sections 2.9 to 2.16
2. Figures 2.9 to 2.20
3. Equations S1 to S4

2.9 Supplementary Information - Simulating the Last Glacial Maximum

For atmospheric trace gases, we adopted Last Glacial maximum (LGM) values of 190*ppm* for CO_2 (Bereiter et al., 2015), 375 parts per billion (ppb) for CH_4 (Loulergue et al., 2008), and a slightly lower concentration of 193*ppb* for N_2O (compared to 200*ppb* in the protocol) (Schilt et al., 2010), which corresponds to the 21 ka BP point in the interpolation between transient records of ice cores (Ivanovic et al., 2016). For the ice sheets, and associated fields, ice sheet extent, surface elevation and the resulting land-sea mask and ocean bathymetry were all derived from the GLAC-1D ice sheet reconstruction (Tarasov and Peltier, 2002; Tarasov et al., 2012; Briggs et al., 2014; Ivanovic et al., 2016) at year 21 ka BP. The ice sheet geometries (Figure 2.9) and associated palaeogeographical fields were not modified at any time of any simulations. The GLAC-1D reconstruction contains patches of ice over central Siberia and southern sectors of the Rocky Mountains (e.g. Tarasov et al., 2012) that can reach up to 100 m thick. Because they correspond to regions where the fractional ice mask is less than 0.5 (Ivanovic et al., 2016), these were not considered nor discussed further in this study.

The remaining parameters were set to the values indicated in Kageyama et al. (2017), including radiative forcing from insolation and dust.

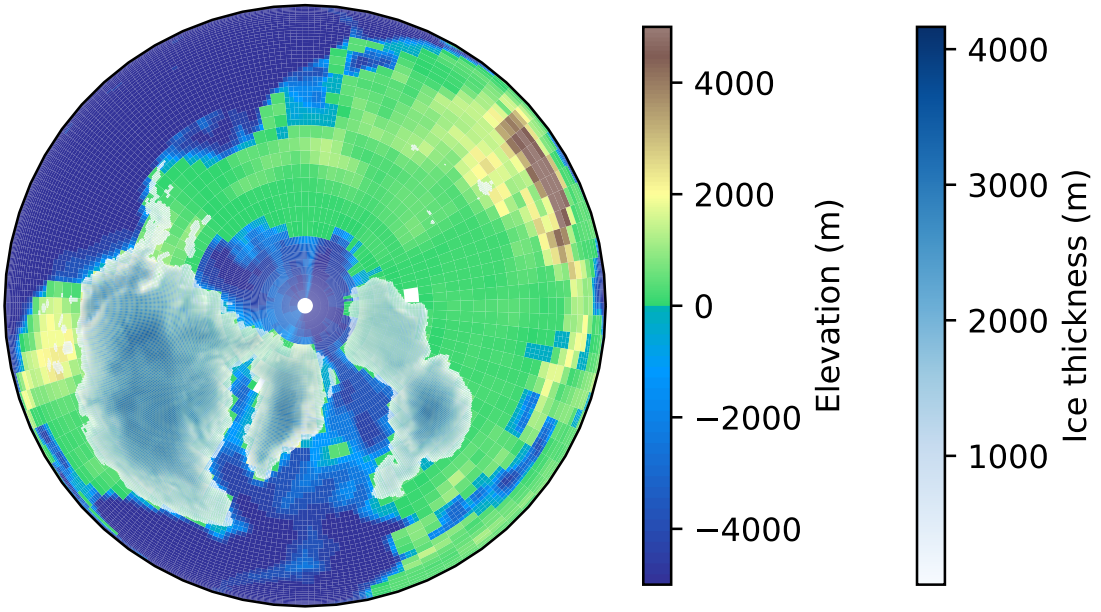

Figure 2.9: **LGM boundary conditions.** Orography, bathymetry, land sea mask and ice sheet elevation boundary conditions in the Arctic region. Ice sheets were reconstructed from GLAC-1D at 21 ka BP. Terrestrial ice is shown where it is thicker than 50 m.

2.10 Supplementary Information - Meltwater discharge protocol

The algorithm used to create the meltwater discharge input was adapted from Ivanovic et al. (2017). We started by creating the meltwater discharge history. At each 100-years time step and for each spatial grid cell where ice is present, ice elevation changes were converted into a freshwater-equivalent flux. To avoid generating strong peaks during the transformation of discrete snapshots of ice sheet geometry into a continuous time series, the flux was smoothed by taking the average of two consecutive time steps. Because we do not have a physically robust way to displace freshwater from the ocean back to the ice sheet, only ice losses were taken into account, ice accumulation being subsequently turned to zero. These steps can be summarised by equation S1, where $flux$ $(kg\,m^{-2}\,s^{-1})$ is the mass flux at a grid cell, $hice$ (m) the ice elevation at the same grid cell, $\rho = 1000\,kg\,m^{-3}$ water density, n represents the time step and $\Delta t = 100\,yrs$ the interval between two time steps.

$$flux_n = max(0, \rho \frac{hice_{n+1} - hice_n}{\Delta t}) \tag{S1}$$

Next, the 100-years time-step series was linearly interpolated into an annual series. The fluxes were then routed to an ocean cell following a global drainage network map consistent with GLAC-1D topography, using the routing coordinates provided with the PMIP4

last deglaciation protocol (Ivanovic et al., 2016). To be consistent with our model, this scattered discharge pattern was remapped to the coarser HadCM3 ocean grid, ensuring that the meltwater reaches the ocean by redistributing any routing points overlapping the land mask to their closest ocean cell.

Because the ocean model is a rigid-lid model (Gordon et al., 2000), oceanic freshwater forcing (including runoff, ice melting, precipitation/evaporation) is prescribed as virtual salinity fluxes. One possible consequence of this parameterisation is that large fluxes can lead to some grid cells being capped at $0PSU$ (minimum salinity) in the case of large freshwater inputs. This can be problematic, since we would approach the limits of the equation of state (Bryan and Cox, 1972; Fofonoff and Millard Jr, 1983; Fofonoff, 1985), and would prevent the full freshwater forcing from being applied to the ocean during episodes of rapid, voluminous meltwater discharge. Instead of trying to estimate when the salinity saturation may be reached, we adopt a cautious approach by reproducing and updating the spreading algorithm employed by Ivanovic et al. (2018a) and Ivanovic et al. (2018b). This algorithm collects all the freshwater from its grid-cell point of entry to the ocean, and spreads it uniformly at the surface of neighbouring discharge regions of at least 500 m depth. The new version of the algorithm used here only modifies the definition of some spreading regions and collection boxes in accordance with the new inputs (i.e. the old algorithm would have missed some of the new meltwater fluxes as a new ice sheet and palaeogeography is being applied in accordance with GLAC-1D; the previous studies follow ICE-6G_C). These areas are plotted in Figure 2.1*b*. It is possible, although rare, that some discharge grid cells may not be caught by the spreading protocol. We checked at each time step that the residual's signal did not exceed 0.1% of the initial flux, a value we consider small enough to be thought of as noise.

Tests for a previous study (Ivanovic et al., 2018a) showed that there was a negligible difference between the results simulated using point-source or more distributed meltwater patterns during the Heinrich Stadial period, and although these freshwater fluxes are different (the previous study used the ICE-6G_C ice sheet history), they are of sufficiently similar rate/amplitude that we are confident that a similar inference applies to the new simulations presented here, whilst also ensuring that we avoid hitting the $0PSU$ lower cap (see above). The freshwater is only discharged in the top layer of the spreading regions. We don't consider that case of hyperpycnal flow that can arise when the water is flooded with sediments (Quadfasel et al., 1990) because (i) this would require major modifications of the model and the algorithm to be possible and (ii) we do not think that this would result in a more realistic spreading region, but would very likely impact the effect on the deep water convection sites (Roche et al., 2007).

The resulting fluxes, including the signal in key regions, are plotted in Figure 2.1*a*. Note the difference in this figure panel between smaller collection boxes (bold contours offshore), larger spreading regions (constituent coloured boxes), and key regions (colours) considered

for plotting the fluxes (e.g. as time series in Figure 2.1*a*). We did not use the transient history as such for the meltwater input files, but instead took six snapshots at specific time steps that we used as constant forcing. Snapshots in time of the meltwater distribution are shown by Figure 2.1*c*.

Once the meltwater input file was created, we added the contribution of the river and iceberg run-off that was calculated to close the hydrological cycle during the Pre-Industrial. Note that meteoric runoff routing follows the configuration calculated when producing the HadCM3 PMIP4 LGM palaeogeography.

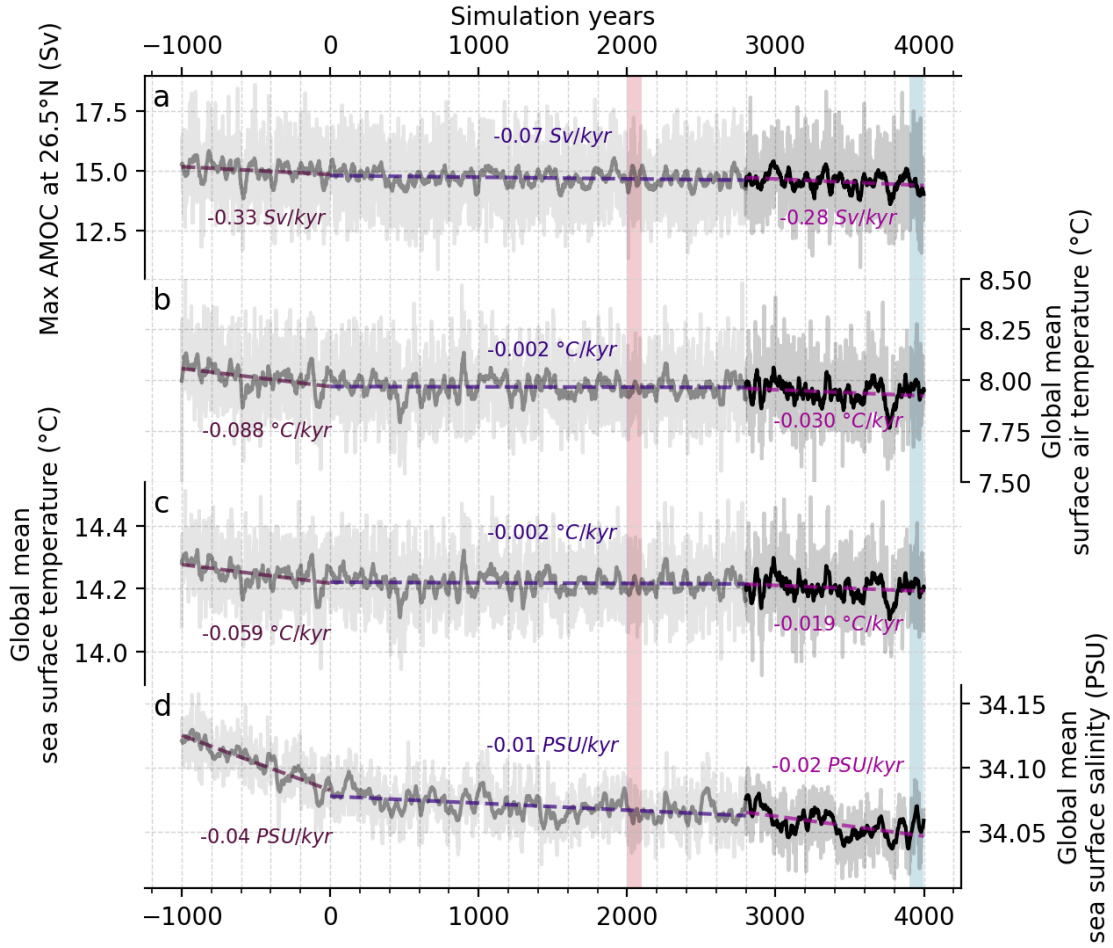

Figure 2.10: **Control climate drifts.** *a.* AMOC index, *b.* global mean surface air temperature, *c.* sea surface temperature and *d.* sea surface salinity trends in the *CTRL* simulation. Light/dark colours correspond to before/after the application of the smoothing algorithm, respectively. The last thousand years of spin-up are shown at the start of the run, for context. The drifts (purple) are calculated from linear regression of the time series before (darker purple) and after (lighter purple) the restart of the run and during the last thousand years of spin-up (medium purple). Red and blue shading highlights the pre and post smoothing phases used in Figure 2.17, respectively.

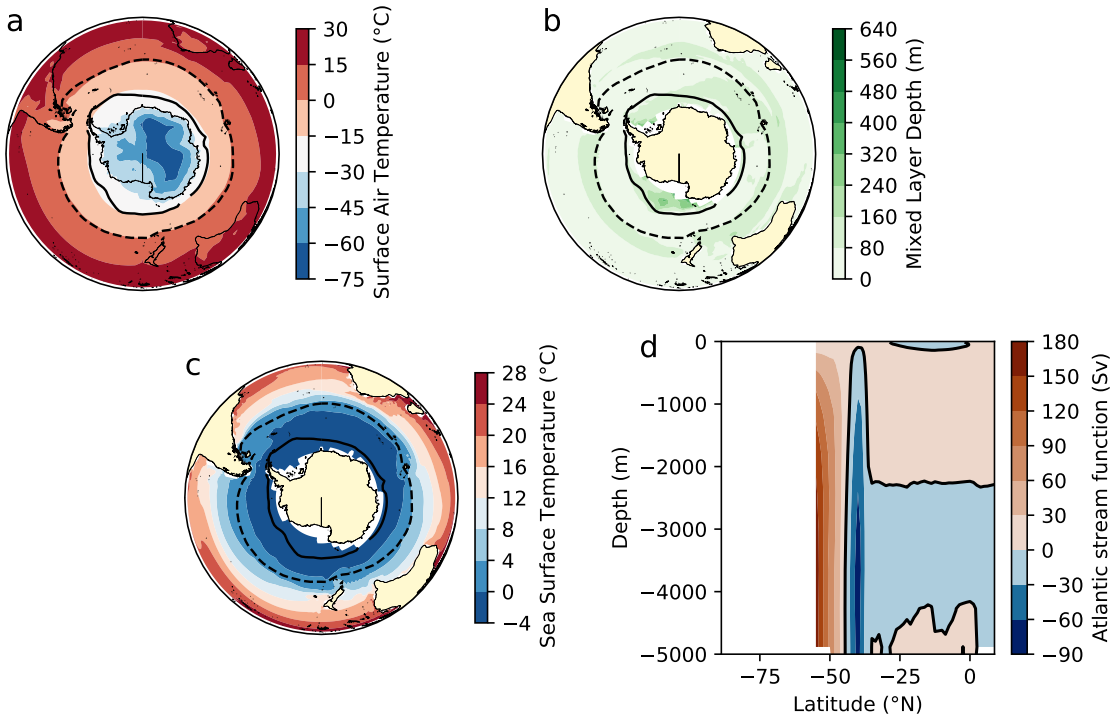

Figure 2.11: **Control climate state - Southern Ocean.** Mean annual conditions between simulation years 3900 and 4000 for *CTRL* in the Southern Ocean. *a.* Surface air temperature. *b.* Mixed layer depth. *c.* Sea surface temperature. *d.* Meridional overturning stream function in the Atlantic basin. Dashed/solid lines indicate the September/-March 50% sea-ice extent.

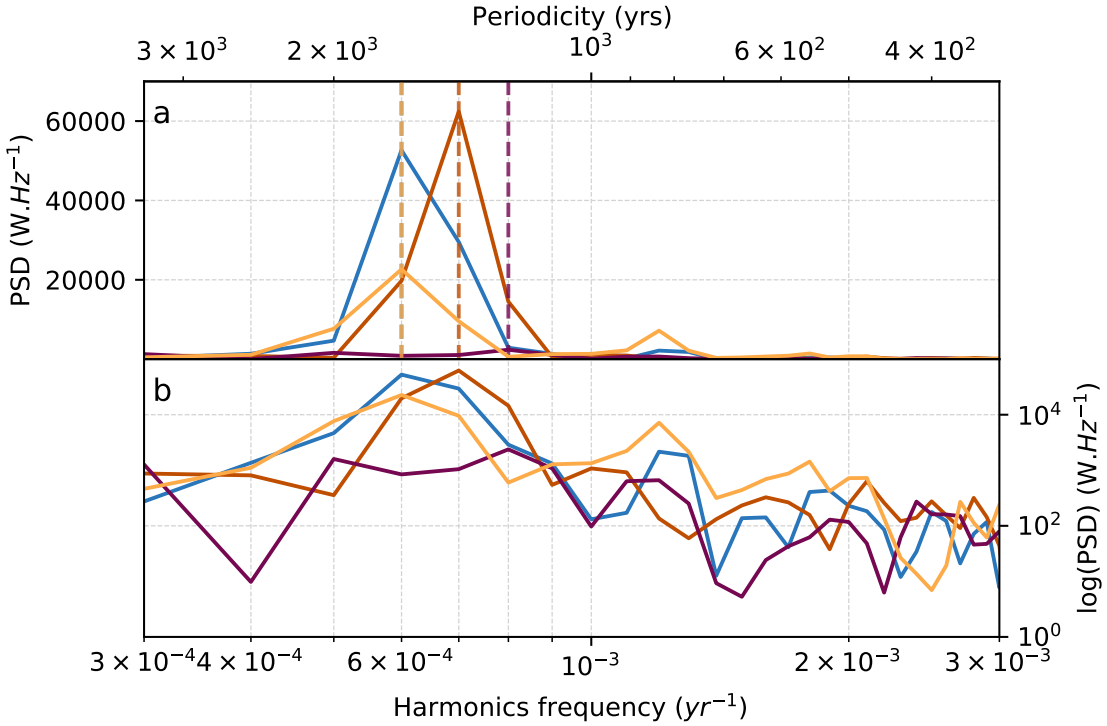

Figure 2.12: **Spectral analysis logarithmic.** *a.* Power Spectral density (PSD, left hand scale) of the unfiltered signal. Dotted lines indicate the dominant frequency/period for each simulation. *b.* Same as *a* but showing the logarithm of the PSD.

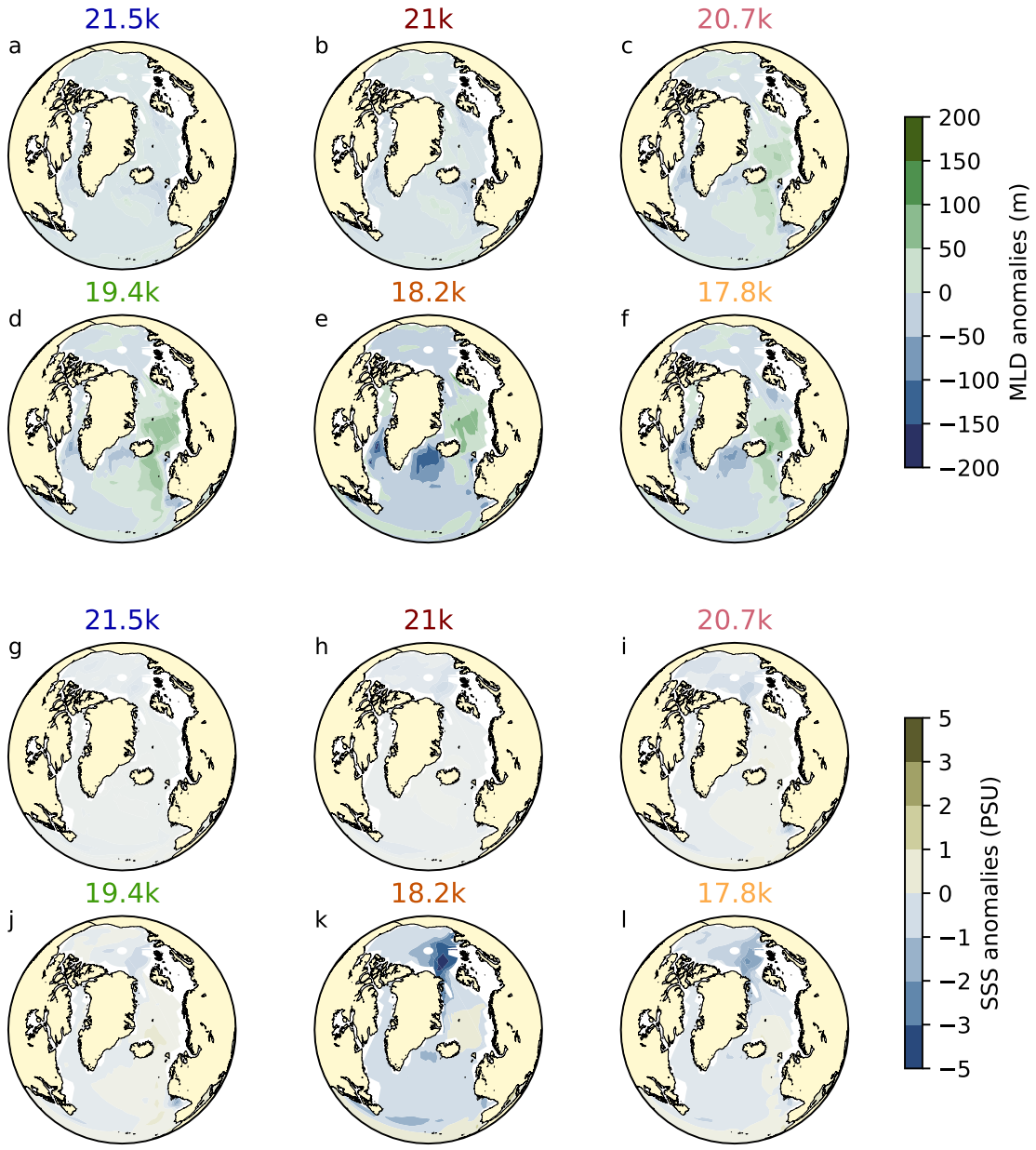

Figure 2.13: **MLD anomalies between composite modes.** Mean annual Mixed Layer Depth (MLD) anomalies between the meltwater simulations and *CTRL* over the composite warm modes *a–f*. Mean annual Sea Surface Salinity (SSS) anomalies between the meltwater simulations and *CTRL* over the composite warm modes *g–l*.

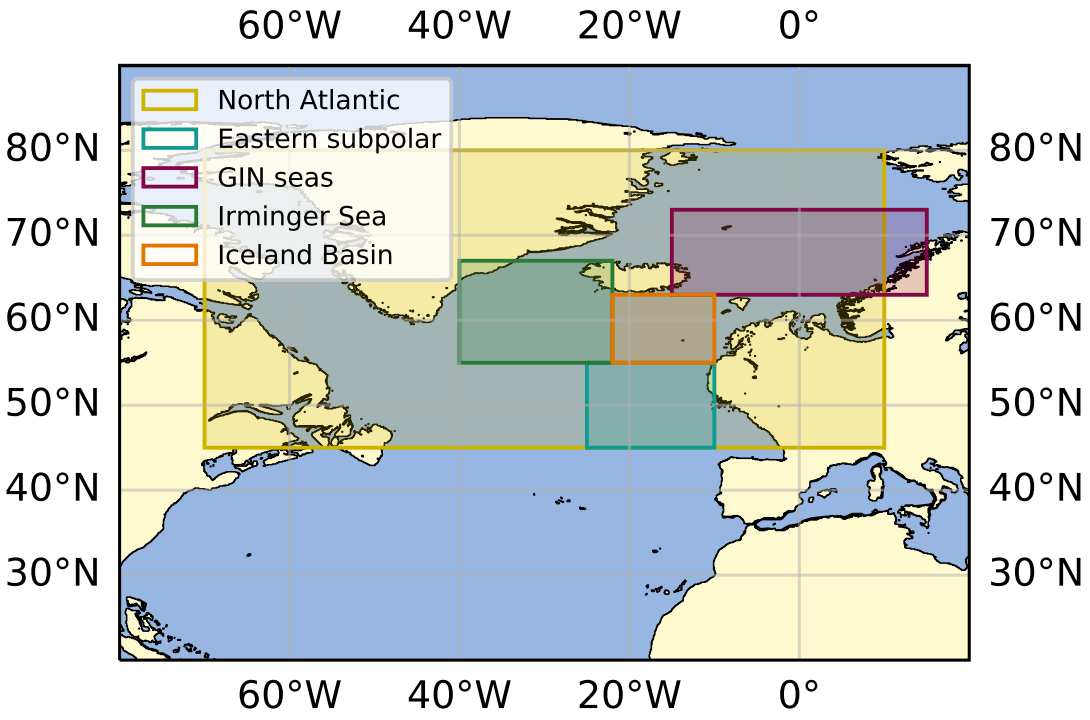

Figure 2.14: **Zone definitions.** Definition of North Atlantic zones used for the analysis summarised by Figure 2.6.

2.11 Supplementary Information - Global mean salinity target

In multi-millennial simulations on the scale presented here, long-term drifts in global mean salinity can arise under equilibrium climate forcings due to internal imbalances in snowfall/melt and iceberg calving (which is prescribed and therefore cannot vary dynamically), and evaporation/precipitation over inland seas, which are not hydrologically connected to the ocean. To conserve water in the model and avoid these long-term drifts, we apply a method for keeping global mean salinity constant that distributes any required correction across the whole volume of the ocean. This approach was preferred to a surface correction, because the latter has a greater propensity for inducing surface salinity drifts that impact large scale ocean circulation, as concluded by Dentith et al. (2019b). The method applied for this study is the VFLUX method described fully by Dentith et al. (2019b). At each ocean model time step, global mean salinity is corrected so that the global mean salinity hits the prescribed target in accordance with the terrestrial ice volume and global ocean volume at that timestep with respect to the pre-industrial. The target is calculated following equation S2, where sal_{target} $(g\,kg^{-1})$ is the global salinity target of the experiment, $sal_{ref} = 34.83\,g\,kg^{-1}$ is the reference HadCM3 salinity at 0 ka, V_{ocn} (m^3) is the ocean volume at 0 ka BP and ΔV_{ice} (m^3) is the difference in ice volume between 0 ka BP and

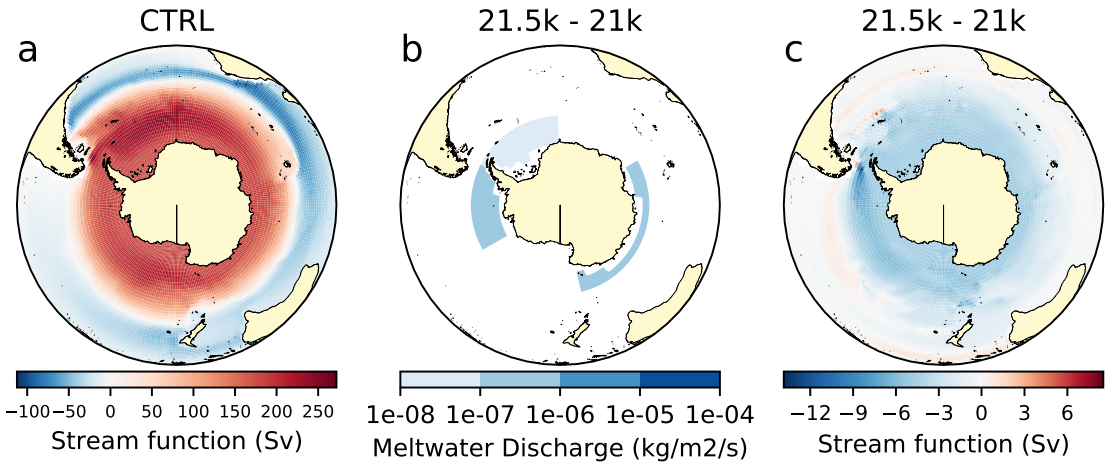

Figure 2.15: **Southern Ocean streamfunction change.** *a.* Barotropic stream function in the Southern Ocean in *CTRL*. **b.** Ice sheet meltwater discharge snapshot anomaly in the Southern Ocean between *21.5k* and *21k*. *c.* Barotropic stream function anomaly in the Southern Ocean between *21.5k* and *21k*.

the current timestep of the simulation. Thus, even though the LGM ice sheet layout (i.e. as prescribed to the atmosphere model) stays constant in our experiments, the effects of changes in terrestrial ice volume on global mean ocean salinity are taken into account through the global salinity target. Thus, each simulation has a global mean salinity target that corresponds exactly with the ice sheet configuration at the time of the meltwater snapshot (Table 2.1), with the *CTRL* target set to $35.8334\,g\,kg^{-1}$.

$$sal_{target} = sal_{ref} * \frac{V_{ocn}}{V_{ocn} + \Delta V_{ice}} \tag{S2}$$

Introducing a global salinity correction in response to local freshwater perturbations can have large implications. In particular, the buyoancy-driven Southern Ocean can be impacted. We verified that this was not the case in Figure 2.15, where we compared the two *warm* simulations in their warm modes. *21k* has greater meltwater discharge, therefore a smaller salinity target, but comparable discharge in the Southern Ocean. In Figure 2.15*c*, we observe a small slowdown of the clockwise circulation and a small acceleration of the anti-clockwise circulation, but no major reorganisation of the circulation. In some grid cells, this effect becomes significant (off the Patagonian coast for instance), but we assume that this is due to the changes in the meltwater discharge pattern. To conclude on whether the effect we observe is due to the difference in meltwater discharge pattern, to the different global salinity target or to the algorithm itself, we would need to run dedicated sensitivity experiments. In any cases, the effect is small and does not impact the main findings.

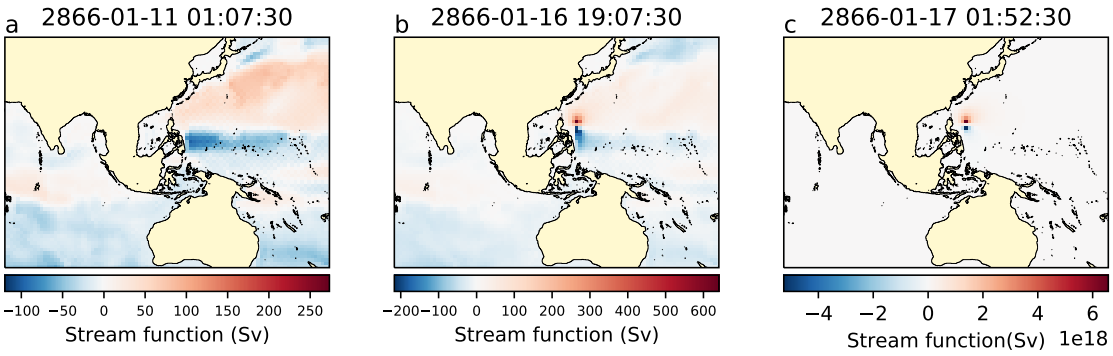

Figure 2.16: **Streamfunction instability.** *a.* Barotropic stream function in *CTRL* during the simulated week before numerical instability causes the model to crash, *b.* at the development of the instability and *c.* at the time of the crash. Note the difference in scales.

2.12 Supplementary Information - Smoothing bathymetry algorithm

After a few thousand years of integration, five out of the seven simulations (*CTRL*, *21.5k*, *21k*, *19.4k*, *18.2k*) presented in this article crashed because of a stream function instability in the Philippines Sea. This instability takes the form of a dipole where two grid cells reach unsustainable high/low barotropic stream function values; for example, as shown for *CTRL* in Figure 2.16. A week (model time) before the crash, the instability is undetectable. When the pattern appears, it gets out of control in less than a simulated day. The precise cause of this crash is not known, but it always occurs at the same location and it appears to be related to the complex bathymetry of the region.

In order to tackle this issue, we restarted the runs having smoothed the bathymetry of the Philippines and South China Seas (Figure 2.17*f*). Because we cannot exactly determine the inception of the instability, we restarted the simulations a few model years/decades before the crashes: *CTRL* at year 2,800, *21.5k* at year 3,060, *21k* at year 2,650, *19.4k* at year 8,610 and *17.8k* at year 8,900. The same smoothing was applied to all simulations and all the other boundary conditions remain unchanged. After this one intervention, all experiments successfully ran to completion.

Small disruptions of the climate are induced by the smoothing and restart process. For example, there is a slight increase of long-term drifts in *CTRL* (Figure 2.10), probably caused by a slight perturbation to the equilibrium state from introducing a small amount of noise at the restart alongside the smoothing of South China Sea and Indonesian bathymetry; the model is adjusting to the minor modifications. However, the trends are of the same order of magnitude as in the previous two and a half thousand years of simulation, and significantly smaller than during the last one thousand years of spin-up, implying that climate

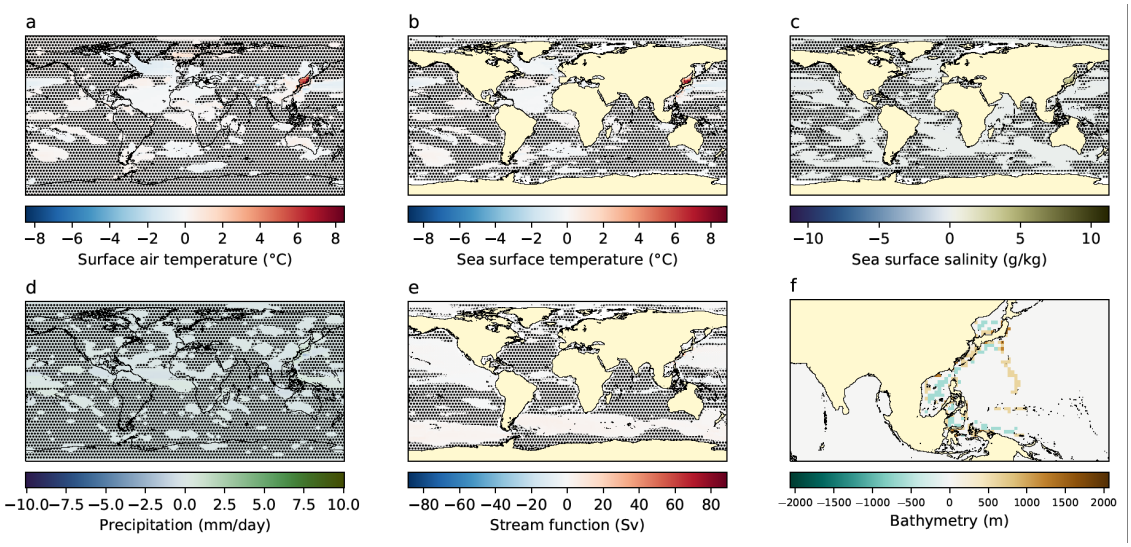

Figure 2.17: **Effect of the smoothing bathymetry algorithm.** *a.* Changes in surface air temperature, *b.* sea surface temperature, *c.* surface salinity, *d.* precipitation, *e.* stream function and *f.* bathymetry in *CTRL* after applying the smoothing algorithm (using the pre/post-smoothing time windows defined in Figure 2.10). Hatching is applied where values are considered statistically insignificant using a student t-test with a p-value of 0.1 .

remains close to its equilibrium state. Similar changes in the long term drifts are seen in *21.5k* and *21k* (not shown), but are impossible to assess for *19.4k* and *17.8k* because of their oscillatory variability. Nonetheless, any impact of the smoothing and restart on the oscillations is imperceptible if it is exists at all. After the introduction of the smoothing algorithm (arrows in Figure 2.3*b*), there is no significant change of behaviour in any of the time series. We cannot determine conclusively whether the smoothing influences the periodicity of the oscillations. However, the climate and ocean behaviours at the end of the restarted simulations are consistent with the variability observed before the smoothing.

Here, we show the spatial response induced by the change of bathymetry for *CTRL* only (Figure 2.17), but all the other simulations were analysed and returned comparable results. The resulting smoothed bathymetry has the greatest impact on the surface air temperatures, sea surface temperatures and sea surface salinity in the Philippines Sea and the Sea of Japan, with changes of up to $7°C$, $8°C$ and $5g\,kg^{-1}$ respectively, but only in grid cells very local to the bathymetric modifications. Outside of these cells, the effect is either very small or statistically insignificant. In particular, we do not see any significant response from the climate system in the North Atlantic, which is the primary domain of interest for this study. In conclusion, we infer that the modifications induced by smoothing South China Sea and Indonesian bathymetry mid-run are minor and do not impact the main findings of the study.

2.13 Supplementary Information - Spectral analysis of the oscillating simulations

Averaging model outputs over time, whether it is by using running means or taking snapshots, is a useful tool for assessing the main trends of a simulation. The downside is that we lose information on the dynamics and variability that are shorter/faster or of comparable duration to the length of the averaging period. Because our aim is to focus on millennial-scale variability only, we here propose a method based on spectral analysis.

Fourier theory, implemented in the Scilab Python project, allows for calculating the harmonics and the Power Spectral Density (PSD) of a time series. By applying that method to the simulated time series of Greenland temperatures at the NGRIP site, we derive a spectrum for each *oscillating* and *cold* simulations in 2.4*c*. Note that the mean value of the signals were subtracted before calculating the PSD to compensate the offset from the fixed component (at $0Hz$). The amplitude of the harmonics corresponds to the most significant frequencies in the time series' signals. The frequencies of millennial-scale variability peak around $10^{-3}\,yrs^{-1}$ (corresponding to a period of $1000\,yrs$), while the frequencies associated with inter-annual variability are higher around $1\,yrs^{-1}$. In *oscillating simulations*, we do indeed observe a clear dominant periodicity of about a thousand years, which corresponds to frequencies previously estimated from Figure 2.3. On the other hand, *18.2k* does not display such a significant peak in the Fourier space and cannot, therefore, be considered as quasi-oscillating. In order to only conserve millennial-scale events and filter inter-annual signal, we decided to apply a first-order low pass filter calibrated with a cut-off frequency of $2 \times 10^{-3}\,yrs^{-1}$ (corresponding to a period of $5000\,yrs$). This is slightly higher than the dominant frequency of the *oscillating simulations* in order not to lose the information contained in the smaller secondary peaks, mainly observed in *17.8k*. This cut-off frequency, and consequently the filters, are the same for every simulation. The resulting filtered signals are shown by Figure 2.4*b*.

Compared to the NGRIP temperatures running mean series of Figure 2.3*c*, Figure 2.4*b* provides a clearer view of the main features of our time series and neither the periodicity of the signals nor the range of temperatures are significantly altered. Nonetheless, we still note a smoothing during sharper climate changes, where some information contained in higher frequencies may have been obscured by the processing. For example, we do not observe the overshoots at the onset of some warm phases in the filtered signals, and the most extreme warming/cooling rates are also damped.

This spectral analysis is useful for quantitatively assessing *oscillating simulations* with dominant frequencies around a thousand years, but fall short of providing useful information for lower dominant frequencies. For instance, the algorithm does not capture the longer periodicity (of a few thousand years) of *18.2k*. This is because Fourier transforms require a sufficient number of cycles to compute robustly. Hence, our algorithm does not

have enough material to establish either way whether the *18.2k* simulation is slowly oscillating, or showing other behaviour such as a complex permanent recovery. Similarly, but more extreme, the absence of a periodic signal in the *warm simulations* prevents the Fourier analysis from being correctly handled, and their responses were therefore not included in this analysis.

For all the stated reasons, we emphasise that it is not appropriate to use the frequency analysis alone to understand our simulations. Instead, we utilise such an approach to complement the running-mean analysis, contributing an objective quantification of cyclical behaviour to identify oscillations, determine the main frequencies of the millennial-scale variability, and isolate the typical features within our experiments. It also helps to clarify the dynamics of the simulations, which is useful for understanding the behaviours depicted by Figure 2.6.

2.14 Supplementary Information - Definition of warm and cold composite modes

In order to accurately characterise the simulations in this study, it is useful to be able to analyse aggregate features of the cold and warm climate modes, e.g. as presented in Figures 2.5. The intricate climate response of the meltwater simulations makes it difficult to adopt an objective definition that is commonly applicable to all simulations of cold and warm modes. A simple approach could be to define a fixed period of time before, after or spanning either side of the coldest/warmest points of the time series. However, this relatively unintelligent algorithm would be heavily susceptible to biases. For example, the warm modes could be biased towards the overshoot during the recovery phase, and the cold modes by the initial transition to a weak AMOC stage. Trying to widen the time spans to avoid this would result in the inclusion of the transition times. A further consideration is that the results need to be consistent between the NGRIP temperatures and the AMOC index time series despite the small lag between the two.

In light of these remarks, six different methods were tested to design the optimal algorithm for identifying the composite data for the cold and warm modes in our simulations, as depicted in Figures 2.18 and 2.19. *Method 1* defines the warm and cold modes as the highest and lowest thirds of the 30-year running mean AMOC index time series. *Method 1b* is similar, only it defines the warm and cold modes on the *filtered* time series of the AMOC index. *Method 2* defines the warm and cold modes as the highest and lowest thirds of the 30-year running mean NGRIP temperature time series. *Method 3* defines the warm and cold modes as the highest and lowest quarters of the 30-year running mean AMOC index time series, excluding the first 1000 years for all experiments except *21.5k* and *21k* to define the quarters; *20.7k*, *19.4k*, *18.2k* and *17.8k* generally show better consistency after the first 1000 years, excluding their adjustment to the initial meltwater perturbation,

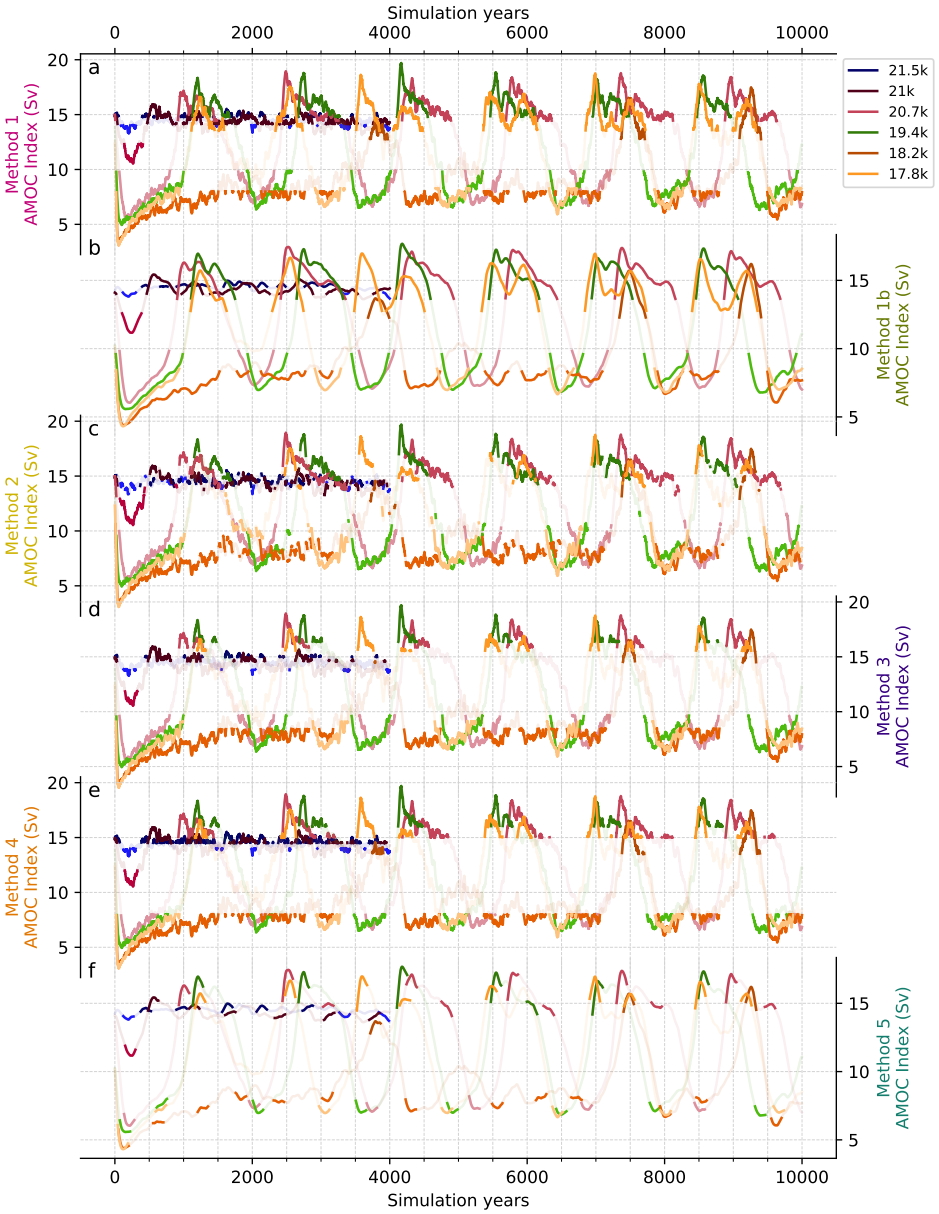

Figure 2.18: **Definition of composite modes on AMOC index.** Depiction of the constituent data (here, showing the AMOC index; max Atlantic overturning circulation at 26.5° N) for the warm and cold climate phases arising from the different methods for creating the composite warm and cold modes analysed in the main article (introduced in section 2.4). Panels *a*, *c*, *d* and *e* used 30-year running-mean of the AMOC index time series. Panels *b* and *f* used the filtered AMOC index time series as described in section 2.13. See Section 2.14 text for the detail of the different methods.

.

which has a strong early impact in these simulations. In *Method 4*, we manually defined the warm and cold limits for each simulation to visually fit what looks like a warm or cold period from the 30-year running mean AMOC index time series. *Method 5* defines the warm modes as the 150 year period centred around the maximum of the filtered AMOC time series and the cold modes as the 150 year period centred around the minimum of the AMOC time series. The maximum and minimum have to be spaced 500 years apart and in the highest/lowest thirds and concave/convex for warm/cold modes.

Comparing the effects of each algorithm on the zonal mean anomalies in Figure 2.20, we observe consistent behaviours during cold modes and slightly more variability in warm modes despite showing similar zonal mean patterns. *Method 3* returns a stronger AMOC in both cold and warm modes of the oscillating and slow-recovery simulations, with the lowest sea ice cover in warm modes. *Method 2* also tends to simulate warmer weak modes of the oscillating and warm experiments. *Method 1* and *Method 5*'s definition of warm modes is too broad in the warm simulations, leading to $1°C$ cooling of the warm modes. A significant amount of the transition times in cold modes are included in *Method 1* and *Method 3*. Finally, we do not recommend using the filtered time series for non-oscillating simulations as they create artefacts in the NGRIP time series that affect the modes-selection algorithm, which rules out methods Method 1b and *Method 5* from being useful.

Method 4 is the only approach not to present any strong irregularities in the composite warm/cold modes. Although it relies on a visual identification, which could induce bias, the results always rank within the mean behaviour in zonal mean anomalies. The method is simple, but provides the required information needed for the analysis. It is the algorithm that best filters-out the transition periods between the cold and warm phases, and it has the advantage of being easily adaptable and applied to all six simulations. It is, therefore, the algorithm we adopted for this study.

We note that when the amplitude range is small compared to the running mean variability, some time slices may end up being assigned to the wrong mode by the chosen categorisation method (*Method 4*). This is the case for *21.5k* in both warm and cold modes and for *21k* in the warm mode. We decided to exclude them from the analysis presented in Figure 2.5.

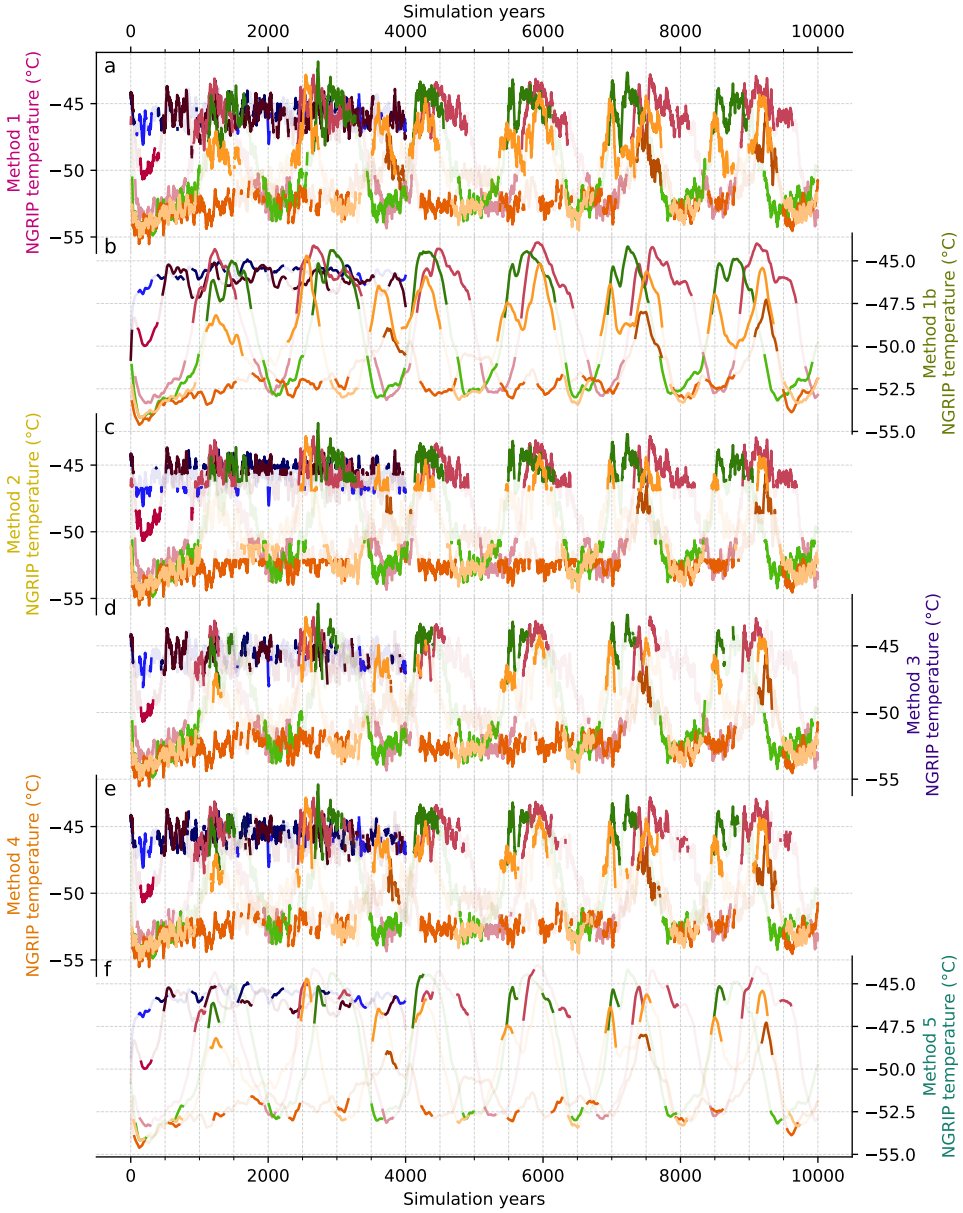

Figure 2.19: **Definition of composite modes on Greenland surface air temperature.** Depiction of the constituent data (here, showing the NGRIP surface air temperature, 42.32° W, 75.01° N) for the warm and cold climate phases arising from the different methods for creating the composite warm and cold modes analysed in the main article (introduced in section 2.4). Panels *a*, *c*, *d* and *e* show the 30-year running-mean of the NGRIP temperature time series. Panels *b* and *f* show the filtered NGRIP temperature time series as described in section 2.13. See 2.14 text for the detail of the different methods.

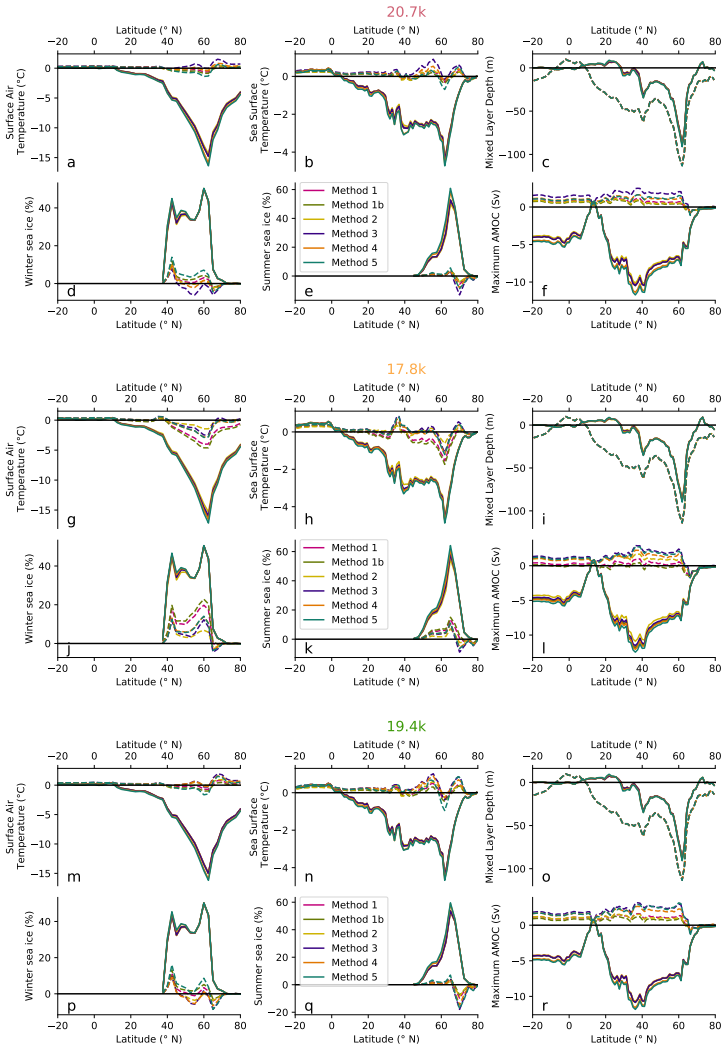

Figure 2.20: **Zonal means depending on composite mode method.** Composite warm and cold modes mean zonal anomalies between the meltwater simulations and the reference state in the Atlantic (70° W – 10° E). Solid lines are cold modes and dashed lines are warm modes, which have been compiled using the five methods described in the text (section 2.14). Panels show the zonally averaged surface air temperature, sea surface temperature, mixed layer depth, winter sea ice concentration, summer sea ice and maximum overturning circulation flow over the water column for the different methods and applied to three simulations corresponding to the three different clusters identified in section 2.4. Figures 2.18 and 2.19 highlight the constituent data for the warm and cold modes identified by each method.

2.15 Supplementary Information - Intertropical Convergence Zone (ITCZ) index

The Intertropical Convergence Zone (ITCZ) index (Figure 2.3) was inspired by the work of Braconnot et al. (2007) and Singarayer et al. (2017) and corresponds to the mean northern limit of the ITCZ. It was calculated following equation S3, where $lat(pr_{max})$ is the latitude of the maximum zonally averaged precipitation, pr ($kg\,m^{-2}\,s^{-1}$). Compared to Singarayer et al. (2017), we computed the mean latitude instead of the maximum latitude of the rainbelt to gain a better view of the global displacement of the ITCZ.

$$ITCZ_{index} = mean(\frac{\sum_{y=lat(pr_{max})}^{35°N} pr(lon,y)lat(y)}{\sum_{y=lat(pr_{max})}^{35°N} lat(y)}) \tag{S3}$$

2.16 Supplementary Information - Locating the centre of mass

The lontitude and latitude of the centre of mass of a value $V(lon, lat)$ (used in section 2.6 and Figure 2.6) is defined in equation S4. For the sake of simplicity, the volume of each grid cell was not considered in this definition.

$$[lon_{COM}, lat_{COM}]_V = \frac{\sum_{i,j} V(i,j)[lon(i), lat(j)]}{\sum_{i,j} V(i,j)} \tag{S4}$$

Chapter 3

Simulated glacial millennial-scale variability driven by a coupled inter-basin salt oscillator

Abstract

The climate of the last glacial period ($\sim$ 115 to 12 thousand years before present) recorded a strong millennial-scale variability including Dansgaard-Oeschger (D-O) events. D-O events are recurring transitions between cold and warm climates where North Atlantic temperatures can change by up to 16° in a few decades. Switches in regimes of the Atlantic Overturning Meridional Circulation (AMOC) are believed to play a crucial role, but the exact mechanisms behind AMOC mode switches are still poorly understood.

This Chapter introduces a new mechanism to explain the millennial-scale variability observed in HadCM3 general circulation model simulations forced with snapshots of deglacial meltwater history. The oscillator is composed of two components: a fast North Atlantic component driven by changes of stratification in deep water formation sites and a slow global component where a salt anomaly is transported between the Atlantic and the Pacific basins. The AMOC plays the coupling agent between the two components.

The right background conditions and freshwater input combination are necessary to kick-start both oscillator components. If one of the components is not activated, the climate system will stabilise in one of the warm or cold modes. This mechanism shares similarities with the existing literature and provides a general framework to understand abrupt climate changes in general circulation models.

3.1 Introduction

North Atlantic climate records of the last glacial period are dominated by millennial-scale variability (Wolff et al., 2010) such as Dansgaard-Oeschger (D-O) events (Dansgaard et al., 1993; Bond et al., 1993). D-O events consist of irregular pseudo-oscillations between cold *stadial* states and warm *interstadial* states with recorded temperature changes in the Greenland ice cores of up to $16°C$ (Huber et al., 2006; Kindler et al., 2014; Buizert et al., 2014) in only a few decades (Rasmussen et al., 2014). Abrupt climate changes have been widely associated with changes in the Atlantic Meridional Overturning Circulation (AMOC Rahmstorf, 2002; Clark et al., 2002), primarily because the AMOC can exist in more than one stable mode: a *warm* mode where a vigorous AMOC reaches high latitudes and the North Atlantic Deep Waters (NADW) can go as deep as 5000 meters, a cold mode where a shallower AMOC does not extend past the Greenland-Iceland-Scotland (GIS) ridge, and an off mode where the AMOC has collapsed (Böhm et al., 2015). Modern days measurements along the RAPID array at 26.5° N (Frajka-Williams et al., 2019) estimated that a strength of the AMOC of $\sim 17Sv$ with a northwards meridional heat transport of $1.25PW$ (McCarthy et al., 2015). The AMOC is believed to have shifted between its different modes during the last glacial period (Broecker et al., 1985; Weijer et al., 2019), and such shifts to have disrupted the flux of heat and salt into the North Atlantic. These shifts may have modified the climate in this region, but the extent of their impact is nonetheless disputed. This is because both the wind-driven subpolar gyre, reaching up to $50Sv$ in the North Atlantic (Jungclaus et al., 2013), and atmosphere circulation, transporting $\sim 5PW$ into the North Atlantic (Seager et al., 2002; Wunsch, 2006), are the primary source of North Atlantic energy.

Because of our lack of understanding of its dynamics, a future collapse of the AMOC in response to climate change remains highly uncertain, but its impact would be dramatic (Armstrong McKay et al., 2022). CMIP6 models tend to simulate a weakening of the AMOC in 2100 compared to present day, but the projections range between a $2Sv$ drop to a complete collapse of the AMOC (Bellomo et al., 2021). Modern measurements of the North Atlantic overturning circulation (Frajka-Williams et al., 2019; Danabasoglu et al., 2021) are still too short to draw any statistically significant conclusion on potential shifts in the AMOC regime (Jackson et al., 2022; Lobelle et al., 2020). On the other hand, fingerprints of AMOC changes observed in ocean variables such as sea surface and subsurface temperatures and density gradients, warn about the possible approach of a tipping point for the AMOC (Thornalley et al., 2018; Boers, 2021; Michel et al., 2022).

Climate simulations in glacial conditions, and in particular around the last glacial maximum – about 21 ka BP (thousand years ago) – and marine isotope stage 3 – about 60 ka BP to 30 ka BP – have proven to be an essential tool to study AMOC stability, a review can be found in Weijer et al. (2019). General Circulation Models (GCMs) tend to be

more biased towards more stable climates (Valdes, 2011; Mecking et al., 2017; Liu et al., 2017), contrary to Earth systems Model of Intermediate Complexity (EMICs) (Kageyama et al., 2010). In the past decade, the palaeo-modelling community addressed this issue by further exploring the parameter space. As a result, GCMs have become more numerous to show millennial-scale variability in the past decade (e.g. Peltier and Vettoretti, 2014; Brown and Galbraith, 2016; Klockmann et al., 2018; Zhang et al., 2021; Armstrong et al., 2022; Kuniyoshi et al., 2022), and these oscillations were obtained with a wide range of background conditions, forcing and model parametrisation (Malmierca-Vallet et al., 2023).

Following the definition of Barker and Knorr (2021), we call the window of opportunity the region in the parameter space where millennial-scale variability can occur. The parameters influencing the window of opportunity can be evaluated from climate models. The extensive ice sheets covering North America and northern Europe during the last glacial maximum (Hughes et al., 2016; Batchelor et al., 2019) can affect the location of the window of opportunity and it is generally easier to trigger transitions with smaller ice sheets (Zhang et al., 2014; Brown and Galbraith, 2016; Klockmann et al., 2018). A more extensive ice sheet cover increases the North Atlantic winds and forces a more southern, less variable jet stream (Merz et al., 2015; Li and Born, 2019). Such changes in the atmospheric circulation can, in turn, have consequences on the AMOC (Czaja, 2009) and the salt and heat transported by the subpolar gyre (Montoya et al., 2011; Li and Born, 2019). The topography and the albedo of the ice sheets also modify the energy balance at the surface and the inter-hemispheric heat fluxes (Roberts and Valdes, 2017). On the other hand, larger ice sheets tend to release more meltwater that can isolate the subsurface waters and reduce the mixing, eventually weakening the AMOC when the water is targeted at critical deep water formation sites such as the Nordic Seas (Smith and Gregory, 2009; Roche et al., 2010). The extent of this effect is still discussed (Birchfield et al., 1994; Bethke et al., 2012). Lastly, atmospheric CO_2 concentrations (Brown and Galbraith, 2016; Zhang et al., 2017; Klockmann et al., 2018; Vettoretti et al., 2022) and insolation (Zhang et al., 2021; Kuniyoshi et al., 2022) have very likely played a primary role in creating suitable conditions for abrupt climate change by changing subsurface North Atlantic stratification.

The mechanisms behind millennial-scale variability remain an open question. There is a consensus on the role of multi-modality of the AMOC since Stommel (1961)'s early box-model. The processes leading to switches between the different modes, however, are elusive. Broecker et al. (1990) introduced the salt oscillator theory, stating that feedback between salt advection, evaporation and convection in the Atlantic could produce regular transitions. This mechanism depends on the sign of the net salt export out of the Atlantic (Drijfhout et al., 2011) and requires an initial perturbation to start the oscillator. In GCM simulations, it is still unclear whether the model's salt oscillator behaviour is a driver of or a response to millennial-scale variability (Peltier and Vettoretti, 2014; Klockmann et al., 2020; Kuniyoshi et al., 2022). Spontaneous oscillations in a simple mixed-layer model

were demonstrated by Welander (1982), and Cessi (1996) argued that a freshwater input could kick-start this oscillator. In climate models, freshwater hosing experiments have historically been an effective way to trigger abrupt climate changes – reviews can be found in Kageyama et al. (2010) and Kageyama et al. (2013b). Colin de Verdière (2007) proposed that both the salt-oscillator theory and the vertical oscillations can work in concert to produce the glacial millennial-scale variability.

The mechanisms proposed by GCMs consist of a combination of the theoretical processes presented above. Vettoretti and Peltier (2018) explained the periodic cycle of Peltier and Vettoretti (2014) by a salt oscillator linked to the interplay between North Atlantic sea ice and convection. The salt oscillator is also at the centre of Armstrong et al. (2022)'s theory, only this time it is winds and meridional and density gradients that act on the North Atlantic convection. The role of the SubPolar Gyre (SPG) is the cornerstone of Li and Born (2019)'s theory and its influence is observed in Klockmann et al. (2018). In Klockmann et al. (2020), they argue that wind-driven or density-driven feedback between the AMOC and the SPG can result in positive and negative coupling, respectively. Kuniyoshi et al. (2022) also observes the effect of the subpolar gyre, but in their case, the mechanism is heat-driven rather than salinity-driven. Similar observations were made by Brown and Galbraith (2016), and thermal control of millennial-scale variability was already widely discussed (Oka et al., 2012; Dokken et al., 2013; Bassis et al., 2017; Oka et al., 2021). One common bias of these theories is that they focus on the Atlantic and, more precisely, the North Atlantic processes. Weijer and Dijkstra (2003) argues that a salinity anomaly propagates along the different ocean basins and sets the oscillations' pace. The Southern Ocean has been identified as a potential critical region to understand the coupling mechanism (Knorr and Lohmann, 2003; Banderas et al., 2015; Buizert and Schmittner, 2015; Thompson et al., 2019; Oka et al., 2021) and the contribution from other ocean basins is also considered (Nuber et al., 2023).

The Hadley Centre Climate Model 3, also known as HadCM3 (Valdes et al., 2017), is one of the models that can simulate abrupt climate changes. Signs of AMOC modes transition were reported in response to freshwater forcing (Matero et al., 2017; Ivanovic et al., 2018a), but only recently did two independent experiments manage to observe climate pseudo-oscillations: Chapter 2 triggered oscillations using deglacial meltwater patterns in a last glacial maximum background and Armstrong et al. (2022) for a specific snapshot in marine isotope stage 3 conditions. This Chapter describes the processes at stake for the Chapter 2 simulations and explores how they connect to the other mechanisms published. The first section presents the experimental design of the simulations. The second section summarises the results and terminology introduced in Chapter 2. The third section portrays the changes in stratification in the North Atlantic convection sites. The fourth section describes the global salt motion. The fifth section introduces the mechanism and the tendencies analysis. The sixth section analyses how this mechanism applies to the

non-oscillating simulations. Lastly, the seventh section discusses the stability of AMOC in general circulation models.

3.2 Methods

3.2.1 HadCM3 general circulation model

All the simulations in this paper used the BRIDGE (Bristol Research Initiative for the Dynamic Global Environment group) version of the HadCM3 (HadCM3B) atmosphere-ocean general circulation model put together by Valdes et al. (2017). The atmosphere model, described by Pope et al. (2000), consists of a 2.5° x 3.75° grid on 19 elevation levels. The ocean model, described by Gordon et al. (2000), is a 1.25° x 1.25° grid on 20 depth layers. In order to verify the equation of state (Bryan and Cox, 1972; Fofonoff and Millard Jr, 1983; Fofonoff, 1985), the ocean model uses a rigid surface lid (Gordon et al., 2000), meaning that the ocean volume stays constant throughout the simulations. On top of the ocean and atmosphere components are included the MOSES 2.1 land model (Cox et al., 1999), and the TRIFFID dynamic vegetation model (Cox, 2001). The land-sea mask matches the ice sheet reconstruction. The Gibraltar Strait is closed during the LGM, and Mediterranean salt and heat exchanges are parametrised by a diffusive pipe (Ivanovic et al., 2014). HadCM3B was optimised for multi-millennial palaeoclimate runs (Valdes et al., 2017) and has been used for meltwater forced simulations by Ivanovic et al. (2018a) and in Chapter 2.

3.2.2 Global salinity target

Because HadCM3 uses a rigid lid ocean model, the hydrological budget is not closed, and salinity drifts of the order of $0.25 PSU.kyr^{-1}$ can occur (Dentith et al., 2019b). When freshwater is discharged in the model, it is implemented not as a physical input of water but as a change of the surface layer salinity. An input of meltwater can drive a significant decrease in salinity comparable to that observed during the last deglaciation, which is not the aim of this set of simulations. Global salinity increase can also be observed if the model is biased towards higher evaporation than precipitation, leading to salt accumulation in the tropical oceans. To tackle this issue, we keep the global mean salinity constant by applying a correction to the entire volume of the ocean, compensating for drifts in ocean salinity – this corresponds to the $VFLUX$ method described by Dentith et al. (2019b). The salinity target is calculated to account for the change in ice volume in the ice sheet reconstruction between a given time step and the present, technically, 1950 CE (Common Era). This way, it prevents the continued freshening of the global ocean during the long integration. The salinity target is calculated to account for the change in ice volume only but is not directly linked to the freshwater input. It is implemented at the start of each simulation, and a spin-up phase where the model adjusts to the new salinity forcing can

be observed in the initial years.

3.2.3 Experimental design

The simulations in this paper, presented in Table 3.1, are branched from the *CTRL* (or *control*) simulation at year 0. The *control* simulation is a Last Glacial Maximum (LGM) run following the PMIP4 protocol for 21 ka BP for the boundary condition (greenhouse gas concentrations, orbital parameters and solar constant Kageyama et al., 2017). We used the GLAC-1D (Tarasov and Peltier, 2002; Tarasov et al., 2012; Briggs et al., 2014; Ivanovic et al., 2016) ice sheet reconstruction and the corresponding land-sea mask, orography and bathymetry. It extends to the spin-up realised in previous HadCM3 last glacial maximum simulations (Davies-Barnard et al., 2017). Its start year will be the year 0 in our time series.

Table 3.1: **Experiments summary.** All experiments were designed with LGM boundary conditions, using the LGM GLAC-1D ice sheet extent and associated geographies. The *meltwater* entries indicate the meltwater snapshot used (see Section 3.2.3) and the total meltwater flux. The meltwater flux only corresponds to the freshwater from the ice sheet melting and does not include the other freshwater fluxes (e.g. precipitation, sea ice, etc.). The *Salinity Target (PSU)* entries are the global salinity target used for the salinity correction described in Section 3.2.2. *Tendencies* indicates if the salinity tendencies diagnostic described in 3.9 were included.

Simulation name	Meltwater snapshot *Meltwater flux (Sv)*	Integration length (years)	Salinity Target (PSU)	Tendencies (included)
CTRL	None	4,000	35.8334	No
20.7k	20.7 ka BP *(0.084)*	10,000	35.8225	No
21k	21 ka BP *(0.054)*	4,000	35.8334	No
18.2k	18.2 ka BP *(0.109)*	10,000	35.7348	No
20.7_tdc	20.7 ka BP *(0.084)*	4,000	35.8225	Yes
20.7_no_gst	20.7 ka BP *(0.084)*	3,000	None	No

The main focus of this Chapter will be the *20.7k* simulation described in Chapter 2. The *20.7k* simulation differs from *CTRL* by the addition of a constant meltwater discharge derived from the 20.7 ka BP slice of GLAC-1D ice sheet history following the protocol introduced in Section 2.10. This protocol computes freshwater discharges from changes in the ice sheet elevations at each time step and, for each grid cell, routes them to an ocean grid cell using an offline drainage map of the last glacial maximum (Wickert et al., 2013) and spreads the meltwater across a wider (proximal ocean) region around the point source. The snapshot is then extracted for the year 20.7 ka BP of the resulting dataset and used as a constant forcing for 10,000 years. We also modify the global salinity target corresponding to the ice volume at the time of the snapshot, in this case, $35.8255 PSU$.

To get a more precise picture of the ocean dynamics in our simulations, we repeated the

20.7k simulation for 4,000 years, saving an extra set of salinity diagnostics, or salinity tendencies, in the model output. This simulation is called *20.7k_tdc*. Armstrong et al. (2022) introduced the HadCM3 tendencies diagnosis and includes a comprehensive description of the implementation. We summarise the essential information in Section 3.9.

Additional simulations from Chapter 2 were also included for comparison. The *21k* simulation used the meltwater snapshot corresponding to 21 ka BP, a global salinity target of $35.8334PSU$ and was run for 4,000 years. The *18.2k* simulation used the meltwater snapshot corresponding to 18.2 ka BP, a global salinity target of $35.7348PSU$ and was run for 10,000 years. At last, we investigated the impact of the global salinity target by running a simulation with the salinity correction algorithm turned off. This simulation, called *20.7k_no_gst*, used the same meltwater snapshot as *20.7k* and was run for 3,000 years.

3.2.4 Anatomy of the simulations

In Chapter 2, the *20.7k* simulation was characterised as an *oscillating* simulation due to the periodic alternation of 'warm' – vigorous AMOC with relatively warm North Atlantic temperatures – and 'cold' – weak AMOC with rather cold North Atlantic temperatures – modes observed in its AMOC index time series in Figure 3.1*a*. In this experiment, we do not aim to reproduce D-O events and will therefore avoid using the 'stadial'/'interstadial' terminology (e.g. Thomas et al., 2009; Lohmann and Ditlevsen, 2019). Nonetheless, it can be helpful to think of warm and cold modes in the light of interstadials and stadial states.

To identify the different configurations of the system, we look at its path in the phase space formed by the Mixed Layer Depth (MLD) – an indicator of the mixing and convection – in the Greenland, Iceland, Nordic Seas (GIN Seas) and in the Irminger Sea as plotted in Figure 3.1*b*. A detail of the zones is given in Figure 3.14*b*. In this phase space, we manually define five distinct *modes* or *phases*. The *cold* mode, where convection at high latitudes is weak; the *meridional warm* mode (or simply *meridional* mode) with a main convection region in the GIN Seas and intermediate convection in the Irminger Sea; the *zonal warm* mode (or simply *zonal* mode) dominated by convection in the Irminger Sea and low convection in the GIN Seas, the *warming* phase, a transition from a *cold* mode to any *warm* mode and the *cooling* phase from any *warm* mode to a *cold* mode. Each mode was assigned a colour, and colour bars will be added to time series plots in this Chapter in the style of Figure 3.1*a*. The transition between the *meridional* and the *zonal* modes is not distinguishable enough in this paper's simulations to be considered a separate phase.

The *20.7k* simulation evolves along a well-defined cycle. After an initial drop to a *cold* mode, it starts by *warming* from the *cold* mode to the *meridional* mode, switching to the *zonal* mode before *cooling* back to the *cold* mode. The system always travels through this precise cycle in the same order with a periodicity of about 1,540 years (see Chapter 2,

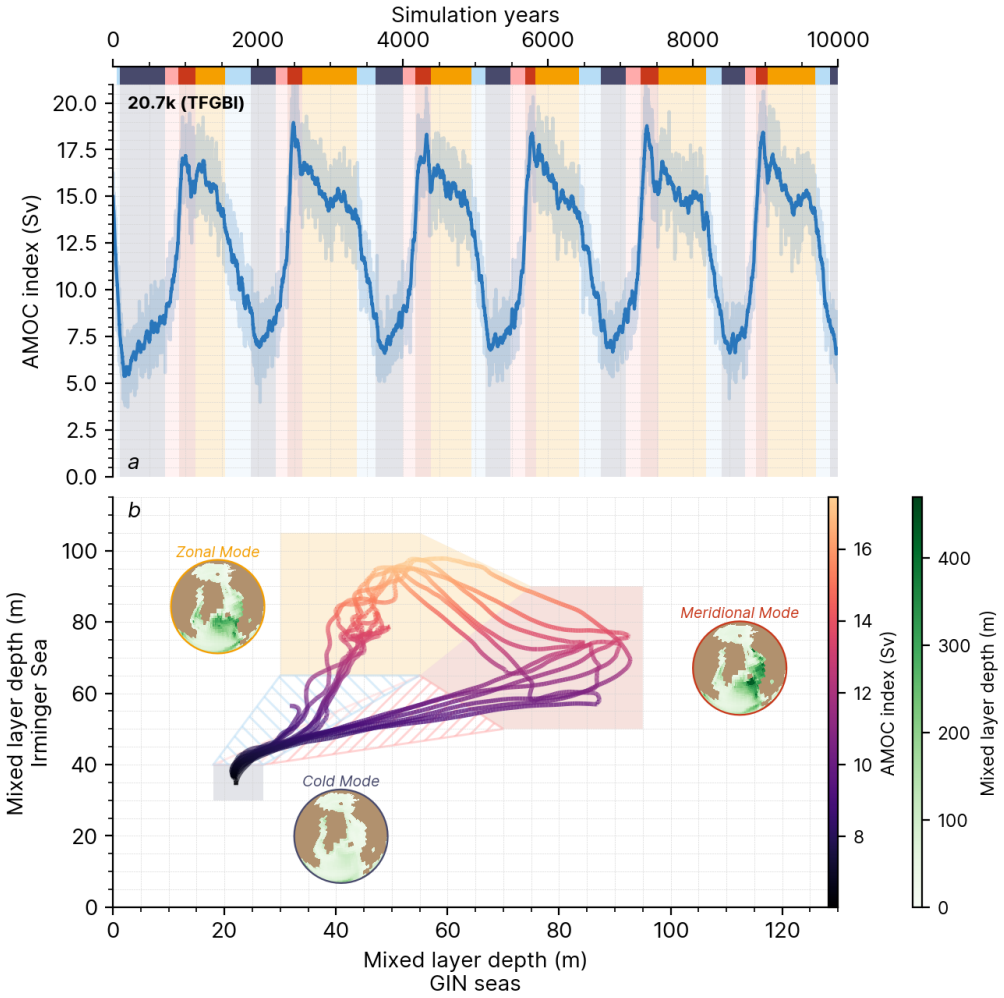

Figure 3.1: **Anatomy of the simulations**. *a* Timeseries of AMOC index (maximum overturning circulation at 26.5° N) in the *20.7k* simulation. The background colour bars indicate the phases with *cold* in dark blue, *warming* in pink, the *meridional* in red, *zonal* in orange and *cooling* in light blue. *b*. Phase space (i.e. scatterplot) of the annual mean mixed layer depth in the Greenland Iceland Nordic (GIN) seas against the mixed layer depth in the Irminger Sea (the zones are defined in Figure 3.14*b*). Each point is the yearly data from simulation *20.7k* processed by a low-pass filtered time series with a cut-off frequency of $10^{-4}yr^{-1}$ – described in detail in Section 2.13. Shaded boxes define the phases shown in panel *a*. In the small globes, the composite means mixed layer depth are plotted for the *cold* and the two *warm* modes.

Table 2).

We split the other simulations of Table 3.1 into similar phases. The definitions of the modes are identical across the simulations, but the spans in the phase space are slightly different from one to another. We reproduce Figure 3.1 for the *18.2k*, *21k*, *20.7k_no_gst* and *20.7k_tdc* in Figure 3.15. The *CTRL* simulation is at equilibrium in a *zonal* mode. *21k* provides an example of a *warm* simulation – a brief multi-centennial *cold* mode drop followed by a recovery into a stable *zonal* mode – and *18.2k* provides an example of a *cold* simulation – a base *cold* mode only interrupted by apparently erratic and short-lived recovery episodes into a *meridional mode*. *20.7k_no_gst* follows one oscillatory cycle before stabilising in a *zonal* mode. Even though *20.7k* and *20.7k_tdc* are effectively the same experiment, the noise introduced during the initial reconfiguration results in slight differences in the periodicity and the shape of the oscillations. We consider the differences between *20.7k* and *20.7k_tdc* to be small enough for the analysis on one to be valid for the other.

3.3 Changes in oceanic conditions in the North Atlantic

We need to understand the dynamics of the deep water formation sites in the North Atlantic to explain the AMOC mode changes. This section details the evolution of the key convection regions in the *20.7k* simulation plotted in Figure 3.2. Since the first cycles are adjusting to the initial perturbation, we focus our analysis on the last five thousand years of the simulation. For better readability, the complete time series, including temperature and salinity profiles, as well as the Labrador Sea and the Arctic deep water formation sites, were not included in Figure 3.2 and plotted in Figure 3.16. The behaviour of the GIN Seas is broadly the same as the Arctic, and the Irminger Sea the same as the Labrador Sea but with a $\sim$ 200 years delay. In the rest of the analysis, we split the water column into three depth regions fitted on the model depth coordinates. The *upper* or *subsurface* depths designates the waters between 5 to 550 meters deep, the *intermediate* depths the waters between 550 and 1800 meters deep, and the *lower* or *deep* depths the waters between 1,800 to 5,500 meters deep.

During the *cold* modes, the North Atlantic subpolar gyre and deep water formation (diagnosed through mixed layer depth) are at their weakest (Figure 3.2*d-f*). Winter sea ice extends down to the Iceland Basin (this region includes the waters west of Ireland and France), and the Nordic seas are covered by ice all year long (Figure 3.2*a-c*). The upper density increases in the Irminger Sea and the Iceland Basin and remains constant in the GIN Seas (Figure 3.2*j-l*). This is because the increase of North Atlantic subsurface salinity (Figure 3.16*p-t*) is only fully compensated by subsurface warming in the GIN Seas (Figure 3.16*k*). In the deep GIN Seas, the density decreases following the warming and the freshening of the water mass (Figure 3.16*k,p*).

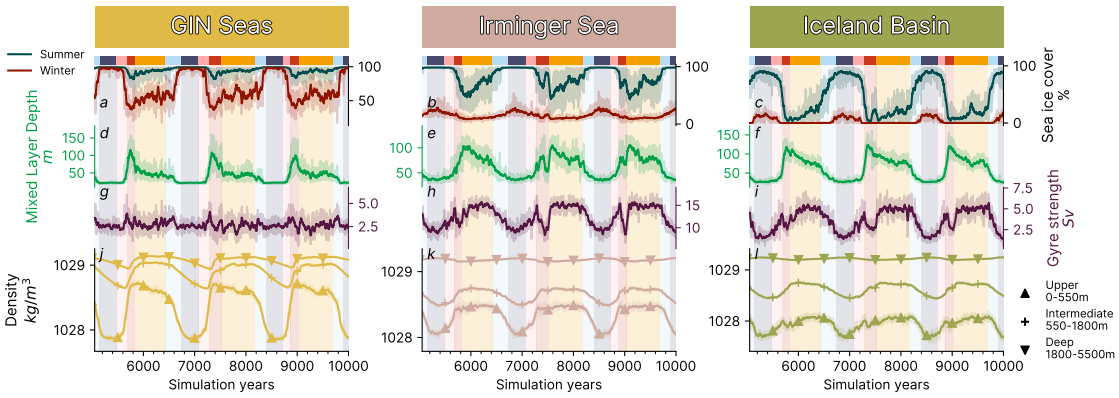

Figure 3.2: North Atlantic dynamics at key deep water formation sites in *20.7k* in the GIN Seas (*a,d,g,j*), the Irminger Sea (*b,e,h,k*) and the Iceland Basin *c,f,i,l*. The zones are defined in Figure 3.14, and the shading is plotted according to Figure 3.1. *a-c.* Winter (March) and Summer (September) sea ice concentration. *d-f.* Annual mean mixed layer depth. *g-i.* Annual mean anti-clockwise barotropic stream function indicating gyre circulation strength. Solid lines indicate 30-year running means, and shaded bands indicate annual means. *j-l.* Annual mean density in the upper, intermediate and deep depth slices.

At the onset of the *warming* phase, sea ice retreats northwards in the North Atlantic (Figure 3.2*a-c*). The subpolar gyre intensifies (Figure 3.2*h,i*) and brings salty waters to the North Atlantic (Figure 3.16*p-t*). At the same time, the heat accumulated in the upper waters is released (Figure 3.16*k-o*) and the subsurface density increases in the three regions (Figure 3.2*j-l*).

At the end of the warming phase, deep water formation resumes in the GIN Seas and in the Iceland Basin (Figure 3.2*d,f*), marking the start of the *meridional* phase. This phase does not lead to a significant reactivation of the Irminger deep water formation site as the subpolar gyre remains weak (Figure 3.2*e,h*). The upper density stabilises around high values in the North Atlantic (Figure 3.2*j-l*). The deep waters density increases in the GIN Seas as the water column is homogenised (Figure 3.2*j*) and observe a slow decrease in the Irminger Sea and the Iceland Basin (Figure 3.2*k,l*).

A switch to the *zonal* mode happens when the subpolar gyre intensifies and starts to expand westward (Figure 3.2*h,i*). The convection halves in the GIN Seas and increases in the Irminger Sea, which now has open waters in winter (Figure 3.2*b,c,e,f*). In the Irminger Sea and the Iceland Basin, the upper density remains constant (Figure 3.2*k,l*) by the combined effect of a reduction in salinity and temperatures (Figure 3.16*l,m,q,r*). The subsurface heat being already evacuated in the GIN Seas, the upper density decreases (Figure 3.2*j*). The deep density tends to increase in the Irminger Sea and in the Iceland Basin (Figure 3.2*k,l*). A gradual decrease in mixed layer depth is also observed in these two regions (Figure 3.2*e,f*).

The slowdown in deep water formation accelerates during the *cooling* phase (Figure 3.2*d-*

f). The subpolar gyre shrinks (Figure 3.2*g-i*), and the upper and intermediate density decrease in the North Atlantic (Figure 3.2*j-l*). This is due to salinity loss and warming at these depths (Figure 3.16*k-t*). In the lower waters, density continues to increase in the Irminger Sea and the Iceland Basin and starts to decrease in the GIN Seas (Figure 3.2*j-l*). When the deep water formation is switched off in the North Atlantic, the system returns to the *cold* mode.

The deep water formation in the North Atlantic depends on the water column stratification at the deep water formation sites. Stratification changes are due to the dynamic evolution of water temperature and salinity. The thermal effect is primarily due to sea ice cover: heat is accumulated when the region is covered in sea ice and evacuated when it is ice-free. Vertical salinity exchanges are insufficient to explain the salinity changes at deep water formation sites. A deeper analysis of the salt exports in and out of the North Atlantic is necessary.

3.4 An inter-basin salt oscillator

Observing the global transportation of salt is necessary to understand the fluxes coming in and out of the North Atlantic. When investigating the density of the seawater, the mean salinity is the primary variable to consider. The most significant changes in mean salinity happen in the North Atlantic and Arctic basins (Figure 3.17). However, in order to track the pattern of global salt transport, salinity budgets are more suitable (Figure 3.18). The budget signal is muted in the North Atlantic and the Arctic oceans because of the relatively small size of the basins, and the largest salt exchanges are between the subtropical Atlantic, the Pacific, the Indian and the Southern oceans (the zones are defined in Figure 3.14). Figure 3.3*a,b* summarises the global absolute and mean salinity exchanges. The detailed salinity budget in each basin's upper, intermediate and deep waters reveals consistent behaviours across the different basins. These behaviours were summarised by grouping the different water masses in *domains* in Figure 3.3*c-e*. To understand the relationship between inter-basin salt transport and AMOC, cross-correlations between salt budgets at each depth region and the AMOC index from Figure 3.1*a* were calculated. Four *domains* can be identified, characterised by similar profiles in the cross-correlation figure (Figure 3.1*c-e*, Figure 3.19*d,h*).

The *surface waters* domain (Figure 3.3*d*) is in phase and very well correlated to the AMOC changes. It includes the upper and intermediate North Atlantic and the upper Arctic basins. The correlation peak is close to 1, indicating an excellent match between the AMOC index and the salinity budgets, and the anti-correlation (the correlation between the AMOC index and the inverse of the salinity budgets) is lower, highlighting the asymmetry of the signal. The intermediate North Atlantic signal is muted as it is also influenced by the deep North Atlantic.

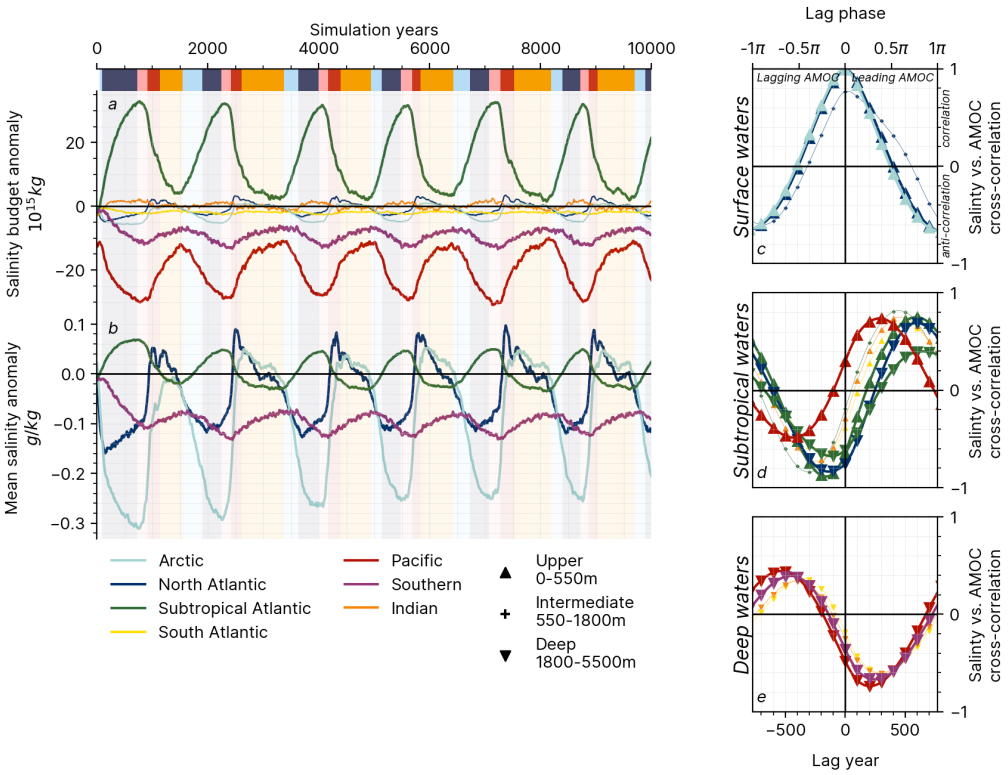

Figure 3.3: **Inter-basin salinity oscillations**. *a,b.* Time-series of salinity budget (*a*) and mean salinity (*b*) differences between *20.7k* and *CTRL*. The background shading indicates the phases as in Figure 3.1). *c-e.* Cross-correlation between the normalised salinity budgets anomalies and AMOC index (see Figure 3.1 *a*) in *d.* the Subsurface North Atlantic, *e.* the Subsurface Atlantic and *f* the Deep Ocean. The lag phase in the cross-correlations is calculated with the 1540-year periodicity derived in Chapter 2. For readability purposes, only the signals from the upper and deep Arctic, North Atlantic, subtropical Atlantic, Southern Ocean and Pacific were plotted in the foreground in Figure 3.3, with the other cross-correlations visible in the background.

The *subtropical* domain (Figure 3.3*e*) leads the AMOC by $\sim$ 500 years, and its inverse signal lags the AMOC by $\sim$ 200 years (i.e. the AMOC index peaks 500 years after the salinity budget, and 200 years before the inverse of the salinity budget). It includes the entire subtropical Atlantic, the deep North Atlantic and the upper Pacific, Indian and South Atlantic basins. The correlation and anti-correlation coefficients are around 0.8 and -0.8, respectively, because the transition phases are not as sharp as the AMOC changes. The deep North Atlantic and subtropical Atlantic variations are weak and poorly correlated to the upper subtropical Atlantic. Finally, a strong correlation is observed between the subtropical Atlantic and the upper South Atlantic and Indian and, to a lesser extent, the upper Pacific oceans.

The *deep waters domain* in Figure 3.3*f*) is in phase inversion compared to the *subtropical Atlantic domain*. It consists of the deep Pacific, Southern, South Atlantic and Indian oceans. This domain lags the AMOC index by $\sim$ 500 years, and its inverse signal leads the AMOC by $\sim$ 200 years. The deep waters signals are smoother than the AMOC index series (Figure 3.19), and neither the correlation nor the anti-correlation coefficients are very high. Overall, this domain has consistent signals (Figure 3.19*c,g*).

A last domain can be identified, including the upper and intermediate Southern Ocean, the intermediate Pacific, Indian, and South Atlantic basins and the intermediate and deep Arctic basins. We call it the *intermediate* domain (Figure 3.19*d,h*). This domain corresponds to the transition regions influenced by the *upper*, *subtropical* and the *deep* domains. Overall, correlations are low in this domain 3.19*d,h*, and this group will not be discussed further in this study.

The global salt fluxes resemble a relaxation oscillator where salt moves from the Pacific to the Atlantic during the *cold* modes and from the Atlantic to the Pacific during the *warm* modes (Figure 3.3*a*). This oscillator shares the same periodicity as AMOC changes, indicating a coupling between the two phenomena.

3.5 The oscillator mechanism

A short review of climate models' millennial-scale variability mechanisms

A variety of mechanisms have been put forward to explain millennial-scale variability. In Armstrong et al. (2022)'s HadCM3 simulations, the meridional salinity gradients between the North and the tropical Atlantic play a central role. During stadials, the gradient is high, and wind forcing can reactivate the convection in the Nordic Seas. During interstadials, the gradient weakens and leads to the deactivation of the deep water formation sites. This set of simulations differs from this Chapter's as it is based on a 30 ka BP background climate where convection is still active in the Irminger Sea and off the European coast during the cold modes, and no additional freshwater is added.

Vettoretti and Peltier (2018) use LGM background conditions in CCSM4 and link the changes in the convection regime to the stratification of the North Atlantic. During interstadial phases, sea ice transported from high latitudes to the North Atlantic decreases the stratification. Large polynyas open in the North Atlantic during stadial phases driven by deep-decoupling processes (Vettoretti and Peltier, 2016). Vettoretti et al. (2022) also discusses the role of the Antarctica Bottom Waters (AABW) in modifying the deep Atlantic density. This mechanism is analogous in many points to early theoretical Stommel box models (Stommel, 1961).

Using MIROC4m, Kuniyoshi et al. (2022) observe more a thermal control rather than a salinity control in their model. A warming (cooling) event results from subsurface warming (cooling) that weakens (strengthens) the stratification in the North Atlantic. Deep decoupling is seen as a way to obtain sharper transitions by accelerating the motion of heat and salt across the water column. The importance of the thermal effect and subsurface warming was similarly discussed in Brown and Galbraith (2016).

Kuniyoshi et al. (2022) also stress the role of the subpolar gyre in this mechanism. The subpolar gyre transports more salt and heat from subtropical waters into the high latitudes than the upper cell of the AMOC (Jungclaus et al., 2013), and this flux is of particular importance in the deep water formation process. Li and Born (2019) suggests that during D-O events, the subpolar gyre was positively correlated to the AMOC if deep water formation occurs in the centre of the gyre, and a negative correlation is observed when deep water formation occurs on the edge (Montoya et al., 2011; Zhang et al., 2011). Klockmann et al. (2020) expanded on this idea by stating that the correlation is positive when the wind-driven feedback dominates and negative when the density-driven feedback dominates.

A new proposed mechanism

Armstrong et al. (2022) found that the salinity effect prevails in their abrupt climate change mechanism. The analysis of Section 3.3 showed that both the subsurface warming in the North Atlantic and the salinity fluxes entering and leaving the North Atlantic are to be considered to explain the buoyancy fluxes in *20.7k*. The oscillator mechanism results from the combination of the fast changes of North Atlantic buoyancy coupled with the slow reorganisation of global salinity. This mechanism is drawn in Figure 3.4. Salinity tendency fluxes, described in Section 3.9, can be used to diagnose the changes in salinity in the different basins. They are plotted in Figure 3.5 along with deep water formation sites' temperature, salinity and density profiles.

At the start of the simulation, the meltwater discharge creates a fresh surface layer in the North Atlantic, reducing the density of the subsurface layer at deep water formation sites. The deep North Atlantic does not have time to respond to the perturbation and

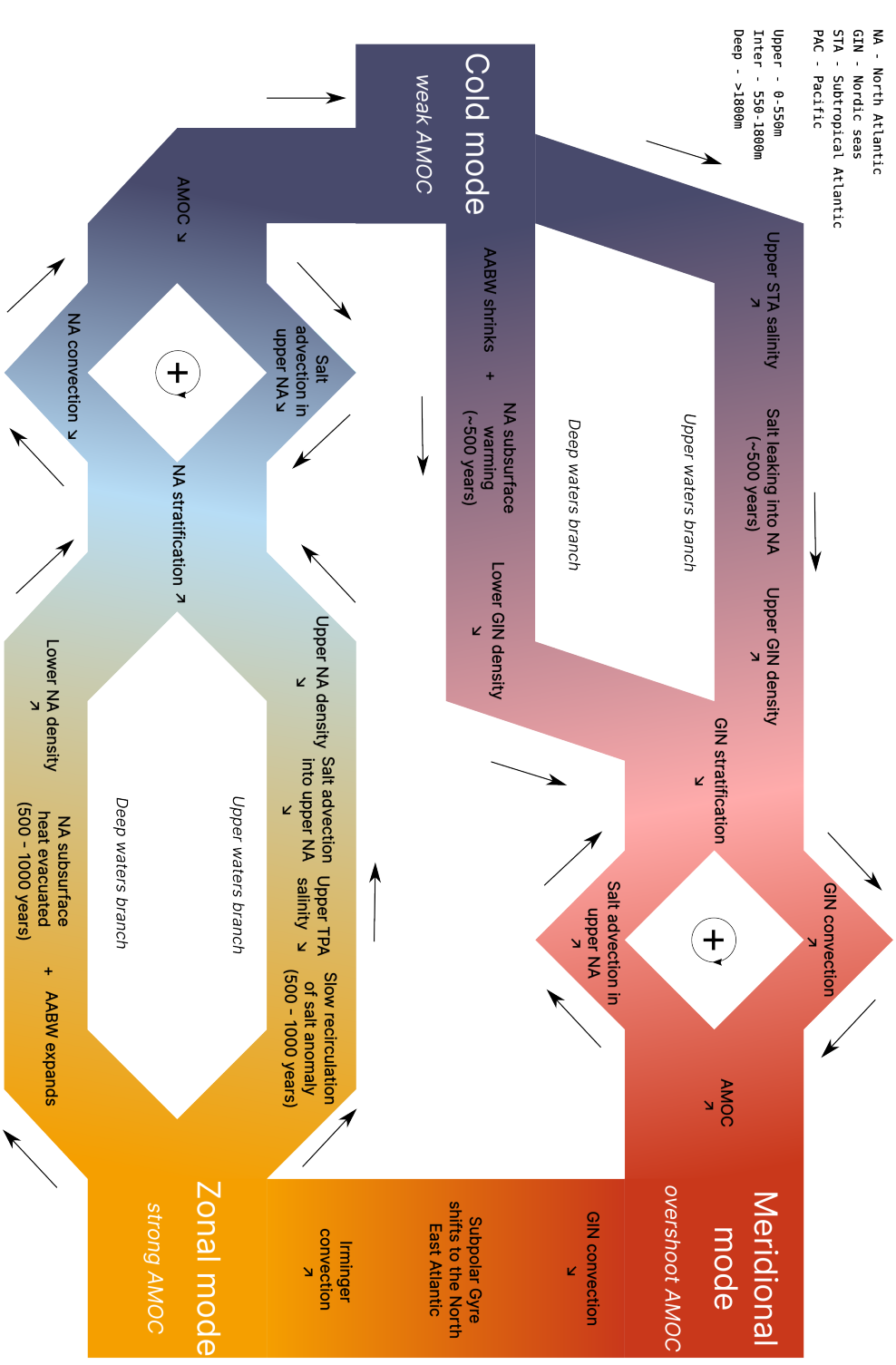

Figure 3.4: **The oscillator mechanism.** Millennial-scale variability mechanism observed in *20.7k*. The colours correspond to the phases defined in Figure 3.1 to the regions defined in Figure 3.14.

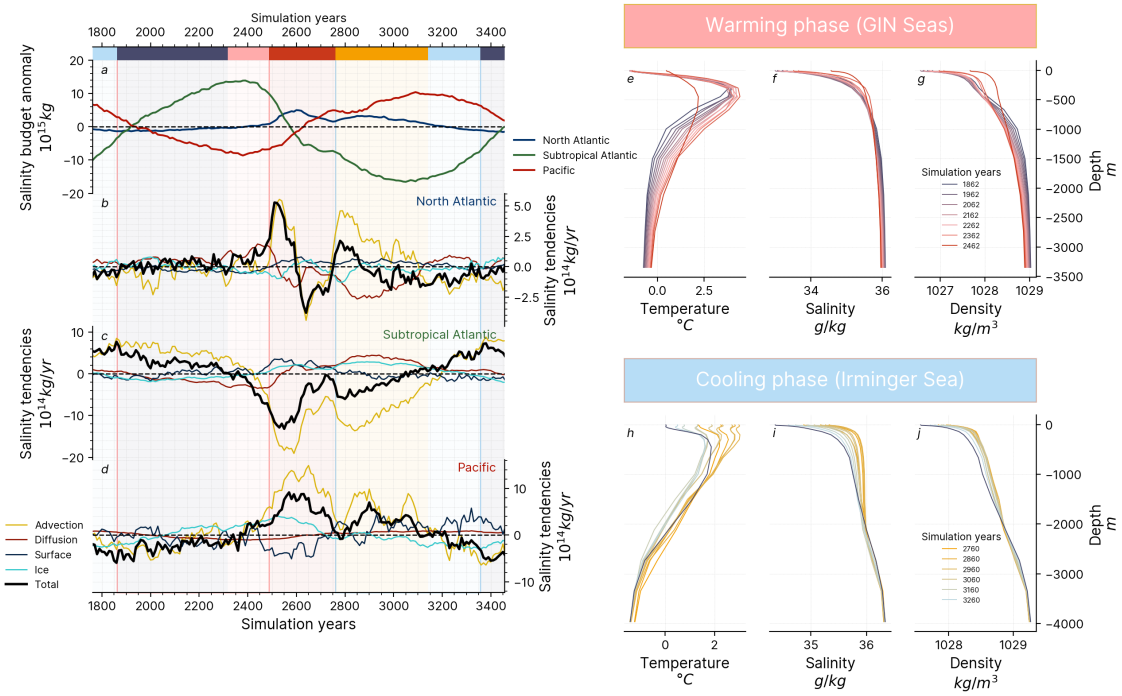

Figure 3.5: **Salinity tendencies and deep water formation sites stratification.** *a-d.* Normalised salinity changes and tendencies in the North Atlantic, subtropical Atlantic and Pacific. *a.* Salinity budget anomalies to *CTRL* centred around 0. *b-d.* 50-years running mean of salinity tendencies in the North Atlantic (b), the subtropical Atlantic (c) and the Pacific (d). The sum of all the tendencies is indicated in black. *e-g.* Vertical temperature (e), salinity (f) and density *(g)* profiles during the *warming* phase in the GIN Seas. *e-g.* Vertical temperature (h), salinity (i) and density *(j)* profiles during the *cooling* phase in the Irminger Sea.

the stratification increases at the deep water formation sites, triggering a deactivation of the convection. This initial perturbation drives a transition from the *control zonal* mode to a *cold* mode in the first hundred years of the *oscillating simulations*. Because the first cycles still lie in the transient state of the *20.7k_tdc* simulation (as observed, for instance, in the deep density profiles in Figure 3.16), the rest of the analysis will focus on the last cycle of the simulation.

The transition from a *cold* to a *meridional* mode (or *warming* phase) is triggered by the decrease of GIN Seas stratification. This change in stratification results from a drop in the subsurface density and an increase in the deep density in the region (Figure 3.5g). The subsurface density decreases because the salt accumulated in the subtropical Atlantic (Figure 3.5a) is leaking into the North Atlantic by gyre advection and diffusion (Figure 3.5b, Figure 3.8d,e). The salt accumulation in the subtropical Atlantic is due to the intense evaporation no longer compensated by advection from the AMOC (Figure 3.5c, Figure 3.8b). Unlike in Armstrong et al. (2022), modifications of precipitation and evaporation patterns in the Atlantic are not dominating the salinity changes in our simulations. The

deep density increase is caused first by the shrinking of the AABW (Figure 3.22*b*), and then subsurface warming in the GIN Seas (Figure 3.5*e*). The subsurface warming during *cold* modes was described by Marcott et al. (2011). The deep waters drop in density is further intensified by the slow drop of salinity (Figure 3.5*f*) due to the deep-decoupling mechanism (Winton, 1993).

When the stratification in the GIN Seas becomes low enough, the convection restarts in the region. This triggers a feedback loop (Figure 3.4) that reactivates deep water formation sites. An increase of the convection drives an intensification of the AMOC, increasing the advection of salt in the North Atlantic, diminishing the stratification in the GIN Seas and leading to a further increase of convection. A similar feedback was described in Drijfhout et al. (2015).

The transition from a *meridional* to a *zonal* mode happens when the convection shifts from the GIN Seas to the Irminger Sea. When the AMOC overshoots (i.e. when the AMOC recovers in a stronger state than the *control* state), the accumulated subsurface heat in the GIN Seas is abruptly evacuated (Figure 3.20*a*, Figure 3.16*k*). As a result, the stratification increases in the GIN Seas and the convection decreases (Figure 3.2 *d,j*). At the same time, the subpolar gyre shifts to the northeast Atlantic and intensifies (Figure 3.2*h*). It leads to an increase in the upper Irminger Sea salinity and an intensification of the convection in this region (Figure 3.2*h*).

The transition from a *zonal* to a *cold* mode is triggered by the increase in stratification in the Irminger Sea and Iceland Basin. The change in stratification is due to a decrease in the upper North Atlantic density and an increase in the lower North Atlantic density. The subsurface density increases in the North Atlantic occurs towards the end of the *zonal* phase (Figure 3.5*e*) when the advection of salt is not large enough to compensate for the diffusion out of the North Atlantic (Figure 3.5*b*). This is because the waters advected into the subtropical Atlantic gets fresher and the region becomes depleted in salt (Figure 3.5*a,c*). In analogy to Weijer and Dijkstra (2003), the global salinity transfer can be seen as a salinity anomaly that is being redistributed from the subtropical Atlantic to the Pacific and has not returned yet to the upper and intermediate subtropical Atlantic. The deep density increase is caused by the expansion of the AABW during the *meridional phase* (Figure 3.22*b*) and the evacuation of subsurface heat that was accumulated in the Irminger and Iceland basins during the *cold* phase (Figure 3.5*h*). Once the stratification in the Irminger Sea and Iceland Basin regions is high enough, the convection dwindles, and the system enters the *cooling* phase. A feedback loop opposite to the one observed in the *warming* phase leads to an abrupt decrease in the North Atlantic deep water formation (Figure 3.4).

The oscillator mechanism is composed of two components coupled by the AMOC. The *slow global* component is an oscillator where a salt anomaly is displaced between the

Atlantic and the Pacific depending on the regime of the AMOC. The *fast North Atlantic* component can be considered an on/off signal where the convection is deactivated or activated depending on whether the deep water formation sites stratification is high or low, respectively. The pace of the oscillations is set by the two limiting processes. In the *cold* mode, it is the time needed for the salt accumulated in the Subtropical Atlantic to leak into the North Atlantic, which takes about 500 years. In the *warm* modes, it is the time for the salt anomaly to return to the Subtropical Atlantic, which takes more than a thousand years.

3.6 Applications of the mechanism to other simulations

The mechanism presented in Section 3.5 was identified on the *20.7k* simulation. In this section, we wonder if this theory can be adapted to explain the non-oscillating simulations introduced in Chapter 2 in Figure 3.6, and comment on its relevance to oscillating simulations from other studies.

The use of freshwater input as a way to take the system into the window of opportunity is one of the most common ways to trigger millennial-scale oscillations (e.g. Timmermann et al., 2003; Kageyama et al., 2010; Brown and Galbraith, 2016). The initial perturbation is weaker in the *21k* simulation than in the *20.7k* simulation. The salt anomaly in Figure 3.6*f* is easily absorbed by the Pacific, which means that the North Atlantic deep water formation never completely shuts down, and the AMOC remains relatively strong (Figure 3.6*b*). Consequently, the subtropical Atlantic salinity has enough time to return to control values before a threshold in North Atlantic stratification is crossed (Figure 3.6*j*). The *21k* simulation finally stabilises in a zonal mode and shows no sign of instability. In the *18.2k* simulation, the initial perturbation is stronger than in the *20.7k* simulation, and the AMOC collapses. The high North Atlantic stratification (Figure 3.6*k*) prevents any recovery of deep water formation before the climate system reaches a new global salinity equilibrium after more than a thousand years (Figure 3.6*g*).

Short-lived recoveries of the AMOC are nonetheless observed in the *18.2k* simulation. These recoveries are the result of the strong subsurface heat accumulation visible in Figure 3.6*o*, that leads to apparently stochastic overshoots of the AMOC and brief *meridional* modes. In the *20.7k* simulation, the overshoot phases correspond to the *meridional* modes, but these modes can also be sustained for longer such as in the *17.8k* simulation in Chapter 2. During the overshoots, the AMOC remains too cold to trigger a significant inversion of the salinity anomaly and to reactivate the global oscillator. The *meridional* modes are not shorter than in the *20.7k* simulation, but the intense freshwater surface layer prevents any convection in the Irminger Sea and, therefore, the transition into a *zonal* mode. As described in Section 3.5, the abrupt warming phase relies on subsurface warming in sea ice-covered regions. In this set of simulations, this implies that the *meridional* mode is

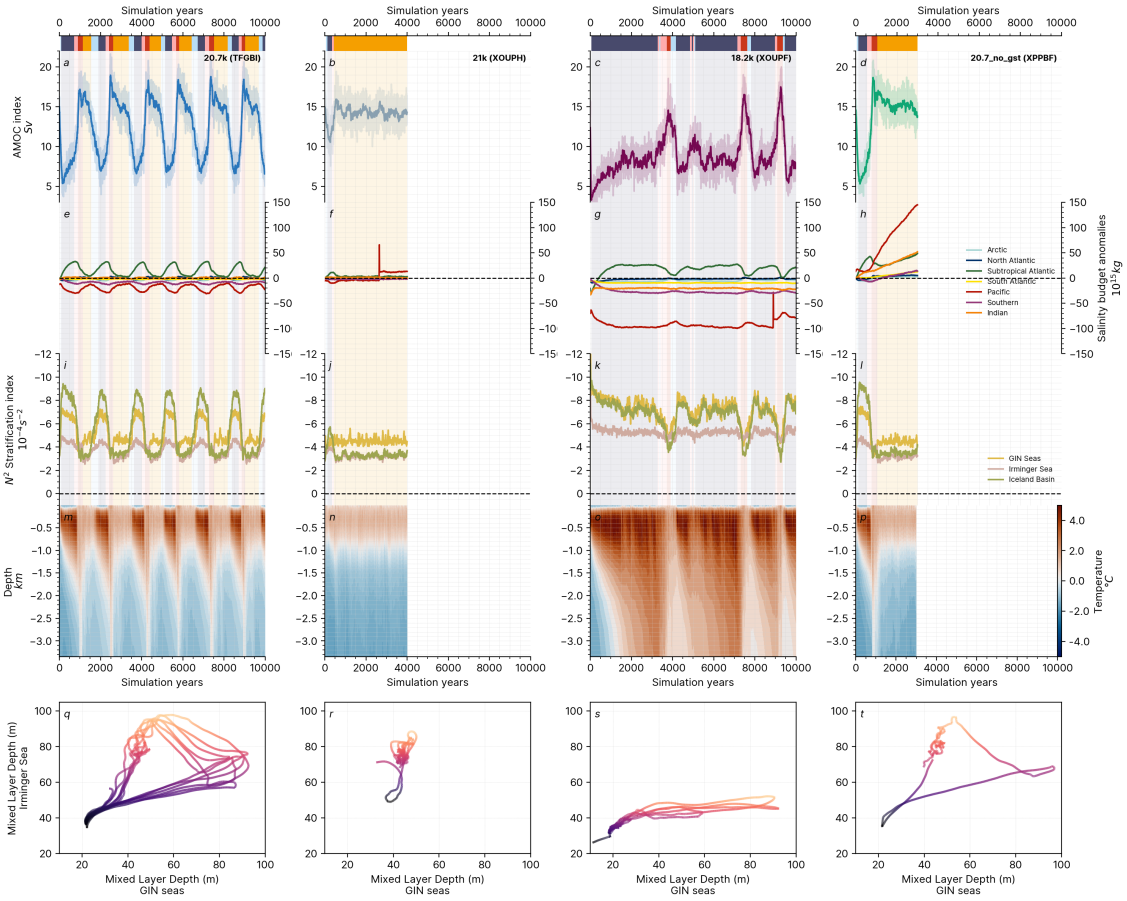

Figure 3.6: **Comparison to the non-oscillating simulations**. 30-years running means (solid lines) and annual mean (transparent lines) AMOC time series (*a*-*d*), salinity budgets in global ocean basins (*e*-*h*, see Figure 3.3*a*), N2 stratification index (Li et al., 2020) in the deep water formation sites (*i*-*l*), and trajectories in the state space defined by the mixed layer depth in the GIN Seas and the Irminger Sea (*q*-*t*, see Figure 3.1*b*) Low negative values of the N2 index indicate high stratification. The abrupt increase of Pacific salinity in panels *j* and *k* correspond to a change of the basin volume introduced by the bathymetry smoothing in the Philippines described in Chapter 2.

necessary to set off the oscillator mechanism. The location of the convection overshoot region depends on the model and the experiment design. Both Vettoretti and Peltier (2016) and Kuniyoshi et al. (2022) observe it in the sea-ice-covered Irminger Sea in the form of polynyas. On the other hand, the GIN Seas deep water formation site is consistently active in Klockmann et al. (2020) and Armstrong et al. (2022), where the subpolar gyre and the winds drive the abrupt warming mechanism. Finally, Cheng et al. (2011) observe a two-step warming phase where abrupt recovery is observed first in the Labrador Sea and then in the GIN Seas.

The *18.2k* simulation is a good example that an overshoot mode is only one of the two conditions to start the oscillatory mechanism: the presence of the salt anomaly is the second one. The salt anomaly is setting the pace of the oscillations. If the global oscillator is restricted to the Atlantic, as in Armstrong et al. (2022), the redistribution of the salt anomaly is shorter, and the periodicity becomes smaller. In the absence of salinity conservation, the salt anomaly cannot exist. This is the case of the *20.7k_no_gst* simulation, described in Figure 3.6*d,h,l,p*. It follows the evolution of the *20.7k* simulation for the first 500 years. At the end of the *cold* phase, the salinity of the Pacific Ocean starts to increase at the same time as the Atlantic salinity (Figure 3.6*l*). Because the tropical Atlantic is never depleted, the North Atlantic subsurface density remains high and deep water formation remains active. The salt accumulation is due to the bias towards evaporation in the tropical Atlantic and Pacific discussed in Section 3.2.2.

20.7k_no_gst highlights the importance of the salinity correction scheme in HadCM3 discussed by Dentith et al. (2019b). This salinity correction is not entirely unrealistic: in the absence of an online ice sheet model, it provides feedback that emulates the stabilising power of the ice sheets on the global salinity. Wickert et al. (2023) proposed a mechanism where the storage and release of freshwater in the Laurentide ice sheet during the stadials and interstadials, respectively, can provide a negative feedback that prevents the deglaciation of the ice sheet. There are certain times during the last glacial period, however, where the destabilisation of the ice sheets has acted as a driver for abrupt climate changes, such as Heinrich events (Menviel et al., 2020) or the saddle collapse (Gregoire et al., 2012). The two cases were observed by Alvarez-Solas et al. (2019), making the case for further coupled-climate ice sheet experiments.

3.7 A theoretical framework for AMOC stability in response to meltwater discharge

Giving a theoretical framing to climate changes induced by meltwater discharge problem is made difficult by the wide range of possible regimes obtainable in a relatively constrained parameter space and the strong non-linearity of the response. We restrict the meltwater forcing to a one-dimensional abstract variable, considering the effect of both the magnitude

and the location of the discharge that we called the *meltwater efficiency*. Along this axis, the *21k* simulation has low efficiency, indicating either insufficient meltwater or not in the right location to trigger a significant change compared to the control state. The *18.2k* simulation has a strong efficiency as the system is taken the furthest from its control state due to the high sensitivity of this system to discharge in the Arctic. The *20.7k* simulation's magnitude and distribution of the discharge are relatively close to the *21k* simulation, but the increase in efficiency is enough to cross a bifurcation point and change the climate regime. The concepts introduced in this section are based on the nonlinear systems theory (Strogatz, 2015).

At low efficiencies, we find that the *warm* simulations such as *21k* behave like an over-damped oscillator. The initial discharge takes the system away from its steady *zonal* state into a short-lived *cold* mode. However, the perturbation is insufficient to reach another attractor and eventually returns to the *zonal* mode, acting as a fixed point in the parameter space. This is reflected in Figure 3.6*f*, where the salinity anomaly is not strong enough to cross a threshold and start the oscillatory cycle, and the internal variability is not sufficient to trigger a transition in the 4000 years of integration.

For high efficiencies, the *cold* simulations (*18.2k* in Chapter 2) are *monostable* with an *excitable* mode (short-lived deviation from a stable state into an unstable state). Only the *cold* mode acts as an attractor, and short excursions into an unstable *meridional* mode occur at what seems to be random intervals, although the probability of transition increases with the time between two warm modes. Stable and unstable modes become close enough for stochastic events, such as the apparition of polynyas or an extraordinary shift of the jets, to start a transition, and we do not observe any build-up of salt that could lead to recovery episodes. In Figure 3.6*g*, the response to such an event also looks like a damped oscillator, with the Pacific absorbing then returning the Atlantic salinity changes.

On the other hand, the *oscillating* simulations, obtained in a small window of opportunity between the *warm* and *cold* simulations, are highly deterministic. The solution is no longer a single fixed point but a periodic *limit cycle* (closed trajectory in phase space) going through the state space along the same path. Small changes in meltwater efficiency result in minor modifications of the shape and periodicity observed in Chapter 2's simulations but do not change the underpinning mechanism. The stochastic component, visible in the inter-annual variability, only induces random fluctuation around the steady state. This oscillator with short/fast components resembles the relaxation oscillators of the FitzHugh–Nagumo model (FitzHugh, 1955; Nagumo et al., 1962).

We extrapolate that at least two further modes could be obtained with different forcing: (i) an *excitable warm* mode by slightly increasing the perturbation from a *cold* mode to trigger stochastic episodes of weak convection and (ii) a *cold stable* mode by increasing

the discharge from the *excitable warm* experiment to prevent recoveries despite subsurface warming. More sensitivity simulations are needed to conclude the existence of these two modes.

3.8 Conclusion

This Chapter presents a new mechanism for millennial-scale variability observed in a last glacial maximum HadCM3 climate simulation forced with a snapshot of deglacial meltwater. The simulation displays a periodical evolution along a limit cycle from a *cold* mode – where the AMOC is weak and there is no deep water formation in the North Atlantic, a *meridional* warm mode – where the AMOC is strong and convection is primarily located in the Nordic seas, and a *zonal* warm mode – where the AMOC is strong and convection situated primarily in the Irminger Sea.

The oscillator mechanism is composed of a *slow global* component and a *fast North Atlantic* component, and the AMOC plays the coupling mediator. The *slow global* component transports a salt anomaly between the subtropical Atlantic and the deep oceans, specifically the deep Pacific basin. The *fast North Atlantic* component responds to thresholds in North Atlantic stratification driving the reactivation or deactivation of deep water formation. During *cold* modes, the salt excess in the subtropical Atlantic leaks into the North Atlantic and increases the upper waters density, and subsurface warming decreases the deep density of the ice-covered regions. This leads to decreased GIN Seas stratification until the convection abruptly reactivates in the regions. A switch between two warm modes is then observed, where the GIN Seas deep water formation site of the *meridional* mode gives way to the Irminger Sea deep water formation site of the *zonal* mode. During *zonal* modes, the Atlantic becomes depleted in salt because of the slow re-circulation of the salt anomaly, and the heat accumulated during cold modes is progressively being evacuated in the North Atlantic. This leads to an increase in the stratification of the Irminger Sea and Iceland Basin until the convection abruptly deactivates.

The system is initially taken out of its equilibrium by the introduction of freshwater perturbation. This perturbation has to be big enough to trigger deactivation of the deep water formation site before the salt anomaly is redistributed and small enough to allow for recovery of the deep water formation sites due to advective transfer of salt from the subtropical Atlantic. In the absence of salinity correction, the global salinity anomaly between the Pacific and the subtropical Atlantic is erased by the global salinity drift.

The simulations presented in the Chapter explore the concept of the window of opportunity associated with meltwater discharge. Depending on the forcing, we observe a *stable warm* simulation, where the system can sustain North Atlantic deep water formation despite the freshwater input, an *oscillating limit cycle* simulation, following the oscillator mechanism, and an *excitable cold* simulation, where the AMOC is collapsed apart from short-lived

recovery of North Atlantic convection. We suggest that *stable cold* and *excitable warm* modes also exist. More sensitivity experiments involving a more comprehensive range of parameters (i.e. atmospheric greenhouse gas concentrations, the orbital parameters, the ice sheet geometry, the salinity conservation scheme and the physical parameters) are needed to constrain the region of existence of these different behaviours.

The conclusions of this study are model-dependent, and even within the same model, different background conditions and forcing can lead to disparate processes. Nonetheless, common patterns between the different mechanisms start to emerge, and the fast-slow component framework presented in this study can be applied to a broader range of glacial simulations. The salinity conservation is necessary to obtain millennial-scale oscillations in HadCM3 simulations in the absence of the ice sheet feedback, and the introduction of such feedback would represent a significant step towards the simulations of realistic millennial-scale variability.

Chapter 3 - Supplementary Information

The supplementary information includes

1. Sections 3.9 to 3.10
2. Figures 3.7 to 3.22

3.9 Supplementary Information - Salinity tendencies diagnostic

The salinity diagnostics were introduced in HadCM3 by Armstrong et al. (2022) as a tool to map the salinity fluxes between the grid cells of the ocean model. At each time step and for each ocean grid cell, each process adding or removing salt is saved independently as well as the total salinity changes. They are clustered in 10 categories. The horizontal and vertical advection are linked to the water motion coming in and out of the cell. The diffusion is calculated at a sub-grid scale, and the Gent and McWilliams diffusion (Gent and McWilliams, 1990), which represents the isopycnal advection by eddies, is saved separately. The convection is represented as a one-dimensional field. The surface processes include the precipitation, evaporation and river run-off. The sea ice processes include brine rejection and sea ice melting. The mixed layer field includes all the processes that relate to mixing. Finally, the Mediterranean field captures the salt exchanges coming from the Mediterranean outflow pipe (Ivanovic et al., 2014).

In the following plots, we combined the Diffusion and Gent and McWilliams diffusion in a single field. The freshwater forcing is included in the surface fluxes. The global salinity corrections are not visible in any of the tendencies fields. This can result in a small shift between the sum of all tendencies (plotted in grey in the following plots) and the derivative of the basin salinity (plotted in black in the following plots), but its effect is assumed to be negligible. In Section 3.9, we also combined the vertical and horizontal advection and diffusion fields, and did not include the Mediterranean flux, which signal is small in the large basins considered, and the mixed layer and convection fields because their sum is zero over the entire water column.

In the following section, we describe the tendencies of the different regions during the warming, meridional to zonal and cooling phases. The detailed tendencies are plotted for the Arctic in Figure 3.7, the North Atlantic in Figure 3.8, the Subtropical Atlantic in Figure 3.9, the South Atlantic in Figure 3.10, the Pacific in Figure 3.11, the Indian in Figure 3.12 and the Southern basins in Figure 3.13. The basins are defined in Figure 3.14.

3.9.1 Warming phase

The upper North Atlantic salinity tendencies are characterised by the competition between a steady freshwater flux at the surface due to the high precipitation, sea ice melting and meltwater discharge, and horizontal advection and diffusion of salt coming from the subtropical Atlantic (Figure 3.8*d,e*). At the onset of a cold mode, in the absence of overturning circulation, the salt advection does not provide a sufficient input of salt to compensate for the surface losses, and the salinity decreases (Figure 3.8*b,c*). As we progress through the cold mode, the upper salinity advection and diffusion increase, leading to a net salt import in the region. This is likely to be the response of the upper subtropical Atlantic

salt accumulation, almost anti-phased with the AMOC (Figure 3.3*d*), that provides saltier water to the upper North Atlantic. Subtropical Atlantic salt accumulation is primarily due to intense evaporation that is no longer flushed by the AMOC (Figure 3.9*b*). Contrary to Vellinga and Wu (2004) and Armstrong et al. (2022), we do not see a significant change in surface processes in the subtropical Atlantic in our simulations (Figure 3.9*b,d*). The AMOC (Figure 3.3*c*) and the subpolar gyre (Figure 3.2*g,f*) start recovering slowly and further increase the subsurface advection of salt into the North Atlantic.

Meanwhile, the lower North Atlantic gets isolated from the other deep water masses. The shrinking of the AABW leads to an initial increase of deep North Atlantic salinity, but it stabilises after $\sim$ 200 years (Figure 3.8*h,i*), and the region does not record a significant change before the end of the cold mode (Figure 3.8*a*). The vertical exchanges between the upper and the lower (and intermediate) waters of the North Atlantic, as well as the horizontal advection in the deep waters, are stopped (Figure 3.8*h,i*).

As a result, there is no mechanism to compensate for the loss of salinity in the lower GIN seas and in the Arctic basin (Figure 3.2*m*, Figure 3.16*a*). This freshening may be due to two factors. First, they are regions of intense meltwater discharge, which, when the surface processes are reduced (Figure 3.8*d*), can freshen the entire water column. Second, they are covered in sea ice all year long, which results in subsurface warming (Figure 3.5*e*). To compensate for the loss of upper density, saltier deep waters are carried to the subsurface in a process that recalls the deep-decoupling mechanism described in Winton (1993). Both the subsurface warming and the leak of deep salinity tend to lower the density of the deep GIN seas.

The combined effect of the subsurface density increase and deep density decrease in the GIN seas reduces the stratification (Figure 3.5*g*). At the onset of the *warming* phase, a threshold is crossed and deep water formation starts to resume. This then triggers a positive feedback that accelerates the recovery of the convection (Figure 3.4). When NADW production is reactivated, the AMOC starts to increase. This leads to reduced sea ice and an expansion of the subpolar gyre, bringing even more salt to the region to increase the upper Nordic Seas' density. This process recalls a mechanism described in Drijfhout et al. (2015). The recovery happens in a warm waters corridor along the East coast of Europe, following the Subpolar Gyre and the North Atlantic Current, and convection overshoots in the GIN seas.

During the *cold* mode, we also observe that the global deep waters get fresher due to the absence of salt from deep convection (Figure 3.3*a*). Changes in surface processes and diffusion in the tropics compensate slightly for this deficit, but only the resumption of the AMOC can reverse the dynamic (Figure 3.11*c*).

3.9.2 Meridional to Zonal transition

During the *meridional* mode, the changes in salinity in the North Atlantic follow the advection dynamics (Figure 3.8*c*). At the onset of the *meridional* mode, there is an overshoot of saline waters entering the upper North Atlantic from the subtropical Atlantic (Figure 3.8*c*, Figure 3.9*c*). This is at this moment that the salinity anomaly is redistributed to the deep Oceans (Figure 3.11*i*).

After the overshoot, the increase of stratification in the Nordic Seas leads to a reduction of the AMOC (Figure 3.5), which in turn reduces the salt transported from the upper subtropical Atlantic to the North Atlantic (Figure 3.8*e*, Figure 3.9*e*). Once the gyre expands and intense convection recovers in the Irminger Sea, the salinity importation resumes in the North Atlantic (Figure 3.8*c*).

3.9.3 Cooling phase

After the resumption of the AMOC, advection brings salt into the upper North Atlantic (Figure 3.8*c*). But as the *zonal* phase progresses, the salinity of the subtropical Atlantic declines (Figure 3.9*a*). The salt accumulated in the *cold* mode is now being redistributed to the deep waters, and this signal lags the AMOC by about 500 years (Figure 3.3*f*). The subsurface salinity of the North Atlantic switches from a net increase to a net decrease. (Figure 3.8*c*).

In the deep North Atlantic, the AABW has expanded back, and the lower North Atlantic is no longer isolated (Figure 3.8*i*). We showed in Figure 3.3*f* that the deep waters of the Pacific (and Indian) and the Southern Ocean and South Atlantic are connected, and as the deep Pacific (and Indian) get saltier (Figure 3.11*a*), so does the AABW. This effect compensates for the influx of salt due to the lower cell of the AMOC (Figure 3.9*i*) and tends to increase the lower North Atlantic salinity as soon as the AMOC diminishes (Figure 3.8*i*).

Despite signs of stabilisation of the global salt distribution at the end of the meridional phase (Figure 3.8*a,c*), a new threshold is crossed in the Irminger Sea and the *cooling phase* is triggered. As convection diminishes, so does the AMOC. Less salt is transferred between the subtropical and North Atlantic, leading to a new positive feedback diminishing the subsurface density (Figure 3.4). Combined with the lower density increase, the AMOC's decline accelerates, and a transition to a *cold* mode is observed after $\sim$ 200 years.

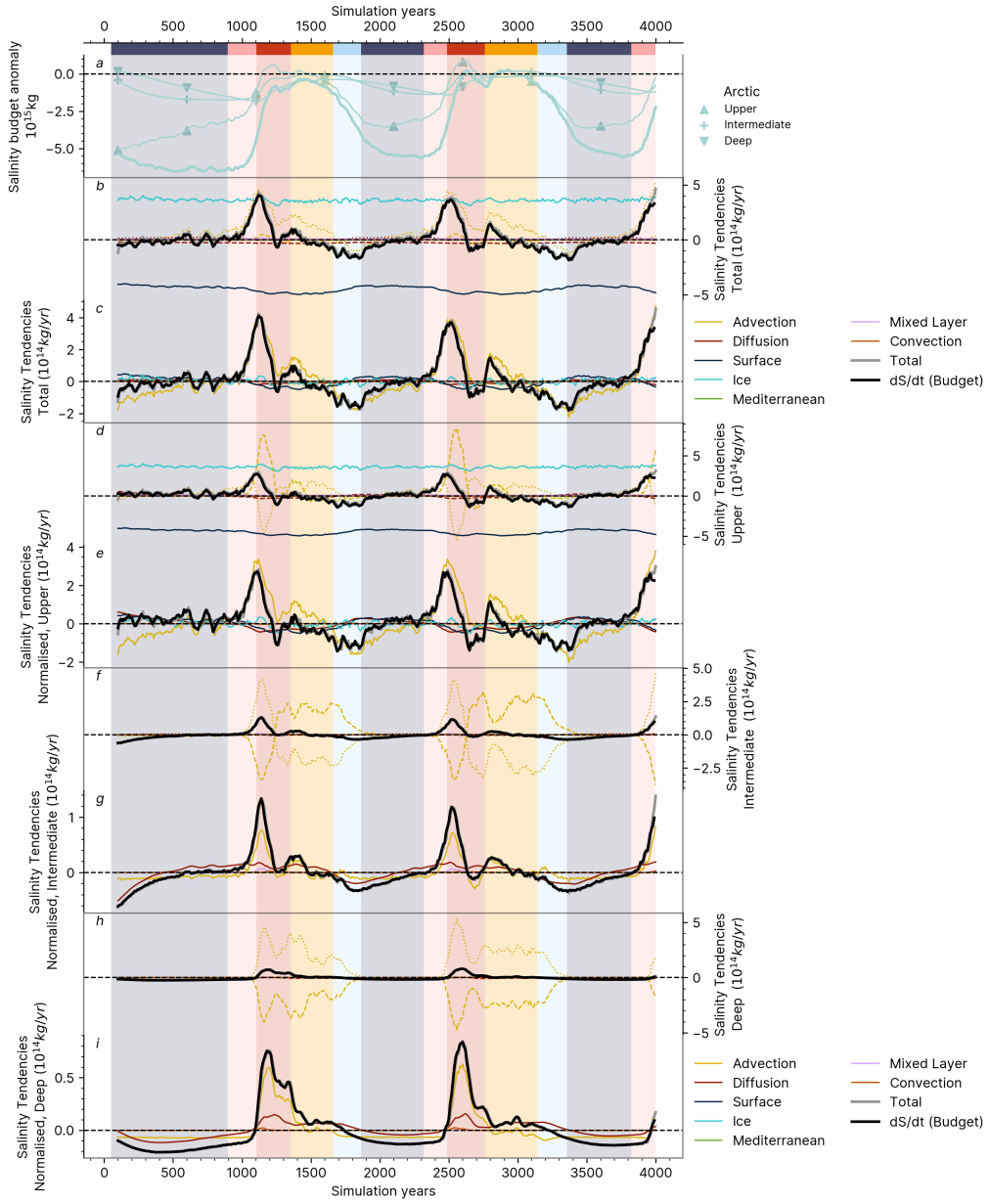

Figure 3.7: **Salinity tendencies in the Arctic.** *a.* Salinity budget at depths slices in the Arctic (see Figure 3.14). *b-i.* 50-year running means of the detailed salinity tendencies, both absolutes and normalised (centred around 0), in the region for the entire water column (*b,c*), the subsurface (*d,e*), the intermediate (*f,g*) and the deep (*h,i*) waters.

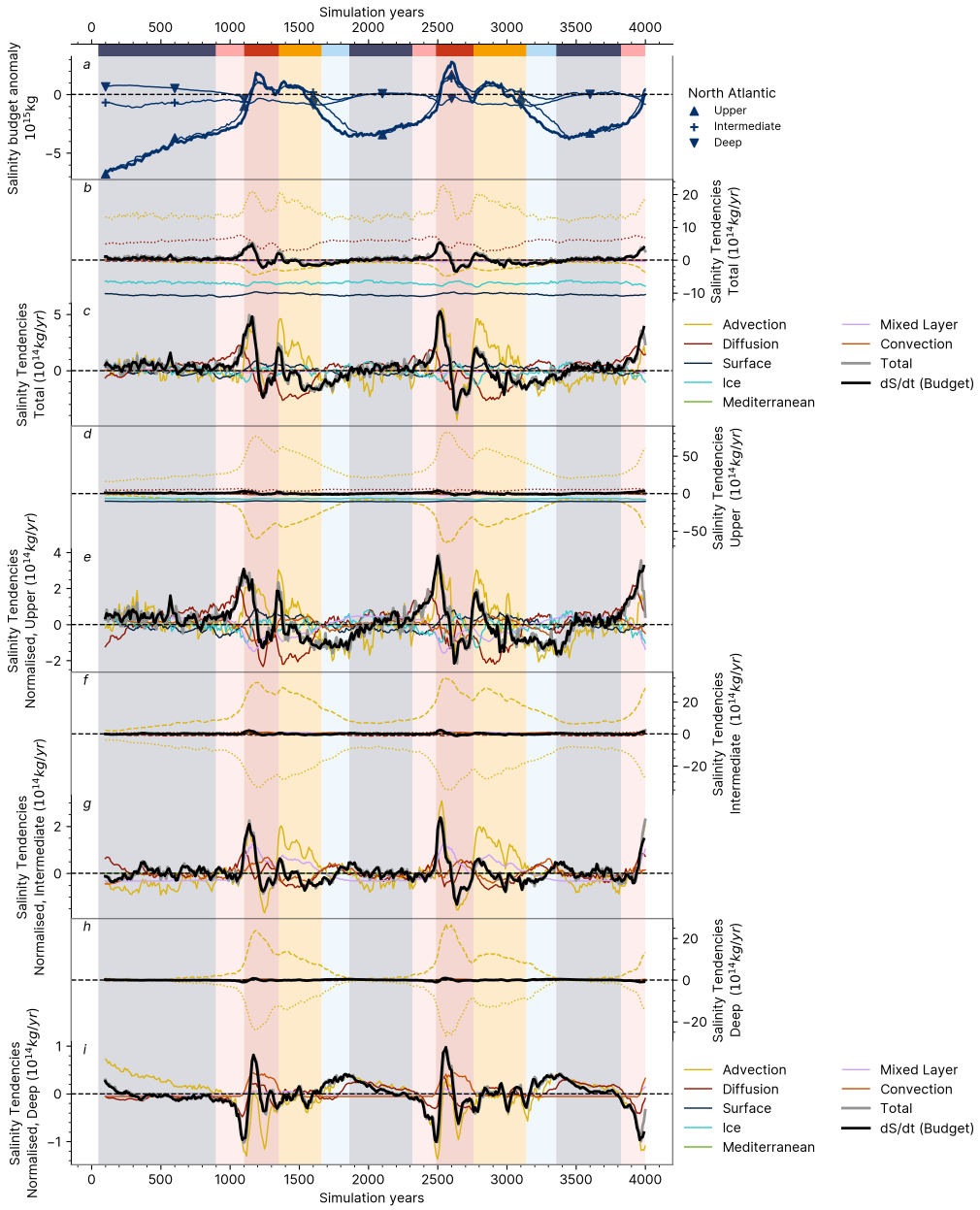

Figure 3.8: **Salinity tendencies in the North Atlantic.** *a.* Salinity budget at depths slices in the North Atlantic (see Figure 3.14). *b-i.* 50-year running means of the detailed salinity tendencies, both absolutes and normalised (centred around 0), in the region for the entire water column (*b,c*), the subsurface (*d,e*), the intermediate (*f,g*) and the deep (*h,i*) waters.

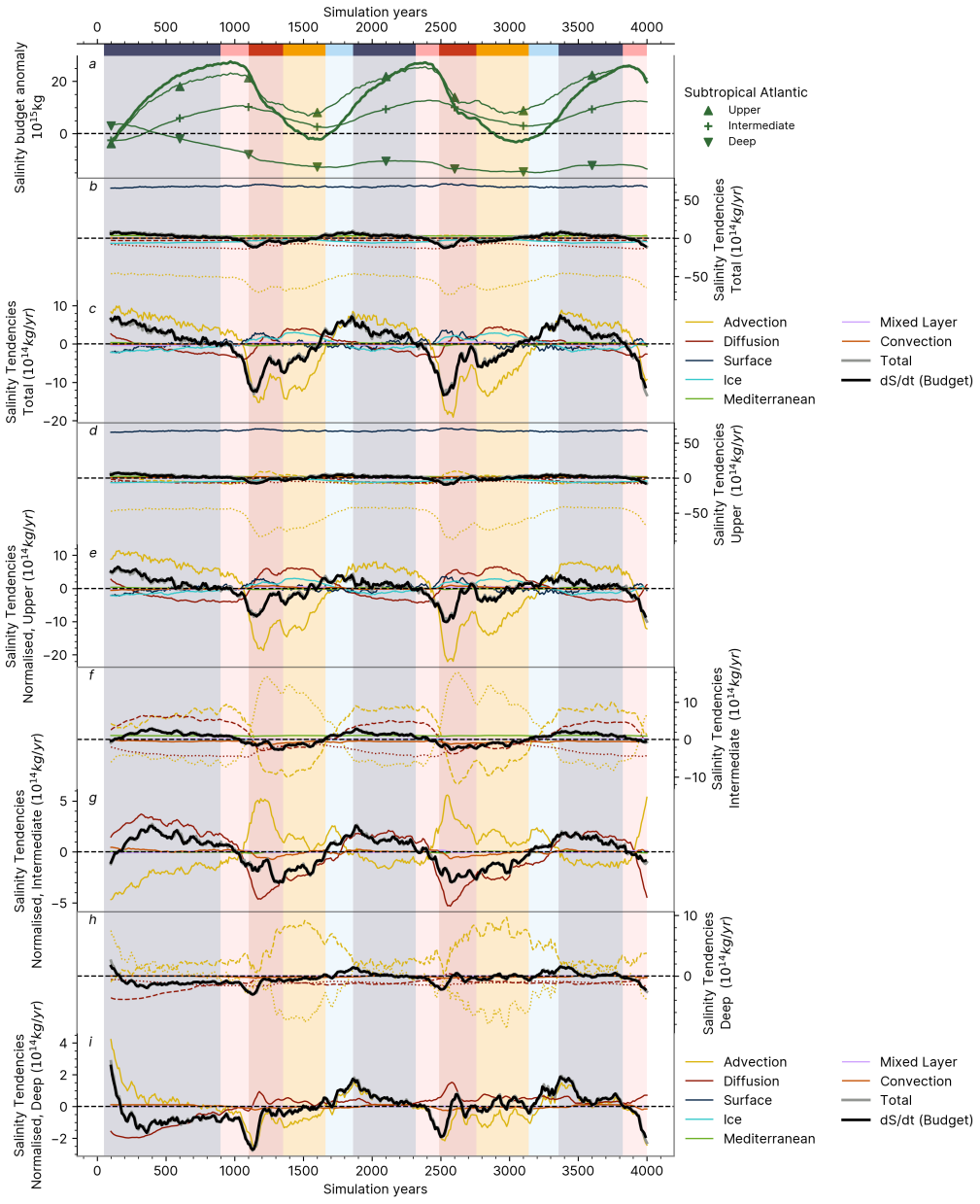

Figure 3.9: **Salinity tendencies in the subtropical Atlantic.** *a.* Salinity budget at depths slices in the subtropical Atlantic (see Figure 3.14). *b-i.* 50-year running means of the detailed salinity tendencies, both absolutes and normalised (centred around 0), in the region for the entire water column (*b,c*), the subsurface (*d,e*), the intermediate (*f,g*) and the deep (*h,i*) waters.

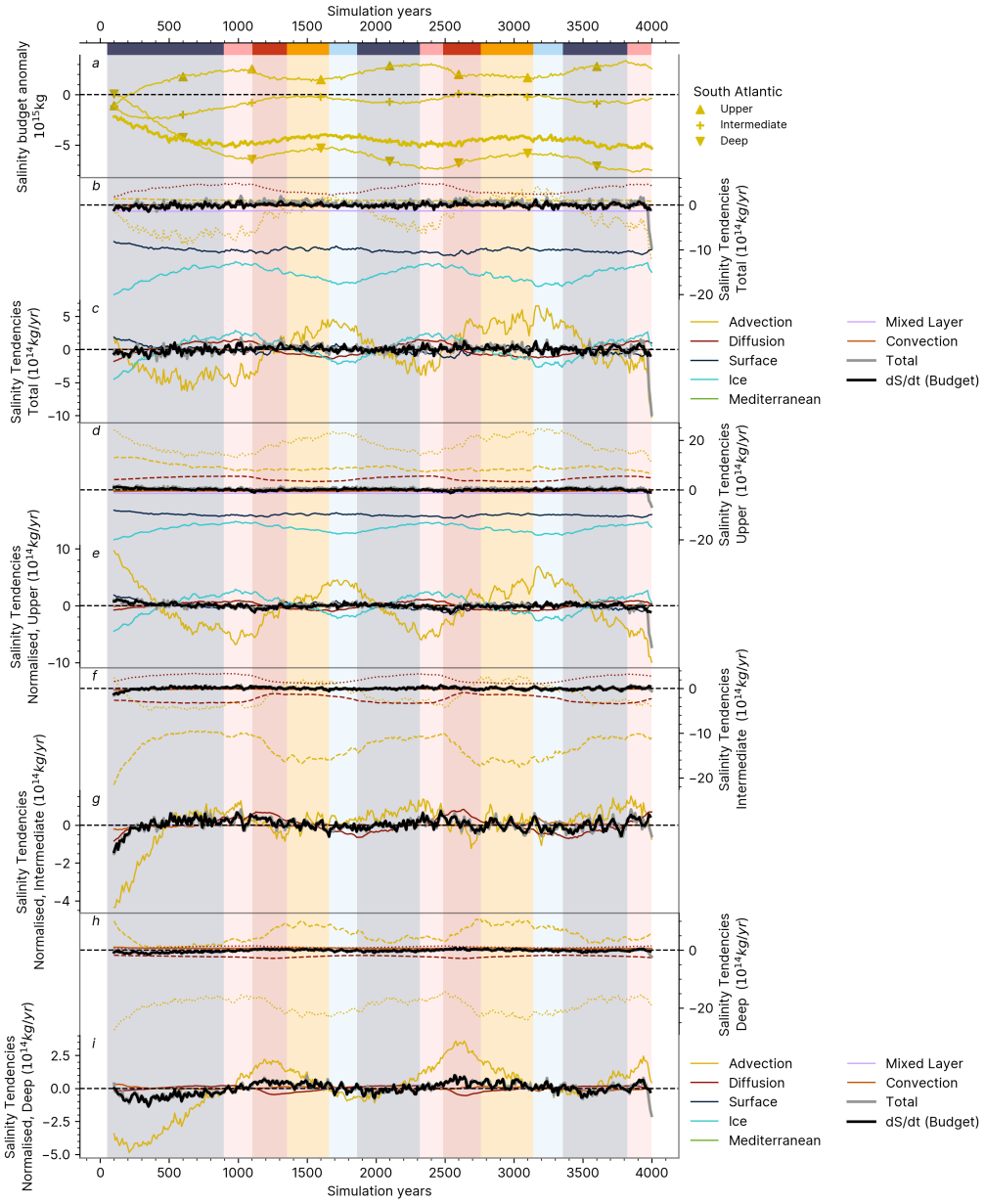

Figure 3.10: **Salinity tendencies in the South Atlantic.** *a.* Salinity budget at depths slices in the South Atlantic (see Figure 3.14). *b-i.* 50-year running means of the detailed salinity tendencies, both absolutes and normalised (centred around 0), in the region for the entire water column (*b,c*), the subsurface (*d,e*), the intermediate (*f,g*) and the deep (*h,i*) waters.

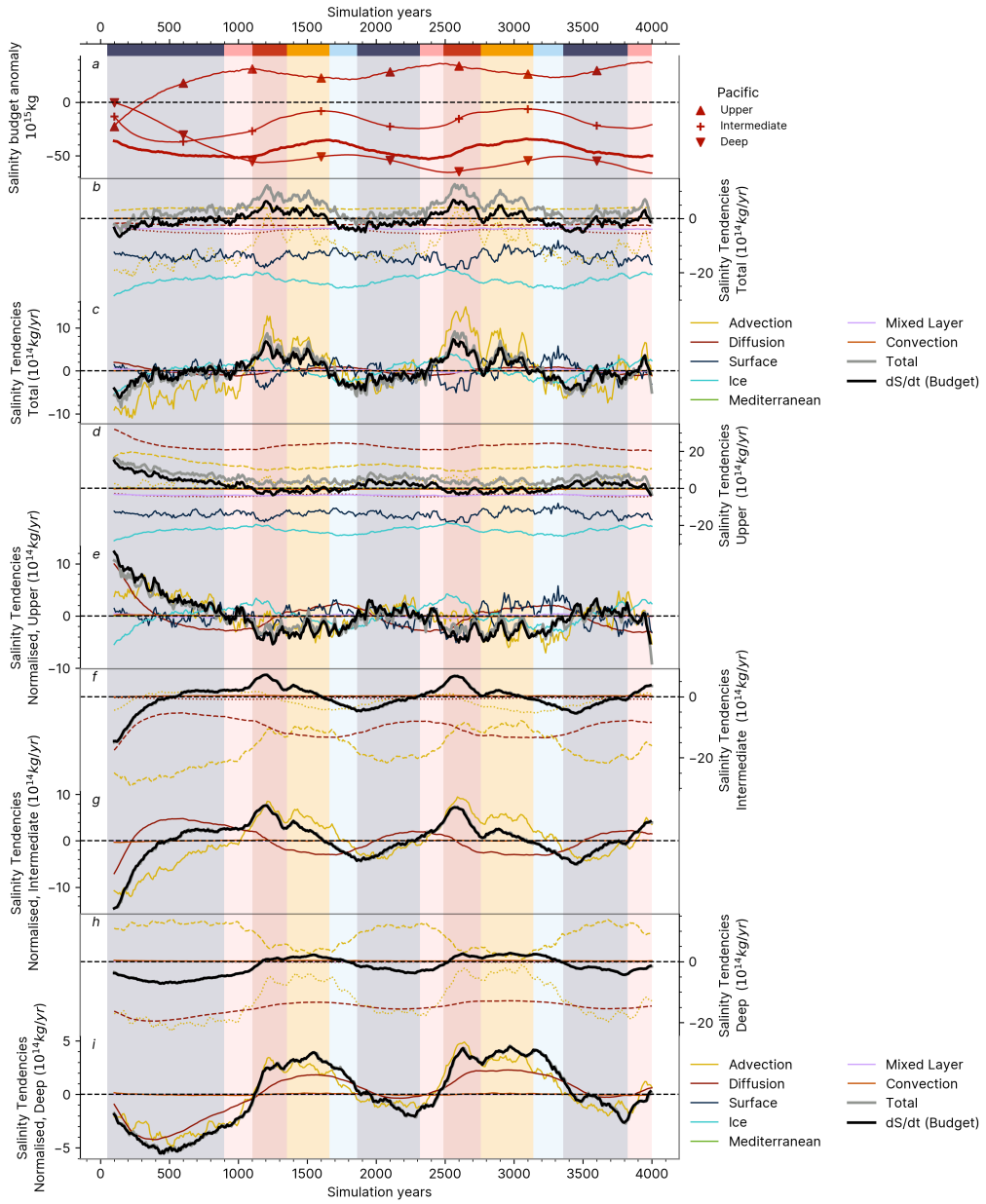

Figure 3.11: **Salinity tendencies in the Pacific.** *a.* Salinity budget at depths slices in the Pacific (see Figure 3.14). *b-i.* 50-year running means of the detailed salinity tendencies, both absolutes and normalised (centred around 0), in the region for the entire water column (*b,c*), the subsurface (*d,e*), the intermediate (*f,g*) and the deep (*h,i*) waters.

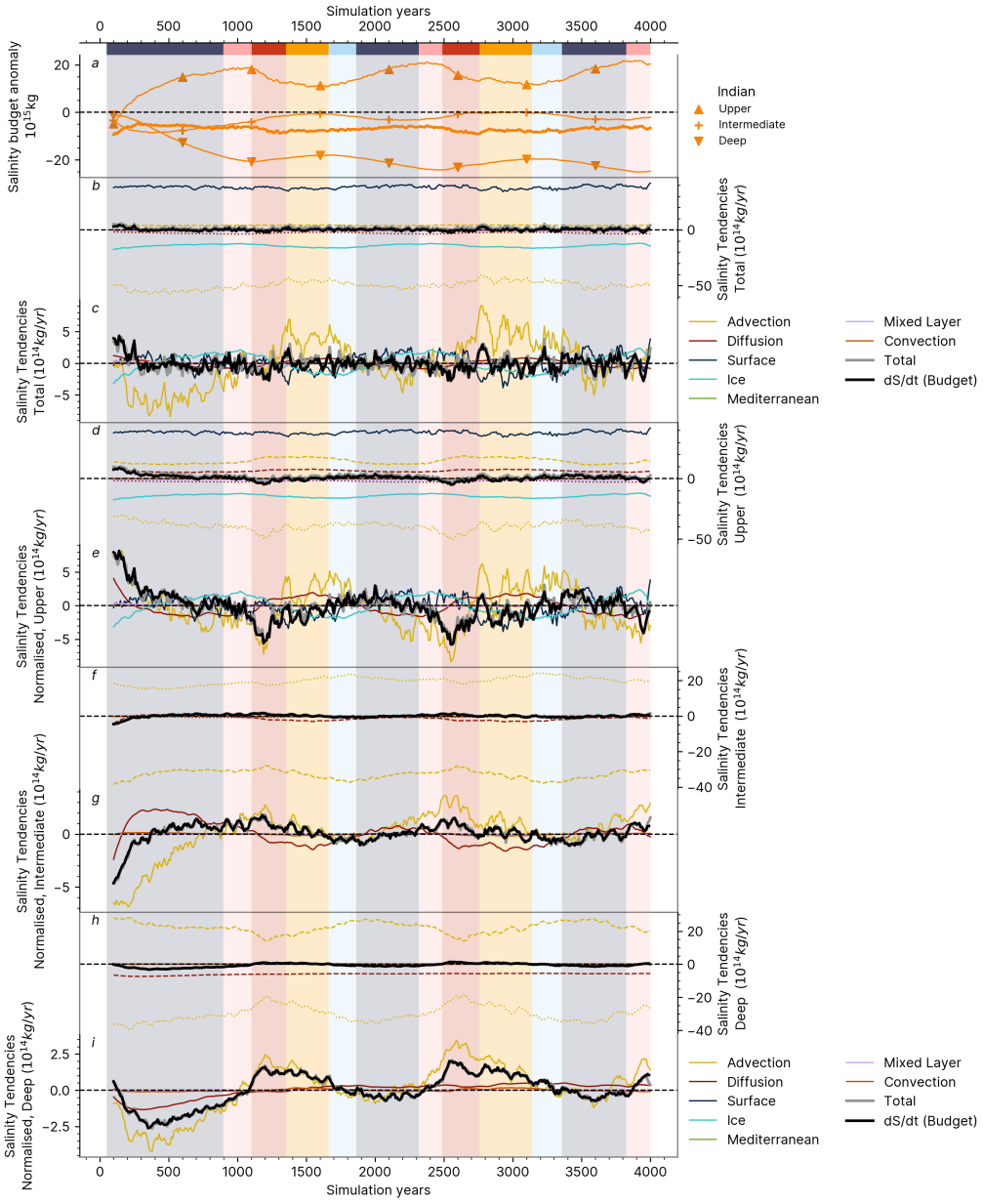

Figure 3.12: **Salinity tendencies in the Indian Ocean.** *a.* Salinity budget at depths slices in the Indian Ocean (see Figure 3.14). *b-i.* 50-year running means of the detailed salinity tendencies, both absolutes and normalised (centred around 0), in the region for the entire water column (*b,c*), the subsurface (*d,e*), the intermediate (*f,g*) and the deep (*h,i*) waters.

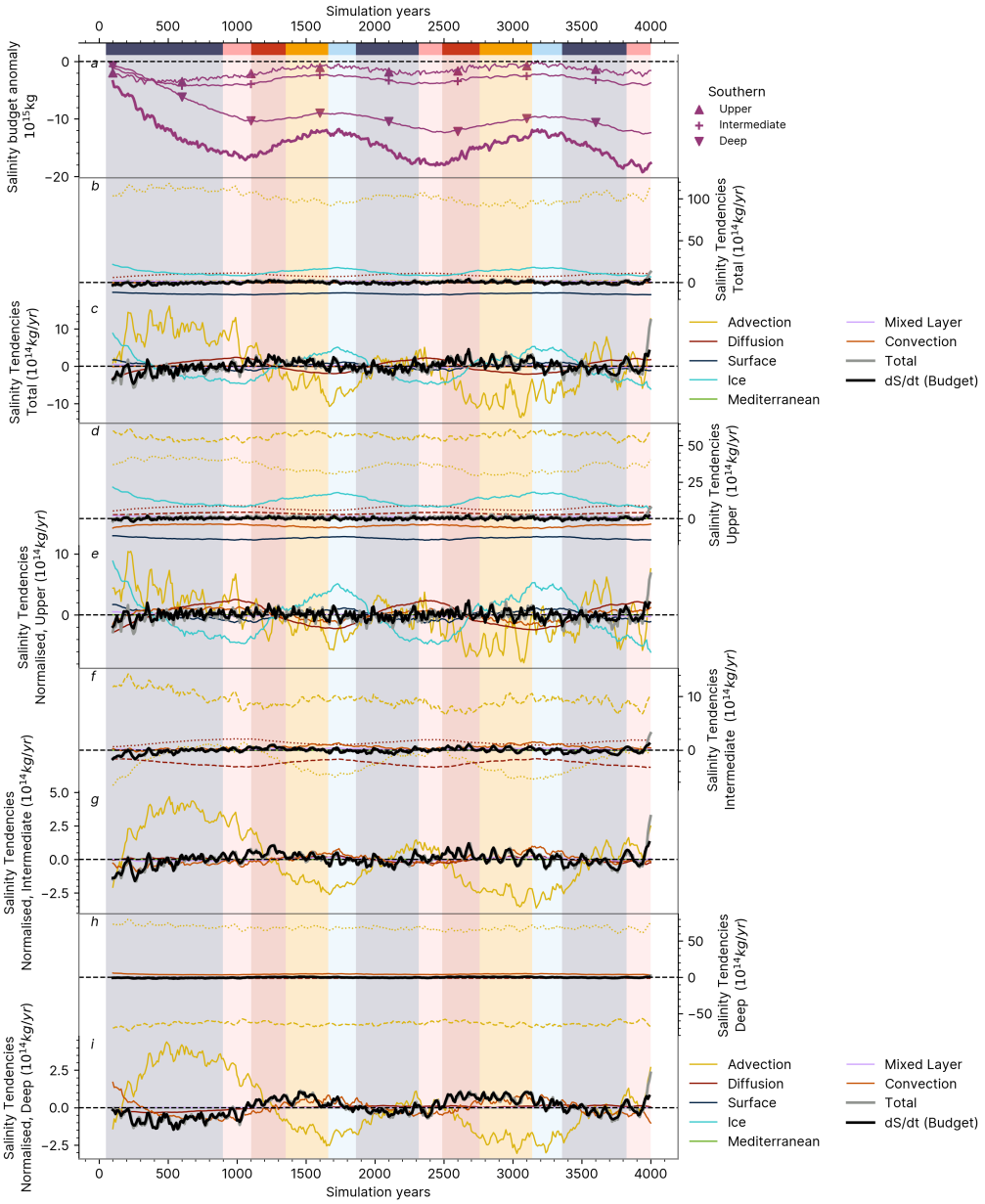

Figure 3.13: **Salinity tendencies in the Southern Ocean.** *a.* Salinity budget at depths slices in the Southern Ocean (see Figure 3.14). *b-i.* 50-year running means of the detailed salinity tendencies, both absolutes and normalised (centred around 0), in the region for the entire water column (*b,c*), the subsurface (*d,e*), the intermediate (*f,g*) and the deep (*h,i*) waters.

3.10 Supplementary Figures

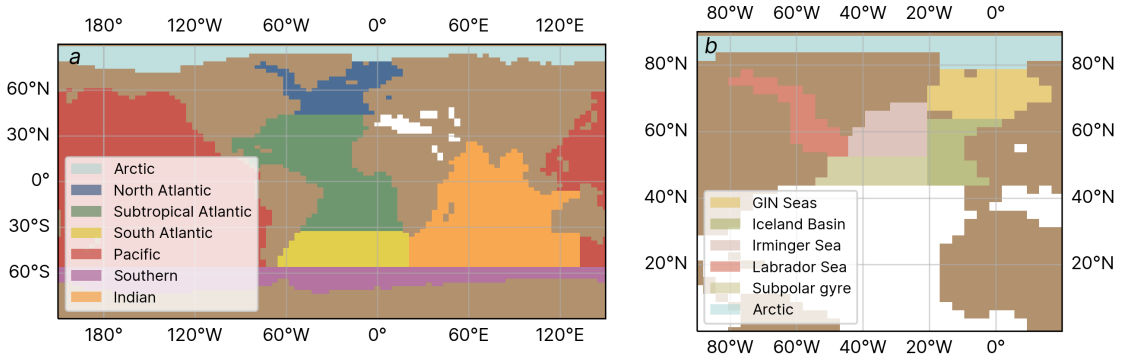

Figure 3.14: **Zone definitions.** Definition of the zones in the global(a) and North Atlantic (b) regions.

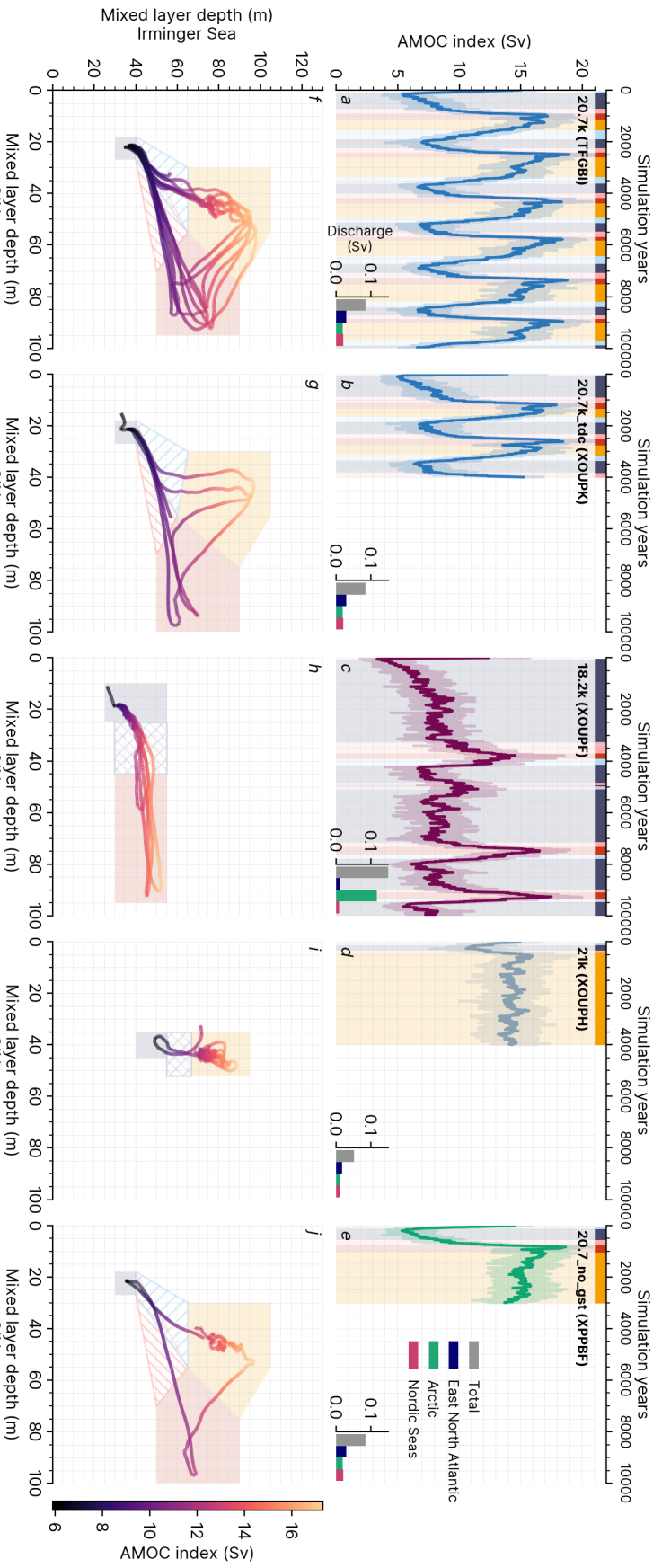

Figure 3.15: **Anatomy of the simulations expanded.** Same than 3.1 but for the *20.7k* (*a,f*), *20.7k_tdc* (*b,g*), *18.2k* (*c,h*), *21k* (*d,i*) and *20.7k_no_gst* *e,j* simulations.

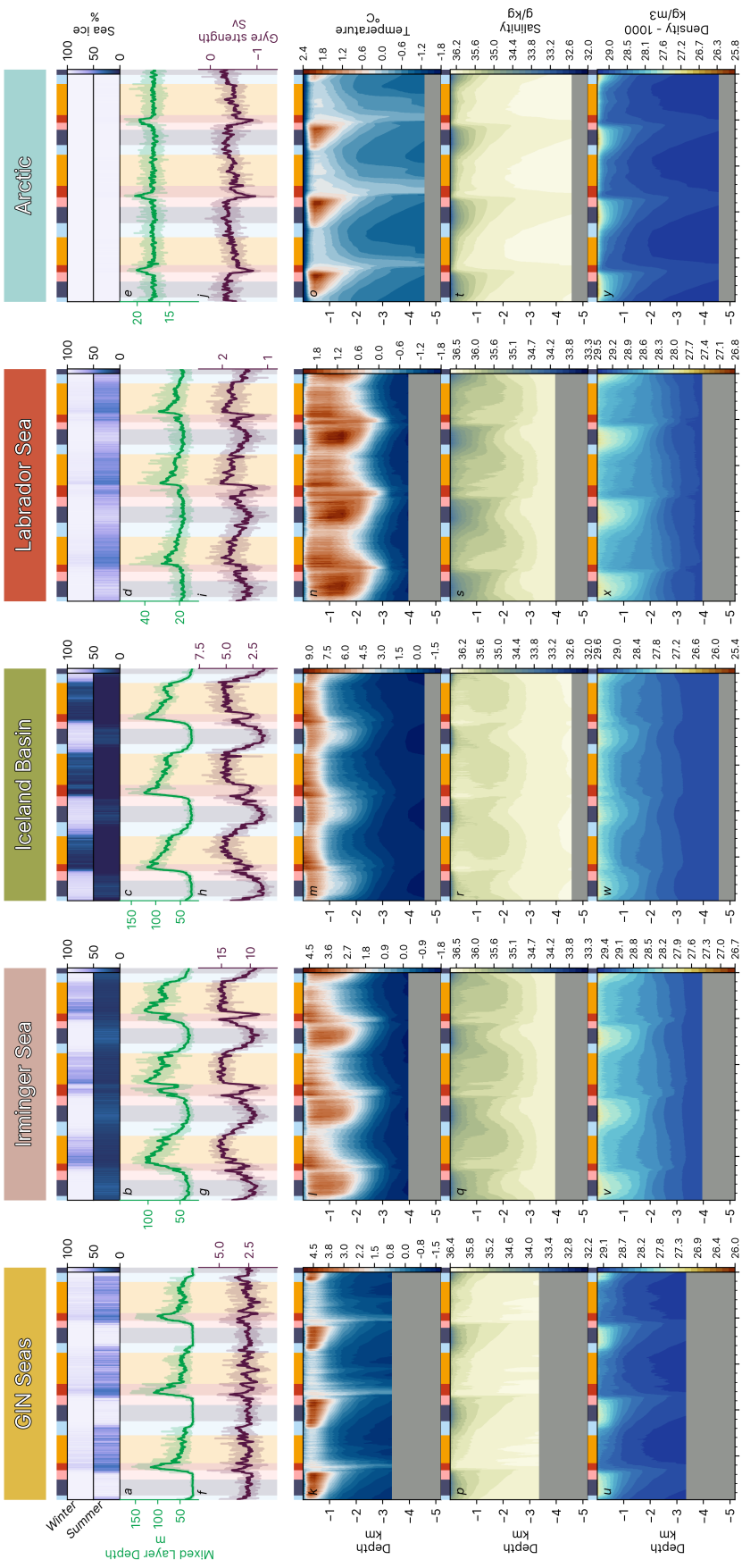

Figure 3.16: **North Atlantic dynamics at key deep water formation sites expanded.** Similar to Figure 3.2 for *20.7k*, but including the temperature and salinity profiles and the Labrador Sea and Arctic regions (see Figure 3.14*b*). The time series were expanded to cover the whole experiment.

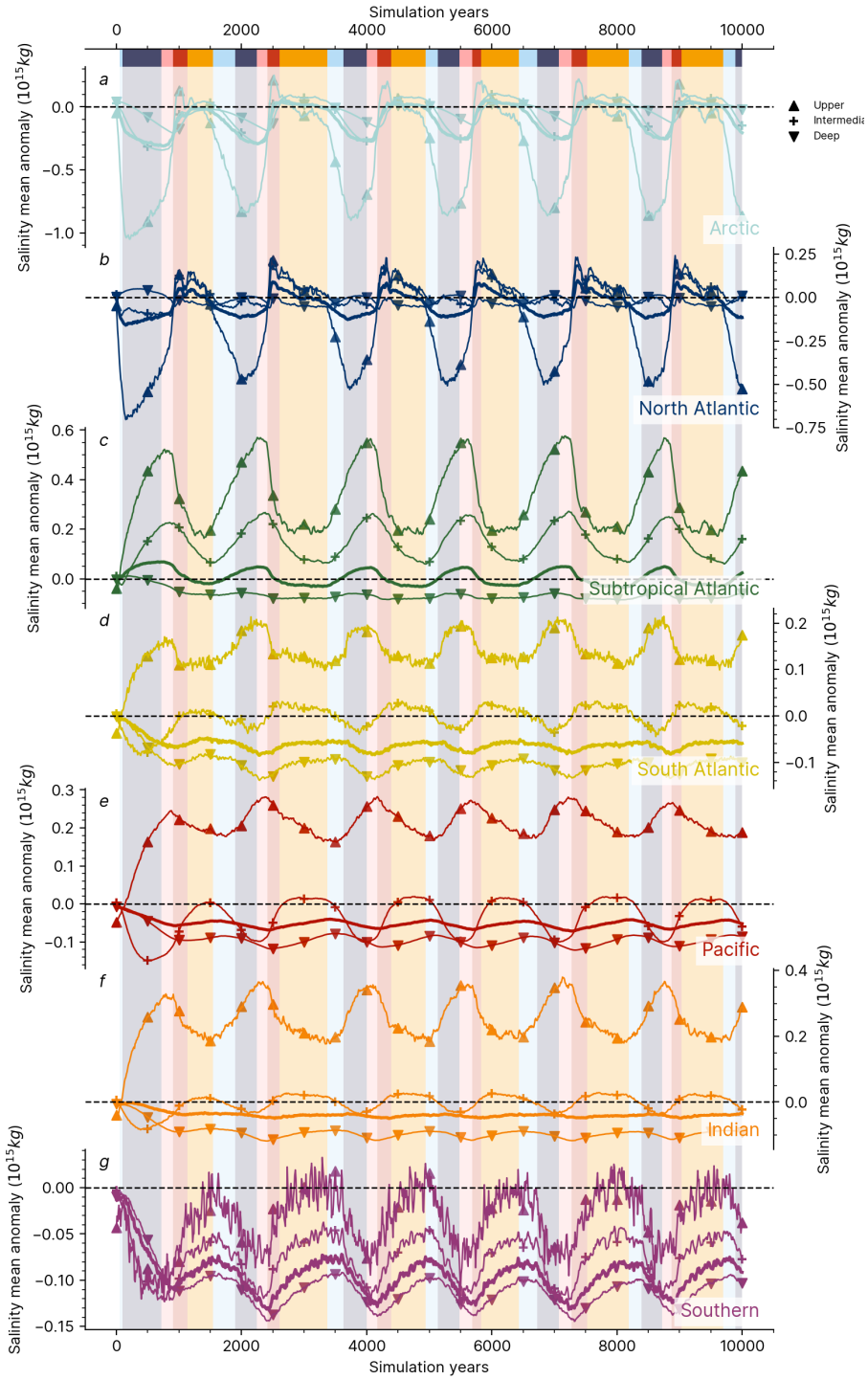

Figure 3.17: **Global salinity means.** Salinity weighted means as in Figure 3.3*b* in the different basins (see Figure 3.14*a*) and depths.

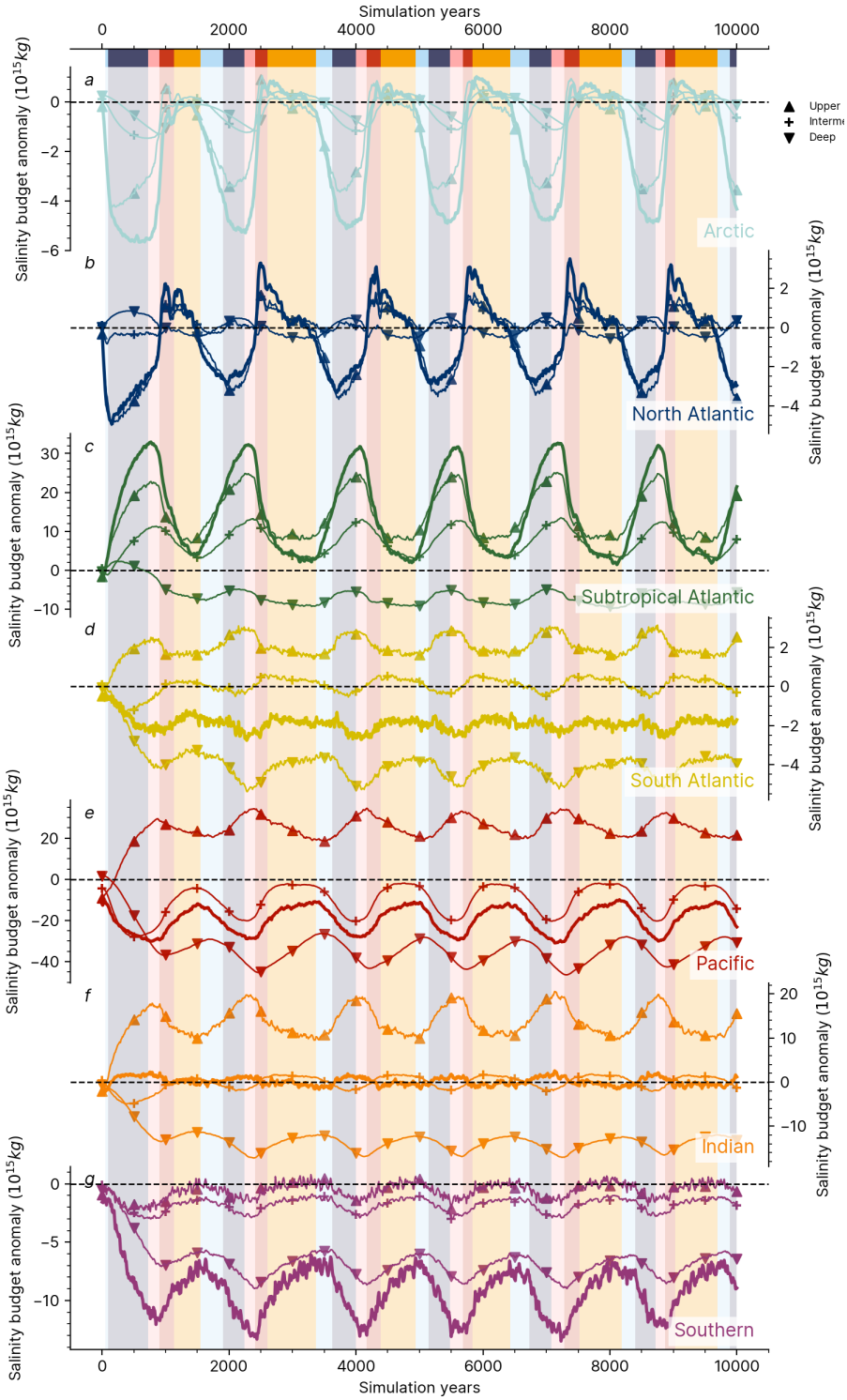

Figure 3.18: **Global salinity budgets.** Salinity budgets as in Figure 3.3*a* in the different basins (see Figure 3.14*a*) and depths.

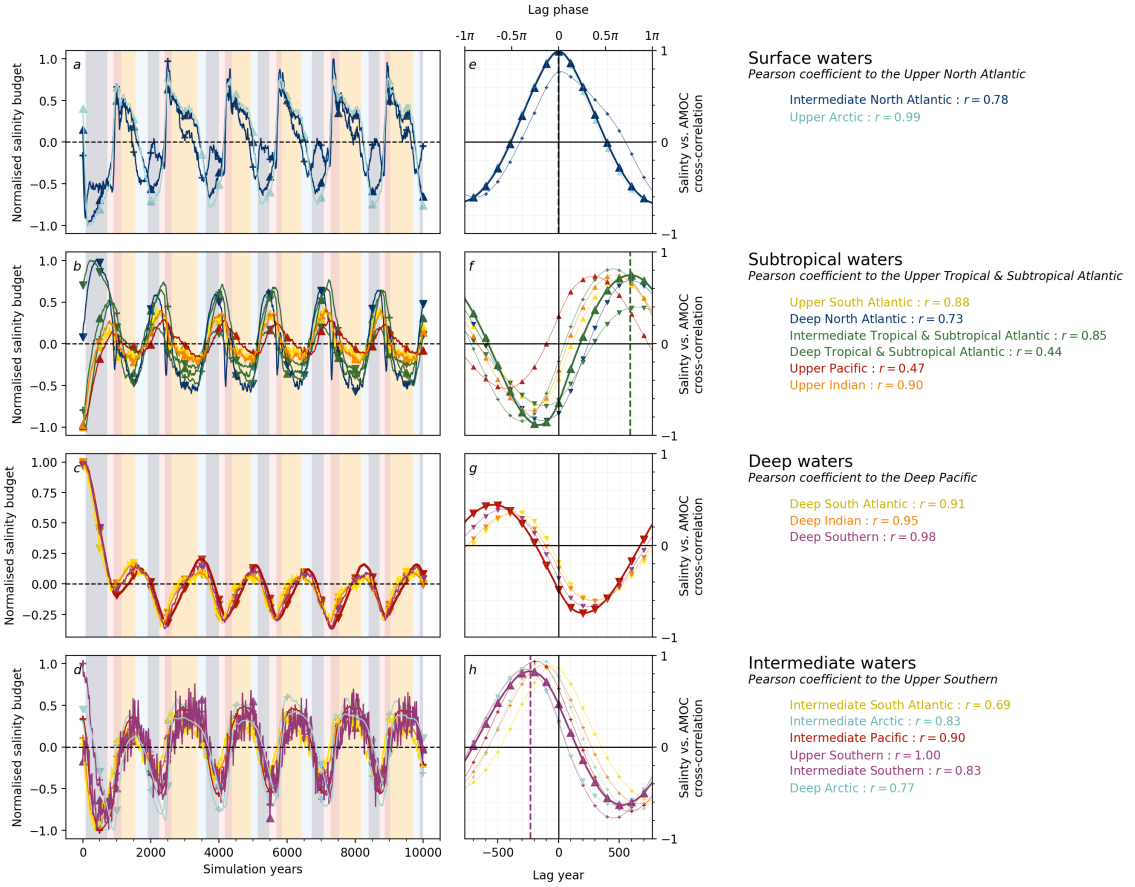

Figure 3.19: **Inter-basin salinity expanded.** *a-d.* Normalised salinity budgets (divided by the maximum value) in each domains defined in Figure 3.3*c-e*, with the addition of the *intermediate* domain. *e-f.* Same as Figure 3.3*d-f* including the *intermediate* domain. For each domain, a main signal was chosen and Pearson correlation coefficients were calculated between the main signal and all the other signals.

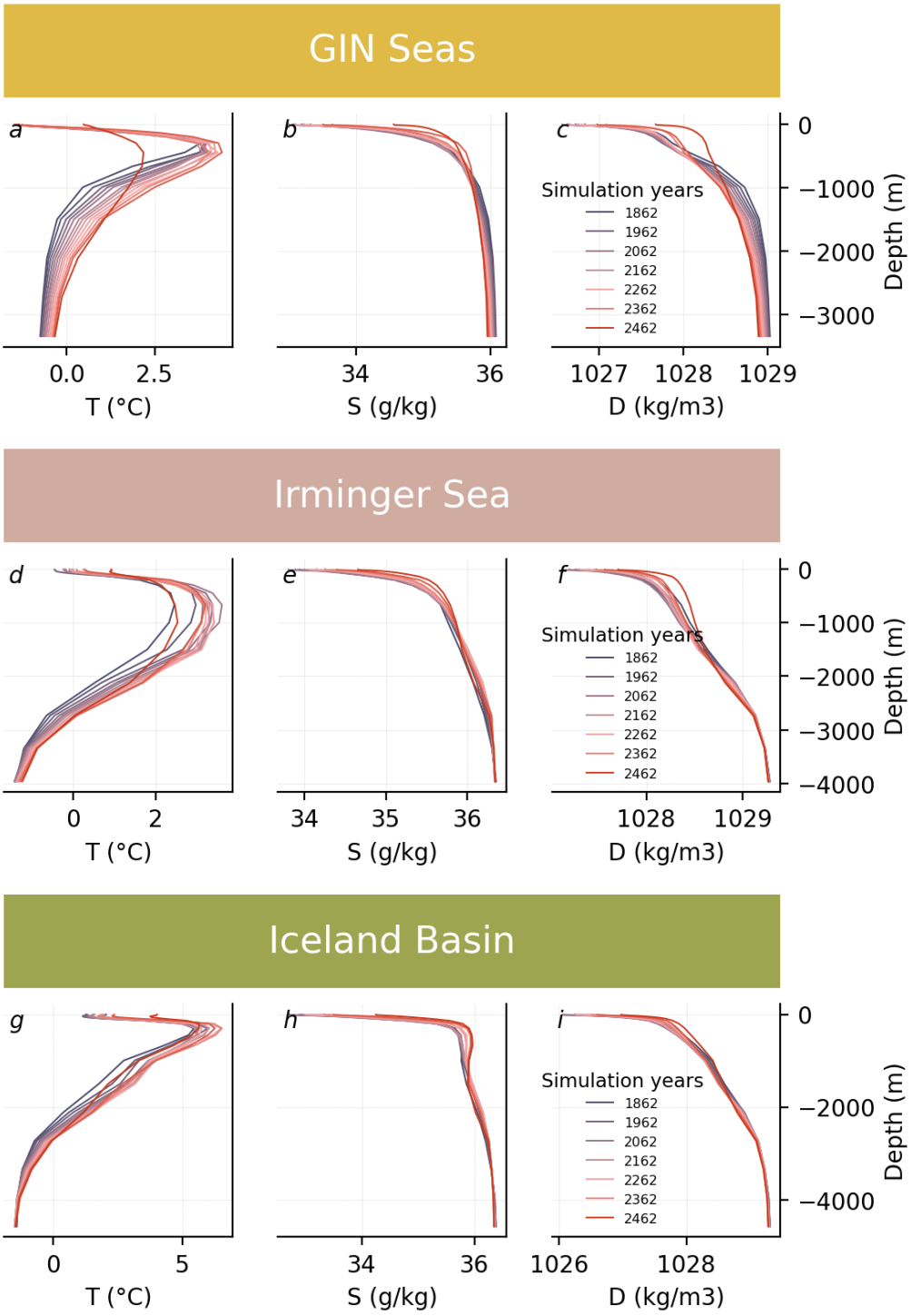

Figure 3.20: **North Atlantic vertical profiles, warming phase.** Vertical profiles of temperature (*a,d,g*), salinity (*b,e,h*) and density (*c,f,i*) in the GIN seas (*a-c*), the Irminger Sea (*d-f*) and the Iceland Basin (*g-i*) every 50 years during the warming phase of the *20.7k_tdc* simulation highlighted in Figure 3.5.

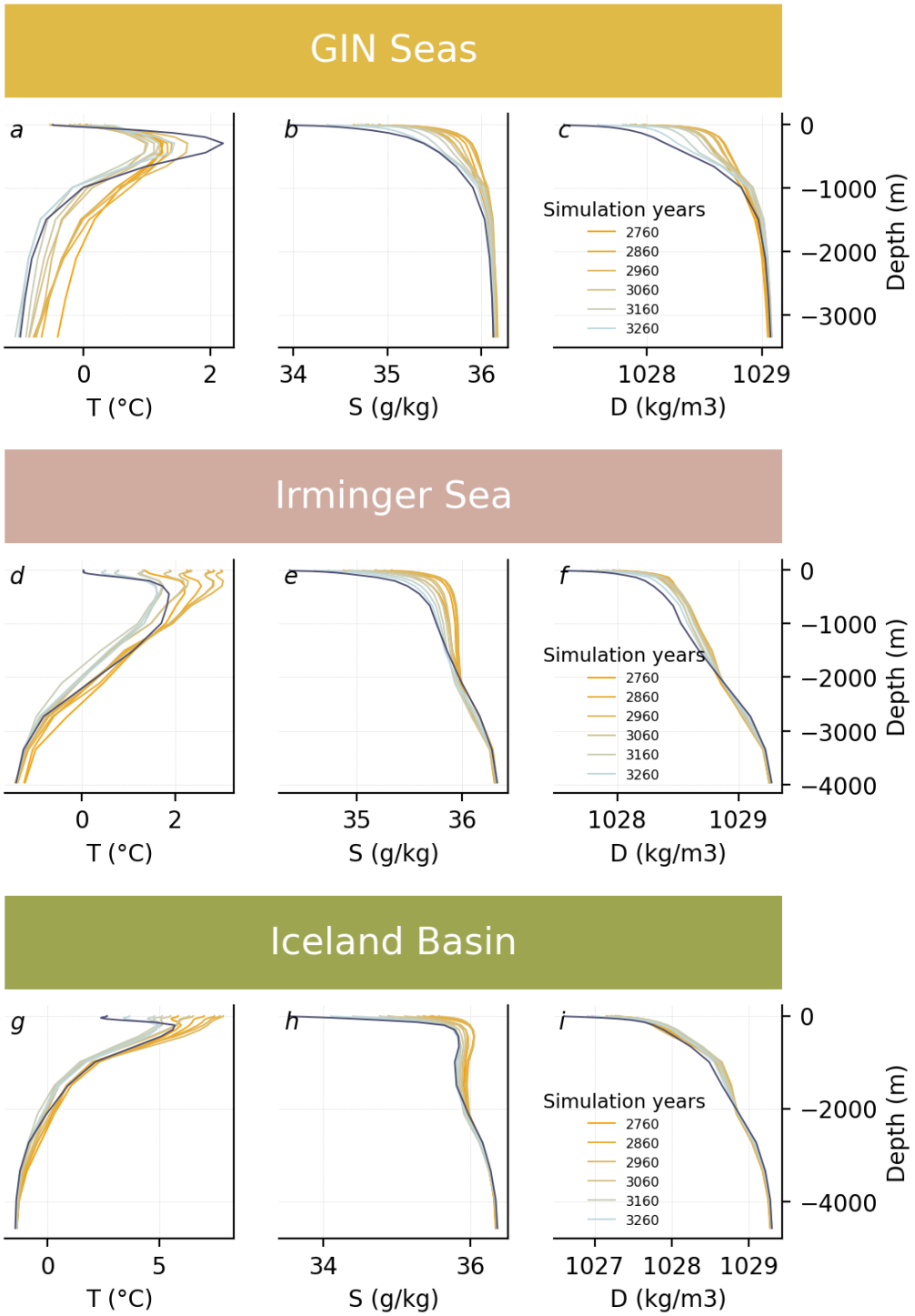

Figure 3.21: **North Atlantic vertical profiles, cooling phase.** Vertical profiles of temperature (*a,d,g*), salinity (*b,e,h*) and density (*c,f,i*) in the GIN seas (*a-c*), the Irminger Sea (*d-f*) and the Iceland Basin (*g-i*) every 50 years during the warming phase of the *20.7k_tdc* simulation highlighted in Figure 3.5.

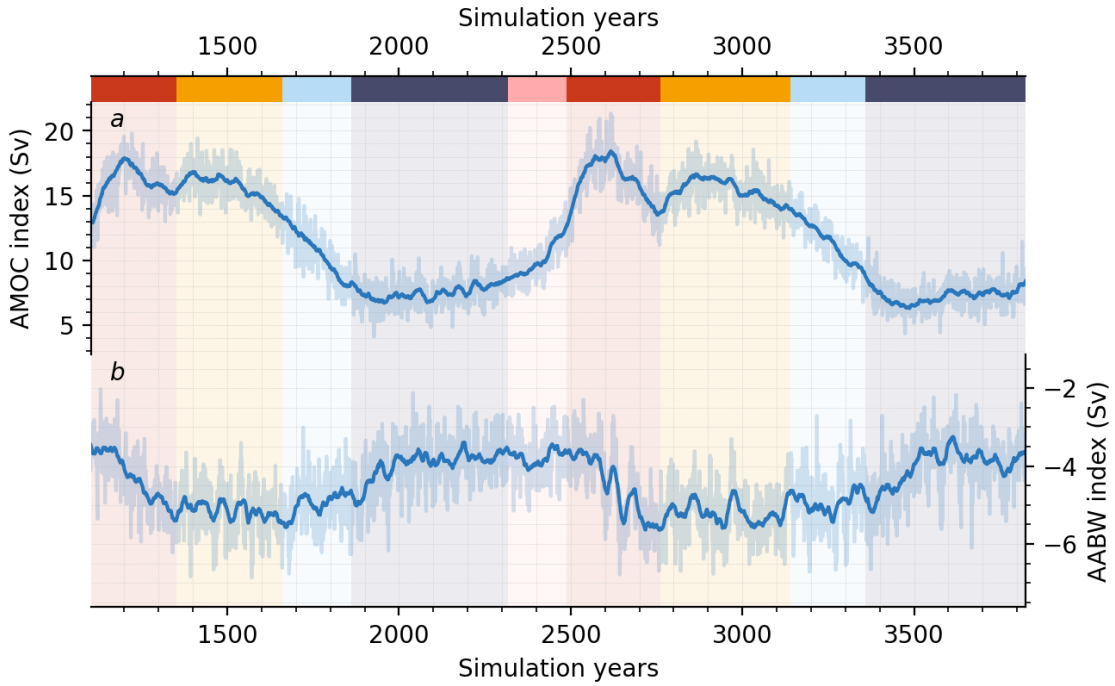

Figure 3.22: **Antarctica bottom waters index.** *a.* AMOC index of the *20.7k_tdc* simulation defined as the maximum overturning circulation at 26.5° N. *b.* AABW index of the *20.7k_tdc* simulation defined as the minimum overturning circulation at 33° S.

Chapter 4

Last deglaciation simulations sensitivity to the choice of ice sheets reconstructions and meltwater discharge pattern

Abstract

In the course of glacial terminations, the increases in greenhouse gas concentrations, summer insolation and the ice sheet demise can trigger episodes of millennial-scale variability. Such variability was observed during the last deglaciation, between 19 ka BP (thousand years ago) and 8 ka BP, in the form of the abrupt North Atlantic temperature shifts of the Bølling–Allerød Warming (14.5 ka BP) and Younger Dryas (12.900 ka BP).

In some climate models, abrupt climate changes can be generated by modifications in the boundary conditions, and freshwater discharge. The sensitivity of climate simulations to the ice sheet geometry and meltwater remains elusive, which is a caveat when considering the rapid demise of the North Atlantic ice sheets during the last deglaciation. In a new set of last glacial maximum HadCM3 simulations that can produce millennial-scale variability, we studied the influence of two ice sheet reconstructions, ICE6G and GLAC-1D, and their associated deglacial meltwater history, on the simulated chain of events of the last deglaciation.

Only the simulations using the GLAC-1D ice sheet reconstruction produced abrupt climate changes. In response to freshwater released close to the Nordic Seas and Iceland Basin deep water formation sites, the GLAC-1D-driven simulations display abrupt shifts in the Atlantic Meridional Overturning Circulation (AMOC) that are decoupled from the meltwater flux. In contrast, the ICE6G ice sheet reconstruction modifies the North Atlantic wind patterns, preventing convection in the Nordic Seas and intensifying the Iceland Basin deep water formation. As a result, no abrupt climate changes are simulated with ICE6G and the AMOC decreases almost linearly with the introduction of freshwater. The simulations do not capture the timing of the last deglaciation chain of events but the abrupt events replicate the main Northern Hemisphere characteristics of the Bølling Warming and the North Atlantic climate changes are very similar to Dansgaard-Oeschger transitions.

4.1 Introduction

The last deglaciation, dated between 19 ka BP (thousand years ago) and 8 ka BP (Clark et al., 2012), is the most recent major climate change event before the Anthropocene. Its proximity to our era implies that a large number of proxy records are available, including ice sheets (e.g. Batchelor et al., 2019), temperatures (e.g. Waelbroeck et al., 2002) and ocean circulation (e.g. Ng et al., 2018) reconstructions. This period provides a great case study to understand better past and future climate changes, but climate simulations still fail to reproduce the complexity of the chain of events of this period.

The last deglaciation sets off at the end of the last glacial maximum, corresponding to a minimum in sea level (Peltier and Fairbanks, 2006; Lambeck et al., 2014) and Greenland surface temperatures (N.G.R.I.P, 2004). It is believed that changes in solar insolation (Berger, 1978) triggered the demise of the large ice sheets formed during the last glacial period (Hays et al., 1976). Temperatures increased in the Southern Hemisphere (Jouzel et al., 1995; Stenni et al., 2011) and the Northern Hemisphere (Shakun et al., 2012; Buizert et al., 2014) and greenhouse gas concentrations rose (Loulergue et al., 2008; Schilt et al., 2010; Bereiter et al., 2015). Over the ten thousand years of the deglaciation, the complete melting of the Cordilleran and Laurentide ice sheets (Dyke et al., 2002) and Eurasian ice sheet (Hughes et al., 2016) along reduction of the Greenland and Antarctica ice sheets (Tarasov and Peltier, 2002; Briggs et al., 2014) led to a sea level rise of 130 to 150 meters (Peltier and Fairbanks, 2006; Lambeck et al., 2014).

The long-term trends were marked by shorter abrupt climate change events, probably linked to massive reorganisations of the Atlantic Meridional Overturning Circulation (AMOC McManus et al., 2004; Ng et al., 2018). During **Heinrich Stadial 1** (∼18 ka BP to ∼15 ka BP Denton et al., 2006; Roche et al., 2011)), a see-saw pattern was observed, with increasing Southern Ocean temperatures (Parrenin et al., 2007) while the North Atlantic cooled (Bard et al., 2000; Buizert et al., 2014) due to a possible slowdown of the AMOC (McManus et al., 2004; Bradtmiller et al., 2014; Ng et al., 2018). This preceded the last of the Heinrich events (Heinrich, 1988), massive discharges of icebergs breaking from the Laurentide ice sheet (Hemming, 2004; Hall et al., 2006; Stanford et al., 2011; Hodell et al., 2017). At the end of Heinrich Event 1, a sharp transition to an interstadial took place around year 14.5 ka BP - this is the **Bølling–Allerød Warming** (Severinghaus and Brook, 1999). The accelerated ice sheet melting during this warm stage led to a peak in meltwater discharge called **Meltwater Pulse 1a** (Deschamps et al., 2012; Gregoire et al., 2012). Around year 13 ka BP, a shift back to a cold state was recorded during the **Younger Dryas** (Murton et al., 2010; Liu et al., 2012), and marked the final event before the slow transition to the Holocene (Clark et al., 2012).

This complex chain of events has still not been simulated in state-of-the-art climate models despite some promising early attempts (Liu et al., 2009). This gap motivated the creation

of a PMIP4 international working group, and a protocol for simulating climate changes of the last deglaciation was written by Ivanovic et al. (2016). A first batch of simulations was analysed by Snoll et al. (2023) and showed that simulations reproduced the timing of the events right (e.g. He et al., 2021) only when fitting the freshwater input to the expected outcome. The simulations using realistic freshwater fluxes come short of capturing the entirety of the records (e.g. Obase and Abe-Ouchi, 2019). Two primary sources of uncertainty have been put forward to explain this issue.

The first uncertainty comes from the choice of ice sheet reconstructions. PMIP protocol provides the option of using two reconstructions: ICE6G (Peltier et al., 2015) and GLAC-1D (Tarasov and Peltier, 2002; Tarasov et al., 2012; Briggs et al., 2014; Ivanovic et al., 2016). They are using different methods to fit the proxy records for ice extent and sea level change which results in significant discrepancies in their thickness and ice surface elevation. GLAC-1D provides a glaciologically consistent reconstruction derived from an ice sheet model, while ICE6G prioritises the fit of the sea level records and global isostatic rebound measurements (Ivanovic et al., 2016). Such differences in ice sheets can have significant impacts on the albedo and radiative balance (Roberts and Valdes, 2017), winds and gyres (Montoya et al., 2011; Roberts et al., 2014b; Madonna et al., 2017) and on the atmospheric circulation (Izumi et al., 2023). As a result, groups who have run transient simulations with the two different ice sheets have observed different amplitude and timing of climate changes (e.g. Kapsch et al., 2022; Bouttes et al., 2023). No HadCM3 last deglaciation run has been published with GLAC-1D ice sheet reconstruction. This is despite the Ivanovic et al. (2018b) hypothesis that it could be more suited to the simulation of Heinrich Stadial 1 due to higher rates of melting from the Eurasian ice sheet during the early deglaciation, a hypothesis backed by the abrupt cooling obtained with meltwater snapshots of the period in Chapter 2.

The second source of uncertainty comes from the meltwater effect on the North Atlantic climate (Bethke et al., 2012). The AMOC is very sensitive to freshwater hosing (Paillard and Labeyrie, 1994; Vidal et al., 1997), which can consequently alter the global climate (Clark et al., 2002; Rahmstorf, 2002). The location of meltwater discharge is the key factor affecting the efficiency of the disruption, with regions close to deep water formation sites being the most sensitive to freshwater (Roche et al., 2010). This aspect is crucial as freshwater discharge is believed to have been a main driver of change in the early Heinrich Stadial 1 (Zaragosi et al., 2001; Toucanne et al., 2015; Peck et al., 2006), especially since meltwater could be directly routed to deep water formation sites (Condron and Winsor, 2012). However, uncertainties still exist regarding its provenance (Scourse et al., 2009; Bigg et al., 2012), and the diverse implementation of meltwater discharge in climate simulations (Kageyama et al., 2013b; Snoll et al., 2023) is a primary source of discrepancy, considering how sensitive climate models are to the location of freshwater discharge (Smith and Gregory, 2009; Roche et al., 2010).

In this Chapter, we isolate these two primary sources of uncertainty to analyse their impact in the context of simulations of the last deglaciation. We expand on the findings of a new set of HadCM3 simulations of the last glacial maximum presented in Chapter 2 that have shown strong millennial-scale variability to include time-evolving meltwater patterns. The first Section presents the model and experimental design of the new meltwater transient simulations. The second Section introduces the four new simulations and gives a detailed view of their dynamic evolution. The third Section explores the role of the ice sheet reconstruction in changes in the atmospheric circulation and its consequences on the deep water formation sites. The fourth Section quantifies the impact of meltwater discharge in HadCM3. Finally, we compare our results to other deglacial simulations and to climate records of climate change.

4.2 Methods

4.2.1 The HadCM3 model

The simulations presented here all use the same model and a similar set-up as Ivanovic et al. (2018a). This is the HadCM3B atmosphere/ocean/land and vegetation general circulation model (GCM) described in Valdes et al. (2017) and put together by the BRIDGE (Bristol Research Initiative for the Dynamic Global Environment) group. The atmosphere model, described by Pope et al. (2000), is a 2.5° × 3.75° grid with 19 elevation layers. It is coupled every simulation day with a 20 layer 1.25° × 1.25° ocean model, described by Gordon et al. (2000). The land model is MOSES 2.1 (Cox et al., 1999) with the addition of the TRIFFID dynamic vegetation model (Cox, 2001).

HadCM3 has historically been used as a CMIP3 model (Stott et al., 2000) and was still part of the CMIP5 ensemble (Taylor et al., 2012). It has been widely used for palaeoclimate simulations and has contributed to PMIP3 and PMIP4 analysis (e.g. Lunt et al., 2012; Haywood et al., 2016; Kageyama et al., 2021; Snoll et al., 2022). The ocean model uses a rigid lid geometry, which means that the ocean volume is not modified by the model during the run, and exchanges of water between the ocean and atmosphere or ice sheets are not done by adding (removing) water to the ocean, but instead reducing (increasing) salinity (Gordon et al., 2000). The water can accumulate in inland seas or ice sheets, potentially leading to drifts of global ocean salinity. To prevent these drifts, the global mean salinity has to be set manually using a global salinity conservation algorithm described by Dentith et al. (2019b) and Chapter 3. This correction flux is applied to the entire volume of the ocean to meet a global salinity. Here, we apply a temporally varying global salinity target by matching the ice volume changes from the ice sheet reconstruction imposed.

4.2.2 Transient meltwater discharge algorithm

We updated the methods presented by Ivanovic et al. (2017) to create the transient meltwater patterns. The algorithm derives the amount of freshwater released in every ocean grid point from changes in ice sheet elevation at each time step of the ice sheet reconstruction. Once the ice thickness loss has been converted into freshwater, the water is routed to the corresponding ocean discharge point following an offline routing map provided by Wickert et al. (2013). In order to work around the fixed volume of the ocean in the model and to avoid the $0PSU$ saturation phenomenon (Section S2), we created capture zones where the routed freshwater release points are spread uniformly across the entire region. The configuration of this algorithm is the same as in Ivanovic et al. (2018a), with just minor modifications on the catchment and release regions.

Some examples of using such an algorithm are given for snapshots of discharge in Chapter 2 and a transient meltwater history in Ivanovic et al. (2018a). In this study, transient meltwater histories were calculated for two different ice sheet reconstructions. For ICE6G (Peltier et al., 2015), we extended the time series calculated by Ivanovic et al. (2018a). For GLAC-1D, we extended the time series calculated for Section 2.10. To account for the changes in global salinity due to the changes in ice volume throughout the deglaciation, the global salinity of the ocean was derived for each ice sheet reconstruction and used as the global salinity target even if the ice volume does not change in our simulations.

4.2.3 Experiment design

This Chapter's simulations build on the work by Ivanovic et al. (2018a) to produce a new set of meltwater transient simulations. All the simulations are based on the two last glacial maximum runs created following the PMIP4 protocol (Kageyama et al., 2017). The atmospheric greenhouse gas concentrations are set for all simulations to $190ppm$ for CO_2 (Bereiter et al., 2015), $375ppb$ for CH_4 (Loulergue et al., 2008), and $200ppb$ for N_2O (Schilt et al., 2010), and orbital parameters to their 21 ka BP values taken from Berger (1978). The simulations only differ by choice of the ice sheet reconstruction and associated freshwater flux correction (or waterfix), using GLAC-1D at 21 ka BP for *GLAC1D_noMw*, initially run for Chapter 2, and ICE6G at 21 ka BP for *ICE6G_noMw*, initially run by Ivanovic et al. (2018a). Because they have no extra meltwater discharge, they will be referred to as the *control* simulations. A summary of the different simulations is given in Table 4.1.

The *transient* simulations used the temporally evolving meltwater patterns described in Section 4.2.2. The simulations using GLAC-1D ice sheet and meltwater pattern were named *GLAC-1DMw*. The simulation using ICE6G ice sheet and meltwater pattern was called *ICE6GMw*. In addition, two extra simulations were run with inverted meltwater discharge: *GLAC_1D-ICE6GMw* using GLAC-1D ice sheet and ICE6G meltwater, and

Table 4.1: **Experiments summary**. All simulations use HadCM3 with LGM boundary conditions. *Control* simulations have no freshwater input, and *transient* simulations derive the meltwater from one of the ice sheet reconstructions. The ice sheet geometries are fixed at their LGM boundary conditions. The *Icelandic ice sheet* column is explained in Section 4.10.

Simulation	Start year	Integration length	Ice sheet geometry	Meltwater discharge	Icelandic ice sheet
GLAC-1D_noMw	-22000	$\sim$ 4,000 years	GLAC-1D	Control	Absent
GLAC-1D_Mw	-21500	9,500 years	GLAC-1D	Transient (GLAC-1D)	Absent
GLAC-1D_GLAC-ICE6GMw	-21500	9,500 years	GLAC-1D	Transient (ICE6G)	Absent
ICE6G_noMw	-22000	5,000 years	ICE6G	Control	Present
ICE6G_Mw	-21500	9,500 years	ICE6G	Transient (ICE6G)	Present
ICE6G_GLAC-1DMw	-21500	9,500 years	ICE6G	Transient (GLAC-1D)	Present
ICE6G_noMw_noIcd	-22000	5,000 years	ICE6G	Control	Removed

ICE6G-GLAC_1DMw using ICE6G ice sheet and GLAC-1D meltwater. The land-sea mask was fitted to the ice sheet reconstruction. This implies that in some cases, the meltwater patterns of *GLAC_1D-ICE6GMw* and *ICE6G-GLAC_1DMw* indicated discharge in a grid cell that is now land rather than an ocean grid cell. In these cases, the freshwater was respread over the remaining spreading region.

At last, a sensitivity simulation to assess the influence of the Iceland ice sheet in ICE6G was run and called *ICE6G_noMw_noICD*. It copies *ICE6G_noMw*, and only the Iceland ice sheet was removed. The detail of the algorithm used to modify the Icelandic ice sheet is given in Section 4.10, and resulted in the ablation of an average of 1655 meters in the region. The changes in albedo and vegetation were also included, although these are minor, considering that Iceland is mostly covered in snow in GLAC-1D simulations.

4.3 A new set of meltwater transient simulations

Figure 4.1 shows the two meltwater discharge histories (*a,b*), and the AMOC indexes, defined as the maximum of the overturning circulation at 26.5° N to match the RAPID array (Smeed et al., 2014), for the *control* and *transient* simulations (*c,d*). In the same way as Chapter 2, a *warm* (*cold*) mode is obtained when the AMOC index remains high (low) for a prolonged time, as these correspond to warm (cold) climate in the North Atlantic. The two simulations with no meltwater, *GLAC-1D_noMw* and *ICE6G_noMw* do not show significant millennial-scale variability in the AMOC index and remain stable in a warm mode with an AMOC index of about $15Sv$. In the rest of this Chapter, these two simulations will be used as *control* states.

GLAC-1D_Mw displays regular and abrupt transitions between warm and cold modes (Figure 4.1*c*). For the first 7,000 years of the simulation, a stable warm mode is disrupted by regular meltwater discharge events (Figure 4.1*a*). When the discharge increases, the AMOC index dwindles and reaches a minimum of about a hundred years after the meltwater peaks (Figure 4.1*e*). The cold modes are sustained for less than a hundred years, and the AMOC index drops range between $2Sv$ and $11Sv$. After the meltwater discharge peak and before the meltwater discharge minimum, the AMOC index recovers sharply to a warm mode through an overshoot phase. The peaks every thousand years in the cross-correlation patterns in Figure 4.1*e* are due to the strong millennial-scale variability of the meltwater discharge, highlighted by the auto-correlations patterns in Figure 4.12. During the final 2,000 years, the discharge is more substantial and the warm mode is no longer stable. A cold mode is sustained for several hundred years around the 14.2 ka BP meltwater pulse 1A. Over the last 2,000 years, a similar behaviour is observed for the *GLAC-1D_ICE6GMw* simulation in Figure 4.1*d*. Before $\sim$ 16 ka BP, however, the ICE6G meltwater discharge is less fluctuating and generally weaker than the GLAC-1D pattern (Figure 4.1*b*). Consequently, the climate remains in a warm, stable and with a slightly

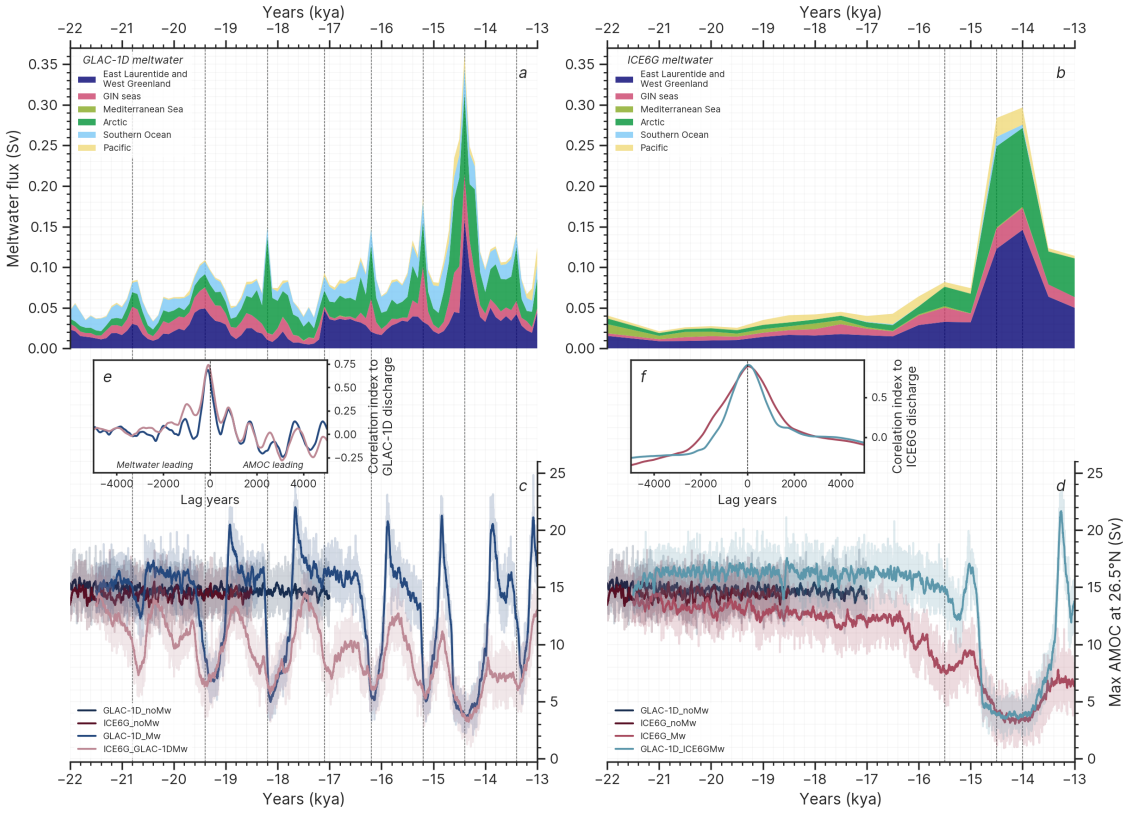

Figure 4.1: **Meltwater fluxes and AMOC changes.** *a,b.* Time-series of Meltwater discharge derived from GLAC-1D (*a*) and ICE6G (*b*) following the algorithm presented in Section 4.2.2. The regions are defined in Figure 4.11*a*. *c,d.* Time-series of AMOC index, defined as the maximum overturning circulation at 26.5° N, in the *control* and *transient* simulations. Solid lines are 30-year running means and shaded bands are annual data. *e,f.* Cross-correlation between the AMOC index and the meltwater discharge.

stronger AMOC mode than *GLAC-1D_noMw*. The intensification of the discharge in two main events around 15.5 ka BP and 14 ka BP triggers a first weak and short-lived drop followed by an abrupt and prolonged transition to a cold mode ended by an overshoot of the AMOC.

In Figure 4.1*d*, *ICE6G_Mw* follows a similar evolution to *GLAC-1D_ICE6GMw*, only the transitions to and back from a cold mode are not as abrupt. The AMOC index decreases slowly from the onset of the simulation and does not return to the warm control state within the simulation running time. As a result of the absence of abrupt warming, it does not contain any overshoot phase. In Figure 4.1*c*, *ICE6G_GLAC-1DMw* shows dips in the AMOC index aligned with the meltwater discharge (Figure 4.1*f*). There does not seem to be a stable warm or cold mode, or at least the climate system does not reach them, and the AMOC index responds more linearly to the meltwater discharge.

There is a clear link between the ice sheet reconstruction used and the abruptness of the model's response to the meltwater discharge. Further exploration of the dynamical evolution of the simulations in Figure 4.2 gives an insight into the fundamental differences between the GLAC-1D simulations (i.e. the simulations using the GLAC-1D ice sheets boundaries) and the ICE6G simulations (i.e. the simulations using the ICE6G ice sheets boundaries). In Figure 4.2*i,j*, both *GLAC-1D_Mw* and *GLAC-1D_ICE6GMw* follow the tri-modal pattern described in Chapters 2 and 3. In addition to the *cold* mode, indicated here by a weak AMOC and sporadic convection in the Nordic seas and the Irminger Sea (shallow mixed layer depth), we observe two *warm modes*. The *meridional* mode is an overshoot mode of the AMOC, where convection is primarily located in the GIN Seas and the Iceland Basin. The *zonal* mode corresponds to the control mode, with a relatively strong AMOC and a main deep water formation site in the Irminger Sea and the Iceland Basin. The time-evolving global salinity imposes a freshening of the global mean salinity (Figure 4.13*i-l*). In the GLAC-1D simulations, this slow drift is overlaid by transfers of salt between the Atlantic and the Pacific Basin around times of AMOC disruptions (Figure 4.13*i,j*). These patterns recall the global component of the oscillating mechanism described in Chapter 3. The changes in global salt disruptions are linked to fast modifications in North Atlantic stratification, represented by the N_2 index (Li et al., 2020) in Figure 4.2*e,f*. The oscillating motion is not sustained as in the *oscillating* simulations in Chapter 2, but the cycles around a meltwater peak resemble an oscillating cycle.

The *meridional* mode is never obtained in *ICE6G_Mw* and *ICE6G_GLAC-1D_Mw*, as demonstrated by Figure 4.2*k,l*. Instead, all the points are situated on a line between the *cold* and the *zonal* modes in the state space. The absence of convection in the GIN Seas is likely linked to a strong stratification in this region in simulations forced with the ICE6G ice sheet (Figure 4.2*g,h*). In the ICE6G simulations, there is no obvious activation of the global salt oscillator. As a result, these cycles resemble more the *cold* simulations in Chapter 2 and do not have the characteristic of an oscillating cycle.

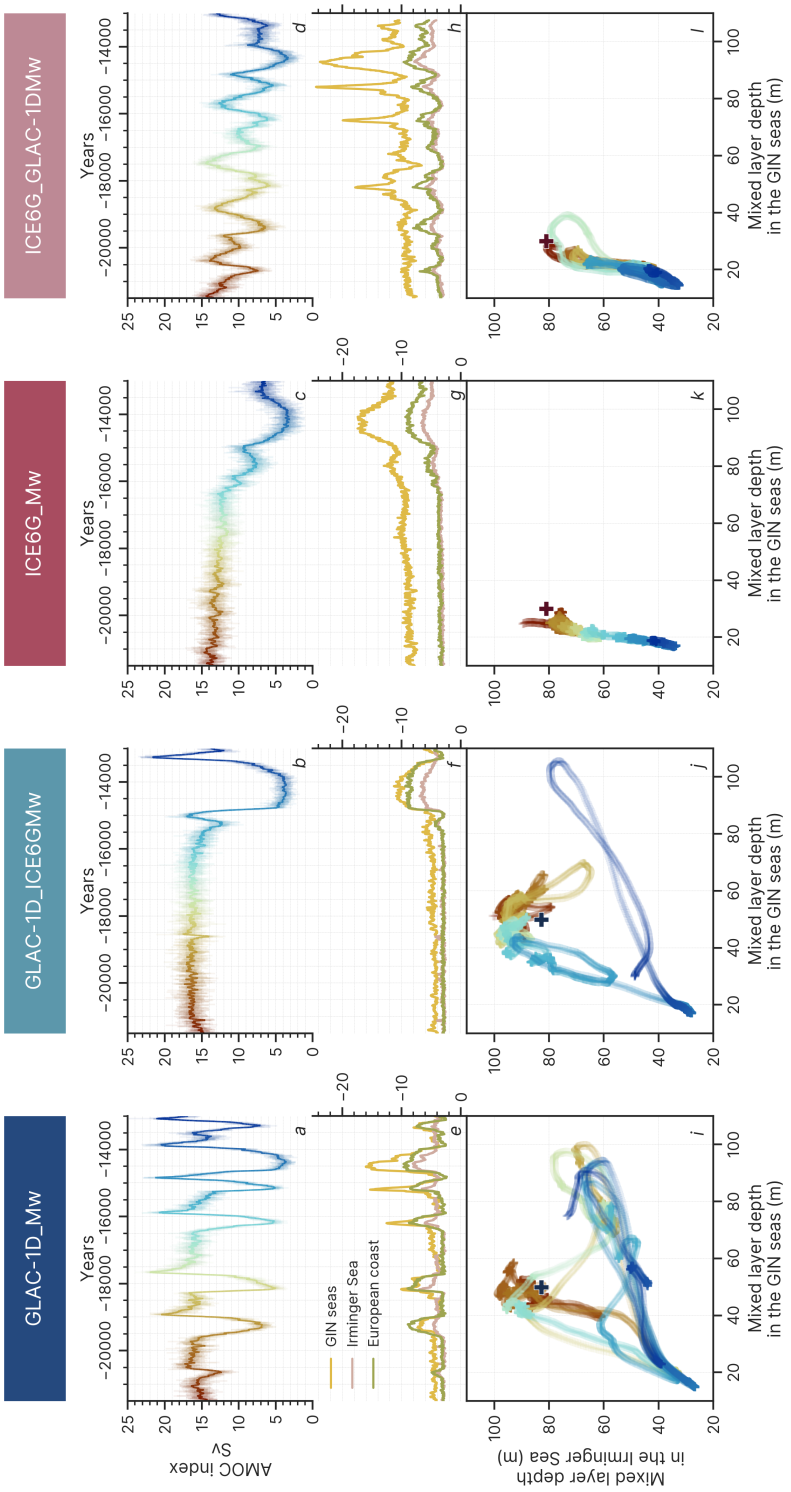

Figure 4.2: **Dynamics of the transient simulations.** *a-d.* Time-series of AMOC index (maximum overturning circulation at 26.5° N). Solid lines are 30-year running means and transparent lines are annual data. Colours are used as time markers for panels *i-l.* *e-h.* N_2 stratification index for the three main regions of deep water formation. Zones are defined in Figure 4.11*c*. More negative values indicate higher ocean stratification. *i-l.* Mixed layer depth in the Greenland Iceland Nordic seas (GIN Seas) plotted against the mixed layer depth in the Irminger Sea. Each individual point represents the yearly data processed by a low-pass filtered time series centred around 1000 years – described in detail in Section 2.13. The blue and red crosses represent the mean state of *GLAC-1D_noMw* and *ICE6G_noMw*, respectively. The colours match panels *a-d.*

4.4 The influence of the ice sheet reconstruction - deep water formation sites and atmospheric circulation

The previous Section showed that only simulations using the GLAC-1D ice sheet reconstruction exhibit abrupt climate transitions. GLAC-1D and ICE6G were created using separate methods, which resulted in significantly different ice sheet geometries (Ivanovic et al., 2016). The impact of the ice sheet layout on the atmospheric circulation of the last glacial maximum has been regularly highlighted in climate models (e.g. Pausata et al., 2011; Kageyama et al., 2013a; Merz et al., 2015; Izumi et al., 2023). To isolate the influence of the ice sheets in this Chapter's simulations, the last hundred years of the two *control* simulations were compared in Figure 4.3.

There is a striking dissimilarity in the mixed layer patterns between the two simulations (Figure 4.3*a-c*). In *ICE6G_noMw*, convection is intense and concentrated along the GIS (Greenland-Iceland-Scotland) ridge, with mixed layer reaching 600 meters deep in the Iceland Basin. In return, the mixed layer is shallow in the GIN Seas and in the Labrador Sea and Baffin Bay, where a check-board pattern is visible. *GLAC-1D_noMw*'s deep water formation sites are more spread across the North Atlantic and do not have an average mixed layer deeper than 200 meters. Compared to *ICE6G_noMw*, convection is more vigorous in the Nordic Seas and more localised in the Labrador Sea. The intensification of the North Atlantic current in *ICE6G_noMw* drives sea surface temperatures to increase by up to $7.5°C$ between 35° N and 60° N (Figure 4.14*c*), resulting in a warmer surface atmosphere by an average of $1.5°C$ (Figure 4.14*f*). In the Nordic Seas, however, the absence of convection in *ICE6G_noMw* drives a cooling of the region's sea surface temperatures by $\sim 3.5°C$.

The mixed layer depth anomaly in Figure 4.3*c* shares noticeable similarities with the wind stress anomaly in Figure 4.3*f*. The more intense Iceland Basin convection matches an increase in surface wind stress by up to $4.5m.s^{-1}$ in *ICE6G_noMw* compared to *GLAC-1D_noMw*, and the lower Nordic Sea's mixed layer depth anomaly matches a surface wind drop by as low as $5.5m.s^{-1}$. The difference in wind patterns in the Nordic Seas is clearly linked to GLAC-1D's Eurasian ice sheets, which are higher and smoother than ICE6G's (Figure 4.3*g*). This results in stronger and more consistent winds around the Eurasian ice sheet in the *GLAC-1D_noMw* simulation (Figure 4.3*e*). Higher winds are also simulated at the northeastern and western edges of the Laurentide ice sheet in *GLAC-1D_noMw* where the slope is more regular than in *ICE6G_noMw*. The wind patterns around the ice sheets in the different reconstructions can explain the mixed layer depth anomaly in the Nordic Seas and the Labrador Sea. It does not, however, provide an explanation for the North Atlantic positive wind anomaly at 60° N and the negative wind anomaly at 50° N between *ICE6G_noMw* and *GLAC-1D_noMw* in Figure 4.3*f*.

The wind anomalies in the North Atlantic between 50° N and 60° N can result from three

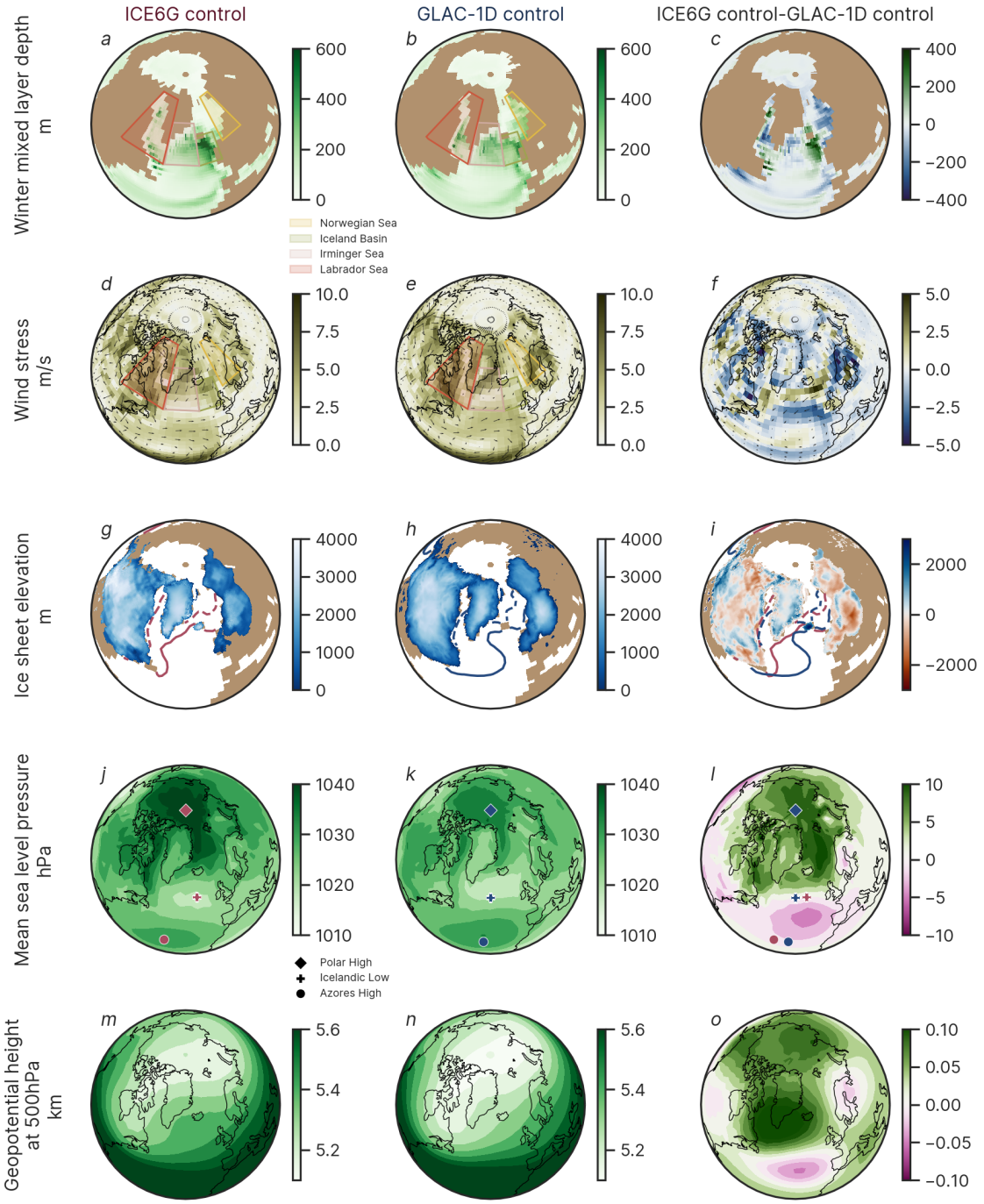

Figure 4.3: **Influence of ice sheets reconstructions on the control simulations.** Climatologies of the final hundred years' annual means of *ICE6G_noMw* (panels *a,d,g,j,m*), *GLAC-1d_noMw* (panels *b,e,h,k,n*) and the anomalies between *ICE6G_noMw* and *GLAC-1d_noMw* (panels *c,f,i,l,o*) for the winter mixed layer depth (panels *a-c*), the wind stress (panels *d-f*), the ice sheet elevation and sea ice extent (panels *g-j*), the mean sea level pressure (panels *j-l*) and the 500hPa geopotential height (panels *m-o*). The zones in panels *a-f* correspond to the main deep water formation regions. Winter (solid line) and summer (dashed line) 50% sea ice concentration is indicated in panels *g-j*.

distinct (but not independent) points: (i) a movement of the jet stream, (ii) changes in North Atlantic sea level pressure, and (iii) the influence of the Icelandic ice sheet. (i) Glacial ice sheets are believed to have modified the strength and the tilt of the jet stream (Merz et al., 2015), and therefore the choice of ice sheet reconstructions can impact the geometry of the jet (Izumi et al., 2023). In the *control* simulations, this is reflected by a higher geopotential height at high latitudes in *ICE6G_noMw*, reaching more than a hundred meters off the southeastern tip of Greenland, and a lowering of the geopotential height around the Azores (Figure 4.3*o*). This drives the jet in a more zonal and equatorward position, with higher wind speeds between 30° N and 40° N. This conclusion is shared with Kapsch et al. (2022) and Izumi et al. (2023). The tilted jet in *GLAC-1D_noMw* brings stronger winds in the North Atlantic and can explain the negative wind anomaly at 50° N in Figure 4.3*f*, but its influence is weak further North, and especially in the Iceland Basin (Figure 4.14*i,l*). (ii) The ice sheets can also modify the sea level pressure around them through changes of the local sea surface temperatures and sea ice extent (Pausata et al., 2011). The Arctic mean sea level pressure is higher by $\sim 6hPa$ in ICE6G simulations than in GLAC-1D simulations, and lower by $\sim 2.5hPa$ below 55° N in the eastern North Atlantic. Both the Icelandic low and the Azores high lie outside the main changes, and the meridional gradient of sea level pressure at 60° N, and in particular East of Iceland, fuels an intense wind belt around this latitude in *ICE6G_noMw*. (iii) The Icelandic ice sheet is only present in the ICE6G ice sheet reconstruction (Figure 4.3*i*) and can modify the winds in the Iceland Basin and the Nordic Seas. To evaluate its influence, a sensitivity experiment, *ICE6G_noMw_noIcd*, was run with the Icelandic ice sheet cropped out of *ICE6G_noMw*. The results are presented in Figure 4.10. Overall, the Icelandic ice sheet increases the winds by up to 1.5m/s in the Iceland Basin and does not change significantly the winds in the Nordic Seas. This does not drive, however, any noticeable differences in the mixed layer depth pattern in the Iceland Basin, and the AMOC index remains at similar levels in both *ICE6G_noMw* and *ICE6G_noMw_noIcd*. In conclusion, the influence of the Icelandic ice sheet is fairly limited in this set of simulations.

The discrepancies in deep water formation layout between the two *control* simulations are the result of changes in the atmospheric circulation in the North Atlantic forced by the different ice sheets geometries and their effect on local climate. In particular, an intensification of the Eurasian ice sheet winds in *GLAC-1D_noMw* and of the Arctic-North Atlantic sea level pressure meridional gradient in *ICE6G_noMw* results in a strengthening of convection in the Nordic Seas in the former, and a strengthening of convection in the Iceland Basin in the latter. In order to determine how these conclusions relate to the behaviour in the *transient* simulations, the distribution of the winds, jet indices and mean sea level pressure in the *control* and the *transient* simulations are plotted in Figure 4.4.

There is a lack of response of the atmospheric circulation to the introduction of meltwater. The jet indices distributions plotted in Figure 4.4*d-g* are hardly modified between

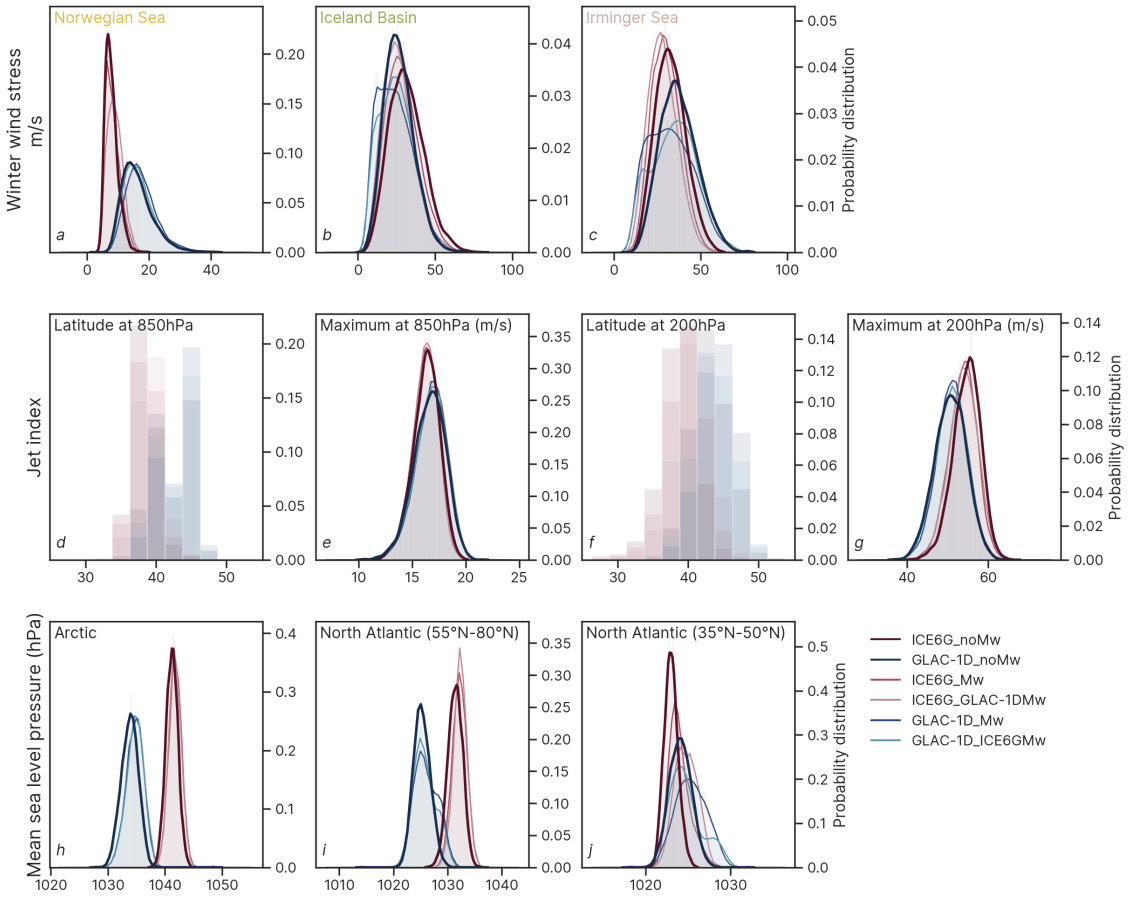

Figure 4.4: **Atmospheric variable distribution in transient simulations.** Distribution of the transient simulations' annual means of Norwegian Sea wind stress (a) and Iceland Basin wind stress (b) as defined in Figure 4.3, and the Irminger Sea wind stress (c) as defined in Figure 4.11, the latitude (d,f) and value (e,g) of the maximum westerly winds in the North Atlantic at 850hPa (d,e) and 200hPa (f,g), and the mean sea level pressure in the Arctic (h), the North Atlantic between 55° N and 80° N (i) and the North Atlantic between 35° N and 50° N (j).

the *control* and the *transient* simulations. A similar conclusion can be drawn for sea level pressure in the Arctic and the North Atlantic over 55° N (Figure 4.4*h,i*). The influence of the meltwater discharge is clearer in the North Atlantic between 30° N and 55° N, where the *transient* simulations distributions do not match the *control* simulations distributions. In this region, the GLAC-1D simulations tend to simulate higher sea level pressure, and the $\sim 2.5hPa$ increase recorded between *GLAC-1D_noMw* and *ICE6G_noMw* is also present between *GLAC-1D_Mw* and *ICE6G_Mw*. The wind patterns modifications between *GLAC-1D_noMw* and *ICE6G_noMw* are consistent for all the GLAC-1D and ICE6G simulations. Winds speed are $\sim 5m.s^{-1}$ faster in the Nordic Seas in GLAC-1D simulations, slightly higher in the Iceland Basin in the ICE6G simulations and in the Irminger Sea in the GLAC-1D simulations. The differences in the last two regions can reach up to $10m.s^{-1}$ on average, but the standard deviation in GLAC-1D simulations' wind patterns is higher than in ICE6G's simulations. It is not possible to precisely estimate the direct influence of wind changes on the deep water formation in the North Atlantic, as the mixed layer depth is heavily influenced by the introduction of meltwater and the AMOC changes (Figure 4.15). Nonetheless, these conclusions give a strong indication of the nature of the atmospheric forcing in the *transient* simulations.

In Chapter 3, we linked the abruptness of the cold-warm transitions to their ability to simulate an abrupt recovery of the Nordic Seas deep water formation site. From this analysis, it appears that only GLAC-1D ice sheet reconstruction can create strong enough winds around the Eurasian ice sheet to simulate abrupt transitions in the Nordic Seas. The stronger convection in the Iceland Basin in ICE6G simulations is favoured by stronger winds in the region, but is not crucial in triggering the oscillating mechanism. In conclusion, the choice of the ice sheet reconstruction, through its influence on the atmospheric circulation, determines almost entirely the dynamical evolution of *transient* simulations in response to meltwater discharge.

4.5 HadCM3 response to deglacial meltwater patterns

In Section 4.3, the choice of reconstruction was identified as the main reason behind changes in *transient* simulations response to time-evolving meltwater discharge. In Section 4.4, the ice sheet layout was shown to influence where convection can occur, and where it is the easiest to deactivate. The two meltwater release histories derived from GLAC-1D and ICE6G ice sheet reconstructions provide an opportunity to map the sensitivity of HadCM3's last glacial maximum simulations to freshwater discharge in two different background conditions. The evolution of the AMOC index against the total meltwater discharge is plotted in Figure 4.5*a,b*. It was realised by concatenating the GLAC-1D simulations (panel *a*) and ICE6G simulations (panel *b*) so that both panels explore the same parameter space plotted in panel *c*. A more precise estimation of the expected AMOC state in each point of the accessible parameter space was realised using a binning

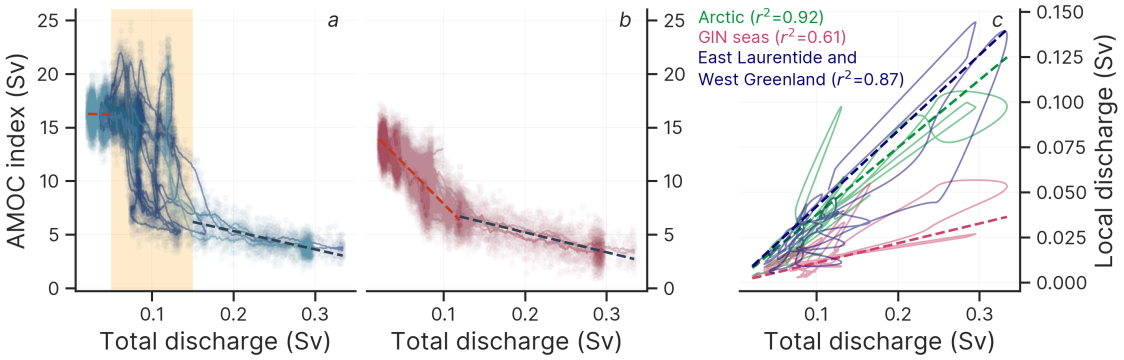

Figure 4.5: **AMOC response to freshwater introduction.** AMOC index against meltwater discharge for the GLAC-1D simulations (*GLAC-1D_Mw* and *GLAC-1D_ICE6GMw*, *a*) and the ICE6G simulations (*ICE6G_Mw* and *ICE6G_GLAC-1DMw*, *b*). The lines indicate the 30-year running mean AMOC index and the points the annual mean AMOC indexes. The colours correspond to the simulation's colours defined in Figure 4.1. *c.* Points and correlations in the parameter space.

algorithm detailed in Section 4.9, and produced the cross-correlations maps of regional discharge in ICE6G (Figure 4.9) and GLAC-1D (Figure 4.8) simulations.

In GLAC-1D transient simulations, the AMOC response to the introduction of meltwater can be *linear* or *decoupled*. For a total discharge below $0.05Sv$, the AMOC is strong with high certainty and the AMOC index is stable around a value of $16Sv$. For a total discharge above $0.15Sv$, the AMOC is weak with high certainty, and the AMOC index decreases by $\sim 1.7Sv$ per $0.1Sv$ of total meltwater. Between $0.05Sv$ and $0.15Sv$ lies the window of opportunity, where the AMOC can exist in both the warm and the cold state. In the window of opportunity, the AMOC index is decoupled from the discharge as the dynamics of the oscillating mechanism (Section 3.5) supersedes the direct response to the discharge. A hysteresis cycle can be guessed from the individual path in the parameter space (lines in Figure 4.5), and indicates different values of the threshold for a warm to cold and cold to warm modes transitions, as it was hypothesised in Section 3.9.

In ICE6G transient simulations, the AMOC response to the introduction of meltwater is *linear*. For a total discharge below $0.12Sv$, the AMOC index decreases by $\sim 7.7Sv$ per $0.1Sv$ of total meltwater. For a total discharge above $0.12Sv$, the AMOC index decreases by $\sim 1.8Sv$ per $0.1Sv$ of total meltwater. There is no clearly identifiable *warm* mode in the ICE6G simulations, and the similar value of the slope for high meltwater efficiency indicates a cold mode analogous to the one in the GLAC-1D simulations. There is a higher AMOC index variability for low meltwater efficiency, but the standard deviation does not exceed $8Sv$ compared to more than $20Sv$ in the GLAC-1D simulations, which is insufficient to label this region a window of opportunity.

In both GLAC-1D and ICE6G simulations, the North Atlantic climate is very sensitive

to freshwater introduction in the Arctic, the GIN Seas, and the East Laurentide-West Greenland regions, which can be referred to as *key discharge* regions. It is not sensitive to freshwater in the Mediterranean, the Southern Ocean and the Pacific within the last deglaciation range that was reconstructed for these simulations (Figures 4.9 and 4.8). It is not possible to disentangle the precise sensitivity of the North Atlantic climate to each precise zone because most of the points of the parameter space are located along a diagonal (Figure 4.5c), i.e. a high discharge in one of the key regions does not exist without a high discharge in the other key regions. A more systematic study of the effect of freshwater discharge in the key regions, testing the entire parameter space with more spin-up time and different initial states, is necessary to complete this analysis. In general, it can be hypothesised that the GIN Seas is the most efficient region to release freshwater as no warm AMOC can exist with either of the ice sheet reconstructions above $0.02Sv$ (Figures 4.8 and 4.9). This conclusion is consistent with the conclusions of Roche et al. (2010) with the LOVECLIM EMIC and Smith and Gregory (2009) with the FAMOUS EMIC.

This new study implies that a window of opportunity where abrupt climate changes can occur may have been crossed during the last deglaciation because of the melting of the Northern Hemisphere ice sheets. When the ice sheet layout is in the right configuration, it can take less than $0.05SV$ of total meltwater discharge to trigger millennial-scale variability. On the other hand, for a non-optimal ice sheet configuration, the response of the AMOC to freshwater discharge becomes linear and abrupt transitions are no longer observed. This analysis reasserts the importance of the choice of ice sheet reconstruction and its associated meltwater discharge in the set-up of deglacial simulations.

4.6 Implication for simulations of the last deglaciation

This study aimed to assess the sensitivity of glacial simulations to the choice of ice sheet reconstructions and their associated meltwater discharge history. The simulations presented in this Chapter were not designed to be accurate representations of the last deglaciation and, therefore, to replicate the timing and magnitude of the deglacial chain of events. Nonetheless, they provide valuable information to understand the processes at stake in simulations of this period. A review of the most recent simulations of the early last deglaciation was assembled by Snoll et al. (2023). They followed the Ivanovic et al. (2016)'s PMIP4 protocol, including either ICE6G or GLAC-1D ice sheet reconstructions and meltwater discharge. In Figure 4.6, a selection of full transient runs from Snoll et al. (2023) are compared to the *ICE6G_Mw* and *GLAC-1D_Mw* simulations of this study, and proxy reconstructions for overturning circulation (Ng et al., 2018) and Greenland temperatures (Martin et al., 2023).

The comparison between the full-transient simulations and the meltwater-only simulations highlights the effect of increasing greenhouse gas concentrations and solar insolation on

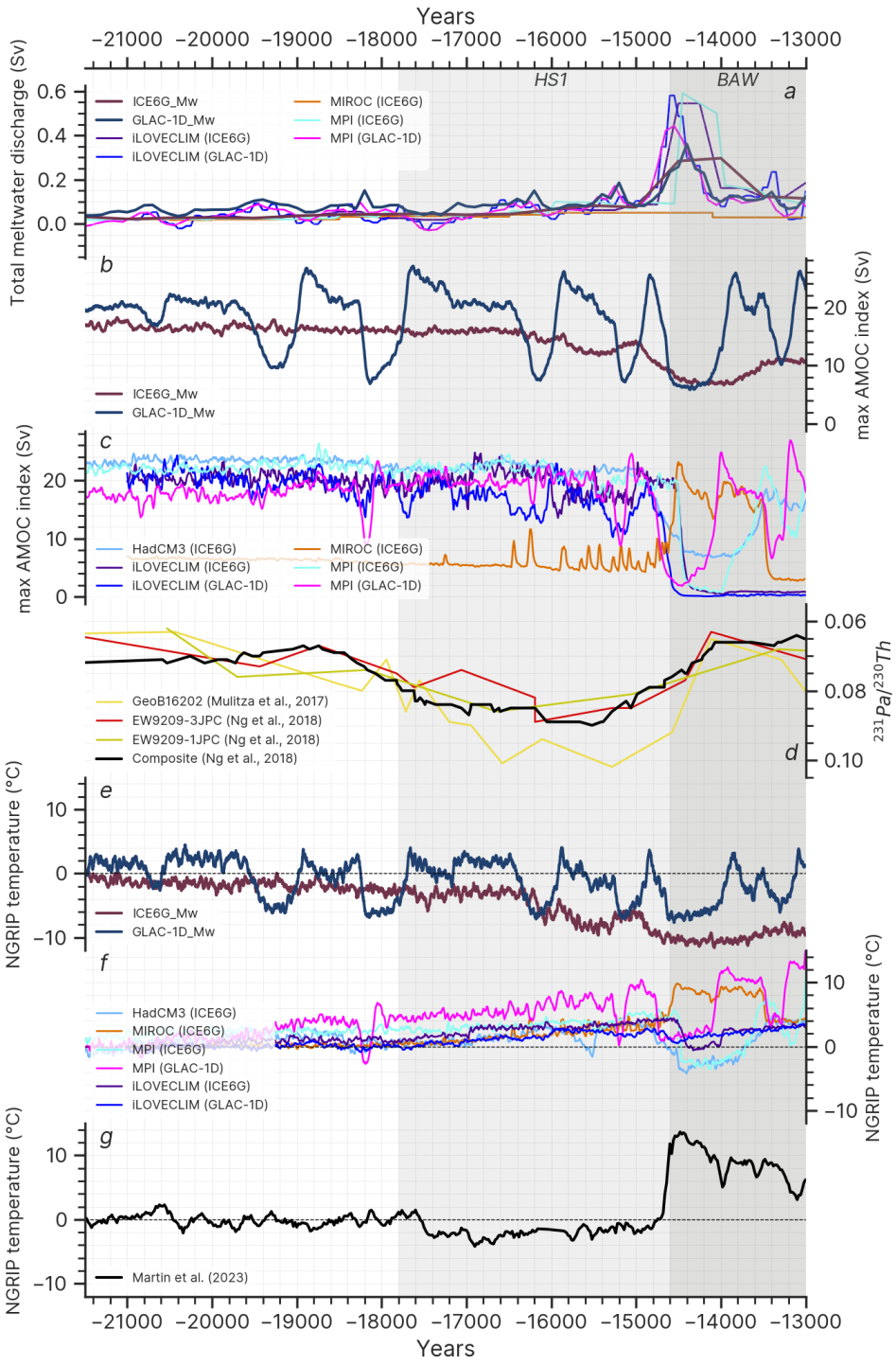

Figure 4.6: **Comparison to simulations and proxy reconstructions.** *a.* Total meltwater discharge calculated in this study and the iLOVECLIM, MIROC and MPI deglacial simulations (Bouttes et al., 2023; Obase and Abe-Ouchi, 2019; Kapsch et al., 2022) compiled by Snoll et al. (2023). *b,c.* Maximum AMOC of the Northern Hemisphere at depths between 500 and 3500 meters in *ICE6G_Mw* and *GLAC-1D_Mw* (*b*) and the deglacial simulations (*c*). *d.* AMOC proxy $^{231}Pa/^{230}Th$ composite record published by Ng et al. (2018). *e,f.* Greenland surface atmosphere temperatures at NGRIP (42.32° W, 75.01° N) in *ICE6G_Mw* and *GLAC-1D_Mw* (*e*) and the deglacial simulations (*f*). *g.* Greenland Summit surface air temperature proxy record from Martin et al. (2023). Heinrich Stadial 1 (HS1) and Booling-Allerod Warming (BAW) from Buizert et al. (2014) and Rasmussen et al. (2014).

causing a slow background increase in global temperatures. Between 21 ka BP and 16 ka BP, the full-transient simulations displayed a Greenland warming between $3°C$ and $10°C$ (Figure 4.6*f*), when *ICE6G_Mw* saw its temperature decrease by $2°C$ (Figure 4.6*e*). The frequency of AMOC mode shifts is also affected by the background conditions. *ICE6G_Mw* is the meltwater-only version of the full-transient *HadCM3_ICE6G*, and only *ICE6G_Mw* displays an AMOC slowdown between 15.9 ka BP and 15 ka BP. A short cooling episode is observed in *HadCM3_ICE6G* at 15.6 ka BP, but it was associated with a change in the ice sheet configuration (Snoll et al., 2022). In conclusion, the evolving background conditions modify the location of the window of opportunity over time, and meltwater-only simulations have a different sensitivity to climate forcings than full-transient simulations.

None of the HadCM3 simulations of the last deglaciation using ICE6G ice sheet reconstruction (Ivanovic et al. (2018a), Snoll et al. (2022) and this study) managed to display abrupt climate warming with high enough rates to fit the temperature records (Figure 4.6*g*). The highest warming rate in HadCM3 with ICE6G ice sheets was obtained in *HadCM3_ICE6G* with $3°C$ in 200 years, far from the $14°C$ in 200 years reconstructed in the Greenland ice cores (Martin et al., 2023). The absence of abrupt climate transitions is not consistent with ICE6G simulations in other models: the *MPI_ICE6G* (Kapsch et al., 2022), *MIROC_ICE6G* (Obase and Abe-Ouchi, 2019) and *iLOVECLIM_ICE6G* (Bouttes et al., 2023) simulations managed to reach temperature change rates of the order of 4 to $7°C$ in a century. One reason why HadCM3 ICE6G simulations do not reach such high rates may lie in the freshwater forcing used around MWP1a (14.65 ka BP to 14.31 ka BP), which is twice as weak and significantly less abrupt in HadCM3 compared to iLOVECLIM and MPI-ESM with ICE6G ice sheets. In order to conclude on the ability of HadCM3 ICE6G simulations to simulate abrupt climate changes, higher discharge rates should also be tested.

On the other hand, there is a strong correlation in the AMOC time series between the GLAC-1D simulations, *GLAC-1D_Mw*, *MPI_GLAC-1D* (Kapsch et al., 2022), and *iLOVECLIM_GLAC-1D* (Bouttes et al., 2023) in Figure 4.6*b,c*. They generally observe higher millennial-scale variability during the early part of the deglaciation, and a similar abrupt cooling at MWP1a. The North Atlantic temperature response to AMOC changes differs from model to model and can be instantaneous (GLAC-1D_Mw), in advance (MPI_GLAC-1D) or muted (iLOVECLIM_GLAC-1D). The existence of early deglaciation disruptions is highly dependent on the meltwater discharge history. In particular, both iLOVECLIM and MPI-ESM allow for negative fluxes that were not considered in HadCM3. This method discrepancy is visible at, for instance, 16.2 ka BP, where a small peak in meltwater discharge present only in *HadCM3_GLAC-1D* (Figure 4.6*a*) led to a deactivation of the AMOC in this simulation, whereas hardly any effect was seen in *MPI_GLAC-1D* and *iLOVECLIM_GLAC-1D*. The meltwater pattern, however, is not enough to explain the differences, as a small meltwater peak at 19.4 ka BP is present in all three simulations

and only has a clear effect on the HadCM3 AMOC time series. This indicates different locations of the window of opportunity in the three experimental designs.

The mechanism for abrupt climate changes in glacial simulations of MPI-ESM was described in Klockmann et al. (2018) and Klockmann et al. (2020). They highlighted that it was easier to trigger abrupt climate changes with higher CO_2 concentrations and lower Northern Hemisphere ice sheets. This may explain why meltwater efficiency is weaker closer to the LGM rather than around the Bølling Warming in *MPI_ICE6G* and *MPI_GLAC-1D*. In iLOVECLIM, the differences in models' physics between EMICs and GCMs can modify the mechanism behind millennial-scale variability (Weber, 2010). Despite the model-dependency of the processes at stake in abrupt climate changes, the relative agreement between all the ICE6G and GLAC-1D simulations but *MIROC_ICE6G* indicated that the mechanism described in Chapter 3 is still consistent with most of the climate models' behaviours during the last deglaciation. It is, therefore, surprising that Obase and Abe-Ouchi (2019) was the simulation with the most accurate reproduction on the Bølling Warming. This simulation, like the TRACE simulations (Liu et al., 2009; He et al., 2021), did not fit the meltwater release to any ice sheet reconstruction and the resulting discharge is relatively small but consistent with the other simulation meltwater chronology (Figure 4.6*a*). The mechanism in this simulation is likely to be different from the one presented in this thesis: the HadCM3 oscillations occur because, at a given point in the parameter space, the stable solution becomes a limit cycle that oscillates between cold and warm modes (see 3.7). In Obase and Abe-Ouchi (2019), the transition is more likely to be due to the modifications in the background conditions that change the stability of different AMOC modes and eventually force a switch from one mode to another. The simulation starts in a weak and stable AMOC mode. As the radiative forcing increases, the AMOC tends to intensify but is kept weak by the increasing meltwater discharge. When the climate system approaches the Bølling Warming, the radiative forcing dominates the freshwater forcing and the weak AMOC mode becomes unstable. This is indicated by the higher frequency of excitable warm modes during Heinrich stadial 1. A positive feedback mechanism exists in MIROC (Kuniyoshi et al., 2022), so that when the threshold where the weak mode becomes completely unstable is crossed at the Bølling Warming, the climate abruptly transitions to a warm mode. This simulation makes a case for new deglacial simulations starting from a cold AMOC mode, as they offer a different mechanism to explain the chain of events of the last deglaciation.

4.7 Comparison to proxy records

The meltwater *transient* simulations presented in this Chapter do not match the timing of the last deglaciation chain of events. This corroborates the "meltwater paradox" discussed in Snoll et al. (2023). The "meltwater paradox" states that simulations using realistic meltwater fluxes derived from ice sheet reconstructions fail to capture the abrupt

climate changes of the period, when the simulations that obtained the best fit to the data were using meltwater fluxes that did not match sea level constraints. Comparing the AMOC index, defined in Figure 4.6 as the maximum overturning circulation of the Northern Hemisphere between 500 and 3500 meters deep, to the overturning circulation reconstructions during the last deglaciation compiled from $^{231}Pa/^{230}Th$ records by Ng et al. (2018), none of the simulations captured the weakening of the AMOC during HS1 (17.8 ka BP to 14.6 ka BP) and its abrupt increase during the Bølling Warming (14.6 ka BP to 13 ka BP). The circulation rate is difficult to reconstruct from proxy records (see Section 1.2.2) and the state of the AMOC during HS1 is still an active topic of discussion (Oppo et al., 2015; Repschläger et al., 2015, 2021). Nonetheless, because most of the records of the North Atlantic circulation agree on the sign of the change (Figure 4.6*d*) during the early deglaciation, we can conclude that either the simulations have the wrong sensitivity to the meltwater fluxes, or that the meltwater fluxes input are incorrect.

According to Kageyama et al. (2021), HadCM3 simulations of the LGM tend to simulate colder oceans than observations (Tierney et al., 2020b), but are a good match to temperatures over land (Cleator et al., 2020). In Figure 4.7 the climatologies of *GLAC-1D_noMw* (panel *a*) and *ICE6G_noMw* (panel *b*) calculated over the last hundred years of the simulations are plotted against the surface atmosphere and ocean temperatures at the LGM (20-–19.5 ka BP) compiled by Shakun et al. (2012). The temperature pattern of the *control* simulations resembles the Shakun et al. (2012)'s stack everywhere but in Bering Strait and Antarctica. In the North Atlantic, the mean annual sea surface temperature at *NA87-22* (Waelbroeck et al., 2011, 55.5° N, 14.7° W) and at *MD01-2461* (Peck et al., 2008, 51.8° N, 12.9° W) matches the simulated range of $\sim 5°C$ to $\sim 8°C$. There is a bias towards an overestimation of Greenland temperatures in the model which goes up to $12°C$ warmer in *GLAC-1D_noMw* and $17°C$ in *ICE6G_noMw* compared to the NGRIP record.

The abrupt climate changes displayed in the GLAC-1D simulations, however, prove to be a good match to the warming event observed for the Bølling Warming. In the simulations, the Greenland temperatures warm by between $6°C$ and $10°C$ in ∼150 years (Figure 4.6*c*), a rate of warming comparable to the records where the Greenland temperature warmed by $14°C$ in 200 years (Figure 4.6*g*). The geographical pattern of change simulated also matches observations, with stronger warming in West Greenland than in East Greenland, as shown in Figure 4.7*c,d*. In this Figure, composite warm (NGRIP temperatures over $-43°C$) and cold (NGRIP temperatures under $-49.5°C$) modes of *ICE6G_Mw* and *GLAC-1D_Mw* are compared to the difference between Heinrich Stadial 1 and the Bølling warming in the Shakun et al. (2012) stack, with the addition of two cores from Eldevik et al. (2014) and one core from Naafs et al. (2013). There is a good agreement between land temperature changes in the Northern Hemisphere of the simulations and the reconstructions. For instance, the model captures the $\sim 2°C$ warming in the Chinese Loess Plateau (34.9° N, 113.3° E), and the $\sim 2°C$ warming of the Nile Delta (31.7° N, 34.1° N).

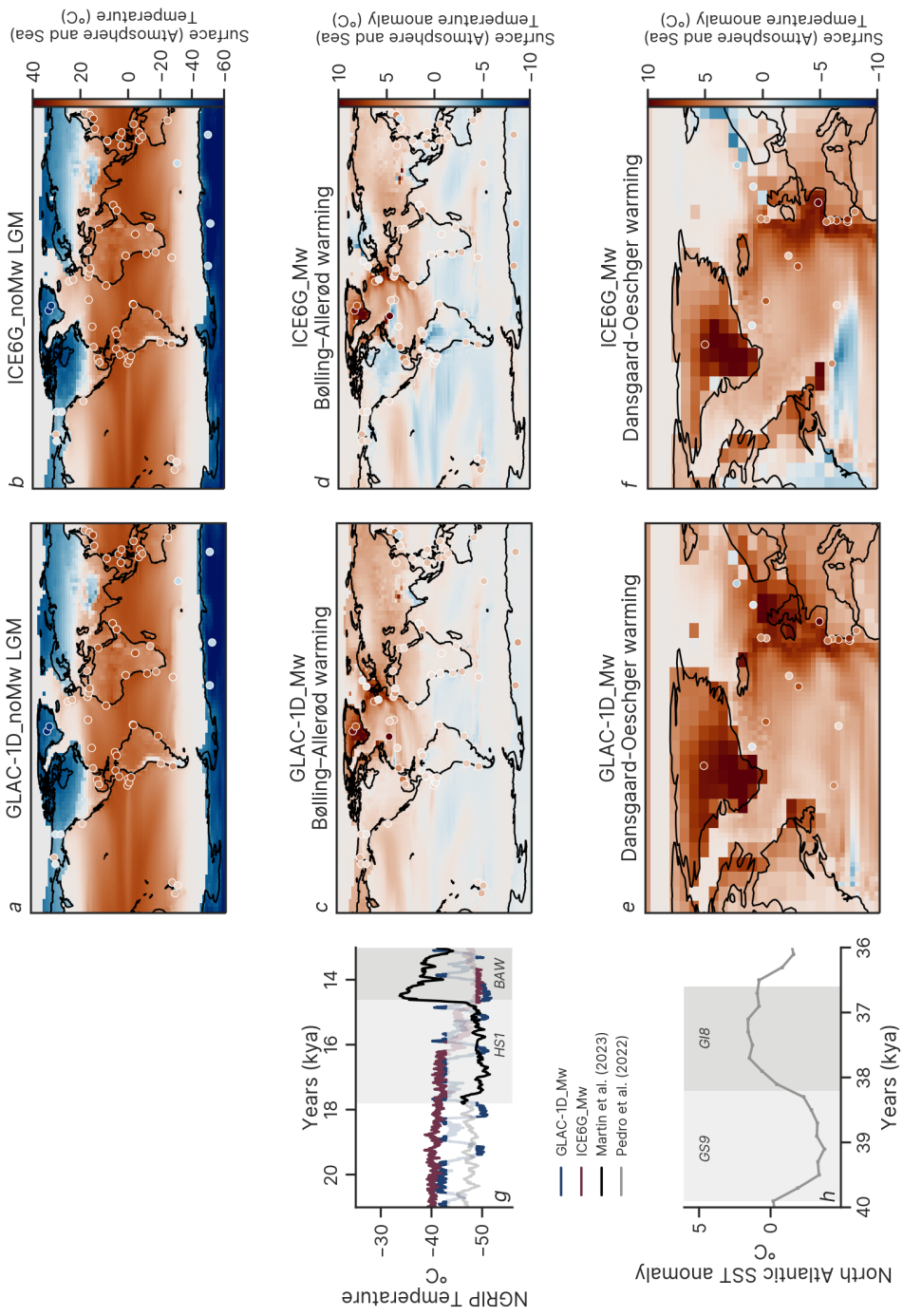

Figure 4.7: **Comparison to proxy records.** *a,b.* The colour maps indicate the GLAC-1D_noMw (*a*) and *ICE6G_noMw* (*b*) temperatures (over the final hundred years of each simulation), and the points the LGM (20—19.5 ka BP) atmosphere and sea surface temperature stacks from Shakun et al. (2012). *c,d.* The colour maps indicate the *GLAC-1D_Mw* (*c*) and *ICE6G_Mw* (*d*) temperature anomalies between the warm and cold times defined in panels *g*, and the points atmosphere and sea surface temperature anomalies from Shakun et al. (2012), Eldevik et al. (2014) and Naafs et al. (2013) between 14 kya-13 kya and 17-16 kya. *e,f.* Same than *c,d* but the points are the GI8-GS9 anomalies from Pedro et al. (2022). *g.* Greenland temperatures over the last deglaciation in the *transient* simulations and in Martin et al. (2023). *h.* North Atlantic SST anomalies from Pedro et al. (2022) over GI8 and GS9.

The simulations do not display the warming of the Southern Hemisphere expected from the climate records (Figure 4.7*c,d*). This effect is unlikely to be related to the Bølling Warming millennial-scale variability, but rather to the increase of radiative forcing by greenhouse gases that is absent from this Chapter's *transient* simulations. In the simulations, the eastern North Atlantic sea surface temperature anomaly is around $8°C$, almost $6°C$ more than the anomaly in the western North Atlantic. This zonal temperature gradient is not obvious in proxy records during the Bølling Warming. In general, the temperature changes in the eastern North Atlantic during this period are slightly overestimated in the model. In the Gulf of Cadiz, records indicate warming by up to $2.3°C$, slightly below the $2.8°C$ and $3.0°C$ obtained in *GLAC-1D_Mw* and *ICE6G_Mw*, respectively. In the Iceland Basin, the $5.2°C$ warming at *NA87-22* matches the $5.1°C$ warming of *GLAC-1D_Mw*, but not the $8.7°C$ in *ICE6G_Mw*. In the western North Atlantic, the temperature changes pattern does not fit well with the records, as demonstrated by the *CH 69-09* core (41.8° N, 47.4° W), although the influence of the nearby Laurentide ice sheet could introduce biases in the proxy reconstructions. Finally, the absence of warming recorded in the GIN Seas in Eldevik et al. (2014) are consistent with the *ICE6G_Mw* simulation, but inconsistent with the $\sim 7°C$ warming displayed in *GLAC-1D_Mw*.

The mismatch between the model and the data can arise from various biases in the proxy reconstructions for temperature. Proxy records for temperature of different natures were used in Shakun et al. (2012), and these different proxies can yield different results depending on the signal they capture in terms of depth, seasonality and temporal resolution. Extreme seasonality in the North-East Atlantic during stadial to interstadial transitions has been hypothesised by Denton et al. (2005) but not observed consistently in the marine records, and biases in the sea ice extent of the model can have a strong effect on the simulated seasonality. Seasonality may explain the inconsistency between the *NA87-22* and *MD01-2461* sites in the North-West Atlantic where the response of *MD01-2461* is muted. These two cores use different methods for reconstructing temperatures (foraminifera assemblages in *NA87-22*, and $U^{k'}_{37}$ in *MD01-2461*), which may capture different temperature signals depending on their blooming seasons and lifespan. The habitat of the species (depth, freshwater, etc.) in this region may be another reason for inconsistency, as highlighted by Wary et al. (2015) who found different signals between planktonic foraminifera and dinocysts-based temperature proxies. Comparing the reconstructed temperatures to simulated ocean temperatures between 100m and 300m may be more representative of the pattern of changes recorded by planktonic foraminifera. The temporal resolution of the records compared to the spans defined in Figure 4.7*g* is also to be considered. South-East of Newfoundland, a cold anomaly is consistently simulated during the Bølling Warming (Figure 4.7*c-f* Ivanovic et al., 2018a; Snoll et al., 2023). In Ivanovic et al. (2018a), this cold anomaly was matched with the Naafs et al. (2013) record (32.9° N, 41.0° W). However, the time spans to plot the model and data anomalies in Figure 4.7 are longer than in

Ivanovic et al. (2018a), which may smooth out the stronger anomalies at the time of the transitions and lead to an underestimation of the changes. Finally, the absence of Nordic Seas warming is a robust result for temperature reconstructions of the Bølling Warming (Eldevik et al., 2014). An abrupt warming by $4°C$ to $8°C$ matching the $\sim 5°C$ warming in *GLAC-1D_Mw* is observed at the end of the Younger Dryas (11.7 ka BP), but in very different background conditions than the *transient* simulations.

The millennial-scale variability simulated in *GLAC-1D_Mw* may be a better match to other abrupt climate change events of the last glacial period. In Section 2.7, it was highlighted that the *oscillating* simulations matched well the D-O records in Greenland and Antarctica. To test if the GLAC-1D *transient* simulations in this article are a good representation of D-O variability, the simulated North Atlantic climate changes were compared to the sea surface temperature changes during D-O transition, between Greenland Stadial (GS)9 (39.2 ka BP to 38.2 ka BP) and Greenland Interstadial (GI)8 (38.2 ka BP to 36.6 ka BP) compiled by Pedro et al. (2022) in Figure 4.7*e,f*. Both the $\sim 7.5°C$ warming in the Northeastern Atlantic and the $\sim 10°C$ warming off the Iberian margin are a good match to the *GLAC-1D_Mw* warming events. *GLAC-1D_Mw*'s temperature anomaly does not extend as far west as the temperature signal in the records, and *ICE6G_Mw*'s warming pattern is a better match to the records. Similarly to the *ICE6G_Mw*, there is no significant warming in the GIN Seas, indicating an absence of convection in this region. This is likely to be due to the mid-glacial conditions of the stadial and interstadial states when the sea ice does not extend as far South. The abrupt recovery, therefore, is more likely to happen outside of the Nordic Seas, and probably through different processes, than in the *GLAC-1D* simulations, during MIS3 - see Armstrong et al. (2022) and the analysis in Section 3.6. Overall, the mechanism at stake in the D-O events is probably similar to the one identified in this thesis, but the mechanism described in Chapter 3 may need to be adapted to take into account mid-glacial background conditions and deep water formation sites.

4.8 Conclusion

This Chapter explored the sensitivity of last glacial maximum simulations to two different ice sheet reconstructions, GLAC-1D and ICE6G, and their associated meltwater discharge patterns. The aim of this Chapter was not to produce a realistic set of simulations of the last deglaciation but to understand the main parameters to observe millennial-scale variability in glacial general circulation model simulations.

Only the simulations in which the ice sheet topography and extent follow the GLAC-1D ice sheet reconstruction produced climate changes that resemble the last glacial period millennial-scale variability. This is because of the scattered convection in the North Atlantic, including the Norwegian Sea deep water formation site, identified as a critical region to trigger the overshoot necessary for the abrupt climate change mechanism. Convection

in the Nordic seas is due to the strong wind forcing around the Eurasian ice sheet, resulting from its smooth geometry. As a result, the model responds to the introduction of meltwater in the Nordic seas, the Arctic, the Labrador Sea and East America along threshold-based hysteresis cycles. The thresholds depend on the distribution of the discharge as well as the history of AMOC changes.

ICE6G simulations also observe cold and warm AMOC modes, but the transitions are never abrupt. The Nordic Seas deep water formation sites are permanently deactivated due to weaker wind forcing from the Eurasian ice sheet. Conversely, the high Arctic sea level pressure creates a strong convection region in the Iceland Basin. The system is sensitive to the same freshwater input locations as GLAC-1D simulations, but the response is linear until the almost deactivation of the AMOC.

Due to the higher resolution of the GLAC-1D-derived meltwater discharge history, we generally observe more substantial variability than in deglacial simulations using ICE6G meltwater discharge history. Contrary to HadCM3 simulations, the presence of abrupt transitions in response to freshwater input is not dependent on the ice sheet reconstruction. The transient simulations did not obtain the timing of the last deglaciation chain of events right, and overestimated the magnitude of deglacial transitions in the North East Atlantic. The abrupt climate changes simulated fit better the geographical pattern of Dansgaard-Oeschger events.

At this point of advancement, we believe we still lack knowledge in both the models and the data to produce accurate simulations of the last deglaciation. The discrepancies between different ice sheet reconstructions are too significant, and their impact too substantial to correctly constrain the experimental designs. Further modelling studies are also necessary to fully comprehend the relation between ice sheets, meltwater, overturning circulation and climate. In particular, a systematic study of the impact of the release region and tracking the freshwater input are necessary to understand the deep water formation site dynamics on a finer level. This initiative is crucial to anticipate the AMOC response to melting ice sheets and adapt our response to present and future climate change.

Chapter 4 - Supplementary Information

The supplementary information includes

1. Sections 4.9 to 4.11
2. Figures 4.8 to 4.15

4.9 Binning Algorithm and AMOC response to meltwater discharge

By using realistic meltwater patterns derived from ice sheet reconstructions, the *transient* simulations do not explore the entire parameter space formed by the meltwater forcing in the discharge regions. The distribution of points is uneven and follows favoured paths of discharge. In order to get a wider understanding of the AMOC evolution in this parameter space, we do not use the individual points but a binning algorithm to produce the AMOC response to discharge pattern plots for GLAC-1D in Figure 4.8 and ICE6G in Figure 4.9.

The algorithm divides each normalised meltwater dimension into ten even bins. For each bin in the two-dimensional parameter space, the AMOC index mean and standard deviation are calculated from the time steps corresponding to this bin, i.e. when the normalised discharge pattern falls into this bin. Transition regions are observed when the AMOC index can take many different values for the same bin, which are indicated by a high standard deviation. Thresholds are indicated when the index goes out of a transition regions to stabilise around a fixed value.

A region is considered sensitive in this experiment when the AMOC index has a consistent response along the discharge axis regardless of the discharge in the other regions. For instance, a normalised discharge lower than $0.02Sv$ in the GIN seas will lead to a strong AMOC with high certainty, and a normalised discharge higher than $0.06Sv$ to a weak AMOC with high certainty. The AMOC is therefore sensitive to discharge in the GIN seas. Conversely, the AMOC can stay strong for all discharge values in the Mediterranean Sea, and can be either strong or weak when the Mediterranean Sea discharge is weak. The AMOC is therefore not sensitive to discharge in the Mediterranean Sea. These results are only valid for this set of experiments and this range of forcing. One can imagine that a stronger discharge in the Mediterranean Sea would eventually lead to a response from the AMOC. However, because these values are likely not to have been reached during the first part of the Last Deglaciation, they are not explored here.

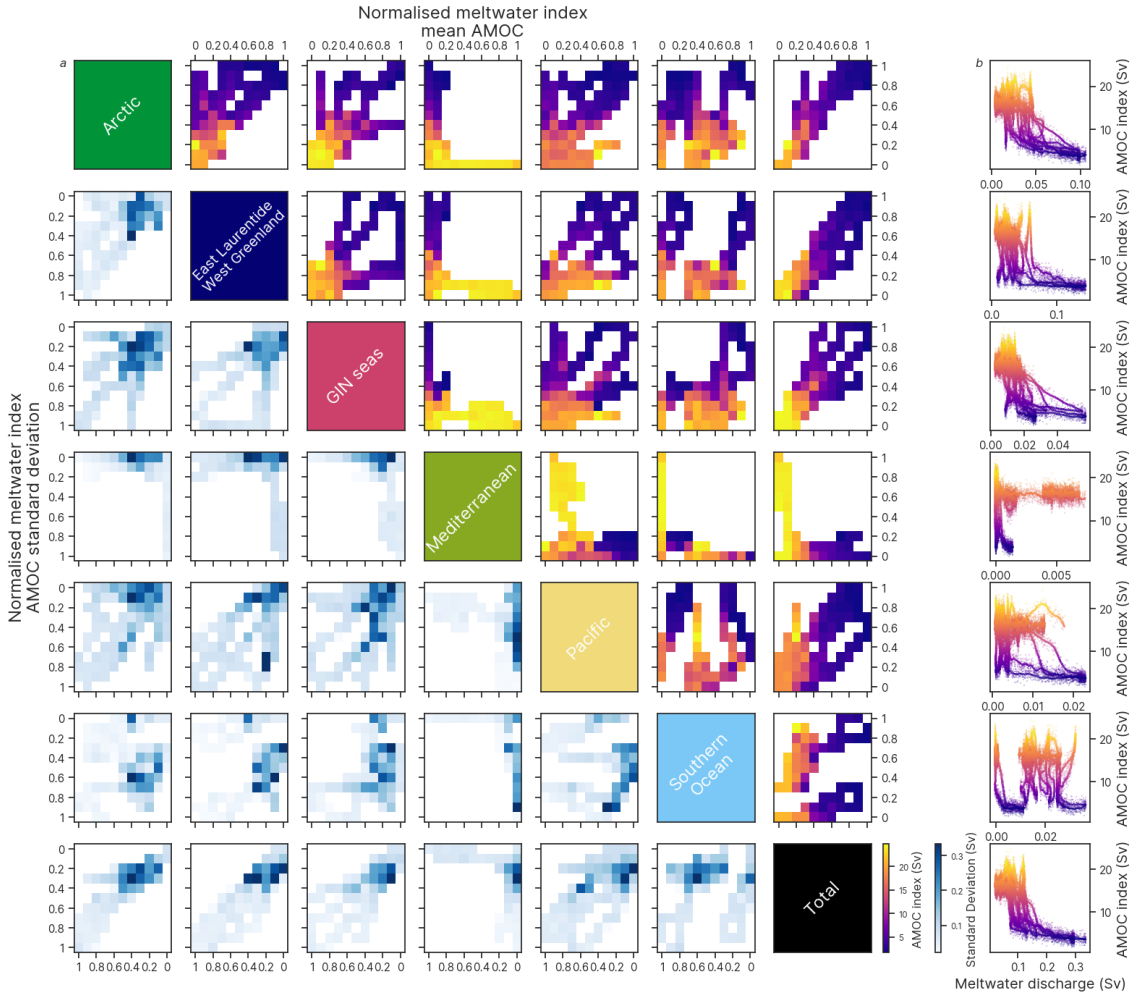

Figure 4.8: **AMOC response to meltwater discharge pattern - GLAC-1D.** *Left panel.* AMOC strength (top right panels) and standard deviation (bottom left panels) in the parameter space formed by normalised meltwater release in the discharge regions defined in Figure 4.11. This was created by following the binning algorithm for *GLAC-1D_Mw* and *GLAC-1D_ICE6GMw*. The meltwater discharge was normalised in each zone. *Right Panel.* AMOC index against meltwater discharge for the GLAC-1D simulations in the discharge regions. The lines indicate the 30-year running mean AMOC index and the points the annual mean AMOC indexes.

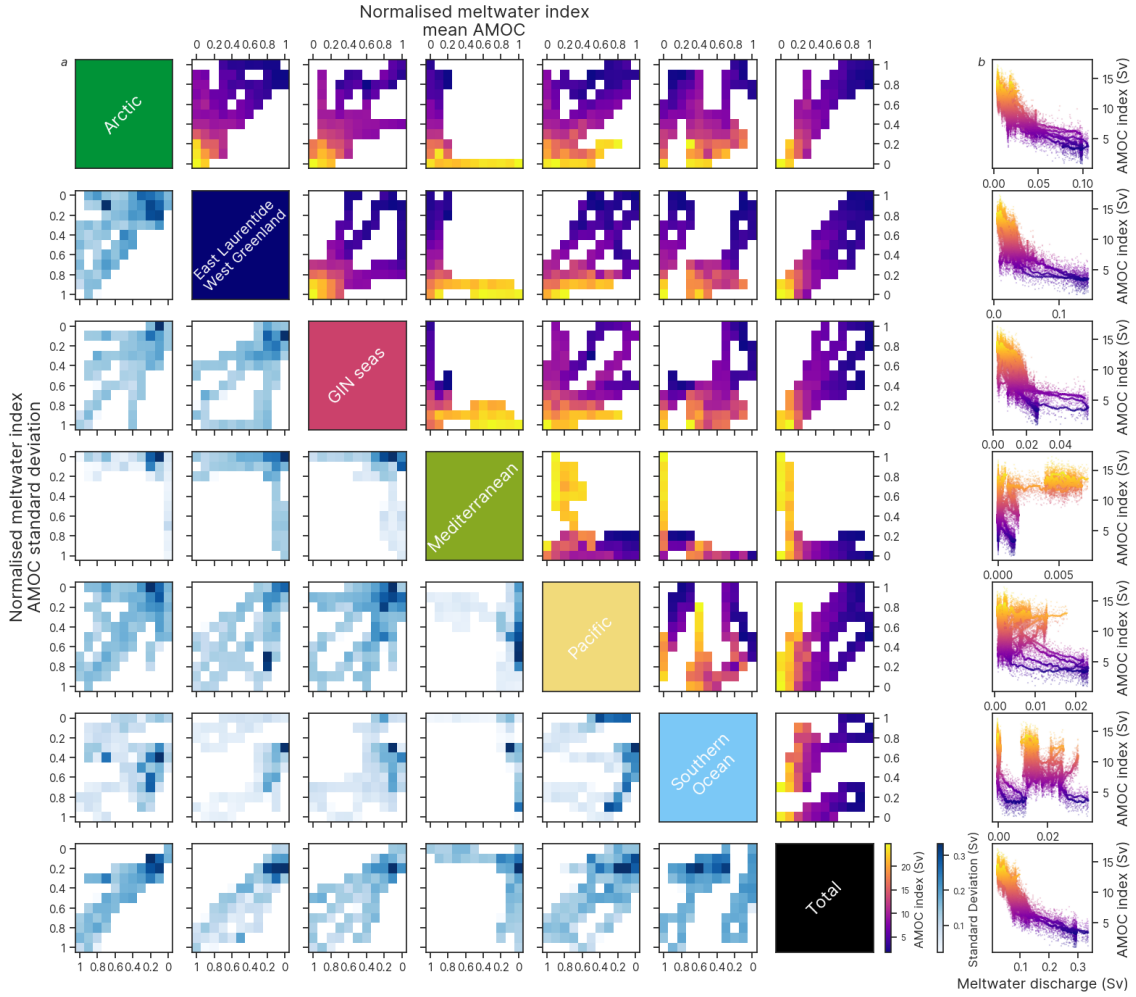

Figure 4.9: **AMOC response to meltwater discharge pattern, ICE6G.** *Left panel.* AMOC strength (top right panels) and standard deviation (bottom left panels) in the parameter space formed by normalised meltwater release in the discharge regions defined in Figure 4.11. This was created by following the binning algorithm for *ICE6G_Mw* and *ICE6G_GLAC-1DMw*. The meltwater discharge was normalised in each zone. *Right Panel.* AMOC index against meltwater discharge for the ICE6G simulations in the discharge regions. The lines indicate the 30-year running mean AMOC index and the points the annual mean AMOC indexes.

4.10 Icelandic ice sheet analysis

To test the sensitivity of the North Atlantic wind patterns and mixed layer depth to the presence of the Icelandic ice sheet in *ICE6G_noMW*, an additional simulation, *ICE6G_noMw_noIcd* was created. To remove the Icelandic ice sheet, the four grid cells corresponding to Iceland were replaced in the ancil files (i.e. model inputs) by their values in *GLAC-1D_noMw*. This includes the orography, vegetation, albedo and land-atmosphere exchanges. The comparison between *ICE6G_noMw* and *ICE6G_noMw_noIcd* is given in Figure 4.10.

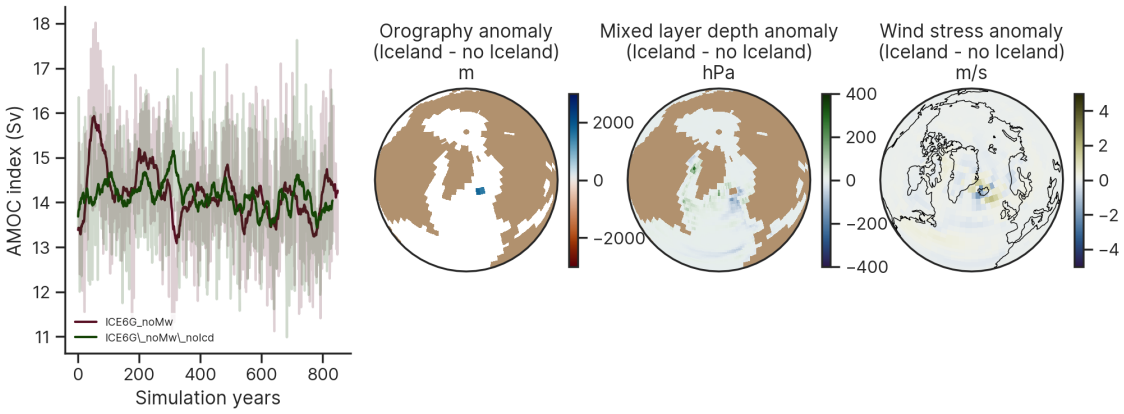

Figure 4.10: **Icelandic ice sheet sensitivity experiment.** *a.* AMOC index, defined as the maximum overturning circulation at 26.5° N, in *ICE6G_noMw* and *ICE6G_noMw_noIcd*. *ICE6G_noMw* minus *ICE6G_noMw_noIcd* anomaly in *b.* orography, *c.* mixed layer depth and *d.* wind stress.

4.11 Supplementary Figures

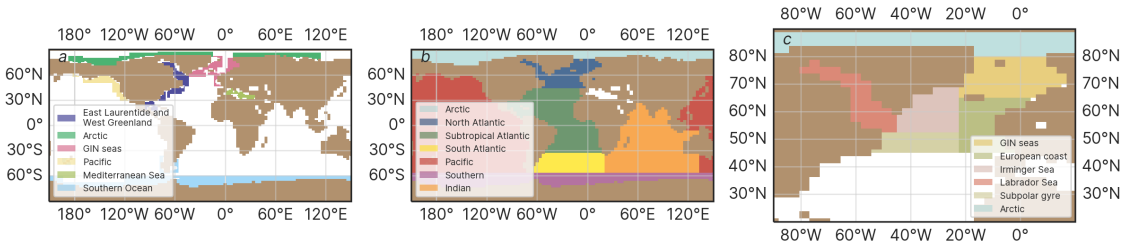

Figure 4.11: **Zone definitions.** for the discharge (a), global (b) and North Atlantic (c) regions.

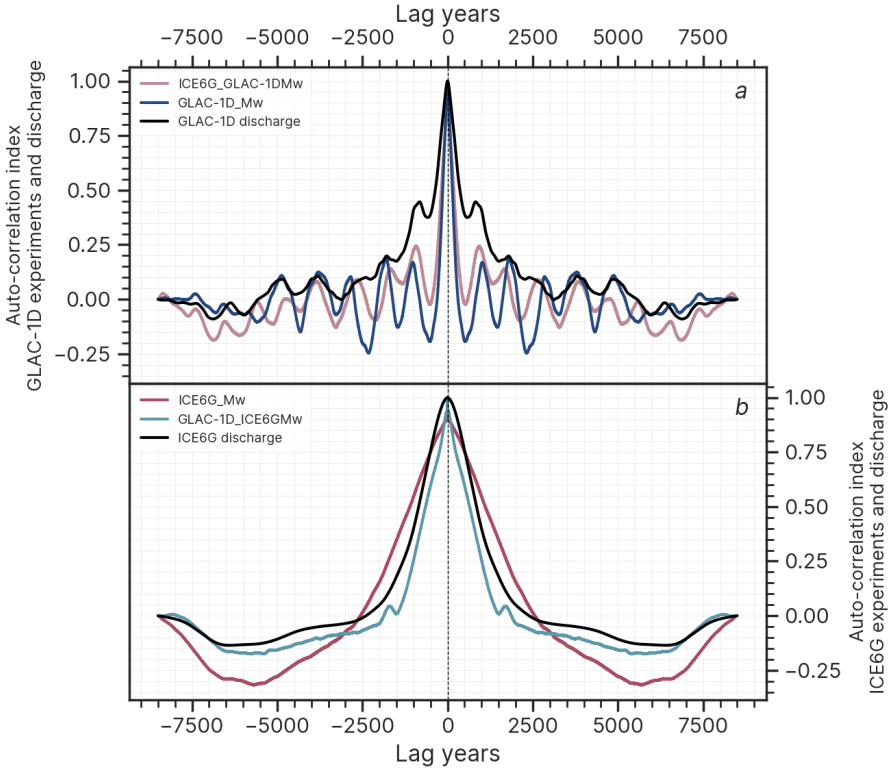

Figure 4.12: **Auto-correlation of the AMOC and meltwater discharge.** Auto-correlation of the AMOC index time series of the *transient* simulations using the *GLAC-1D* meltwater pattern (a) and the *ICE6G* meltwater pattern (b). The auto-correlation of the meltwater discharge histories is plotted in black.

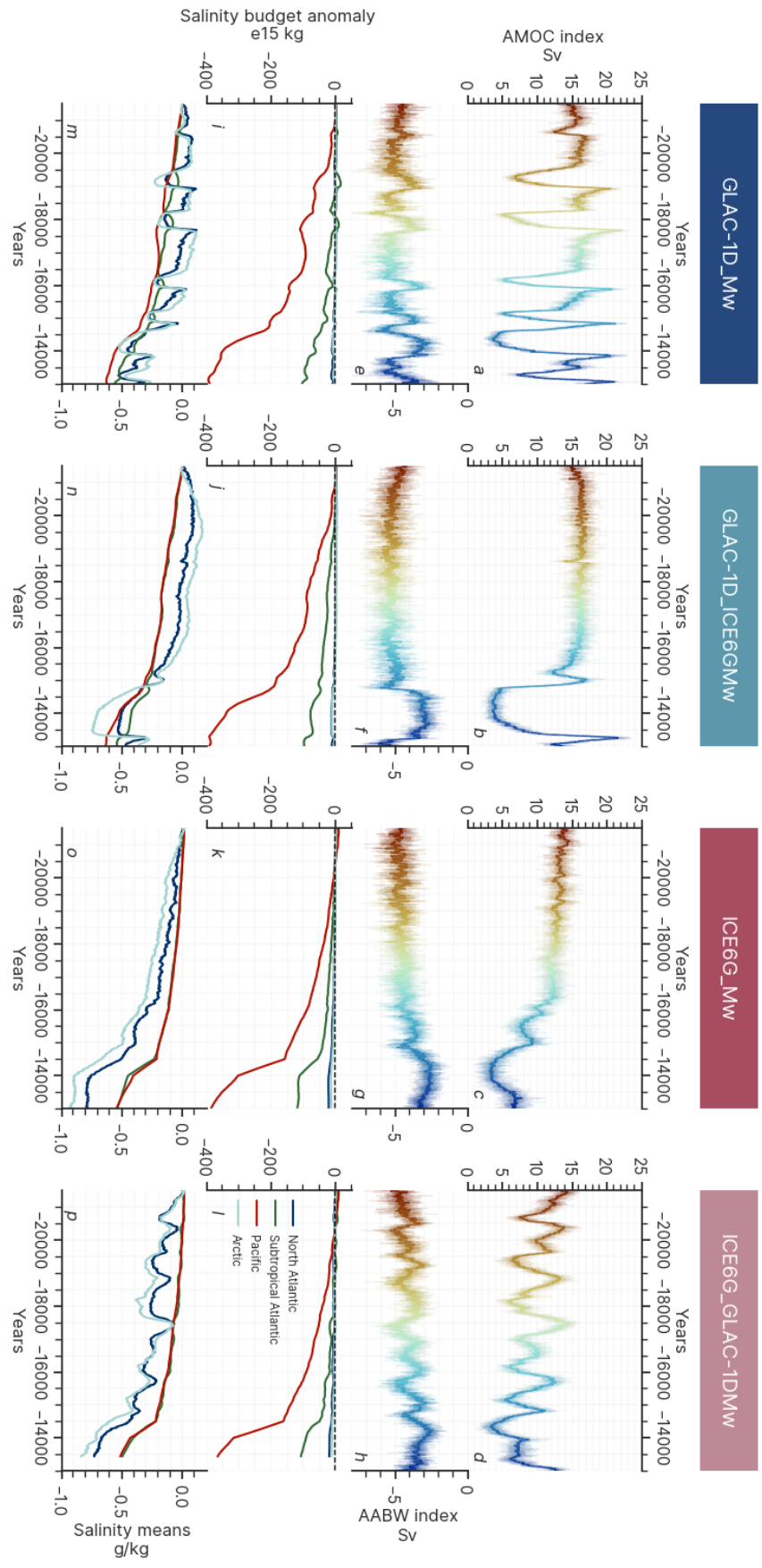

Figure 4.13: **Dynamics of the transient simulations expanded.** *a-d* AMOC indexes, defined as the maximum overturning circulation at 26.5° N. Solid lines are 30-year running means and transparent lines are annual data. *e-h* AABW indexes, defined as the minimum overturning circulation at 33° S. Solid lines are 30-year running means and transparent lines are annual data. The colours of *a-h* are used as a time indicator and match Figure 4.2. *i-l* Salinity budget anomaly compared to the initial time step in global zones defined in Figure 4.11*b*. *m-p* Mean salinity anomaly compared to the initial time step in global zones defined in Figure 4.11*b*.

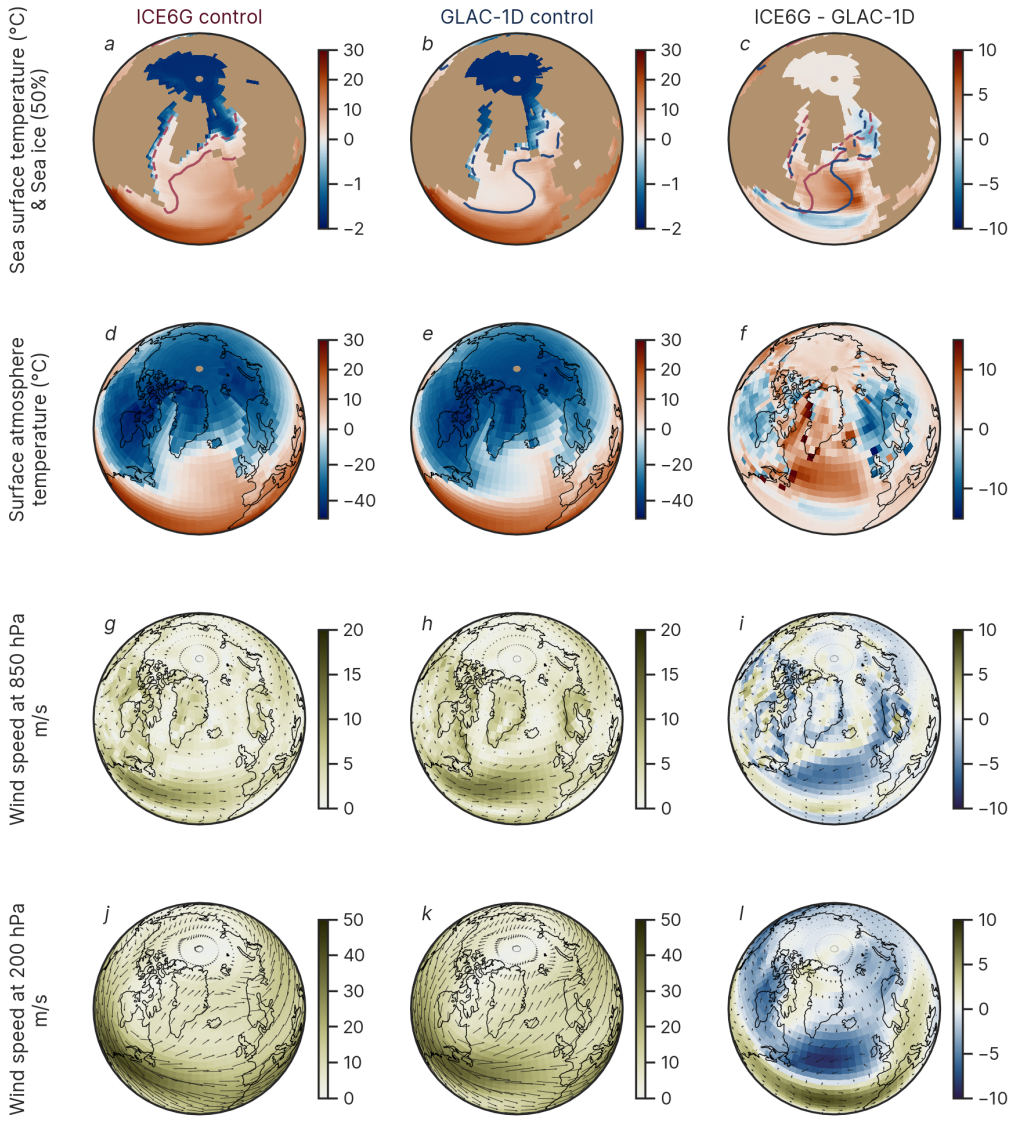

Figure 4.14: **Influence of ice sheets reconstructions on the control simulations expanded**. Climatologies of the final hundred years of *ICE6G_noMw* (panels *a,d,g,j*), *GLAC-1d_noMw* (panels *b,e,h,k*) and the anomalies between *ICE6G_noMw* and *GLAC-1d_noMw* (panels *c,f,i*) for the sea surface temperatures (panels *a-c*), the surface atmosphere temperatures (panels *d-f*), the wind speed at 850hPa (panels *g-i*) and the the wind speed at 200hPa (panels *j-l*). Winter (solid line) and summer (dashed line) 50% sea ice concentration is indicated in panels *a-c*.

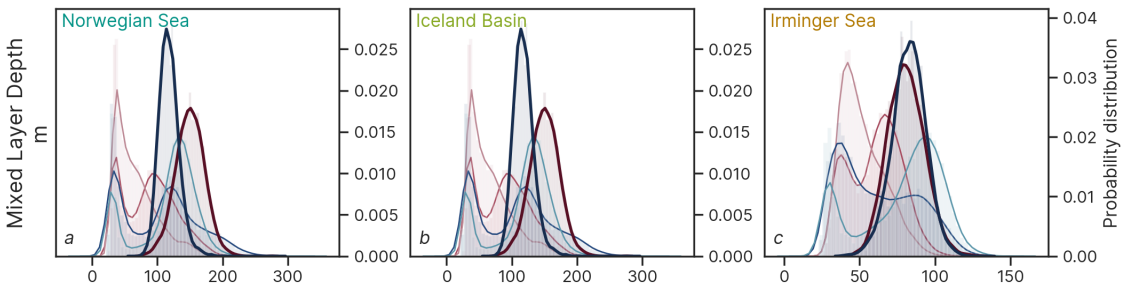

Figure 4.15: **Mixed layer depth distribution in transient simulations.** Distribution of the transient simulations' values of the mixed layer depth in the regions defined in Figure 4.3.

Chapter 5

Discussion and Conclusion

5.1 Summary

This thesis aimed *to investigate the mechanism that caused millennial-scale variability during the last deglaciation using a general circulation model forced with different ice sheet reconstructions.* This was done by creating a new set of HadCM3 simulations of the last glacial maximum using constant and time-evolving meltwater discharge with two different ice sheet reconstructions. A mechanism for millennial-scale variability was identified from the oscillating snapshot simulations, and meltwater-only transient simulations of the last deglaciation were compared to the chain of events of this period.

To answer **RQ1**, I investigated the mechanisms behind millennial-scale variability in HadCM3 simulations and compared this mechanism to the existing literature on abrupt climate changes. The mechanism was described in Chapter 3 based on an oscillating simulation produced in Chapter 2. Chapter 3 includes an in-depth analysis of the global budget of ocean salinity fluxes and provides a theoretical framework to study abrupt climate changes in climate simulations. In Chapter 4, the mechanism was applied to explain the evolution of LGM simulations forced with meltwater discharge history from the last deglaciation.

To answer **RQ2**, I explored the sensitivity of HadCM3 glacial simulations to the choice of ice sheet reconstruction for boundary conditions and freshwater forcing. Chapter 2 demonstrated that GLAC-1D ice sheet configuration at the LGM is able to produce millennial-scale variability when realistic meltwater fluxes are added to the oceans, but only with the right magnitude and distribution of freshwater. In Chapter 4, ICE6G and GLAC-1D ice sheet reconstructions were used to assess how simulations with two background conditions of the same period respond to time-evolving meltwater discharge.

To answer **RQ3**, I questioned if LGM simulations forced with deglacial patterns of meltwater can reproduce the climate variability observed during the last glacial period. The abrupt climate transitions displayed in the GLAC-1D simulations in Chapter 2 and 4 share similar magnitude, abruptness and regional impact to the Bølling Warming and Younger Dryas transitions and Dansgaard-Oeschger events. Although the absence of transient radiative forcing and ice sheet geometry may contribute to preventing a realistic reproduction of the last deglaciation, the simulations in Chapter 4 highlight the key processes necessary to simulate the last deglaciation chain of events in general circulation models.

Six research objectives were designed to conduct the analysis. *RO1* aimed to simulate millennial-scale variability in HadCM3. *RO2* aimed to identify the mechanism behind millennial-scale variability in HadCM3. *RO3* aimed to define the conditions for the validity of the millennial-scale variability mechanism. *RO4* aimed to explore the sensitivity of millennial-scale variability occurrence to ice sheets layout and meltwater discharge. *RO5* aimed to simulate abrupt climate changes that resemble the last deglaciation chain of events with time-evolving meltwater simulations. *RO6* aimed to compare the simulated

millennial-scale variability to past and future abrupt climate changes.

This Discussion Chapter details how the research questions were answered in the previous Chapters and discusses the limitation of the thesis and the leads for future work to fill the gaps. Finally, it includes a general conclusion and a discussion on the broad impact of the thesis in the research area.

5.2 Research questions

5.2.1 RQ1 - What are the mechanisms behind millennial-scale climate variability during the last glacial period?

Theoretical models inspire the discussion about millennial-scale variability, and both the salt oscillator described by Broecker et al. (1990) and the mixed layer oscillator from Welander (1982) have been used as a framework to describe the oscillating behaviours in climate models. The salt oscillator, in particular, has been reported in numerous simulations (e.g. Peltier and Vettoretti, 2014; Klockmann et al., 2018; Armstrong et al., 2022), but is only a description of large-scale salt transfers without a comprehensive study of the causes and consequences of the oscillations. Moreover, building a mechanism based on the sole salt transfers neglects the thermal control that has been demonstrated essential to some models (e.g. Oka et al., 2012; Kuniyoshi et al., 2022). The theory of Colin de Verdière (2007), which involves both an inter-basin oscillator and the North Atlantic convection, offers the right level of complexity to describe the millennial-scale variability. Despite significant progress over the last decade, the complexity of the processes at stake in GCM simulations of millennial-scale variability makes it difficult to diagnose the mechanism behind abrupt climate changes.

In Chapter 3, I described a mechanism to explain the millennial-scale variability displayed by the *oscillating* simulations of Chapter 2 (*RO2*). This mechanism involves two components: a *slow global* component where a salt anomaly is transported back and forth between the Atlantic and the Pacific, and a *fast North Atlantic* component driven by changes in stratification at deep water formation sites. The two components are coupled by the AMOC, regulating the salinity and temperature in the North Atlantic. The periodicity of the oscillations is dictated by the time it takes for a salt anomaly resulting from the freshwater discharge to be redistributed by the AMOC into the North Atlantic. In Section 3.6, I relied on this mechanism to discuss how meltwater discharge can trigger millennial-scale variability in the regions of the parameter space where a window of opportunity (*RO3*) exists, introducing the concept of meltwater efficiency. If the meltwater perturbation is not efficient enough, the vertical stratification in the North Atlantic does not cross the threshold that activates the fast component. If the meltwater perturbation is too efficient, the salt anomaly does not bring enough salt into the North Atlantic to reactivate the fast component and the global salinity distribution reaches a new equilibrium.

In Section 3.6, I explained why the coupled inter-basin oscillator is more likely to work in an environment where global salinity is constrained rather than free-evolving. The time-evolving meltwater simulations of Chapter 4 provide a good case study for this argument (*RO3*) because of the melting of the ice sheet is constantly changing the salinity. This way, the salt anomaly can be wiped out of the ocean before it has time to influence the North Atlantic stratification. When the global salt oscillator is not activated, stratification in the North Atlantic responds directly to the freshwater forcing: a higher discharge increases the stratification and weakens the AMOC, and a lower discharge decreases the stratification and strengthens the AMOC. In Section 4.2.2, I argued that the relative position of meltwater discharge and the deep water formation sites determine if the AMOC response to freshwater forcing is *linear* or *decoupled*. Furthermore, the presence of a positive feedback mechanism, such as subsurface warming or salt advection feedback, determines if the transitions are progressive or abrupt.

The research community has wondered if a one-size-fits-all mechanism for millennial-scale variability existed (Malmierca-Vallet et al., 2022). The findings of this thesis provide a framework to synthesise the behaviours of different box models and climate models, which I summarised in Figure 5.1. The framework lies in the interplay between a fast component, a slow component, and a forcing field. The fast component can be a combination of fast responding processes changing convection in the North Atlantic deep water formation sites such as changes in stratification (Chapter 3), winds (Armstrong et al., 2022), gyres (Klockmann et al., 2020), or polynyas (Vettoretti and Peltier, 2016). The slow component affects the vertical density gradients in the North Atlantic. It sets the pace of the oscillations and can be, for example, a salt oscillator (Peltier and Vettoretti, 2014; Armstrong et al., 2022; Klockmann et al., 2020), subsurface warming (Vettoretti and Peltier, 2016) or deep-decoupling oscillations (Kuniyoshi et al., 2022). Note that different fast and slow components can be triggered in the warming and cooling phases. Only the meltwater discharge was considered as a forcing field in this thesis, but additional forcing like wind patterns modifications due to sudden ice sheet topography changes could be studied.

The deterministic nature of the millennial-scale variability is imposed by the coupling of the slow and the fast components. If the slow component is not activated, the fast component responds directly to changes in the forcing field. In this case, AMOC mode shifts can be observed by *(i)* a stochastic activation of the fast component, similar to the *18.2k* simulation in Chapter 2, *(ii)* a modification of the background climatic conditions (e.g. from orbit and CO_2 changes), similar to Obase and Abe-Ouchi (2019) and *(iii)* a change in the forcing field, as simulated in Chapter 4's simulations. A combination of points *(i)* and *(iii)* can lead to oscillating behaviours if the forcing itself is periodic, as is the case in the stochastic resonance theory (Alley et al., 2001; Ganopolski and Rahmstorf, 2002; Cimatoribus et al., 2013). The ice sheet feedback offers a potential link between the stochastic resonance and the last glacial period millennial-scale variability following Wickert et al.

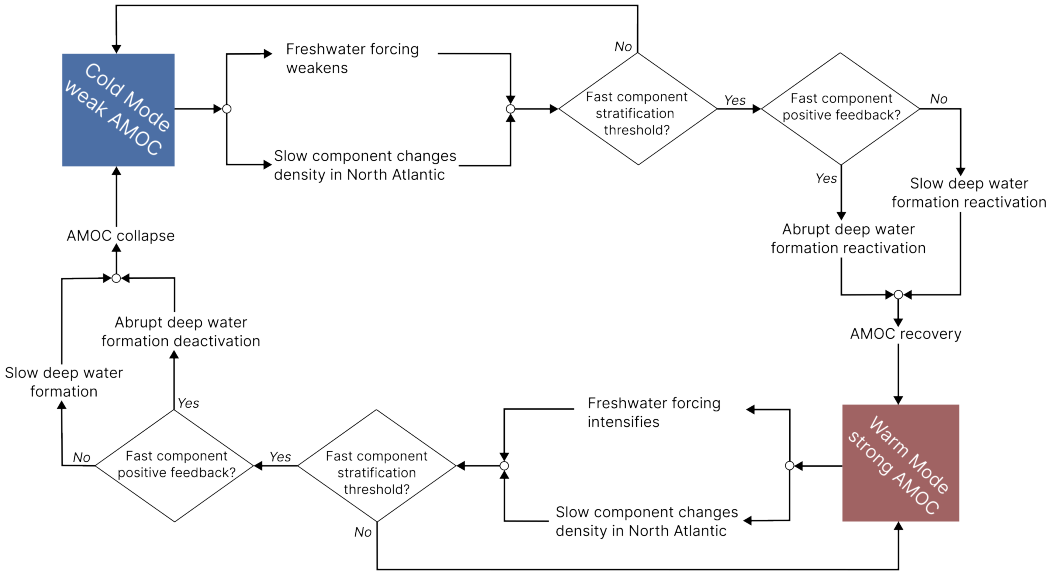

Figure 5.1: **A general concept for millennial-scale variability.**

(2023)'s theory that the ice sheets extent may have oscillated with a periodicity of about 1,500 years during the last deglaciation. This could provide the necessary forcing field for millennial-scale variability, that would only be triggered when the background climate is located in the window of opportunity. Finally, if neither the slow component nor the fast component is activated, the North Atlantic feedback responds linearly to changes in climate forcing in the same way as the ICE6G simulations in Section 4.2.2.

Future work

The absence of coupling between the ice sheets and the atmosphere is a significant limitation in simulating millennial-scale variability in HadCM3. The effect of the ice sheet feedback has often been discussed as a critical component of abrupt climate change mechanisms (Broecker et al., 1990; Menviel et al., 2020), and has been used to simulate the chain of events of the last glacial period in simple climate models (Boers et al., 2018; Alvarez-Solas et al., 2019). The main limitation of running coupled climate-ice sheets simulations is that they are computationally expensive and can return a wide range of results in response to small parameter changes (Gandy et al., 2023). To overcome this problem, Gandy et al. (2023) used ensemble runs to constrain the parameter space only to plausible results, and Sherriff-Tadano et al. (2023) used a simplified slab ocean model to allow more comprehensive coverage of the parameter space. This solution could be simplified even further to test this thesis' mechanism by coupling the ice sheet model to a simple

ocean model in the style of Stommel (1961), including only the processes relevant to the slow and fast oscillator components. Connecting general circulation models to theoretical concepts is essential to enhance cross-disciplinarity in the study of the millennial-scale variability. If, for instance, a simple box model based on the Fitz-Nakamura oscillator were to fit the broad lines of the GCMs' oscillating behaviour, this would be an opportunity to analyse millennial-scale variability in the light of oscillating behaviour observed in other research areas, such as biology or theoretical physics, where the mechanisms are better understood.

The modelling of meltwater discharge also needs further development to capture the entire complexity of abrupt climate changes. The ice sheet melt river routing method introduced by Ivanovic et al. (2017) is a step forward from the classical freshwater hosing experiments (Manabe and Stouffer, 1988). Still, it does not allow for precise and time-evolving distribution of meltwater as it can be obtained in models with integrated hydrological components such as the MPI-ESM (Kapsch et al., 2022). In particular, the absence of the modelling of production and transport of icebergs consists of a significant gap in the mapping of freshwater fluxes. Different approaches have been proposed to better model freshwater flux from iceberg discharge by using coupled iceberg-climate model (Martin and Adcroft, 2010; Marsh et al., 2015), but it has seldom been used in the context of Heinrich events (Levine and Bigg, 2008). Going further on this topic would require the implementation of iceberg tracking models (Bigg et al., 1998; Roberts et al., 2014a) in a GCM and better handling of surface currents and gyres (Monegato et al., 2017), requiring a high-resolution surface ocean model.

5.2.2 RQ2 - What is the influence of the ice sheet geometry and meltwater discharge history on the occurrence and characteristics of millennial-scale variability?

In the past decade, general circulation models have managed to overcome the assumption that they were too stable to trigger abrupt climate changes with realistic forcing (Valdes, 2011). Simulations displaying millennial-scale variability have been obtained with a wide range of conditions from pre-industrial (Brown and Galbraith, 2016) to full-glacial (Peltier and Vettoretti, 2014). The concept of window of opportunity was introduced to characterise the sweet spots in the parameter space formed by boundary conditions in response to climate forcing (Barker and Knorr, 2021). The main background conditions influencing the location of the window of opportunity are the ice sheet layout, the greenhouse gas concentrations and the orbital parameters, and only the latter two have been studied expansively. Glacial concentrations of CO_2 fall more often in the window of opportunity than high pre-industrial CO_2 concentrations (Brown and Galbraith, 2016; Zhang et al., 2017; Klockmann et al., 2018; Vettoretti et al., 2022). Lower solar insolation is more suitable for abrupt climate changes (Zhang et al., 2021; Kuniyoshi et al., 2022). The effect

of the ice sheet layout, however, remains more elusive. Smaller ice sheets tend to offer favourable conditions to millennial-scale variability (Brown and Galbraith, 2016; Klockmann et al., 2018), but such variability also exists with full-glacial ice sheets (Peltier and Vettoretti, 2014). The main forcing relevant to abrupt climate changes is the freshwater discharge that can disrupt the stratification at the deep water formation sites (Kageyama et al., 2013b). For a given set of background conditions that do not display spontaneous oscillations, millennial-scale variability can only be obtained with the right balance of location and magnitude of freshwater release (Chapter 2). Otherwise, the AMOC either recovers or completely collapses. Finally, changes in the parameterisation of the model were not considered in this thesis but were used in other studies to trigger abrupt climate changes, such as Peltier and Vettoretti (2014) and vertical mixing. The models' window of opportunity might be shifted relative to the real-world one, due to errors/uncertainty in the model structure and model parameters, and this requires the model to be tuned to observations and reconstructions.

In this thesis, new simulations were introduced showing clear millennial-scale variability in last glacial maximum background conditions forced with deglacial meltwater (*RO1*). In Chapter 2, six snapshots of meltwater discharge were derived from the GLAC-1D early last deglaciation history and used as forcing on an LGM background climate using GLAC-1D ice sheet reconstruction. In Chapter 4, two background conditions with ICE6G and GLAC-1D ice sheet layout at the LGM were forced with time-evolving meltwater histories derived from these two reconstructions. This combination of ice sheet layout and meltwater history enables the investigation of the sensitivity of HadCM3 to specific background conditions and forcing in the context of millennial-scale variability (*RO4*). A summary of the main experiments run for this thesis is presented in Figure 5.2.

Chapter 4's discussion gives an insight into the impact of the ice sheet layout on the location of the window of opportunity. ICE6G did not simulate abrupt transitions in HadCM3 simulations of the Last Glacial Maximum, mainly because its geometry over the Eurasian ice sheet does not produce the strong katabatic winds necessary to create deep water formation in the Nordic Seas. This is a strong limiting factor for abrupt climate transitions as this region was identified as crucial to obtain an abrupt overshoot in Chapter 3. In addition, ICE6G ice sheets produce an intensification of the high Arctic mean sea level pressure, which drives a strong deep water formation site in the Iceland Basin. This deep water formation site is very stable and difficult to deactivate, which may explain why it only responds linearly rather than abruptly to the introduction of freshwater (Section 4.2.2 Matero et al., 2017; Ivanovic et al., 2018a). This behaviour may not be true for different time slices of the ICE6G ice sheet reconstruction. Armstrong et al. (2022) showed that with ICE5G, an ice sheet reconstruction that preceded ICE6G, abrupt climate shifts can occur spontaneously in HadCM3 under mid-glacial conditions. One can imagine that similar conditions in ICE6G could result in a more favourable background for

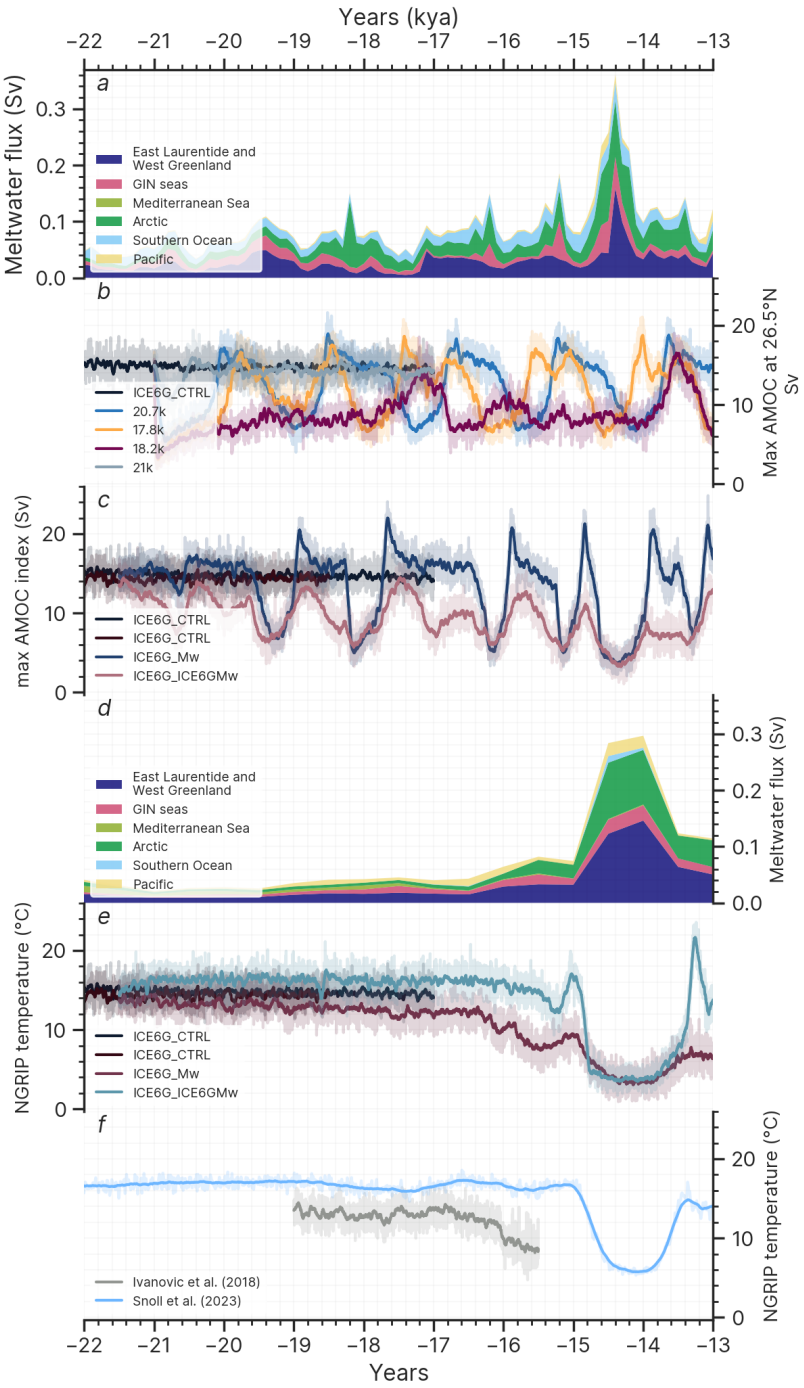

Figure 5.2: **HadCM3 simulations of the last deglaciation.** *a,d.* Meltwater discharge patterns obtained from GLAC-1D (*a*) and ICE6G (*d*) following the algorithm presented in Section 4.2.2. The regions are defined in Figure 4.11*a*. *b,c,e,f.* AMOC indexes, defined as the maximum overturning circulation at 26.5° N, for the simulations described in Chapter 2 (*b*), Chapter 4 using GLAC-1D meltwater (*c*), Chapter 4 using GLAC-1D meltwater (*e*) and the ICE6G meltwater transient simulation from Ivanovic et al. (2018a) and the ICE6G transient simulation from Snoll et al. (2023) (*f*). Solid lines are 30-year running means and transparent lines are annual data.

millennial-scale variability. On the other hand, the GLAC-1D ice sheet geometry provides a background climate suitable for producing abrupt climate changes. In the GLAC-1D LGM background climate, convection is present in the GIN Seas and none of the deep water formation sites are particularly strong. As a result, the introduction of freshwater disruptions around the deep water formation sites can trigger positive feedback, leading to abrupt AMOC mode shifts.

Future work

The ice sheet reconstruction is only one example of a boundary condition that can influence the ability of climate models to replicate millennial-scale variability. This thesis investigates a limited number of combinations within the last glacial maximum and the last deglaciation and, therefore, only gives an incomplete mapping of the window of opportunity. Similarly, Armstrong et al. (2019) presented a collection of snapshot simulations of the last glacial period that explore specific historical background conditions. In order to take the observation of the window of opportunity further, a systematic sensitivity study of all the key boundary conditions (i.e. ice sheet geometry, greenhouse gas concentration and orbital parameters) in the style of Brown and Galbraith (2016) or Klockmann et al. (2018) is necessary. Varying ice sheet geometries, orbital parameters and greenhouse gas concentrations around sweet spots of the climate model would give a thorough view of the model's behaviour in the climate forcing parameter space of the last glacial period. Because of the model-dependency of such a conclusion, this initiative should be repeated with all the general circulation models that displayed millennial-scale variability.

Chapter 2 investigated the sensitivity of glacial climate simulations to external forcing, in this case, the introduction of meltwater. To isolate the effect of the freshwater input only, all the other background conditions were fixed to last glacial maximum values and the meltwater was kept constant for the entire length of the oscillations. The precise location of the release was found to be as important, if not more, than the magnitude of the discharge. Despite a comparable amount of total freshwater discharged, *19.4k* showed regular oscillations, while *18.2k* ended up in an excitable cold mode. Roche et al. (2010) hypothesised that discharge in the GIN seas and the Arctic have the most direct influence on the deep water formation sites. This was verified in both Chapter 2, when comparing *19.4k* and *18.2k*, and in Chapter 4 where $0.02Sv$ in the GIN seas was enough to lead to an AMOC collapse compared to more than $0.05Sv$ in the Arctic and $0.07Sv$ in the Labrador Sea.

In the same way as for the boundary conditions, a systematic study of the effect of freshwater discharge is needed to get a deeper understanding of the window of opportunity. A one-dimensional sensitivity analysis was realised by Roche et al. (2010) and needed to be updated to explore the multi-dimensional parameter space introduced in Figure 4.5*c*. The main challenge of such a study is that simulating millennial-scale variability depends not

only on the instantaneous discharge pattern for a given background climate but also on the discharge history of the simulation. Testing all combinations of discharge, boundary conditions and meltwater history in multi-millennial simulations to see past the transition period would require unrealistic computer resources. Three methods can be imagined to conduct this analysis. The first would be to run an ensemble of 30-50 simulations and train a statistical emulator to interpolate between these results. This has, to my knowledge, never been attempted in a palaeo context, but could be attempted for a limited window of the parameter space. The main caveat is that emulators are not always reliable for non-linear behaviour and could miss key behaviours such as abrupt climate changes if they are not simulated in the training dataset. The second would be the use a lower-resolution model, such as FAMOUS that is based on HadCM3. However, lower-resolution models have different modelling of key physical components and, therefore, different responses to meltwater introduction; see Kageyama et al. (2013b) and the iLOVECLIM simulations in Figure 4.6. Finally, a dye study could help constrain the freshwater discharge dimension of the parameter space by tracking the actual path of meltwater discharge along surface currents and clustering the different discharge regions. Similar initiatives have been realised on specific examples, such as Heinrich event 1 (Roberts et al., 2014a), the 8.2 ka BP event (Born and Levermann, 2010), or to constrain overturning circulation proxies (Wunsch and Heimbach, 2008). This methodology could be applied to the oscillating simulations presented in Chapter 2.

The last factor that is often overlooked in millennial-scale variability research is the initial stage of the AMOC. This is especially limiting in simulations of the last deglaciation, as the AMOC was likely weaker during Heinrich stadial 1 prior to the Bølling warming (Ng et al., 2018), an effect commonly associated with the freshwater discharged by melting ice sheets (Toucanne et al., 2015; Hodell et al., 2017). It is possible that this particularity explains why the last deglaciation was the only of the last four deglaciations to exhibit millennial-scale variability (Cheng et al., 2009). In the multi-model analysis of the period by Snoll et al. (2023), only the MIROC simulation ran by Obase and Abe-Ouchi (2019) managed to simulate the Bølling warming. They were also the only run to start from a cold, almost collapsed, AMOC mode. None of the HadCM3 simulations presented in this thesis or in the literature have simulated a stable cold mode under glacial climate conditions. The *18.2k* simulation from Chapter 2 is arguably the closest, but it requires a significant amount of freshwater and occasionally produces "excitable" modes. Running two last deglaciation simulations starting from a warm and cold mode would be a good development in the PMIP protocol to test the importance of the initial state.

5.2.3 RQ3 - How did the transient evolution of ice sheet meltwater discharge influence the occurrence of millennial-scale variability during the last deglaciation and the last glacial period?

This thesis presents a new set of simulations using forcing from the last deglaciation. The primary aim of these simulations was not to produce an accurate reconstruction of the chain of events of the last deglaciation, but to inform on the processes at stake during this period. To that extent, the boundary conditions and forcing were fit to the actual reconstruction of the period, and the model results were compared to proxy data. This is also a statement for less compartmentalisation of climate research and to 'escape model world' (Thompson and Smith, 2019) of the historical modelling studies (e.g. Manabe and Stouffer, 1988).

The timing of the main events of the last deglaciation is fairly well reconstructed (Clark et al., 2012). However, their magnitude and geographical extent rely on limited data and are still open to interpretation. In particular, the state of the overturning circulation during the last deglaciation is an open topic of discussion (Muglia and Schmittner, 2021; Repschläger et al., 2021; Pöppelmeier et al., 2023). The state of the ice sheets during this period has also been at the centre of the debate of the past decade, and their geometry (Tarasov et al., 2012; Peltier et al., 2015; Batchelor et al., 2019; Gowan et al., 2021) can differ significantly depending on the methods. The lack of direct constraints of freshwater discharge resulting from the melting of the deglacial ice sheets is arguably even more limiting when it comes to climate simulations, considering the effect it can have on abrupt climate shifts. Bethke et al. (2012) argued that without further constraints of the ice sheet reconstructions and meltwater discharge history, climate models might not be able to produce much better simulations of the last deglaciation than the early attempts of Liu et al. (2009) and Menviel et al. (2011). Following the PMIP4 protocol for the last deglaciation instigated by Ivanovic et al. (2016), the guidelines for ice sheet and meltwater handling led to more consistent behaviours have been observed in the new generation of deglacial simulations (Snoll et al., 2023). The most convincing results, however, were obtained with non-ice-sheet reconstruction-derived freshwater fluxes fitted to the expected results (He et al., 2021). This raised the "meltwater paradox", stating that realistic freshwater fluxes cannot trigger the sequence of abrupt climate changes of the last deglaciation with state-of-the-art models.

Even though they did not manage to capture the timing of the chain of events of the last deglaciation, the new simulations introduced in Chapter 4 represent a step forward from the conclusions of Ivanovic et al. (2018a) in that abrupt climate changes can now be observed in glacial HadCM3 simulations forced with deglacial meltwater (*RO5*). The resulting transitions resemble the millennial-scale variability observed during the Bølling Warming/Younger Dryas transitions. During these transitions, the Greenland temperature signal is an excellent fit with what is expected from climate records, and the AMOC

mode shifts are consistent with reconstructions of the overturning circulations. In general, there is a good agreement between the temperature changes of the Northern Hemisphere, but the non-inclusion of the increase of radiative forcing means that the simulations do not capture the Southern Hemisphere warming. In the North Atlantic, the temperature changes are over-estimated at high latitudes but capture the main pattern of changes. The one significant caveat is that the warming of the Nordic Seas, essential to the mechanism presented in Chapter 3, is not apparent in climate records of the Bølling Warming and D-O events (Pedro et al., 2022).

The mismatch between this thesis' simulations and the proxy reconstructions for Nordic Seas temperature changes in abrupt warming events may come from the different processes that exist to trigger abrupt North Atlantic warming. The idea that changing ice sheet geometry, greenhouse gas concentrations and orbital parameters during the last deglaciation took the climate system into a sweet spot is appealing. Obase and Abe-Ouchi (2019), however, provides a new potential explanation of the Bølling Warming transition in that the weak AMOC of Heinrich Stadial 1 is maintained by the high freshwater flux of the melting Northern Hemisphere ice sheets, which eventually is not enough to compensate for the increase of the radiative forcing due to the increase of insolation and greenhouse gas concentrations. If, in addition, a positive feedback mechanism for abrupt transition exists in the model, then an abrupt warming can occur. The actual mechanism probably lies between these two theories, as the latter cannot explain abrupt cooling and requires to start from a cold AMOC mode. The melting of the ice sheets during the Bølling Warming may have eventually taken the system into a window of opportunity and triggered the Younger Dryas. Dynamical boundary conditions and climate forcings are necessary to test this hypothesis.

This process would fit the observations of Wickert et al. (2023), where a series of Laurentide ice sheet expansion and retreat may have occurred during the last deglaciation. In the same way, as in Section 5.2.1, an ice sheet component in climate models is necessary to test this hypothesis.

The transitions simulated in Chapters 2 and 4 better fit the DO sequence of the last glacial period, where the background conditions were more stable (*RO6*). With a periodicity of about 1500 years and Greenland temperature changes of about $10°C$, they fit the typical shape of such events in climate records (Lohmann and Ditlevsen, 2019). The simulation clustering that was done in Section 2.4 can also be applied to the D-O events sequences as illustrated in Figure 5.3. The *oscillating* simulations cluster fits D-Os 12-9 and 8-5, with similar shape, strong periodicity and a transition period over the first two cycles. The absence of dampening of the oscillations in the simulations could be a consequence of the fixed forcing and background conditions. The *cold* with *excitable warm* cluster fits D-O 18, 4, 3 and 2, where a base cold mode is disrupted by short-lived stochastic recovery of the AMOC. The *warm* cluster is less frequently observed in the D-O records,

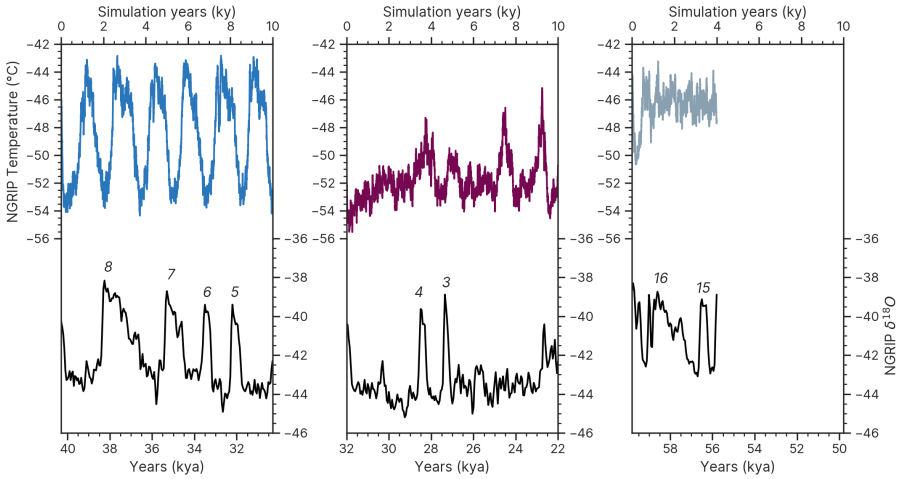

Figure 5.3: **Identifying Dansgaard-Oeschger events.** Comparison between Dansgaard-Oeschger events in Greenland $\delta^{18}O$ records (N.G.R.I.P, 2004) and selected simulations from Chapter 2.

but D-O 17 may be a good analogy where the forcing field can have triggered a short-lived cold mode transition from a base warm mode. Finally, DO 20 and 19 may be caused by the mechanism described for the Booling Warming/Younger Dryas transition, where an abrupt initial climate change took the system into a window of opportunity and stimulated the millennial-scale variability. It is nonetheless essential to remind the reader that none of these simulations were made with the prior intention to be compared to D-O events, and one can only conclude on the ability of HadCM3 to reproduce the D-O sequence if these oscillations are reproduced in a background where D-O events are observed, such as MIS3.

Future work

Three tracks to improve the last deglaciation simulations can be imagined from the conclusions of this study. The first lead rests on the continuous improvement of proxy records frequency, variety and constraints, and therefore to produce higher temporal and geographical resolution data for ice sheets extent and volume. Model-data comparison can help not only with the interpretation of climate records but also to provide suitable parameters for climate simulations. In particular, Chapter 4 makes the case for more consistent ice sheet reconstructions. The method used to reconstruct the past ice sheets from the climate records has been a subject of contention; nonetheless, it is an improvement to now have GLAC-1D as an alternative to the ICExG family. The new ice sheet reconstructions, such as Gowan et al. (2021), should also be tested in the framework of this study for a more comprehensive coverage of the parameter space. Finally, ICE6G may be missing some critical processes due to its 500-year resolution, and the 100-year resolution of GLAC-1D should be used as a standard to make sure that theories such as Wickert et al. (2023) can

be tested.

The ice sheet reconstruction is only one side of the problem, and the meltwater discharge patterns are also primordial when it comes to millennial-scale variability. Because small changes in discharge can dramatically impact climate simulations, improving the temporal resolution of the ice sheet reconstructions discussed in the previous paragraph would already be a way to improve the meltwater forcing field. However, Kapsch et al. (2022) showed the influence of re-routing and land storage in MPI-ESM deglacial simulations. This discussion could also include the calving fluxes and ice sheet feedback to climate models. This level of detail exists in ice sheet models, and even without a full coupling, they could be used to refine the forcing fields.

The TRACE simulations He et al. (2021) and Obase and Abe-Ouchi (2019) inspire a last track. Perturbed parameter ensembles of simulations, in a similar way to what was discussed in Section 5.2.1, could be designed based on the simulations of Chapter 4. Varying meltwater discharge magnitude, location, and the ice sheet layout to match the timing and magnitude of the deglacial chain of events can give a good insight into the location of the window of opportunity at each time step and inform the data reconstructions. The computer resources are, here again, a limitation, but this thesis already provides a good constraint of the sweet spots in the ice sheet and meltwater distributions in the context of the last deglaciation.

Past climate simulations are now able to capture millennial-scale variability better than CMIP climate models (Bellomo et al., 2021). Yet, the early climate warning (e.g. Ditlevsen and Ditlevsen, 2023) metrics for AMOC collapse have never been tested in past climate simulations. Testing these early climate warnings on the set of simulations presented in this thesis could be a good way to prevent any misinterpretation of the signals. Because the location of sea-ice cover and deep water formation sites is different in modern and glacial contexts, it is unclear if the mechanism presented in Chapter 3 would apply to modern climate. Nonetheless, the framework introduced in Section 5.2.1 could be helpful to future climate tipping points, particularly in the identification of the necessary positive feedback mechanisms.

5.3 General conclusions and future development

State-of-the-art climate models are now able to simulate millennial-scale variability in past glacial conditions, and this is mainly because they use boundary conditions and forcings more accurately than ever before. To that extent, the creation of a PMIP working group dedicated to simulations of the last glacial maximum and the last deglaciation was crucial as model-data comparisons are the most efficient way of testing and constraining simulation inputs. The response of climate simulations to boundary conditions and climate forcing, however, is still highly dependent on the model used and the experimental design in terms

of magnitude, sensitivity and the processes at stake. In this thesis, I investigated the influence of two model parameters, the ice sheet reconstructions and meltwater discharge, on the occurrence of abrupt climate changes in HadCM3 climate simulations.

I presented a robust and detailed mechanism for abrupt millennial-scale variability that consists of the interplay of a slow global component and a fast North Atlantic component coupled by AMOC mode shifts. The activation of the fast component relies on katabatic winds originating from the Eurasian ice sheets to force an abrupt recovery of the deep water formation site at high latitudes, in this case, in the Nordic Seas. The set-off of the oscillations requires an initial freshwater discharge forcing to start the oscillator and does not require an unrealistic amount of meltwater as long as it is targeted directly at the deep water formation sites. The mechanism can be adapted to different models and experimental designs by changing the processes at stake to modify the Atlantic conditions and the feedback to trigger abrupt climate transitions in the North Atlantic.

The last deglaciation simulations produced in this thesis are a step forward from the previous HadCM3 deglaciation simulations as they display abrupt climate changes. The simulations only used time-evolving meltwater discharge on top of an LGM climate background, and the magnitude and rate of change of the abrupt climate changes resemble the Bølling Warming/Younger Dryas transitions. The timing of the chain of events of the last deglaciation is not captured in any of the simulations. The absence of transient ice sheet layout, atmospheric trace gases and orbital parameters may prevent the window of opportunity to adapt to the deglacial climate, and the absence of land-sea mask change can mute potentially crucial mechanisms such as the Bering Strait opening or changes in the Mediterranean overflow. However, I argued that a more comprehensive and systematic sensitivity study to map the deglacial evolution window of opportunity is necessary before realising realistic fully transient simulations. In particular, understanding the precise impact of the choice of ice sheet reconstruction is key, as ICE6G does not enable convection overshoot in the Nordic Seas, and GLAC-1D is too sensitive to the introduction of meltwater. A combination of the two ice sheet reconstructions could be used with the Greenland and Icelandic ice sheets from ICE6G to boost the deep water formation in the Iceland Basin and Irminger Sea, and a Eurasian ice sheet from GLAC-1D to enable convection in the Nordic Seas.

Without the time-evolving background conditions, the simulated abrupt climate changes presented in Chapters 2 and 4 better match Dansgaard-Oeschger variability. They captured the reconstructed Northern Hemisphere temperature changes very well and displayed the right shape and rate of warming and cooling. The regularity of the simulated oscillations and the short cold periods could be an artefact of the absence of carbon and ice sheet feedback. The ice sheet feedback handling by climate models should be a priority to test the entire mechanism, whether by coupled climate-ice sheets simulations or GCM parametrisation. Different types of transitions were presented in response to more or less

efficient forcing fields, and they could explain the variety of Dansgaard-Oeschger events observed. These conclusions, however, need to be verified with background climate where millennial-scale variability is expected, such as MIS3.

The main source of uncertainty in these simulations comes from the constraints of the ice sheet layout, the meltwater discharge history, and how they are implemented in the climate model. From a modeller perspective, greater care should be given to the ice melting and calving processes, particularly iceberg calving and ice shelf instabilities. The efficiency of freshwater forcing should also be reviewed using the Lagrangian approach instead of the commonly used Eulerian approach. After their discharge, the freshwater parcel should be followed through dye tracer studies to trace their precise area of influence. Regarding the ice sheet reconstruction uncertainties, they should be considered with perturbed parameter ensemble not only for the ice sheet layout but also for the meltwater discharge.

This study provides a new way to consider millennial-scale variability not only for past climate changes but also for future climate changes. The debate about potential tipping points in the overturning circulation is mostly addressed using modern climate simulations when past climate models are generally more successful at triggering abrupt climate changes. The current metrics used for early climate warnings should be reviewed on palaeo simulations, and new metrics should be created based on the simulated millennial-scale variability.

Bibliography

Abe-Ouchi, A., Saito, F., Kawamura, K., Raymo, M. E., Okuno, J., Takahashi, K., and Blatter, H.: Insolation-driven 100,000-year glacial cycles and hysteresis of ice-sheet volume, Nature, 500, 190–193, doi:10.1038/nature12374, URL https://www.nature.com/articles/nature12374, number: 7461 Publisher: Nature Publishing Group, 2013.

Abe-Ouchi, A., Saito, F., Kageyama, M., Braconnot, P., Harrison, S. P., Lambeck, K., Otto-Bliesner, B. L., Peltier, W. R., Tarasov, L., Peterschmitt, J.-Y., and Takahashi, K.: Ice-sheet configuration in the CMIP5/PMIP3 Last Glacial Maximum experiments, Geoscientific Model Development, 8, 3621–3637, doi:https://doi.org/10.5194/gmd-8-3621-2015, URL https://www.geosci-model-dev.net/8/3621/2015/, publisher: Copernicus GmbH, 2015.

Alexander-Turner, R., Ortega, P., and Robson, J. I.: How Robust Are the Surface Temperature Fingerprints of the Atlantic Overturning Meridional Circulation on Monthly Time Scales?, Geophysical Research Letters, 45, 3559–3567, doi:10.1029/2017GL076759, URL https://onlinelibrary.wiley.com/doi/abs/10.1029/2017GL076759, important - To read, 2018.

Alley, R. B., Anandakrishnan, S., and Jung, P.: Stochastic resonance in the North Atlantic, Paleoceanography, 16, 190–198, doi:10.1029/2000PA000518, URL https://agupubs.onlinelibrary.wiley.com/doi/10.1029/2000PA000518, 2001.

Alvarez-Solas, J., Charbit, S., Ritz, C., Paillard, D., Ramstein, G., and Dumas, C.: Links between ocean temperature and iceberg discharge during Heinrich events, Nature Geoscience, 3, 122–126, doi:10.1038/ngeo752, URL https://www.nature.com/articles/ngeo752, number: 2 Publisher: Nature Publishing Group, 2010.

Alvarez-Solas, J., Robinson, A., Montoya, M., and Ritz, C.: Iceberg discharges of the last glacial period driven by oceanic circulation changes, Proceedings of the National Academy of Sciences, 110, 16 350–16 354, doi:10.1073/pnas.1306622110, URL https://www.pnas.org/content/110/41/16350, 2013.

Alvarez-Solas, J., Banderas, R., Robinson, A., and Montoya, M.: Ocean-driven millennial-scale variability of the Eurasian ice sheet during the last glacial period simulated with

a hybrid ice-sheet–shelf model, Climate of the Past, 15, 957–979, doi:https://doi.org/10.5194/cp-15-957-2019, URL https://www.clim-past.net/15/957/2019/, 2019.

Andel, T. H. v.: The Climate and Landscape of the Middle Part of the Weichselian Glaciation in Europe: The Stage 3 Project, Quaternary Research, 57, 2–8, doi:10.1006/qres.2001.2294, publisher: Cambridge University Press, 2002.

Annan, J. D. and Hargreaves, J. C.: A new global reconstruction of temperature changes at the Last Glacial Maximum, Climate of the Past, 9, 367–376, doi:https://doi.org/10.5194/cp-9-367-2013, URL https://www.clim-past.net/9/367/2013/, publisher: Copernicus GmbH, 2013.

Argus, D. F., Peltier, W. R., Drummond, R., and Moore, A. W.: The Antarctica component of postglacial rebound model ICE-6G_C (VM5a) based on GPS positioning, exposure age dating of ice thicknesses, and relative sea level histories, Geophysical Journal International, 198, 537–563, doi:10.1093/gji/ggu140, URL https://academic.oup.com/gji/article/198/1/537/2874192, publisher: Oxford Academic, 2014.

Armstrong, E., Hopcroft, P. O., and Valdes, P. J.: A simulated Northern Hemisphere terrestrial climate dataset for the past 60,000 years, Scientific Data, 6, 265, doi:10.1038/s41597-019-0277-1, URL https://doi.org/10.1038/s41597-019-0277-1, 2019.

Armstrong, E., Izumi, K., and Valdes, P.: Identifying the mechanisms of DO-scale oscillations in a GCM: a salt oscillator triggered by the Laurentide ice sheet, Climate Dynamics, doi:10.1007/s00382-022-06564-y, URL https://doi.org/10.1007/s00382-022-06564-y, 2022.

Armstrong McKay, D. I., Staal, A., Abrams, J. F., Winkelmann, R., Sakschewski, B., Loriani, S., Fetzer, I., Cornell, S. E., Rockström, J., and Lenton, T. M.: Exceeding 1.5°C global warming could trigger multiple climate tipping points, Science, 377, eabn7950, doi:10.1126/science.abn7950, URL https://www.science.org/doi/10.1126/science.abn7950, publisher: American Association for the Advancement of Science, 2022.

Banderas, R., Alvarez-Solas, J., Robinson, A., and Montoya, M.: An interhemispheric mechanism for glacial abrupt climate change, Climate Dynamics, 44, 2897–2908, doi:10.1007/s00382-014-2211-8, URL https://doi.org/10.1007/s00382-014-2211-8, 2015.

Barbante, C., Barnola, J.-M., Becagli, S., Beer, J., Bigler, M., Boutron, C., Blunier, T., Castellano, E., Cattani, O., Chappellaz, J., Dahl-Jensen, D., Debret, M., Delmonte, B., Dick, D., Falourd, S., Faria, S., Federer, U., Fischer, H., Freitag, J., Frenzel, A., Fritzsche, D., Fundel, F., Gabrielli, P., Gaspari, V., Gersonde, R., Graf, W., Grigoriev, D., Hamann, I., Hansson, M., Hoffmann, G., Hutterli, M. A., Huybrechts, P., Isaksson, E., Johnsen, S., Jouzel, J., Kaczmarska, M., Karlin, T., Kaufmann, P., Kipfstuhl, S., Kohno, M., Lambert, F., Lambrecht, A., Lambrecht, A., Landais, A., Lawer,

G., Leuenberger, M., Littot, G., Loulergue, L., Lüthi, D., Maggi, V., Marino, F., Masson-Delmotte, V., Meyer, H., Miller, H., Mulvaney, R., Narcisi, B., Oerlemans, J., Oerter, H., Parrenin, F., Petit, J.-R., Raisbeck, G., Raynaud, D., Röthlisberger, R., Ruth, U., Rybak, O., Severi, M., Schmitt, J., Schwander, J., Siegenthaler, U., Siggaard-Andersen, M.-L., Spahni, R., Steffensen, J. P., Stenni, B., Stocker, T. F., Tison, J.-L., Traversi, R., Udisti, R., Valero-Delgado, F., van den Broeke, M. R., van de Wal, R. S. W., Wagenbach, D., Wegner, A., Weiler, K., Wilhelms, F., Winther, J.-G., Wolff, E., and EPICA Community Members: One-to-one coupling of glacial climate variability in Greenland and Antarctica, Nature, 444, doi:10.1038/nature05301, URL https://www.nature.com/articles/nature05301, 2006.

Bard, E., Rostek, F., Turon, J.-L., and Gendreau, S.: Hydrological Impact of Heinrich Events in the Subtropical Northeast Atlantic, Science, 289, 1321–1324, doi:10.1126/science.289.5483.1321, URL https://science.sciencemag.org/content/289/5483/1321, publisher: American Association for the Advancement of Science Section: Report, 2000.

Barker, S. and Knorr, G.: Millennial scale feedbacks determine the shape and rapidity of glacial termination, Nature Communications, 12, 2273, doi:10.1038/s41467-021-22388-6, URL https://www.nature.com/articles/s41467-021-22388-6, 2021.

Barker, S., Chen, J., Gong, X., Jonkers, L., Knorr, G., and Thornalley, D.: Icebergs not the trigger for North Atlantic cold events, Nature, 520, 333–336, doi:10.1038/nature14330, URL https://www.nature.com/articles/nature14330, 2015.

Bassis, J. N., Petersen, S. V., and Mac Cathles, L.: Heinrich events triggered by ocean forcing and modulated by isostatic adjustment, Nature, 542, 332–334, doi:10.1038/nature21069, URL https://www.nature.com/articles/nature21069, 2017.

Batchelor, C. L., Margold, M., Krapp, M., Murton, D. K., Dalton, A. S., Gibbard, P. L., Stokes, C. R., Murton, J. B., and Manica, A.: The configuration of Northern Hemisphere ice sheets through the Quaternary, Nature Communications, 10, 1–10, doi:10.1038/s41467-019-11601-2, URL https://www.nature.com/articles/s41467-019-11601-2, 2019.

Batchelor, C. L., Christie, F. D. W., Ottesen, D., Montelli, A., Evans, J., Dowdeswell, E. K., Bjarnadóttir, L. R., and Dowdeswell, J. A.: Rapid, buoyancy-driven ice-sheet retreat of hundreds of metres per day, Nature, 617, 105–110, doi:10.1038/s41586-023-05876-1, URL https://www.nature.com/articles/s41586-023-05876-1, number: 7959 Publisher: Nature Publishing Group, 2023.

Beerling, D. J. and Royer, D. L.: Convergent Cenozoic CO2 history, Nature Geoscience, 4, 418–420, doi:10.1038/ngeo1186, URL https://www.nature.com/articles/ngeo1186, number: 7 Publisher: Nature Publishing Group, 2011.

Beghin, P., Charbit, S., Dumas, C., Kageyama, M., and Ritz, C.: How might the North American ice sheet influence the northwestern Eurasian climate?, Climate of the Past, 11, 1467–1490, doi:10.5194/cp-11-1467-2015, URL https://cp.copernicus.org/articles/11/1467/2015/, publisher: Copernicus GmbH, 2015.

Bellomo, K., Angeloni, M., Corti, S., and von Hardenberg, J.: Future climate change shaped by inter-model differences in Atlantic meridional overturning circulation response, Nature Communications, 12, 3659, doi:10.1038/s41467-021-24015-w, URL https://www.nature.com/articles/s41467-021-24015-w, important - To Read, 2021.

Bereiter, B., Eggleston, S., Schmitt, J., Nehrbass-Ahles, C., Stocker, T. F., Fischer, H., Kipfstuhl, S., and Chappellaz, J.: Revision of the EPICA Dome C CO2 record from 800 to 600 kyr before present, Geophysical Research Letters, 42, 542–549, doi:10.1002/2014GL061957, URL https://agupubs.onlinelibrary.wiley.com/doi/abs/10.1002/2014GL061957, 2015.

Berger, A.: Long-Term Variations of Daily Insolation and Quaternary Climatic Changes, Journal of the Atmospheric Sciences, 35, 2362–2367, doi:10.1175/1520-0469(1978)035⟨2362:LTVODI⟩2.0.CO;2, URL https://journals.ametsoc.org/doi/abs/10.1175/1520-0469%281978%29035%3C2362%3ALTVODI%3E2.0.CO%3B2, publisher: American Meteorological Society, 1978.

Berger, A. and Loutre, M. F.: Insolation values for the climate of the last 10 million years, Quaternary Science Reviews, 10, 297–317, doi:10.1016/0277-3791(91)90033-Q, URL https://www.sciencedirect.com/science/article/pii/027737919190033Q, 1991.

Bethke, I., Li, C., and Nisancioglu, K. H.: Can we use ice sheet reconstructions to constrain meltwater for deglacial simulations?, Paleoceanography, 27, doi:10.1029/2011PA002258, URL https://agupubs.onlinelibrary.wiley.com/doi/abs/10.1029/2011PA002258, 2012.

Bigg, G. R. and Wadley, M. R.: Millennial-scale variability in the oceans: an ocean modelling view, Journal of Quaternary Science, 16, 309–319, doi:10.1002/jqs.599, URL https://onlinelibrary.wiley.com/doi/abs/10.1002/jqs.599, 2001.

Bigg, G. R., Wadley, M. R., Stevens, D. P., and Johnson, J. A.: Simulations of two Last Glacial Maximum ocean states, Paleoceanography, 13, 340–351, doi:10.1029/98PA00402, URL https://agupubs.onlinelibrary.wiley.com/doi/abs/10.1029/98PA00402, 1998.

Bigg, G. R., Clark, C. D., Greenwood, S. L., Haflidason, H., Hughes, A. L. C., Levine, R. C., Nygård, A., and Sejrup, H. P.: Sensitivity of the North Atlantic circulation to break-up of the marine sectors of the NW European ice sheets during the last Glacial: A synthesis of modelling and palaeoceanography, Global and Planetary Change, 98-99,

153–165, doi:10.1016/j.gloplacha.2012.09.004, URL http://www.sciencedirect.com/science/article/pii/S0921818112001816, 2012.

Birchfield, E. G., Wang, H., and Rich, J. J.: Century/millennium internal climate oscillations in an ocean-atmosphere-continental ice sheet model, Journal of Geophysical Research: Oceans, 99, 12 459–12 470, doi:10.1029/94JC00523, URL https://agupubs.onlinelibrary.wiley.com/doi/10.1029/94JC00523, important - Abstract, 1994.

Blunier, T. and Brook, E. J.: Timing of Millennial-Scale Climate Change in Antarctica and Greenland During the Last Glacial Period, Science, 291, 109–112, doi:10.1126/science.291.5501.109, URL https://science.sciencemag.org/content/291/5501/109, publisher: American Association for the Advancement of Science Section: Report, 2001.

Boers, N.: Observation-based early-warning signals for a collapse of the Atlantic Meridional Overturning Circulation, Nature Climate Change, 11, 680–688, doi:10.1038/s41558-021-01097-4, URL https://www.nature.com/articles/s41558-021-01097-4, high - To Read - SST fingerprint, 2021.

Boers, N., Ghil, M., and Rousseau, D.-D.: Ocean circulation, ice shelf, and sea ice interactions explain Dansgaard–Oeschger cycles, Proceedings of the National Academy of Sciences, 115, E11 005–E11 014, doi:10.1073/pnas.1802573115, URL https://www.pnas.org/doi/10.1073/pnas.1802573115, publisher: Proceedings of the National Academy of Sciences, 2018.

Bond, G., Broecker, W., Johnsen, S., McManus, J., Labeyrie, L., Jouzel, J., and Bonani, G.: Correlations between climate records from North Atlantic sediments and Greenland ice, Nature, 365, 143–147, doi:10.1038/365143a0, URL https://www.nature.com/articles/365143a0, number: 6442 Publisher: Nature Publishing Group, 1993.

Born, A. and Levermann, A.: The 8.2 ka event: Abrupt transition of the subpolar gyre toward a modern North Atlantic circulation, Geochemistry, Geophysics, Geosystems, 11, doi:10.1029/2009GC003024, URL https://agupubs.pericles-prod.literatumonline.com/doi/abs/10.1029/2009GC003024, 2010.

Bouttes, N., Lhardy, F., Quiquet, A., Paillard, D., Goosse, H., and Roche, D. M.: Deglacial climate changes as forced by different ice sheet reconstructions, Climate of the Past, 19, 1027–1042, doi:10.5194/cp-19-1027-2023, URL https://cp.copernicus.org/articles/19/1027/2023/, publisher: Copernicus GmbH, 2023.

Bower, A. S., Lozier, M. S., Gary, S. F., and Böning, C. W.: Interior pathways of the North Atlantic meridional overturning circulation, Nature, 459, 243–247, doi:10.1038/nature07979, URL https://www.nature.com/articles/nature07979, number: 7244 Publisher: Nature Publishing Group, 2009.

Braconnot, P., Otto-Bliesner, B., Harrison, S., Joussaume, S., Peterchmitt, J.-Y., Abe-

Ouchi, A., Crucifix, M., Driesschaert, E., Fichefet, T., Hewitt, C. D., Kageyama, M., Kitoh, A., Loutre, M.-F., Marti, O., Merkel, U., Ramstein, G., Valdes, P., Weber, L., Yu, Y., and Zhao, Y.: Results of PMIP2 coupled simulations of the Mid-Holocene and Last Glacial Maximum – Part 2: feedbacks with emphasis on the location of the ITCZ and mid- and high latitudes heat budget, Climate of the Past, 3, 279–296, doi:10.5194/cp-3-279-2007, URL https://cp.copernicus.org/articles/3/279/2007/, publisher: Copernicus GmbH, 2007.

Bradtmiller, L. I., McManus, J. F., and Robinson, L. F.: 231 Pa/ 230 Th evidence for a weakened but persistent Atlantic meridional overturning circulation during Heinrich Stadial 1, Nature Communications, 5, 5817, doi:10.1038/ncomms6817, URL https://www.nature.com/articles/ncomms6817, number: 1 Publisher: Nature Publishing Group, 2014.

Bradwell, T., Small, D., Fabel, D., Clark, C. D., Chiverrell, R. C., Saher, M. H., Dove, D., Callard, S. L., Burke, M. J., Moreton, S. G., Medialdea, A., Bateman, M. D., Roberts, D. H., Golledge, N. R., Finlayson, A., Morgan, S., and Cofaigh, C. O.: Pattern, style and timing of British–Irish Ice Sheet retreat: Shetland and northern North Sea sector, Journal of Quaternary Science, 36, 681–722, doi:10.1002/jqs.3163, URL https://onlinelibrary.wiley.com/doi/abs/10.1002/jqs.3163, 2021.

Briggs, R. D., Pollard, D., and Tarasov, L.: A data-constrained large ensemble analysis of Antarctic evolution since the Eemian, Quaternary Science Reviews, 103, 91–115, doi:10.1016/j.quascirev.2014.09.003, URL http://www.sciencedirect.com/science/article/pii/S0277379114003448, 2014.

Broecker, W. S.: The Great Ocean Conveyor, Oceanography, 4, 79–89, URL https://www.jstor.org/stable/43924572, publisher: Oceanography Society, 1991.

Broecker, W. S.: Thermohaline Circulation, the Achilles Heel of Our Climate System: Will Man-Made CO2 Upset the Current Balance?, Science, 278, 1582–1588, doi:10.1126/science.278.5343.1582, URL https://www.science.org/doi/10.1126/science.278.5343.1582, publisher: American Association for the Advancement of Science, 1997.

Broecker, W. S. and Peng, T. H.: Tracers in the Sea, Palisades, NY, 1982.

Broecker, W. S., Peteet, D. M., and Rind, D.: Does the ocean–atmosphere system have more than one stable mode of operation?, Nature, 315, 21–26, doi:10.1038/315021a0, URL https://www.nature.com/articles/315021a0, number: 6014 Publisher: Nature Publishing Group, 1985.

Broecker, W. S., Bond, G., Klas, M., Bonani, G., and Wolfli, W.: A salt oscillator in the glacial Atlantic? 1. The concept, Paleoceanography, 5, 469–477, doi:10.1029/PA005i004p00469, URL https://agupubs.onlinelibrary.wiley.com/doi/abs/10.1029/PA005i004p00469, 1990.

Brown, N. and Galbraith, E.: Hosed vs. unhosed: Interruptions of the Atlantic Meridional Overturning Circulation in a global coupled model, with and without freshwater forcing, Climate of the Past, 12, 1663–1679, doi:10.5194/cp-12-1663-2016, 2016.

Bryan, K. and Cox, M. D.: An Approximate Equation of State for Numerical Models of Ocean Circulation, Journal of Physical Oceanography, 2, 510–514, doi:10.1175/1520-0485(1972)002⟨0510:AAEOSF⟩2.0.CO;2, URL https://journals.ametsoc.org/view/journals/phoc/2/4/1520-0485_1972_002_0510_aaeosf_2_0_co_2.xml, 1972.

Buizert, C. and Schmittner, A.: Southern Ocean control of glacial AMOC stability and Dansgaard-Oeschger interstadial duration, Paleoceanography, 30, 1595–1612, doi:10.1002/2015PA002795, URL https://agupubs.onlinelibrary.wiley.com/doi/full/10.1002/2015PA002795, 2015.

Buizert, C., Gkinis, V., Severinghaus, J. P., He, F., Lecavalier, B. S., Kindler, P., Leuenberger, M., Carlson, A. E., Vinther, B., Masson-Delmotte, V., White, J. W. C., Liu, Z., Otto-Bliesner, B., and Brook, E. J.: Greenland temperature response to climate forcing during the last deglaciation, Science, 345, 1177–1180, doi:10.1126/science.1254961, URL https://science.sciencemag.org/content/345/6201/1177, publisher: American Association for the Advancement of Science Section: Report, 2014.

Buizert, C., Keisling, B. A., Box, J. E., He, F., Carlson, A. E., Sinclair, G., and DeConto, R. M.: Greenland-Wide Seasonal Temperatures During the Last Deglaciation, Geophysical Research Letters, 45, 1905–1914, doi:10.1002/2017GL075601, URL https://onlinelibrary.wiley.com/doi/abs/10.1002/2017GL075601, _eprint: https://onlinelibrary.wiley.com/doi/pdf/10.1002/2017GL075601, 2018.

Buizert, C., Fudge, T. J., Roberts, W. H. G., Steig, E. J., Sherriff-Tadano, S., Ritz, C., Lefebvre, E., Edwards, J., Kawamura, K., Oyabu, I., Motoyama, H., Kahle, E. C., Jones, T. R., Abe-Ouchi, A., Obase, T., Martin, C., Corr, H., Severinghaus, J. P., Beaudette, R., Epifanio, J. A., Brook, E. J., Martin, K., Chappellaz, J., Aoki, S., Nakazawa, T., Sowers, T. A., Alley, R. B., Ahn, J., Sigl, M., Severi, M., Dunbar, N. W., Svensson, A., Fegyveresi, J. M., He, C., Liu, Z., Zhu, J., Otto-Bliesner, B. L., Lipenkov, V. Y., Kageyama, M., and Schwander, J.: Antarctic surface temperature and elevation during the Last Glacial Maximum, Science, 372, 1097–1101, doi:10.1126/science.abd2897, URL https://www.science.org/doi/10.1126/science.abd2897, publisher: American Association for the Advancement of Science, 2021.

Burckel, P., Waelbroeck, C., Gherardi, J. M., Pichat, S., Arz, H., Lippold, J., Dokken, T., and Thil, F.: Atlantic Ocean circulation changes preceded millennial tropical South America rainfall events during the last glacial, Geophysical Research Letters, 42, 411–418, doi:10.1002/2014GL062512, URL https://agupubs.onlinelibrary.wiley.com/doi/abs/10.1002/2014GL062512, 2015.

Burckel, P., Waelbroeck, C., Luo, Y., Roche, D. M., Pichat, S., Jaccard, S. L., Gherardi, J., Govin, A., Lippold, J., and Thil, F.: Changes in the geometry and strength of the Atlantic meridional overturning circulation during the last glacial (20–50 ka), Climate of the Past, 12, 2061–2075, doi:10.5194/cp-12-2061-2016, URL https://cp.copernicus.org/articles/12/2061/2016/cp-12-2061-2016-discussion.html, 2016.

Böhm, E., Lippold, J., Gutjahr, M., Frank, M., Blaser, P., Antz, B., Fohlmeister, J., Frank, N., Andersen, M. B., and Deininger, M.: Strong and deep Atlantic meridional overturning circulation during the last glacial cycle, Nature, 517, 73–76, doi:10.1038/nature14059, URL https://www.nature.com/articles/nature14059, 2015.

Caesar, L., Rahmstorf, S., Robinson, A., Feulner, G., and Saba, V.: Observed fingerprint of a weakening Atlantic Ocean overturning circulation, Nature, 556, 191–196, doi:10.1038/s41586-018-0006-5, URL https://www.nature.com/articles/s41586-018-0006-5, high, 2018.

Carstens, J., Hebbeln, D., and Wefer, G.: Distribution of planktic foraminifera at the ice margin in the Arctic (Fram Strait), Marine Micropaleontology, 29, 257–269, doi:10.1016/S0377-8398(96)00014-X, URL https://www.sciencedirect.com/science/article/pii/S037783989600014X, 1997.

Cattle, H., Crossley, J., Drewry, D. J., Wadhams, P., Dowdeswell, J. A., and Schofield, A. N.: Modelling Arctic climate change, Philosophical Transactions of the Royal Society of London. Series A: Physical and Engineering Sciences, 352, 201–213, doi:10.1098/rsta.1995.0064, URL https://royalsocietypublishing.org/doi/10.1098/rsta.1995.0064, publisher: Royal Society, 1997.

Cessi, P.: Convective Adjustment and Thermohaline Excitability, Journal of Physical Oceanography, 26, 481–491, doi:10.1175/1520-0485(1996)026⟨0481:CAATE⟩2.0.CO;2, URL https://journals.ametsoc.org/view/journals/phoc/26/4/1520-0485_1996_026_0481_caate_2_0_co_2.xml, publisher: American Meteorological Society Section: Journal of Physical Oceanography, 1996.

Cheng, H., Edwards, R. L., Broecker, W. S., Denton, G. H., Kong, X., Wang, Y., Zhang, R., and Wang, X.: Ice Age Terminations, Science, 326, 248–252, doi:10.1126/science.1177840, URL https://www.science.org/doi/10.1126/science.1177840, publisher: American Association for the Advancement of Science, 2009.

Cheng, H., Edwards, R. L., Sinha, A., Spötl, C., Yi, L., Chen, S., Kelly, M., Kathayat, G., Wang, X., Li, X., Kong, X., Wang, Y., Ning, Y., and Zhang, H.: The Asian monsoon over the past 640,000 years and ice age terminations, Nature, 534, 640–646, doi:10.1038/nature18591, URL https://www.nature.com/articles/nature18591, 2016.

Cheng, J., Liu, Z., He, F., L. Otto-Bliesner, B., Brady, E., and Wehrenberg, M.: Simulated Two-Stage Recovery of Atlantic Meridional Overturning Circulation During the Last

Deglaciation, Abrupt Climate Change: Mechanisms, Patterns, and Impacts, 193, 75–92, doi:10.1029/2010gm001014, 2011.

Cimatoribus, A. A., Drijfhout, S. S., Livina, V., and van der Schrier, G.: Dansgaard–Oeschger events: bifurcation points in the climate system, Climate of the Past, 9, 323–333, doi:10.5194/cp-9-323-2013, URL https://cp.copernicus.org/articles/9/323/2013/, 2013.

Clark, P. U. and Tarasov, L.: Closing the sea level budget at the Last Glacial Maximum, Proceedings of the National Academy of Sciences, 111, 15 861–15 862, doi:10.1073/pnas.1418970111, URL https://www.pnas.org/content/111/45/15861, publisher: National Academy of Sciences Section: Commentary, 2014.

Clark, P. U., Pisias, N. G., Stocker, T. F., and Weaver, A. J.: The role of the thermohaline circulation in abrupt climate change, Nature, 415, 863–869, doi:10.1038/415863a, URL https://www.nature.com/articles/415863a, number: 6874 Publisher: Nature Publishing Group, 2002.

Clark, P. U., Dyke, A. S., Shakun, J. D., Carlson, A. E., Clark, J., Wohlfarth, B., Mitrovica, J. X., Hostetler, S. W., and McCabe, A. M.: The Last Glacial Maximum, Science, 325, 710–714, doi:10.1126/science.1172873, URL https://science.sciencemag.org/content/325/5941/710, publisher: American Association for the Advancement of Science Section: Research Article, 2009.

Clark, P. U., Shakun, J. D., Baker, P. A., Bartlein, P. J., Brewer, S., Brook, E., Carlson, A. E., Cheng, H., Kaufman, D. S., Liu, Z., Marchitto, T. M., Mix, A. C., Morrill, C., Otto-Bliesner, B. L., Pahnke, K., Russell, J. M., Whitlock, C., Adkins, J. F., Blois, J. L., Clark, J., Colman, S. M., Curry, W. B., Flower, B. P., He, F., Johnson, T. C., Lynch-Stieglitz, J., Markgraf, V., McManus, J., Mitrovica, J. X., Moreno, P. I., and Williams, J. W.: Global climate evolution during the last deglaciation, Proceedings of the National Academy of Sciences, 109, E1134–E1142, doi:10.1073/pnas.1116619109, URL https://www.pnas.org/doi/full/10.1073/pnas.1116619109, publisher: Proceedings of the National Academy of Sciences, 2012.

Cleator, S. F., Harrison, S. P., Nichols, N. K., Prentice, I. C., and Roulstone, I.: A new multivariable benchmark for Last Glacial Maximum climate simulations, Climate of the Past, 16, 699–712, doi:10.5194/cp-16-699-2020, URL https://cp.copernicus.org/articles/16/699/2020/, publisher: Copernicus GmbH, 2020.

Clement, A. C. and Peterson, L. C.: Mechanisms of abrupt climate change of the last glacial period, Reviews of Geophysics, 46, doi:10.1029/2006RG000204, URL https://onlinelibrary.wiley.com/doi/abs/10.1029/2006RG000204, 2008.

Colin de Verdière, A.: A Simple Model of Millennial Oscillations of the Thermohaline Circulation, Journal of Physical Oceanography, 37, 1142–1155, doi:10.

1175/JPO3056.1, URL https://journals.ametsoc.org/view/journals/phoc/37/5/jpo3056.1.xml, publisher: American Meteorological Society Section: Journal of Physical Oceanography, 2007.

Condron, A. and Winsor, P.: Meltwater routing and the Younger Dryas, Proceedings of the National Academy of Sciences, 109, 19 928–19 933, doi:10.1073/pnas.1207381109, URL http://www.pnas.org/cgi/doi/10.1073/pnas.1207381109, 2012.

Cox, P.: Description of the TRIFFID dynamic global vegetation model, Hadley Centre Technical Note, 24, 2001.

Cox, P. M., Betts, R. A., Bunton, C. B., Essery, R. L. H., Rowntree, P. R., and Smith, J.: The impact of new land surface physics on the GCM simulation of climate and climate sensitivity, Climate Dynamics, 15, 183–203, doi:10.1007/s003820050276, URL https://doi.org/10.1007/s003820050276, 1999.

Cronin, T. M.: Paleoclimates: Understanding Climate Change Past and Present, Columbia University Press, URL https://www.jstor.org/stable/10.7312/cron14494, 2010.

Czaja, A.: Atmospheric Control on the Thermohaline Circulation, Journal of Physical Oceanography, 39, 234–247, doi:10.1175/2008JPO3897.1, URL https://journals.ametsoc.org/view/journals/phoc/39/1/2008jpo3897.1.xml, middle, 2009.

Danabasoglu, G., Castruccio, F. S., Small, R. J., Tomas, R., Frajka-Williams, E., and Lankhorst, M.: Revisiting AMOC Transport Estimates From Observations and Models, Geophysical Research Letters, 48, e2021GL093 045, doi:10.1029/2021GL093045, URL https://onlinelibrary.wiley.com/doi/abs/10.1029/2021GL093045, 2021.

Dansgaard, W., Johnsen, S. J., Clausen, H. B., Dahl-Jensen, D., Gundestrup, N. S., Hammer, C. U., Hvidberg, C. S., Steffensen, J. P., Sveinbjörnsdottir, A. E., Jouzel, J., and Bond, G.: Evidence for general instability of past climate from a 250-kyr ice-core record, Nature, 364, 218–220, doi:10.1038/364218a0, URL https://www.nature.com/articles/364218a0, 1993.

Davies-Barnard, T., Ridgwell, A., Singarayer, J., and Valdes, P.: Quantifying the influence of the terrestrial biosphere on glacial–interglacial climate dynamics, Climate of the Past, 13, 1381–1401, doi:10.5194/cp-13-1381-2017, URL https://cp.copernicus.org/articles/13/1381/2017/, publisher: Copernicus GmbH, 2017.

Dentith, J. E., Ivanovic, R. F., Gregoire, L. J., Tindall, J. C., Robinson, L. F., and Valdes, P. J.: Simulating oceanic radiocarbon with the FAMOUS GCM: implications for its use as a proxy for ventilation and carbon uptake, Biogeosciences Discussions, pp. 1–46, doi:10.5194/bg-2019-365, URL https://bg.copernicus.org/preprints/bg-2019-365/, publisher: Copernicus GmbH, 2019a.

Dentith, J. E., Ivanovic, R. F., Gregoire, L. J., Tindall, J. C., and Smith, R. S.: Ocean circulation drifts in multi-millennial climate simulations: the role of salinity corrections and climate feedbacks, Climate Dynamics, 52, 1761–1781, doi:10.1007/s00382-018-4243-y, URL https://doi.org/10.1007/s00382-018-4243-y, 2019b.

Denton, G. H., Alley, R. B., Comer, G. C., and Broecker, W. S.: The role of seasonality in abrupt climate change, Quaternary Science Reviews, 24, 1159–1182, doi:10.1016/j.quascirev.2004.12.002, URL https://www.sciencedirect.com/science/article/pii/S027737910500003X, 2005.

Denton, G. H., Broecker, W. S., and Alley, R. B.: The mystery interval 17.5 to 14.5 kyrs ago, PAGES news, 14, 14–16, doi:10.22498/pages.14.2.14, URL http://www.pastglobalchanges.org/products/12189, 2006.

Deschamps, P., Durand, N., Bard, E., Hamelin, B., Camoin, G., Thomas, A. L., Henderson, G. M., Okuno, J., and Yokoyama, Y.: Ice-sheet collapse and sea-level rise at the Bølling warming 14,600 years ago, Nature, 483, 559–564, doi:10.1038/nature10902, URL https://www.nature.com/articles/nature10902, number: 7391 Publisher: Nature Publishing Group, 2012.

Dijkstra, H. A. and Ghil, M.: Low-frequency variability of the large-scale ocean circulation: A dynamical systems approach, Reviews of Geophysics, 43, doi:10.1029/2002RG000122, URL https://onlinelibrary.wiley.com/doi/abs/10.1029/2002RG000122, _eprint: https://onlinelibrary.wiley.com/doi/pdf/10.1029/2002RG000122, 2005.

Ditlevsen, P. and Ditlevsen, S.: Warning of a forthcoming collapse of the Atlantic meridional overturning circulation, Nature Communications, 14, 4254, doi:10.1038/s41467-023-39810-w, URL https://www.nature.com/articles/s41467-023-39810-w, number: 1 Publisher: Nature Publishing Group, 2023.

Dokken, T. M., Nisancioglu, K. H., Li, C., Battisti, D. S., and Kissel, C.: Dansgaard-Oeschger cycles: Interactions between ocean and sea ice intrinsic to the Nordic seas, Paleoceanography, 28, 491–502, doi:10.1002/palo.20042, URL https://agupubs.onlinelibrary.wiley.com/doi/abs/10.1002/palo.20042, 2013.

Drijfhout, S., Bathiany, S., Beaulieu, C., Brovkin, V., Claussen, M., Huntingford, C., Scheffer, M., Sgubin, G., and Swingedouw, D.: Catalogue of abrupt shifts in Intergovernmental Panel on Climate Change climate models, Proceedings of the National Academy of Sciences, 112, E5777–E5786, doi:10.1073/pnas.1511451112, URL https://www.pnas.org/doi/10.1073/pnas.1511451112, high - Read (05/09/2023), 2015.

Drijfhout, S. S., Weber, S. L., and van der Swaluw, E.: The stability of the MOC as diagnosed from model projections for pre-industrial, present and future climates, Climate

Dynamics, 37, 1575–1586, doi:10.1007/s00382-010-0930-z, URL https://doi.org/10.1007/s00382-010-0930-z, classic, 2011.

Du, J., Haley, B. A., and Mix, A. C.: Evolution of the Global Overturning Circulation since the Last Glacial Maximum based on marine authigenic neodymium isotopes, Quaternary Science Reviews, 241, 106 396, doi:10.1016/j.quascirev.2020.106396, URL https://www.sciencedirect.com/science/article/pii/S0277379120303589, 2020.

Dyke, A.: An outline of North American deglaciation with emphasis on central and northern Canada, Developments in Quaternary Sciences, 2, 373–424, doi:10.1016/S1571-0866(04)80209-4, URL https://www.sciencedirect.com/science/article/pii/S1571086604802094, publisher: Elsevier, 2004.

Dyke, A. S., Andrews, J. T., Clark, P. U., England, J. H., Miller, G. H., Shaw, J., and Veillette, J. J.: The Laurentide and Innuitian ice sheets during the Last Glacial Maximum, Quaternary Science Reviews, 21, 9–31, doi:10.1016/S0277-3791(01)00095-6, URL http://www.sciencedirect.com/science/article/pii/S0277379101000956, 2002.

Eddy, J. A.: The Maunder Minimum, Science, 192, 1189–1202, doi:10.1126/science.192.4245.1189, URL https://www.science.org/doi/10.1126/science.192.4245.1189, publisher: American Association for the Advancement of Science, 1976.

Ehrmann, W. U., Grobe, H., and Fütterer, D.: Late Miocene to Holocene glacial history of East Antarctica revealed by sediments from Sites 745 and 746, doi:/doi.org/10.2973/odp.proc.sr.119.208.1991⟩, URL http://dx.doi.org/10.2973/odp.proc.sr.119.208.1991, 1991.

Eldevik, T., Risebrobakken, B., Bjune, A. E., Andersson, C., Birks, H. J. B., Dokken, T. M., Drange, H., Glessmer, M. S., Li, C., Nilsen, J. E. Ø., Otterå, O. H., Richter, K., and Skagseth, Ø.: A brief history of climate – the northern seas from the Last Glacial Maximum to global warming, Quaternary Science Reviews, 106, 225–246, doi:10.1016/j.quascirev.2014.06.028, URL https://www.sciencedirect.com/science/article/pii/S0277379114002650, 2014.

Erhardt, T., Capron, E., Rasmussen, S. O., Schüpbach, S., Bigler, M., Adolphi, F., and Fischer, H.: Decadal-scale progression of the onset of Dansgaard–Oeschger warming events, Climate of the Past, 15, 811–825, doi:10.5194/cp-15-811-2019, URL https://cp.copernicus.org/articles/15/811/2019/, publisher: Copernicus GmbH, 2019.

Ferreira, D., Cessi, P., Coxall, H. K., de Boer, A., Dijkstra, H. A., Drijfhout, S. S., Eldevik, T., Harnik, N., McManus, J. F., Marshall, D. P., Nilsson, J., Roquet, F., Schneider, T., and Wills, R. C.: Atlantic-Pacific Asymmetry in Deep Water Formation, Annual Review of Earth and Planetary Sciences, 46, 327–352, doi:10.1146/annurev-earth-082517-010045, URL https://doi.org/10.1146/annurev-earth-082517-010045, 2018.

FitzHugh, R.: Mathematical models of threshold phenomena in the nerve membrane, The bulletin of mathematical biophysics, 17, 257–278, doi:10.1007/BF02477753, URL https://doi.org/10.1007/BF02477753, 1955.

Fletcher, W. J., Sánchez Goñi, M. F., Allen, J. R. M., Cheddadi, R., Combourieu-Nebout, N., Huntley, B., Lawson, I., Londeix, L., Magri, D., Margari, V., Müller, U. C., Naughton, F., Novenko, E., Roucoux, K., and Tzedakis, P. C.: Millennial-scale variability during the last glacial in vegetation records from Europe, Quaternary Science Reviews, 29, 2839–2864, doi:10.1016/j.quascirev.2009.11.015, URL https://www.sciencedirect.com/science/article/pii/S0277379109003886, 2010.

Fofonoff, N. P.: Physical properties of seawater: A new salinity scale and equation of state for seawater, Journal of Geophysical Research: Oceans, 90, 3332–3342, doi:10.1029/JC090iC02p03332, URL https://agupubs.onlinelibrary.wiley.com/doi/abs/10.1029/JC090iC02p03332, 1985.

Fofonoff, N. P. and Millard Jr, R. C.: Algorithms for the computation of fundamental properties of seawater., UNESCO Technical Papers in Marine Sciences, doi:10.25607/OBP-1450, URL https://repository.oceanbestpractices.org/handle/11329/109, 1983.

Frajka-Williams, E., Ansorge, I. J., Baehr, J., Bryden, H. L., Chidichimo, M. P., Cunningham, S. A., Danabasoglu, G., Dong, S., Donohue, K. A., Elipot, S., Heimbach, P., Holliday, N. P., Hummels, R., Jackson, L. C., Karstensen, J., Lankhorst, M., Le Bras, I. A., Lozier, M. S., McDonagh, E. L., Meinen, C. S., Mercier, H., Moat, B. I., Perez, R. C., Piecuch, C. G., Rhein, M., Srokosz, M. A., Trenberth, K. E., Bacon, S., Forget, G., Goni, G., Kieke, D., Koelling, J., Lamont, T., McCarthy, G. D., Mertens, C., Send, U., Smeed, D. A., Speich, S., van den Berg, M., Volkov, D., and Wilson, C.: Atlantic Meridional Overturning Circulation: Observed Transport and Variability, Frontiers in Marine Science, 6, URL https://www.frontiersin.org/articles/10.3389/fmars.2019.00260, 2019.

Frank, M.: Radiogenic Isotopes: Tracers of Past Ocean Circulation and Erosional Input, Reviews of Geophysics, 40, 1–1–1–38, doi:10.1029/2000RG000094, URL https://onlinelibrary.wiley.com/doi/abs/10.1029/2000RG000094, 2002.

Gandy, N., Astfalck, L. C., Gregoire, L. J., Ivanovic, R. F., Patterson, V. L., Sherriff-Tadano, S., Smith, R. S., Williamson, D., and Rigby, R.: De-Tuning Albedo Parameters in a Coupled Climate Ice Sheet Model to Simulate the North American Ice Sheet at the Last Glacial Maximum, Journal of Geophysical Research: Earth Surface, 128, e2023JF007 250, doi:10.1029/2023JF007250, URL https://onlinelibrary.wiley.com/doi/abs/10.1029/2023JF007250, 2023.

Ganopolski, A. and Rahmstorf, S.: Rapid changes of glacial climate simulated in a

coupled climate model, Nature, 409, 153–158, doi:10.1038/35051500, URL https://www.nature.com/articles/35051500, 2001.

Ganopolski, A. and Rahmstorf, S.: Abrupt Glacial Climate Changes due to Stochastic Resonance, Physical review letters, 88, 038 501, doi:10.1103/PhysRevLett.88.038501, 2002.

Gebbie, G.: How much did Glacial North Atlantic Water shoal?, Paleoceanography, 29, 190–209, doi:10.1002/2013PA002557, URL https://agupubs.onlinelibrary.wiley.com/doi/abs/10.1002/2013PA002557, 2014.

Gebbie, G., Simms, A. R., and Lisiecki, L. E.: Why estimates of deglacial ice loss should be biased low, Earth and Planetary Science Letters, 515, 112–124, doi:10.1016/j.epsl.2019.03.017, URL https://www.sciencedirect.com/science/article/pii/S0012821X19301657, 2019.

Gent, P. R. and McWilliams, J. C.: Isopycnal Mixing in Ocean Circulation Models, Journal of Physical Oceanography, 20, 150–155, doi:10.1175/1520-0485(1990)020⟨0150:IMIOCM⟩2.0.CO;2, URL https://journals.ametsoc.org/view/journals/phoc/20/1/1520-0485_1990_020_0150_imiocm_2_0_co_2.xml, high - Read, 1990.

Gong, X., Liu, H., Wang, F., and Heuzé, C.: Of Atlantic Meridional Overturning Circulation in the CMIP6 Project, Deep Sea Research Part II: Topical Studies in Oceanography, 206, 105 193, doi:10.1016/j.dsr2.2022.105193, URL https://www.sciencedirect.com/science/article/pii/S0967064522001783, high - To Read, 2022.

González, C. and Dupont, L. M.: Tropical salt marsh succession as sea-level indicator during Heinrich events, Quaternary Science Reviews, 28, 939–946, doi:10.1016/j.quascirev.2008.12.023, URL http://www.sciencedirect.com/science/article/pii/S0277379108003582, 2009.

Gordon, C., Cooper, C., Senior, C. A., Banks, H., Gregory, J. M., Johns, T. C., Mitchell, J. F. B., and Wood, R. A.: The simulation of SST, sea ice extents and ocean heat transports in a version of the Hadley Centre coupled model without flux adjustments, Climate Dynamics, 16, 147–168, doi:10.1007/s003820050010, URL https://doi.org/10.1007/s003820050010, 2000.

Gowan, E. J., Zhang, X., Khosravi, S., Rovere, A., Stocchi, P., Hughes, A. L. C., Gyllencreutz, R., Mangerud, J., Svendsen, J.-I., and Lohmann, G.: A new global ice sheet reconstruction for the past 80 000 years, Nature Communications, 12, 1199, doi:10.1038/s41467-021-21469-w, URL https://www.nature.com/articles/s41467-021-21469-w, number: 1 Publisher: Nature Publishing Group, 2021.

Gregoire, L. J., Payne, A. J., and Valdes, P. J.: Deglacial rapid sea level rises caused by ice-sheet saddle collapses, Nature, 487, 219–222, doi:10.1038/nature11257, URL https://

www.nature.com/articles/nature11257, number: 7406 Publisher: Nature Publishing Group, 2012.

Gregoire, L. J., Valdes, P. J., and Payne, A. J.: The relative contribution of orbital forcing and greenhouse gases to the North American deglaciation, Geophysical Research Letters, 42, 9970–9979, doi:10.1002/2015GL066005, URL https://agupubs.onlinelibrary.wiley.com/doi/abs/10.1002/2015GL066005, 2015.

Gregoire, L. J., Otto-Bliesner, B., Valdes, P. J., and Ivanovic, R.: Abrupt Bølling warming and ice saddle collapse contributions to the Meltwater Pulse 1a rapid sea level rise, Geophysical Research Letters, 43, 9130–9137, doi:10.1002/2016GL070356, URL https://onlinelibrary.wiley.com/doi/abs/10.1002/2016GL070356, 2016.

Gregoire, L. J., Ivanovic, R. F., Maycock, A. C., Valdes, P. J., and Stevenson, S.: Holocene lowering of the Laurentide ice sheet affects North Atlantic gyre circulation and climate, Climate Dynamics, 51, 3797–3813, doi:10.1007/s00382-018-4111-9, URL https://doi.org/10.1007/s00382-018-4111-9, 2018.

Gregory, J. M., Saenko, O. A., and Weaver, A. J.: The role of the Atlantic freshwater balance in the hysteresis of the meridional overturning circulation, Climate Dynamics, 21, 707–717, doi:10.1007/s00382-003-0359-8, URL https://doi.org/10.1007/s00382-003-0359-8, 2003.

Grootes, P. M.: Interpreting Continental Oxygen Isotope Records, in: Climate Change in Continental Isotopic Records, pp. 37–46, American Geophysical Union (AGU), doi:10.1029/GM078p0037, URL https://onlinelibrary.wiley.com/doi/abs/10.1029/GM078p0037, 1993.

Grousset, F. E., Labeyrie, L., Sinko, J. A., Cremer, M., Bond, G., Duprat, J., Cortijo, E., and Huon, S.: Patterns of Ice-Rafted Detritus in the Glacial North Atlantic (40–55°N), Paleoceanography, 8, 175–192, doi:10.1029/92PA02923, URL https://agupubs.onlinelibrary.wiley.com/doi/abs/10.1029/92PA02923, 1993.

Guo, C., Nisancioglu, K. H., Bentsen, M., Bethke, I., and Zhang, Z.: Equilibrium simulations of Marine Isotope Stage 3 climate, Climate of the Past, 15, 1133–1151, doi:https://doi.org/10.5194/cp-15-1133-2019, URL https://www.clim-past.net/15/1133/2019/, publisher: Copernicus GmbH, 2019.

Gwiazda, R. H., Hemming, S. R., and Broecker, W. S.: Provenance of icebergs during Heinrich Event 3 and the contrast to their sources during other Heinrich episodes, Paleoceanography, 11, 371–378, doi:10.1029/96PA01022, URL https://agupubs.onlinelibrary.wiley.com/doi/abs/10.1029/96PA01022, 1996.

Gyllencreutz, R., Mangerud, J., Svendsen, J., and Lohne, Ø.: DATED – a dating Database

and GIS-based Reconstruction of the Eurasian Deglaciation, Geological Survey of Finland Special Paper., 46, 113–120, 2007.

Hall, I. R., Moran, S. B., Zahn, R., Knutz, P. C., Shen, C.-C., and Edwards, R. L.: Accelerated drawdown of meridional overturning in the late-glacial Atlantic triggered by transient pre-H event freshwater perturbation, Geophysical Research Letters, 33, doi:10.1029/2006GL026239, URL https://agupubs.onlinelibrary.wiley.com/doi/abs/10.1029/2006GL026239, 2006.

Hassan, F. A.: Historical Nile Floods and Their Implications for Climatic Change, Science, 212, 1142–1145, doi:10.1126/science.212.4499.1142, URL https://www.science.org/doi/10.1126/science.212.4499.1142, 1981.

Hays, J. D., Imbrie, J., and Shackleton, N. J.: Variations in the Earth's Orbit: Pacemaker of the Ice Ages, Science, 194, 1121–1132, doi:10.1126/science.194.4270.1121, URL https://science.sciencemag.org/content/194/4270/1121, publisher: American Association for the Advancement of Science Section: Articles, 1976.

Haywood, A. M., Dowsett, H. J., Dolan, A. M., Rowley, D., Abe-Ouchi, A., Otto-Bliesner, B., Chandler, M. A., Hunter, S. J., Lunt, D. J., Pound, M., and Salzmann, U.: The Pliocene Model Intercomparison Project (PlioMIP) Phase 2: scientific objectives and experimental design, Climate of the Past, 12, 663–675, doi:10.5194/cp-12-663-2016, URL https://cp.copernicus.org/articles/12/663/2016/, publisher: Copernicus GmbH, 2016.

He, C., Liu, Z., Otto-Bliesner, B. L., Brady, E., Zhu, C., Tomas, R., Clark, P., Zhu, J., Jahn, A., Gu, S., Zhang, J., Nusbaumer, J., Noone, D., Cheng, H., Wang, Y., Yan, M., and Bao, Y.: Hydroclimate footprint of pan-Asian monsoon water isotope during the last deglaciation, Science Advances, 7, eabe2611, doi:10.1126/sciadv.abe2611, URL https://www.science.org/doi/10.1126/sciadv.abe2611, publisher: American Association for the Advancement of Science, 2021.

Heinrich, H.: Origin and consequences of cyclic ice rafting in the Northeast Atlantic Ocean during the past 130,000 years, Quaternary Research, 29, 142–152, doi:10.1016/0033-5894(88)90057-9, URL http://www.sciencedirect.com/science/article/pii/0033589488900579, 1988.

Hemming, S. R.: Heinrich events: Massive late Pleistocene detritus layers of the North Atlantic and their global climate imprint, Reviews of Geophysics, 42, doi:10.1029/2003RG000128, URL https://agupubs.onlinelibrary.wiley.com/doi/full/10.1029/2003RG000128, 2004.

Henry, L. G., McManus, J. F., Curry, W. B., Roberts, N. L., Piotrowski, A. M., and Keigwin, L. D.: North Atlantic ocean circulation and abrupt climate change during the last glaciation, Science, 353, 470–474, doi:10.1126/science.aaf5529, URL https://

science.sciencemag.org/content/353/6298/470, publisher: American Association for the Advancement of Science Section: Report, 2016.

Hernández, A., Martin-Puertas, C., Moffa-Sánchez, P., Moreno-Chamarro, E., Ortega, P., Blockley, S., Cobb, K. M., Comas-Bru, L., Giralt, S., Goosse, H., Luterbacher, J., Martrat, B., Muscheler, R., Parnell, A., Pla-Rabes, S., Sjolte, J., Scaife, A. A., Swingedouw, D., Wise, E., and Xu, G.: Modes of climate variability: Synthesis and review of proxy-based reconstructions through the Holocene, Earth-Science Reviews, 209, 103 286, doi:10.1016/j.earscirev.2020.103286, URL https://www.sciencedirect.com/science/article/pii/S0012825220303329, 2020.

Hodell, D. A., Nicholl, J. A., Bontognali, T. R. R., Danino, S., Dorador, J., Dowdeswell, J. A., Einsle, J., Kuhlmann, H., Martrat, B., Mleneck-Vautravers, M. J., Rodríguez-Tovar, F. J., and Röhl, U.: Anatomy of Heinrich Layer 1 and its role in the last deglaciation, Paleoceanography, 32, 284–303, doi:10.1002/2016PA003028, URL https://agupubs.onlinelibrary.wiley.com/doi/abs/10.1002/2016PA003028, 2017.

Hofmann, M. and Rahmstorf, S.: On the stability of the Atlantic meridional overturning circulation, Proceedings of the National Academy of Sciences, 106, 20 584–20 589, doi:10.1073/pnas.0909146106, URL https://www.pnas.org/doi/full/10.1073/pnas.0909146106, middle, 2009.

Howe, J. N. W., Piotrowski, A. M., Noble, T. L., Mulitza, S., Chiessi, C. M., and Bayon, G.: North Atlantic Deep Water Production during the Last Glacial Maximum, Nature Communications, 7, 11 765, doi:10.1038/ncomms11765, URL https://www.nature.com/articles/ncomms11765, number: 1 Publisher: Nature Publishing Group, 2016.

Huber, C., Leuenberger, M., Spahni, R., Flückiger, J., Schwander, J., Stocker, T. F., Johnsen, S., Landais, A., and Jouzel, J.: Isotope calibrated Greenland temperature record over Marine Isotope Stage 3 and its relation to CH4, Earth and Planetary Science Letters, 243, 504–519, doi:10.1016/j.epsl.2006.01.002, URL http://www.sciencedirect.com/science/article/pii/S0012821X06000392, 2006.

Hughes, A. L. C., Gyllencreutz, R., Lohne, Ø. S., Mangerud, J., and Svendsen, J. I.: The last Eurasian ice sheets – a chronological database and time-slice reconstruction, DATED-1, Boreas, 45, 1–45, doi:10.1111/bor.12142, URL https://onlinelibrary.wiley.com/doi/abs/10.1111/bor.12142, 2016.

Huisman, S. E., Toom, M. d., Dijkstra, H. A., and Drijfhout, S.: An Indicator of the Multiple Equilibria Regime of the Atlantic Meridional Overturning Circulation, Journal of Physical Oceanography, 40, 551–567, doi:10.1175/2009JPO4215.1, URL https://journals.ametsoc.org/view/journals/phoc/40/3/2009jpo4215.

1.xml, publisher: American Meteorological Society Section: Journal of Physical Oceanography, 2010.

Hulbe, C. L., MacAyeal, D. R., Denton, G. H., Kleman, J., and Lowell, T. V.: Catastrophic ice shelf breakup as the source of Heinrich event icebergs, Paleoceanography, 19, doi:10.1029/2003PA000890, URL https://agupubs.onlinelibrary.wiley.com/doi/abs/10.1029/2003PA000890, 2004.

Hébert, R., Herzschuh, U., and Laepple, T.: Millennial-scale climate variability over land overprinted by ocean temperature fluctuations, Nature Geoscience, 15, 899–905, doi:10.1038/s41561-022-01056-4, URL https://www.nature.com/articles/s41561-022-01056-4, number: 11 Publisher: Nature Publishing Group, 2022.

Inglis, G. N., Bragg, F., Burls, N. J., Cramwinckel, M. J., Evans, D., Foster, G. L., Huber, M., Lunt, D. J., Siler, N., Steinig, S., Tierney, J. E., Wilkinson, R., Anagnostou, E., de Boer, A. M., Dunkley Jones, T., Edgar, K. M., Hollis, C. J., Hutchinson, D. K., and Pancost, R. D.: Global mean surface temperature and climate sensitivity of the early Eocene Climatic Optimum (EECO), Paleocene–Eocene Thermal Maximum (PETM), and latest Paleocene, Climate of the Past, 16, 1953–1968, doi:10.5194/cp-16-1953-2020, URL https://cp.copernicus.org/articles/16/1953/2020/, publisher: Copernicus GmbH, 2020.

IPCC: Evaluation of Climate Models, in: Climate Change 2013 – The Physical Science Basis: Working Group I Contribution to the Fifth Assessment Report of the Intergovernmental Panel on Climate Change, edited by Intergovernmental Panel on Climate Change, pp. 741–866, Cambridge University Press, Cambridge, doi:10.1017/CBO9781107415324.020, URL https://www.cambridge.org/core/books/climate-change-2013-the-physical-science-basis/evaluation-of-climate-models/94BC2268C864F2C6A18436DB22BD1E5A, 2014.

IPCC: Annex IV: Modes of Variability, p. 2153–2192, Cambridge University Press, 2023a.

IPCC: Changing State of the Climate System, p. 287–422, Cambridge University Press, 2023b.

Isachsen, P. E., Mauritzen, C., and Svendsen, H.: Dense water formation in the Nordic Seas diagnosed from sea surface buoyancy fluxes, Deep Sea Research Part I: Oceanographic Research Papers, 54, 22–41, doi:10.1016/j.dsr.2006.09.008, URL https://www.sciencedirect.com/science/article/pii/S0967063706002573, 2007.

Ivanovic, R. F., Valdes, P. J., Gregoire, L., Flecker, R., and Gutjahr, M.: Sensitivity of modern climate to the presence, strength and salinity of Mediterranean-Atlantic exchange in a global general circulation model, Climate Dynamics, 42, 859–877, doi:10.1007/s00382-013-1680-5, URL https://doi.org/10.1007/s00382-013-1680-5, 2014.

Ivanovic, R. F., Gregoire, L. J., Kageyama, M., Roche, D. M., Valdes, P. J., Burke, A., Drummond, R., Peltier, W. R., and Tarasov, L.: Transient climate simulations of the deglaciation 21–9 thousand years before present (version 1) – PMIP4 Core experiment design and boundary conditions, Geoscientific Model Development, 9, 2563–2587, doi:https://doi.org/10.5194/gmd-9-2563-2016, URL https://www.geosci-model-dev.net/9/2563/2016/, 2016.

Ivanovic, R. F., Gregoire, L. J., Wickert, A. D., Valdes, P. J., and Burke, A.: Collapse of the North American ice saddle 14,500 years ago caused widespread cooling and reduced ocean overturning circulation, Geophysical Research Letters, 44, 383–392, doi:10.1002/2016GL071849, URL https://agupubs.onlinelibrary.wiley.com/doi/abs/10.1002/2016GL071849, 2017.

Ivanovic, R. F., Gregoire, L. J., Burke, A., Wickert, A. D., Valdes, P. J., Ng, H. C., Robinson, L. F., McManus, J. F., Mitrovica, J. X., Lee, L., and Dentith, J. E.: Acceleration of Northern Ice Sheet Melt Induces AMOC Slowdown and Northern Cooling in Simulations of the Early Last Deglaciation, Paleoceanography and Paleoclimatology, 33, 807–824, doi:10.1029/2017PA003308, URL https://agupubs.onlinelibrary.wiley.com/doi/abs/10.1029/2017PA003308, 2018a.

Ivanovic, R. F., Gregoire, L. J., Wickert, A. D., and Burke, A.: Climatic Effect of Antarctic Meltwater Overwhelmed by Concurrent Northern Hemispheric Melt, Geophysical Research Letters, 45, 5681–5689, doi:https://doi.org/10.1029/2018GL077623, URL https://agupubs.onlinelibrary.wiley.com/doi/abs/10.1029/2018GL077623, 2018b.

Izumi, K., Valdes, P., Ivanovic, R., and Gregoire, L.: Impacts of the PMIP4 ice sheets on Northern Hemisphere climate during the last glacial period, Climate Dynamics, 60, 2481–2499, doi:10.1007/s00382-022-06456-1, URL https://doi.org/10.1007/s00382-022-06456-1, 2023.

Jackson, L. C. and Petit, T.: North Atlantic overturning and water mass transformation in CMIP6 models, Climate Dynamics, doi:10.1007/s00382-022-06448-1, URL https://doi.org/10.1007/s00382-022-06448-1, 2022.

Jackson, L. C., Biastoch, A., Buckley, M. W., Desbruyères, D. G., Frajka-Williams, E., Moat, B., and Robson, J.: The evolution of the North Atlantic Meridional Overturning Circulation since 1980, Nature Reviews Earth & Environment, 3, 241–254, doi:10.1038/s43017-022-00263-2, URL https://www.nature.com/articles/s43017-022-00263-2, 2022.

Jeandel, C., Arsouze, T., Lacan, F., Téchiné, P., and Dutay, J. C.: Isotopic Nd compositions and concentrations of the lithogenic inputs into the ocean: A compilation, with an emphasis on the margins, Chemical Geology, 239, 156–164,

doi:10.1016/j.chemgeo.2006.11.013, URL https://www.sciencedirect.com/science/article/pii/S0009254106005158, 2007.

Jeffreys, H.: On fluid motions produced by differences of temperature and humidity, Quarterly Journal of the Royal Meteorological Society, 51, 347–356, doi:10.1002/qj.49705121604, URL https://onlinelibrary.wiley.com/doi/abs/10.1002/qj.49705121604, 1925.

Jiang, W., Gastineau, G., and Codron, F.: Multicentennial Variability Driven by Salinity Exchanges Between the Atlantic and the Arctic Ocean in a Coupled Climate Model, Journal of Advances in Modeling Earth Systems, 13, e2020MS002 366, doi:10.1029/2020MS002366, URL https://onlinelibrary.wiley.com/doi/abs/10.1029/2020MS002366, 2021.

Jouzel, J.: Calibrating the Isotopic Paleothermometer, Science, 286, 910–911, doi:10.1126/science.286.5441.910, URL https://www.science.org/doi/10.1126/science.286.5441.910, 1999.

Jouzel, J., Vaikmae, R., Petit, J. R., Martin, M., Duclos, Y., Stievenard, M., Lorius, C., Toots, M., Mélières, M. A., Burckle, L. H., Barkov, N. I., and Kotlyakov, V. M.: The two-step shape and timing of the last deglaciation in Antarctica, Climate Dynamics, 11, 151–161, doi:10.1007/BF00223498, URL https://doi.org/10.1007/BF00223498, 1995.

Jouzel, J., Masson-Delmotte, V., Cattani, O., Dreyfus, G., Falourd, S., Hoffmann, G., Minster, B., Nouet, J., Barnola, J. M., Chappellaz, J., Fischer, H., Gallet, J. C., Johnsen, S., Leuenberger, M., Loulergue, L., Luethi, D., Oerter, H., Parrenin, F., Raisbeck, G., Raynaud, D., Schilt, A., Schwander, J., Selmo, E., Souchez, R., Spahni, R., Stauffer, B., Steffensen, J. P., Stenni, B., Stocker, T. F., Tison, J. L., Werner, M., and Wolff, E. W.: Orbital and Millennial Antarctic Climate Variability over the Past 800,000 Years, Science, 317, 793–796, doi:10.1126/science.1141038, URL https://www.science.org/doi/10.1126/science.1141038, abstract - Useful for last 800.000 years plots, 2007.

Jungclaus, J. H., Fischer, N., Haak, H., Lohmann, K., Marotzke, J., Matei, D., Mikolajewicz, U., Notz, D., and von Storch, J. S.: Characteristics of the ocean simulations in the Max Planck Institute Ocean Model (MPIOM) the ocean component of the MPI-Earth system model, Journal of Advances in Modeling Earth Systems, 5, 422–446, doi:10.1002/jame.20023, URL https://onlinelibrary.wiley.com/doi/abs/10.1002/jame.20023, 2013.

Kageyama, M., Paul, A., Roche, D. M., and Van Meerbeeck, C. J.: Modelling glacial climatic millennial-scale variability related to changes in the Atlantic meridional overturning circulation: a review, Quaternary Science Reviews, 29, 2931–2956,

doi:10.1016/j.quascirev.2010.05.029, URL http://www.sciencedirect.com/science/article/pii/S0277379110001745, 2010.

Kageyama, M., Braconnot, P., Bopp, L., Caubel, A., Foujols, M.-A., Guilyardi, E., Khodri, M., Lloyd, J., Lombard, F., Mariotti, V., Marti, O., Roy, T., and Woillez, M.-N.: Mid-Holocene and Last Glacial Maximum climate simulations with the IPSL model—part I: comparing IPSL_CM5A to IPSL_CM4, Climate Dynamics, 40, 2447–2468, doi:10.1007/s00382-012-1488-8, URL https://doi.org/10.1007/s00382-012-1488-8, 2013a.

Kageyama, M., Merkel, U., Otto-Bliesner, B., Prange, M., Abe-Ouchi, A., Lohmann, G., Ohgaito, R., Roche, D. M., Singarayer, J., Swingedouw, D., and Zhang, X.: Climatic impacts of fresh water hosing under Last Glacial Maximum conditions: a multi-model study, Climate of the Past, 9, 935–953, doi:10.5194/cp-9-935-2013, URL https://cp.copernicus.org/articles/9/935/2013/, 2013b.

Kageyama, M., Albani, S., Braconnot, P., Harrison, S. P., Hopcroft, P. O., Ivanovic, R. F., Lambert, F., Marti, O., Peltier, W. R., Peterschmitt, J.-Y., Roche, D. M., Tarasov, L., Zhang, X., Brady, E. C., Haywood, A. M., LeGrande, A. N., Lunt, D. J., Mahowald, N. M., Mikolajewicz, U., Nisancioglu, K. H., Otto-Bliesner, B. L., Renssen, H., Tomas, R. A., Zhang, Q., Abe-Ouchi, A., Bartlein, P. J., Cao, J., Li, Q., Lohmann, G., Ohgaito, R., Shi, X., Volodin, E., Yoshida, K., Zhang, X., and Zheng, W.: The PMIP4 contribution to CMIP6 – Part 4: Scientific objectives and experimental design of the PMIP4-CMIP6 Last Glacial Maximum experiments and PMIP4 sensitivity experiments, Geoscientific Model Development, 10, 4035–4055, doi:https://doi.org/10.5194/gmd-10-4035-2017, URL https://www.geosci-model-dev.net/10/4035/2017/, 2017.

Kageyama, M., Harrison, S. P., Kapsch, M.-L., Lofverstrom, M., Lora, J. M., Mikolajewicz, U., Sherriff-Tadano, S., Vadsaria, T., Abe-Ouchi, A., Bouttes, N., Chandan, D., Gregoire, L. J., Ivanovic, R. F., Izumi, K., LeGrande, A. N., Lhardy, F., Lohmann, G., Morozova, P. A., Ohgaito, R., Paul, A., Peltier, W. R., Poulsen, C. J., Quiquet, A., Roche, D. M., Shi, X., Tierney, J. E., Valdes, P. J., Volodin, E., and Zhu, J.: The PMIP4 Last Glacial Maximum experiments: preliminary results and comparison with the PMIP3 simulations, Climate of the Past, 17, 1065–1089, doi:10.5194/cp-17-1065-2021, URL https://cp.copernicus.org/articles/17/1065/2021/, publisher: Copernicus GmbH, 2021.

Kapsch, M.-L., Mikolajewicz, U., Ziemen, F., and Schannwell, C.: Ocean response in transient simulations of the last deglaciation dominated by underlying ice-sheet reconstruction and method of meltwater distribution, Geophysical Research Letters, n/a, e2021GL096 767, doi:10.1029/2021GL096767, URL https://onlinelibrary.wiley.com/doi/abs/10.1029/2021GL096767, 2022.

Kessler, A., Bouttes, N., Roche, D. M., Ninnemann, U. S., and Tjiputra, J.: Dynamics of Spontaneous (Multi) Centennial-Scale Variations of the Atlantic Meridional Overturning Circulation Strength During the Last Interglacial, Paleoceanography and Paleoclimatology, 35, e2020PA003 913, doi:https://doi.org/10.1029/2020PA003913, URL https://agupubs.onlinelibrary.wiley.com/doi/abs/10.1029/2020PA003913, 2020.

Khider, D., Jackson, C., and Stott, L.: Assessing millennial-scale variability during the Holocene: A perspective from the western tropical Pacific, Paleoceanography, 29, 143–159, doi:10.1002/2013PA002534, URL https://onlinelibrary.wiley.com/doi/abs/10.1002/2013PA002534, _eprint: https://onlinelibrary.wiley.com/doi/pdf/10.1002/2013PA002534, 2014.

Kilbourne, K. H., Wanamaker, A. D., Moffa-Sanchez, P., Reynolds, D. J., Amrhein, D. E., Butler, P. G., Gebbie, G., Goes, M., Jansen, M. F., Little, C. M., Mette, M., Moreno-Chamarro, E., Ortega, P., Otto-Bliesner, B. L., Rossby, T., Scourse, J., and Whitney, N. M.: Atlantic circulation change still uncertain, Nature Geoscience, 15, 165–167, doi:10.1038/s41561-022-00896-4, URL https://www.nature.com/articles/s41561-022-00896-4, high - abstract, 2022.

Kindler, P., Guillevic, M., Baumgartner, M., Schwander, J., Landais, A., and Leuenberger, M.: Temperature reconstruction from 10 to 120 kyr b2k from the NGRIP ice core, Climate of the Past, 10, 887–902, doi:https://doi.org/10.5194/cp-10-887-2014, URL https://cp.copernicus.org/articles/10/887/2014/cp-10-887-2014.html, publisher: Copernicus GmbH, 2014.

Kleppin, H., Jochum, M., Otto-Bliesner, B., Shields, C. A., and Yeager, S.: Stochastic Atmospheric Forcing as a Cause of Greenland Climate Transitions, Journal of Climate, 28, 7741–7763, doi:10.1175/JCLI-D-14-00728.1, URL https://journals.ametsoc.org/view/journals/clim/28/19/jcli-d-14-00728.1.xml, high - Abstract, 2015.

Klockmann, M., Mikolajewicz, U., and Marotzke, J.: The effect of greenhouse gas concentrations and ice sheets on the glacial AMOC in a coupled climate model, Climate of the Past, 12, 1829–1846, doi:10.5194/cp-12-1829-2016, URL https://cp.copernicus.org/articles/12/1829/2016/, publisher: Copernicus GmbH, 2016.

Klockmann, M., Mikolajewicz, U., and Marotzke, J.: Two AMOC States in Response to Decreasing Greenhouse Gas Concentrations in the Coupled Climate Model MPI-ESM, Journal of Climate, 31, 7969–7984, doi:10.1175/JCLI-D-17-0859.1, URL https://journals.ametsoc.org/doi/full/10.1175/JCLI-D-17-0859.1, 2018.

Klockmann, M., Mikolajewicz, U., Kleppin, H., and Marotzke, J.: Coupling of the Subpolar Gyre and the Overturning Circulation During Abrupt Glacial Climate Transitions, Geophysical Research Letters, 47, e2020GL090 361, doi:https://doi.org/10.

1029/2020GL090361, URL https://agupubs.onlinelibrary.wiley.com/doi/abs/10.1029/2020GL090361, 2020.

Knorr, G. and Lohmann, G.: Southern Ocean origin for the resumption of Atlantic thermohaline circulation during deglaciation, Nature, 424, 532–536, doi:10.1038/nature01855, URL https://www.nature.com/articles/nature01855, 2003.

Kucera, M., Weinelt, M., Kiefer, T., Pflaumann, U., Hayes, A., Weinelt, M., Chen, M.-T., Mix, A. C., Barrows, T. T., Cortijo, E., Duprat, J., Juggins, S., and Waelbroeck, C.: Reconstruction of sea-surface temperatures from assemblages of planktonic foraminifera: multi-technique approach based on geographically constrained calibration data sets and its application to glacial Atlantic and Pacific Oceans, Quaternary Science Reviews, 24, 951–998, doi:10.1016/j.quascirev.2004.07.014, URL https://www.sciencedirect.com/science/article/pii/S027737910400229X, 2005.

Kuhlbrodt, T., Griesel, A., Montoya, M., Levermann, A., Hofmann, M., and Rahmstorf, S.: On the driving processes of the Atlantic meridional overturning circulation, Reviews of Geophysics, 45, doi:10.1029/2004RG000166, URL https://onlinelibrary.wiley.com/doi/abs/10.1029/2004RG000166, important - Abstract, 2007.

Kuniyoshi, Y., Abe-Ouchi, A., Sherriff-Tadano, S., Chan, W.-L., and Saito, F.: Effect of Climatic Precession on Dansgaard-Oeschger-Like Oscillations, Geophysical Research Letters, 49, e2021GL095 695, doi:10.1029/2021GL095695, URL https://onlinelibrary.wiley.com/doi/abs/10.1029/2021GL095695, important, 2022.

Lambeck, K.: Sea-level change through the last glacial cycle: geophysical, glaciological and palaeogeographic consequences, Comptes Rendus Geoscience, 336, 677–689, doi:10.1016/j.crte.2003.12.017, URL https://www.sciencedirect.com/science/article/pii/S1631071304000896, 2004.

Lambeck, K., Rouby, H., Purcell, A., Sun, Y., and Sambridge, M.: Sea level and global ice volumes from the Last Glacial Maximum to the Holocene, Proceedings of the National Academy of Sciences, 111, 15 296–15 303, doi:10.1073/pnas.1411762111, URL https://www.pnas.org/content/111/43/15296, publisher: National Academy of Sciences Section: Physical Sciences, 2014.

Lambert, F., Tagliabue, A., Shaffer, G., Lamy, F., Winckler, G., Farias, L., Gallardo, L., and De Pol-Holz, R.: Dust fluxes and iron fertilization in Holocene and Last Glacial Maximum climates, Geophysical Research Letters, 42, 6014–6023, doi:10.1002/2015GL064250, URL https://onlinelibrary.wiley.com/doi/abs/10.1002/2015GL064250, 2015.

Larkin, C. S., Ezat, M. M., Roberts, N. L., Bauch, H. A., Spielhagen, R. F., Noormets, R., Polyak, L., Moreton, S. G., Rasmussen, T. L., Sarnthein, M., Tipper, E. T., and Piotrowski, A. M.: Active Nordic Seas deep-water formation during the last

glacial maximum, Nature Geoscience, 15, 925–931, doi:10.1038/s41561-022-01050-w, URL https://www.nature.com/articles/s41561-022-01050-w, number: 11 Publisher: Nature Publishing Group, 2022.

Larsen, G. and Eiríksson, J.: Holocene tephra archives and tephrochronology in Iceland – a brief overview, Jökull, 58, 229–250, doi:10.33799/jokull2008.58.229, URL https://jokull.jorfi.is/articles/jokull2008.58/jokull2008.58.229.pdf, 2008.

Latif, M., Sun, J., Visbeck, M., and Hadi Bordbar, M.: Natural variability has dominated Atlantic Meridional Overturning Circulation since 1900, Nature Climate Change, 12, 455–460, doi:10.1038/s41558-022-01342-4, URL https://www.nature.com/articles/s41558-022-01342-4, medium - abstract, 2022.

Lenton, T. M.: Early warning of climate tipping points, Nature Climate Change, 1, 201–209, doi:10.1038/nclimate1143, URL https://www.nature.com/articles/nclimate1143, number: 4 Publisher: Nature Publishing Group, 2011.

Lenton, T. M., Held, H., Kriegler, E., Hall, J. W., Lucht, W., Rahmstorf, S., and Schellnhuber, H. J.: Tipping elements in the Earth's climate system, Proceedings of the National Academy of Sciences, 105, 1786–1793, doi:10.1073/pnas.0705414105, URL https://www.pnas.org/doi/full/10.1073/pnas.0705414105, middle, 2008.

Lenton, T. M., Rockström, J., Gaffney, O., Rahmstorf, S., Richardson, K., Steffen, W., and Schellnhuber, H. J.: Climate tipping points — too risky to bet against, Nature, 575, 592–595, doi:10.1038/d41586-019-03595-0, URL https://www.nature.com/articles/d41586-019-03595-0, medium - Read (10/08/2023), 2019.

Levine, R. C. and Bigg, G. R.: Sensitivity of the glacial ocean to Heinrich events from different iceberg sources, as modeled by a coupled atmosphere-iceberg-ocean model, Paleoceanography, 23, doi:10.1029/2008PA001613, URL https://agupubs.onlinelibrary.wiley.com/doi/abs/10.1029/2008PA001613, 2008.

Lherminier, P., Mercier, H., Huck, T., Gourcuff, C., Perez, F. F., Morin, P., Sarafanov, A., and Falina, A.: The Atlantic Meridional Overturning Circulation and the subpolar gyre observed at the A25-OVIDE section in June 2002 and 2004, Deep Sea Research Part I: Oceanographic Research Papers, 57, 1374–1391, doi:10.1016/j.dsr.2010.07.009, URL https://www.sciencedirect.com/science/article/pii/S0967063710001615, 2010.

Li, C. and Born, A.: Coupled atmosphere-ice-ocean dynamics in Dansgaard-Oeschger events, Quaternary Science Reviews, 203, 1–20, doi:10.1016/j.quascirev.2018.10.031, URL http://www.sciencedirect.com/science/article/pii/S0277379118305705, 2019.

Li, G., Cheng, L., Zhu, J., Trenberth, K. E., Mann, M. E., and Abraham, J. P.: Increas-

ing ocean stratification over the past half-century, Nature Climate Change, 10, 1116–1123, doi:10.1038/s41558-020-00918-2, URL https://www.nature.com/articles/s41558-020-00918-2, number: 12 Publisher: Nature Publishing Group, 2020.

Lisiecki, L. E. and Raymo, M. E.: A Pliocene-Pleistocene stack of 57 globally distributed benthic $\delta^{18}O$ records, Paleoceanography, 20, doi:10.1029/2004PA001071, URL https://agupubs.onlinelibrary.wiley.com/doi/abs/10.1029/2004PA001071, 2005.

Lisiecki, L. E. and Stern, J. V.: Regional and global benthic $\delta^{18}O$ stacks for the last glacial cycle, Paleoceanography, 31, 1368–1394, doi:10.1002/2016PA003002, URL https://onlinelibrary.wiley.com/doi/abs/10.1002/2016PA003002, 2016.

Liu, W., Xie, S.-P., Liu, Z., and Zhu, J.: Overlooked possibility of a collapsed Atlantic Meridional Overturning Circulation in warming climate, Science Advances, 3, e1601 666, doi:10.1126/sciadv.1601666, URL https://www.science.org/doi/10.1126/sciadv.1601666, high, 2017.

Liu, Z., Otto-Bliesner, B. L., He, F., Brady, E. C., Tomas, R., Clark, P. U., Carlson, A. E., Lynch-Stieglitz, J., Curry, W., Brook, E., Erickson, D., Jacob, R., Kutzbach, J., and Cheng, J.: Transient Simulation of Last Deglaciation with a New Mechanism for Bølling-Allerød Warming, Science, 325, 310–314, doi:10.1126/science.1171041, URL https://science.sciencemag.org/content/325/5938/310, 2009.

Liu, Z., Carlson, A. E., He, F., Brady, E. C., Otto-Bliesner, B. L., Briegleb, B. P., Wehrenberg, M., Clark, P. U., Wu, S., Cheng, J., Zhang, J., Noone, D., and Zhu, J.: Younger Dryas cooling and the Greenland climate response to CO2, Proceedings of the National Academy of Sciences, 109, 11 101–11 104, doi:10.1073/pnas.1202183109, URL https://www.pnas.org/content/109/28/11101, publisher: National Academy of Sciences Section: Physical Sciences, 2012.

Lobelle, D., Beaulieu, C., Livina, V., Sévellec, F., and Frajka-Williams, E.: Detectability of an AMOC Decline in Current and Projected Climate Changes, Geophysical Research Letters, 47, e2020GL089 974, doi:10.1029/2020GL089974, URL https://onlinelibrary.wiley.com/doi/abs/10.1029/2020GL089974, 2020.

Lohmann, J. and Ditlevsen, P. D.: Objective extraction and analysis of statistical features of Dansgaard–Oeschger events, Climate of the Past, 15, 1771–1792, doi:https://doi.org/10.5194/cp-15-1771-2019, URL https://cp.copernicus.org/articles/15/1771/2019/, publisher: Copernicus GmbH, 2019.

Lohmann, J. and Ditlevsen, P. D.: Risk of tipping the overturning circulation due to increasing rates of ice melt, Proceedings of the National Academy of Sciences, 118, e2017989 118, doi:10.1073/pnas.2017989118, URL https://www.pnas.org/doi/full/10.1073/pnas.2017989118, high - To read, 2021.

Loulergue, L., Schilt, A., Spahni, R., Masson-Delmotte, V., Blunier, T., Lemieux, B., Barnola, J.-M., Raynaud, D., Stocker, T. F., and Chappellaz, J.: Orbital and millennial-scale features of atmospheric CH 4 over the past 800,000 years, Nature, 453, 383–386, doi:10.1038/nature06950, URL https://www.nature.com/articles/nature06950, number: 7193 Publisher: Nature Publishing Group, 2008.

Lozier, M. S., Li, F., Bacon, S., Bahr, F., Bower, A. S., Cunningham, S. A., de Jong, M. F., de Steur, L., deYoung, B., Fischer, J., Gary, S. F., Greenan, B. J. W., Holliday, N. P., Houk, A., Houpert, L., Inall, M. E., Johns, W. E., Johnson, H. L., Johnson, C., Karstensen, J., Koman, G., Le Bras, I. A., Lin, X., Mackay, N., Marshall, D. P., Mercier, H., Oltmanns, M., Pickart, R. S., Ramsey, A. L., Rayner, D., Straneo, F., Thierry, V., Torres, D. J., Williams, R. G., Wilson, C., Yang, J., Yashayaev, I., and Zhao, J.: A sea change in our view of overturning in the subpolar North Atlantic, Science, 363, 516–521, doi:10.1126/science.aau6592, URL https://www.science.org/doi/10.1126/science.aau6592, publisher: American Association for the Advancement of Science, 2019.

Lunt, D. J., Dunkley Jones, T., Heinemann, M., Huber, M., LeGrande, A., Winguth, A., Loptson, C., Marotzke, J., Roberts, C. D., Tindall, J., Valdes, P., and Winguth, C.: A model–data comparison for a multi-model ensemble of early Eocene atmosphere–ocean simulations: EoMIP, Climate of the Past, 8, 1717–1736, doi:10.5194/cp-8-1717-2012, URL https://cp.copernicus.org/articles/8/1717/2012/, publisher: Copernicus GmbH, 2012.

Lynch-Stieglitz, J.: 6.16 - Tracers of Past Ocean Circulation, in: Treatise on Geochemistry, edited by Holland, H. D. and Turekian, K. K., pp. 433–451, Pergamon, Oxford, doi:10.1016/B0-08-043751-6/06117-X, URL https://www.sciencedirect.com/science/article/pii/B008043751606117X, 2003.

Lynch-Stieglitz, J.: The Atlantic Meridional Overturning Circulation and Abrupt Climate Change, Annual Review of Marine Science, 9, 83–104, doi:10.1146/annurev-marine-010816-060415, URL https://www.annualreviews.org/doi/10.1146/annurev-marine-010816-060415, publisher: Annual Reviews, 2017.

Lynch-Stieglitz, J., Adkins, J. F., Curry, W. B., Dokken, T., Hall, I. R., Herguera, J. C., Hirschi, J. J.-M., Ivanova, E. V., Kissel, C., Marchal, O., Marchitto, T. M., McCave, I. N., McManus, J. F., Mulitza, S., Ninnemann, U., Peeters, F., Yu, E.-F., and Zahn, R.: Atlantic Meridional Overturning Circulation During the Last Glacial Maximum, Science, URL https://www.science.org/doi/abs/10.1126/science.1137127, publisher: American Association for the Advancement of Science, 2007.

Löfverström, M., Caballero, R., Nilsson, J., and Kleman, J.: Evolution of the large-scale atmospheric circulation in response to changing ice sheets over the last glacial cycle,

Climate of the Past, 10, 1453–1471, doi:10.5194/cp-10-1453-2014, URL https://cp.copernicus.org/articles/10/1453/2014/, publisher: Copernicus GmbH, 2014.

MacAyeal, D. R.: Binge/purge oscillations of the Laurentide Ice Sheet as a cause of the North Atlantic's Heinrich events, Paleoceanography, 8, 775–784, doi:10.1029/93PA02200, URL https://agupubs.onlinelibrary.wiley.com/doi/abs/10.1029/93PA02200, 1993.

Madonna, E., Li, C., Grams, C. M., and Woollings, T.: The link between eddy-driven jet variability and weather regimes in the North Atlantic-European sector, Quarterly Journal of the Royal Meteorological Society, 143, 2960–2972, doi:10.1002/qj.3155, URL https://rmets.onlinelibrary.wiley.com/doi/full/10.1002/qj.3155, high, 2017.

Malmierca-Vallet, I., Sime, L. C., and the D-O community members: Dansgaard-Oeschger events in climate models: Review and baseline MIS3 protocol, EGUsphere, pp. 1–45, doi:10.5194/egusphere-2022-707, URL https://egusphere.copernicus.org/preprints/2022/egusphere-2022-707/, 2022.

Malmierca-Vallet, I., Sime, L. C., and the D–O community members: Dansgaard–Oeschger events in climate models: review and baseline Marine Isotope Stage 3 (MIS3) protocol, Climate of the Past, 19, 915–942, doi:10.5194/cp-19-915-2023, URL https://cp.copernicus.org/articles/19/915/2023/, publisher: Copernicus GmbH, 2023.

Manabe, S. and Stouffer, R. J.: Two Stable Equilibria of a Coupled Ocean-Atmosphere Model, Journal of Climate, 1, 841–866, doi:10.1175/1520-0442(1988)001⟨0841:TSEOAC⟩2.0.CO;2, URL https://journals.ametsoc.org/doi/abs/10.1175/1520-0442%281988%29001%3C0841%3ATSEOAC%3E2.0.CO%3B2, publisher: American Meteorological Society, 1988.

Manabe, S. and Stouffer, R. J.: Coupled ocean-atmosphere model response to freshwater input: Comparison to Younger Dryas Event, Paleoceanography, 12, 321–336, doi:10.1029/96PA03932, URL https://agupubs.onlinelibrary.wiley.com/doi/abs/10.1029/96PA03932, 1997.

Marcott, S. A., Clark, P. U., Padman, L., Klinkhammer, G. P., Springer, S. R., Liu, Z., Otto-Bliesner, B. L., Carlson, A. E., Ungerer, A., Padman, J., He, F., Cheng, J., and Schmittner, A.: Ice-shelf collapse from subsurface warming as a trigger for Heinrich events, Proceedings of the National Academy of Sciences of the United States of America, 108, 13 415, doi:10.1073/PNAS.1104772108, URL http://www.ncbi.nlm.nih.gov/pubmed/21808034http://www.pubmedcentral.nih.gov/articlerender.fcgi?artid=PMC3158189, 2011.

Margari, V., Gibbard, P. L., Bryant, C. L., and Tzedakis, P. C.: Character of vegetational and environmental changes in southern Europe during the last glacial period; evidence from Lesvos Island, Greece, Quaternary Science Reviews, 28, 1317–

1339, doi:10.1016/j.quascirev.2009.01.008, URL https://www.sciencedirect.com/science/article/pii/S0277379109000353, 2009.

Marsh, R., Ivchenko, V. O., Skliris, N., Alderson, S., Bigg, G. R., Madec, G., Blaker, A. T., Aksenov, Y., Sinha, B., Coward, A. C., Le Sommer, J., Merino, N., and Zalesny, V. B.: NEMO-ICB (v1.0): interactive icebergs in the NEMO ocean model globally configured at eddy-permitting resolution, Geoscientific Model Development, 8, 1547–1562, URL http://dx.doi.org/10.5194/gmd-8-1547-2015, 2015.

Martin, K. C., Buizert, C., Edwards, J. S., Kalk, M. L., Riddell-Young, B., Brook, E. J., Beaudette, R., Severinghaus, J. P., and Sowers, T. A.: Bipolar impact and phasing of Heinrich-type climate variability, Nature, 617, 100–104, doi:10.1038/s41586-023-05875-2, URL https://www.nature.com/articles/s41586-023-05875-2, number: 7959 Publisher: Nature Publishing Group, 2023.

Martin, T. and Adcroft, A.: Parameterizing the fresh-water flux from land ice to ocean with interactive icebergs in a coupled climate model, Ocean Modelling, 34, 111–124, doi:10.1016/j.ocemod.2010.05.001, URL http://www.sciencedirect.com/science/article/pii/S146350031000065X, 2010.

Marzocchi, A. and Jansen, M. F.: Connecting Antarctic sea ice to deep-ocean circulation in modern and glacial climate simulations, Geophysical Research Letters, 44, 6286–6295, doi:10.1002/2017GL073936, URL https://agupubs.onlinelibrary.wiley.com/doi/10.1002/2017GL073936, publisher: John Wiley & Sons, Ltd, 2017.

Matero, I. S. O., Gregoire, L. J., Ivanovic, R. F., Tindall, J. C., and Haywood, A. M.: The 8.2 ka cooling event caused by Laurentide ice saddle collapse, Earth and Planetary Science Letters, 473, 205–214, doi:10.1016/j.epsl.2017.06.011, URL https://www.sciencedirect.com/science/article/pii/S0012821X17303205, 2017.

McCarthy, G. D., Smeed, D. A., Johns, W. E., Frajka-Williams, E., Moat, B. I., Rayner, D., Baringer, M. O., Meinen, C. S., Collins, J., and Bryden, H. L.: Measuring the Atlantic Meridional Overturning Circulation at 26°N, Progress in Oceanography, 130, 91–111, doi:10.1016/j.pocean.2014.10.006, URL https://www.sciencedirect.com/science/article/pii/S0079661114001694, 2015.

McManus, J. F., Francois, R., Gherardi, J.-M., Keigwin, L. D., and Brown-Leger, S.: Collapse and rapid resumption of Atlantic meridional circulation linked to deglacial climate changes, Nature, 428, 834–837, doi:10.1038/nature02494, URL https://www.nature.com/articles/nature02494, number: 6985 Publisher: Nature Publishing Group, 2004.

Mecking, J. V., Drijfhout, S. S., Jackson, L. C., and Andrews, M. B.: The effect of model bias on Atlantic freshwater transport and implications for AMOC bi-stability, Tellus A: Dynamic Meteorology and Oceanography, 69, 1299 910, doi:10.1080/16000870.2017.

1299910, URL https://a.tellusjournals.se/articles/10.1080/16000870.2017.1299910, 2017.

Mehling, O., Bellomo, K., Angeloni, M., Pasquero, C., and von Hardenberg, J.: High-latitude precipitation as a driver of multicentennial variability of the AMOC in a climate model of intermediate complexity, Climate Dynamics, doi:10.1007/s00382-022-06640-3, URL https://doi.org/10.1007/s00382-022-06640-3, 2022.

Menviel, L., Timmermann, A., Timm, O. E., and Mouchet, A.: Deconstructing the Last Glacial termination: the role of millennial and orbital-scale forcings, Quaternary Science Reviews, 30, 1155–1172, doi:10.1016/j.quascirev.2011.02.005, URL http://www.sciencedirect.com/science/article/pii/S0277379111000539, 2011.

Menviel, L., Timmermann, A., Friedrich, T., and England, M. H.: Hindcasting the continuum of Dansgaard–Oeschger variability: mechanisms, patterns and timing, Climate of the Past, 10, 63–77, doi:https://doi.org/10.5194/cp-10-63-2014, URL https://www.clim-past.net/10/63/2014/, 2014.

Menviel, L. C., Skinner, L. C., Tarasov, L., and Tzedakis, P. C.: An ice–climate oscillatory framework for Dansgaard–Oeschger cycles, Nature Reviews Earth & Environment, 1, 677–693, doi:10.1038/s43017-020-00106-y, URL https://www.nature.com/articles/s43017-020-00106-y, 2020.

Merz, N., Raible, C. C., and Woollings, T.: North Atlantic Eddy-Driven Jet in Interglacial and Glacial Winter Climates, Journal of Climate, 28, 3977–3997, doi:10.1175/JCLI-D-14-00525.1, URL https://journals.ametsoc.org/view/journals/clim/28/10/jcli-d-14-00525.1.xml, 2015.

Michel, S. L. L., Swingedouw, D., Ortega, P., Gastineau, G., Mignot, J., McCarthy, G., and Khodri, M.: Early warning signal for a tipping point suggested by a millennial Atlantic Multidecadal Variability reconstruction, Nature Communications, 13, 5176, doi:10.1038/s41467-022-32704-3, URL https://www.nature.com/articles/s41467-022-32704-3, high - AMV fingerprint, 2022.

Milillo, P., Rignot, E., Rizzoli, P., Scheuchl, B., Mouginot, J., Bueso-Bello, J. L., Prats-Iraola, P., and Dini, L.: Rapid glacier retreat rates observed in West Antarctica, Nature Geoscience, 15, 48–53, doi:10.1038/s41561-021-00877-z, URL https://www.nature.com/articles/s41561-021-00877-z, number: 1 Publisher: Nature Publishing Group, 2022.

Miller, G. H., Geirsdóttir, Á., Zhong, Y., Larsen, D. J., Otto-Bliesner, B. L., Holland, M. M., Bailey, D. A., Refsnider, K. A., Lehman, S. J., Southon, J. R., Anderson, C., Björnsson, H., and Thordarson, T.: Abrupt onset of the Little Ice Age triggered by volcanism and sustained by sea-ice/ocean feedbacks, Geophysical Research Letters,

39, doi:10.1029/2011GL050168, URL https://onlinelibrary.wiley.com/doi/abs/10.1029/2011GL050168, 2012.

Monegato, G., Scardia, G., Hajdas, I., Rizzini, F., and Piccin, A.: The Alpine LGM in the boreal ice-sheets game, Scientific Reports, 7, 1–8, doi:10.1038/s41598-017-02148-7, URL https://www.nature.com/articles/s41598-017-02148-7, number: 1 Publisher: Nature Publishing Group, 2017.

Montoya, M., Born, A., and Levermann, A.: Reversed North Atlantic gyre dynamics in present and glacial climates, Climate Dynamics, 36, 1107–1118, doi:10.1007/s00382-009-0729-y, URL https://doi.org/10.1007/s00382-009-0729-y, 2011.

Moreno-Chamarro, E., Zanchettin, D., Lohmann, K., and Jungclaus, J. H.: An abrupt weakening of the subpolar gyre as trigger of Little Ice Age-type episodes, Climate Dynamics, 48, 727–744, doi:10.1007/s00382-016-3106-7, URL https://doi.org/10.1007/s00382-016-3106-7, 2017.

Morrill, C., Anderson, D. M., Bauer, B. A., Buckner, R., Gille, E. P., Gross, W. S., Hartman, M., and Shah, A.: Proxy benchmarks for intercomparison of 8.2 ka simulations, Climate of the Past, 9, 423–432, doi:10.5194/cp-9-423-2013, URL https://cp.copernicus.org/articles/9/423/2013/, publisher: Copernicus GmbH, 2013.

Muglia, J. and Schmittner, A.: Glacial Atlantic overturning increased by wind stress in climate models, Geophysical Research Letters, 42, 9862–9868, doi:10.1002/2015GL064583, URL https://agupubs.onlinelibrary.wiley.com/doi/abs/10.1002/2015GL064583, 2015.

Muglia, J. and Schmittner, A.: Carbon isotope constraints on glacial Atlantic meridional overturning: Strength vs depth, Quaternary Science Reviews, 257, 106 844, doi:10.1016/j.quascirev.2021.106844, URL https://www.sciencedirect.com/science/article/pii/S0277379121000512, 2021.

Munk, W. and Wunsch, C.: Abyssal recipes II: energetics of tidal and wind mixing, Deep Sea Research Part I: Oceanographic Research Papers, 45, 1977–2010, doi:10.1016/S0967-0637(98)00070-3, URL https://www.sciencedirect.com/science/article/pii/S0967063798000703, 1998.

Murton, J. B., Bateman, M. D., Dallimore, S. R., Teller, J. T., and Yang, Z.: Identification of Younger Dryas outburst flood path from Lake Agassiz to the Arctic Ocean, Nature, 464, 740–743, doi:10.1038/nature08954, URL https://www.nature.com/articles/nature08954, number: 7289 Publisher: Nature Publishing Group, 2010.

Naafs, B. D. A., Hefter, J., Grützner, J., and Stein, R.: Warming of surface waters in the mid-latitude North Atlantic during Heinrich events, Paleoceanography, 28, 153–163, doi:10.1029/2012PA002354, URL https:

//onlinelibrary.wiley.com/doi/abs/10.1029/2012PA002354, _eprint: https://onlinelibrary.wiley.com/doi/pdf/10.1029/2012PA002354, 2013.

Nagumo, J., Arimoto, S., and Yoshizawa, S.: An Active Pulse Transmission Line Simulating Nerve Axon, Proceedings of the IRE, 50, 2061–2070, doi:10.1109/JRPROC.1962.288235, URL https://ieeexplore.ieee.org/document/4066548, 1962.

Nakada, M., Okuno, J., and Yokoyama, Y.: Total meltwater volume since the Last Glacial Maximum and viscosity structure of Earth's mantle inferred from relative sea level changes at Barbados and Bonaparte Gulf and GIA-induced J2, Geophysical Journal International, 204, 1237–1253, doi:10.1093/gji/ggv520, URL https://doi.org/10.1093/gji/ggv520, 2016.

Ng, H. C., Robinson, L. F., McManus, J. F., Mohamed, K. J., Jacobel, A. W., Ivanovic, R. F., Gregoire, L. J., and Chen, T.: Coherent deglacial changes in western Atlantic Ocean circulation, Nature Communications, 9, 1–10, doi:10.1038/s41467-018-05312-3, URL https://www.nature.com/articles/s41467-018-05312-3, 2018.

N.G.R.I.P, M.: High-resolution record of Northern Hemisphere climate extending into the last interglacial period, Nature, 431, 147–151, doi:10.1038/nature02805, URL https://www.nature.com/articles/nature02805, number: 7005 Publisher: Nature Publishing Group, 2004.

Nuber, S., Rae, J. W. B., Zhang, X., Andersen, M. B., Dumont, M. D., Mithan, H. T., Sun, Y., de Boer, B., Hall, I. R., and Barker, S.: Indian Ocean salinity build-up primes deglacial ocean circulation recovery, Nature, 617, 306–311, doi:10.1038/s41586-023-05866-3, URL https://www.nature.com/articles/s41586-023-05866-3, number: 7960 Publisher: Nature Publishing Group, 2023.

Nürnberg, D., Bijma, J., and Hemleben, C.: Assessing the reliability of magnesium in foraminiferal calcite as a proxy for water mass temperatures, Geochimica et Cosmochimica Acta, 60, 803–814, doi:10.1016/0016-7037(95)00446-7, URL https://www.sciencedirect.com/science/article/pii/0016703795004467, 1996.

Obase, T. and Abe-Ouchi, A.: Abrupt Bølling-Allerød Warming Simulated under Gradual Forcing of the Last Deglaciation, Geophysical Research Letters, 46, 11 397–11 405, doi:10.1029/2019GL084675, URL https://onlinelibrary.wiley.com/doi/abs/10.1029/2019GL084675, 2019.

Oka, A., Hasumi, H., and Abe-Ouchi, A.: The thermal threshold of the Atlantic meridional overturning circulation and its control by wind stress forcing during glacial climate, Geophysical Research Letters, 39, doi:10.1029/2012GL051421, URL https://agupubs.onlinelibrary.wiley.com/doi/abs/10.1029/2012GL051421, 2012.

Oka, A., Abe-Ouchi, A., Sherriff-Tadano, S., Yokoyama, Y., Kawamura, K., and

Hasumi, H.: Glacial mode shift of the Atlantic meridional overturning circulation by warming over the Southern Ocean, Communications Earth & Environment, 2, 1–8, doi:10.1038/s43247-021-00226-3, URL https://www.nature.com/articles/s43247-021-00226-3, 2021.

Oppo, D. W., Curry, W. B., and McManus, J. F.: What do benthic δ13C and δ18O data tell us about Atlantic circulation during Heinrich Stadial 1?, Paleoceanography, 30, 353–368, doi:10.1002/2014PA002667, URL https://onlinelibrary.wiley.com/doi/abs/10.1002/2014PA002667, 2015.

Orsi, A. H., Johnson, G. C., and Bullister, J. L.: Circulation, mixing, and production of Antarctic Bottom Water, Progress in Oceanography, 43, 55–109, doi:10.1016/S0079-6611(99)00004-X, URL https://www.sciencedirect.com/science/article/pii/S007966119900004X, 1999.

Osman, M. B., Tierney, J. E., Zhu, J., Tardif, R., Hakim, G. J., King, J., and Poulsen, C. J.: Globally resolved surface temperatures since the Last Glacial Maximum, Nature, 599, 239–244, doi:10.1038/s41586-021-03984-4, URL https://www.nature.com/articles/s41586-021-03984-4, 2021.

Paillard, D. and Labeyrie, L.: Role of the thermohaline circulation in the abrupt warming after Heinrich events, Nature, 372, 162–164, doi:10.1038/372162a0, URL https://www.nature.com/articles/372162a0, number: 6502 Publisher: Nature Publishing Group, 1994.

Parrenin, F., Barnola, J.-M., Beer, J., Blunier, T., Castellano, E., Chappellaz, J., Dreyfus, G., Fischer, H., Fujita, S., Jouzel, J., Kawamura, K., Lemieux-Dudon, B., Loulergue, L., Masson-Delmotte, V., Narcisi, B., Petit, J.-R., Raisbeck, G., Raynaud, D., Ruth, U., Schwander, J., Severi, M., Spahni, R., Steffensen, J. P., Svensson, A., Udisti, R., Waelbroeck, C., and Wolff, E.: The EDC3 chronology for the EPICA Dome C ice core, Climate of the Past, 3, 485–497, doi:https://doi.org/10.5194/cp-3-485-2007, URL https://cp.copernicus.org/articles/3/485/2007/, publisher: Copernicus GmbH, 2007.

Paul, A., Mulitza, S., Stein, R., and Werner, M.: A global climatology of the ocean surface during the Last Glacial Maximum mapped on a regular grid (GLOMAP), Climate of the Past, 17, 805–824, doi:10.5194/cp-17-805-2021, URL https://cp.copernicus.org/articles/17/805/2021/, publisher: Copernicus GmbH, 2021.

Pausata, F. S. R., Li, C., Wettstein, J. J., Kageyama, M., and Nisancioglu, K. H.: The key role of topography in altering North Atlantic atmospheric circulation during the last glacial period, Climate of the Past, 7, 1089–1101, doi:https://doi.org/10.5194/cp-7-1089-2011, URL https://www.clim-past.net/7/1089/2011/, 2011.

Peck, V. L., Hall, I. R., Zahn, R., Elderfield, H., Grousset, F., Hemming, S. R.,

and Scourse, J. D.: High resolution evidence for linkages between NW European ice sheet instability and Atlantic Meridional Overturning Circulation, Earth and Planetary Science Letters, 243, 476–488, doi:10.1016/j.epsl.2005.12.023, URL http://www.sciencedirect.com/science/article/pii/S0012821X0500885X, 2006.

Peck, V. L., Hall, I. R., Zahn, R., and Elderfield, H.: Millennial-scale surface and subsurface paleothermometry from the northeast Atlantic, 55–8 ka BP, Paleoceanography, 23, doi:10.1029/2008PA001631, URL https://onlinelibrary.wiley.com/doi/abs/10.1029/2008PA001631, _eprint: https://onlinelibrary.wiley.com/doi/pdf/10.1029/2008PA001631, 2008.

Pedro, J. B., Andersson, C., Vettoretti, G., Voelker, A. H. L., Waelbroeck, C., Dokken, T. M., Jensen, M. F., Rasmussen, S. O., Sessford, E. G., Jochum, M., and Nisancioglu, K. H.: Dansgaard-Oeschger and Heinrich event temperature anomalies in the North Atlantic set by sea ice, frontal position and thermocline structure, Quaternary Science Reviews, 289, 107 599, doi:10.1016/j.quascirev.2022.107599, URL https://www.sciencedirect.com/science/article/pii/S027737912200230X, 2022.

Peltier, W. R.: On the hemispheric origins of meltwater pulse 1a, Quaternary Science Reviews, 24, 1655–1671, doi:10.1016/j.quascirev.2004.06.023, URL https://www.sciencedirect.com/science/article/pii/S0277379105000788, 2005.

Peltier, W. R. and Fairbanks, R. G.: Global glacial ice volume and Last Glacial Maximum duration from an extended Barbados sea level record, Quaternary Science Reviews, 25, 3322–3337, doi:10.1016/j.quascirev.2006.04.010, URL http://www.sciencedirect.com/science/article/pii/S0277379106001788, 2006.

Peltier, W. R. and Vettoretti, G.: Dansgaard-Oeschger oscillations predicted in a comprehensive model of glacial climate: A "kicked" salt oscillator in the Atlantic, Geophysical Research Letters, 41, 7306–7313, doi:10.1002/2014GL061413, URL https://agupubs.onlinelibrary.wiley.com/doi/abs/10.1002/2014GL061413, 2014.

Peltier, W. R., Argus, D. F., and Drummond, R.: Space geodesy constrains ice age terminal deglaciation: The global ICE-6G_C (VM5a) model, Journal of Geophysical Research: Solid Earth, 120, 450–487, doi:10.1002/2014JB011176, URL https://agupubs.onlinelibrary.wiley.com/doi/abs/10.1002/2014JB011176, 2015.

Peterson, L. C. and Haug, G. H.: Variability in the mean latitude of the Atlantic Intertropical Convergence Zone as recorded by riverine input of sediments to the Cariaco Basin (Venezuela), Palaeogeography, Palaeoclimatology, Palaeoecology, 234, 97–113, doi:10.1016/j.palaeo.2005.10.021, URL https://www.sciencedirect.com/science/article/pii/S0031018205006115, 2006.

Petit, T., Lozier, M. S., Josey, S. A., and Cunningham, S. A.: Atlantic Deep Water Formation Occurs Primarily in the Iceland Basin and Irminger Sea by Local Buoyancy Forcing,

Geophysical Research Letters, 47, e2020GL091 028, doi:10.1029/2020GL091028, URL https://onlinelibrary.wiley.com/doi/abs/10.1029/2020GL091028, 2020.

Pollard, O. G., Barlow, N. L. M., Gregoire, L. J., Gomez, N., Cartelle, V., Ely, J. C., and Astfalck, L. C.: Quantifying the uncertainty in the Eurasian ice-sheet geometry at the Penultimate Glacial Maximum (Marine Isotope Stage 6), The Cryosphere, 17, 4751–4777, doi:10.5194/tc-17-4751-2023, URL https://tc.copernicus.org/articles/17/4751/2023/, publisher: Copernicus GmbH, 2023.

Pope, V. D., Gallani, M. L., Rowntree, P. R., and Stratton, R. A.: The impact of new physical parametrizations in the Hadley Centre climate model: HadAM3, Climate Dynamics, 16, 123–146, doi:10.1007/s003820050009, URL https://doi.org/10.1007/s003820050009, 2000.

Prahl, F. G. and Wakeham, S. G.: Calibration of unsaturation patterns in long-chain ketone compositions for palaeotemperature assessment, Nature, 330, 367–369, doi:10.1038/330367a0, URL https://www.nature.com/articles/330367a0, number: 6146 Publisher: Nature Publishing Group, 1987.

Pöppelmeier, F., Jeltsch-Thömmes, A., Lippold, J., Joos, F., and Stocker, T. F.: Multi-proxy constraints on Atlantic circulation dynamics since the last ice age, Nature Geoscience, 16, 349–356, doi:10.1038/s41561-023-01140-3, URL https://www.nature.com/articles/s41561-023-01140-3, important - Read, 2023.

Quadfasel, D., Kudrass, H., and Frische, A.: Deep-water renewal by turbidity currents in the Sulu Sea, Nature, 348, 320–322, doi:10.1038/348320a0, URL https://www.nature.com/articles/348320a0, number: 6299 Publisher: Nature Publishing Group, 1990.

Rahmstorf, S.: On the freshwater forcing and transport of the Atlantic thermohaline circulation, Climate Dynamics, 12, 799–811, doi:10.1007/s003820050144, URL https://doi.org/10.1007/s003820050144, 1996.

Rahmstorf, S.: Ocean circulation and climate during the past 120,000 years, Nature, 419, 207–214, doi:10.1038/nature01090, URL https://www.nature.com/articles/nature01090, 2002.

Rahmstorf, S.: Timing of abrupt climate change: A precise clock, Geophysical Research Letters, 30, doi:10.1029/2003GL017115, URL https://onlinelibrary.wiley.com/doi/abs/10.1029/2003GL017115, 2003.

Rasmussen, S. O., Bigler, M., Blockley, S. P., Blunier, T., Buchardt, S. L., Clausen, H. B., Cvijanovic, I., Dahl-Jensen, D., Johnsen, S. J., Fischer, H., Gkinis, V., Guillevic, M., Hoek, W. Z., Lowe, J. J., Pedro, J. B., Popp, T., Seierstad, I. K., Steffensen, J. P., Svensson, A. M., Vallelonga, P., Vinther, B. M., Walker, M. J. C., Wheatley, J. J., and Winstrup, M.: A stratigraphic framework for abrupt climatic changes during

the Last Glacial period based on three synchronized Greenland ice-core records: refining and extending the INTIMATE event stratigraphy, Quaternary Science Reviews, 106, 14–28, doi:10.1016/j.quascirev.2014.09.007, URL https://www.sciencedirect.com/science/article/pii/S0277379114003485, 2014.

Rasmussen, T. L. and Thomsen, E.: The role of the North Atlantic Drift in the millennial timescale glacial climate fluctuations, Palaeogeography, Palaeoclimatology, Palaeoecology, 210, 101–116, doi:10.1016/j.palaeo.2004.04.005, URL https://www.sciencedirect.com/science/article/pii/S0031018204002020, 2004.

Rasmussen, T. L., Thomsen, E., and Moros, M.: North Atlantic warming during Dansgaard-Oeschger events synchronous with Antarctic warming and out-of-phase with Greenland climate, Scientific Reports, 6, 20 535, doi:10.1038/srep20535, URL https://www.nature.com/articles/srep20535, number: 1 Publisher: Nature Publishing Group, 2016.

Raymo, M. E., Oppo, D. W., Flower, B. P., Hodell, D. A., McManus, J. F., Venz, K. A., Kleiven, K. F., and McIntyre, K.: Stability of North Atlantic water masses in face of pronounced climate variability during the Pleistocene, Paleoceanography, 19, doi:10.1029/2003PA000921, URL https://onlinelibrary.wiley.com/doi/abs/10.1029/2003PA000921, 2004.

Rea, D., Basov, L., Scholl, D., and Allan, J., eds.: Proceedings of the Ocean Drilling Program, 145 Scientific Results, vol. 145 of *Proceedings of the Ocean Drilling Program*, Ocean Drilling Program, doi:10.2973/odp.proc.sr.145.1995, URL http://www-odp.tamu.edu/publications/145_SR/145TOC.HTM, 1995.

Reichler, T. and Kim, J.: How Well Do Coupled Models Simulate Today's Climate?, Bulletin of the American Meteorological Society, 89, 303–312, doi:10.1175/BAMS-89-3-303, URL https://journals.ametsoc.org/view/journals/bams/89/3/bams-89-3-303.xml, publisher: American Meteorological Society Section: Bulletin of the American Meteorological Society, 2008.

Renold, M., Raible, C. C., Yoshimori, M., and Stocker, T. F.: Simulated resumption of the North Atlantic meridional overturning circulation – Slow basin-wide advection and abrupt local convection, Quaternary Science Reviews, 29, 101–112, doi:10.1016/j.quascirev.2009.11.005, URL http://www.sciencedirect.com/science/article/pii/S0277379109003680, 2010.

Repschläger, J., Weinelt, M., Kinkel, H., Andersen, N., Garbe-Schönberg, D., and Schwab, C.: Response of the subtropical North Atlantic surface hydrography on deglacial and Holocene AMOC changes, Paleoceanography, 30, 456–476, doi:10.1002/2014PA002637, URL https://onlinelibrary.wiley.com/doi/abs/10.1002/2014PA002637, 2015.

Repschläger, J., Zhao, N., Rand, D., Lisiecki, L., Muglia, J., Mulitza, S., Schmittner,

A., Cartapanis, O., Bauch, H. A., Schiebel, R., and Haug, G. H.: Active North Atlantic deepwater formation during Heinrich Stadial 1, Quaternary Science Reviews, 270, 107 145, doi:10.1016/j.quascirev.2021.107145, URL https://www.sciencedirect.com/science/article/pii/S0277379121003528, 2021.

Roberts, W. H. G. and Valdes, P. J.: Green Mountains and White Plains: The Effect of Northern Hemisphere Ice Sheets on the Global Energy Budget, Journal of Climate, 30, 3887–3905, doi:10.1175/JCLI-D-15-0846.1, URL https://journals.ametsoc.org/jcli/article/30/10/3887/106888/Green-Mountains-and-White-Plains-The-Effect-of, publisher: American Meteorological Society, 2017.

Roberts, W. H. G., Valdes, P. J., and Payne, A. J.: A new constraint on the size of Heinrich Events from an iceberg/sediment model, Earth and Planetary Science Letters, 386, 1–9, doi:10.1016/j.epsl.2013.10.020, URL http://www.sciencedirect.com/science/article/pii/S0012821X13005839, 2014a.

Roberts, W. H. G., Valdes, P. J., and Payne, A. J.: Topography's crucial role in Heinrich Events, Proceedings of the National Academy of Sciences, 111, 16 688–16 693, doi:10.1073/pnas.1414882111, URL https://www.pnas.org/content/111/47/16688, publisher: National Academy of Sciences Section: Physical Sciences, 2014b.

Robinson, L. F., Henderson, G. M., Ng, H. C., and McManus, J. F.: Pa/Th as a (paleo)circulation tracer: A North Atlantic perspective, Past Global Changes Magazine, 27, doi:10.22498/pages.27.2.56, URL http://pastglobalchanges.org/products/pages-magazine/12923, 2019.

Robinson, S., Ivanovic, R., van de Flierdt, T., Blanchet, C. L., Tachikawa, K., Martin, E. E., Cook, C. P., Williams, T., Gregoire, L., Plancherel, Y., Jeandel, C., and Arsouze, T.: Global continental and marine detrital ϵNd: An updated compilation for use in understanding marine Nd cycling, Chemical Geology, 567, 120 119, doi:10.1016/j.chemgeo.2021.120119, URL https://www.sciencedirect.com/science/article/pii/S0009254121000632, 2021.

Roche, D. M., Renssen, H., Weber, S. L., and Goosse, H.: Could meltwater pulses have been sneaked unnoticed into the deep ocean during the last glacial?, Geophysical Research Letters, 34, doi:10.1029/2007GL032064, URL https://onlinelibrary.wiley.com/doi/abs/10.1029/2007GL032064, high - Read, 2007.

Roche, D. M., Wiersma, A. P., and Renssen, H.: A systematic study of the impact of freshwater pulses with respect to different geographical locations, Climate Dynamics, 34, 997–1013, doi:10.1007/s00382-009-0578-8, URL https://doi.org/10.1007/s00382-009-0578-8, 2010.

Roche, D. M., Renssen, H., Paillard, D., and Levavasseur, G.: Deciphering the spatio-

temporal complexity of climate change of the last deglaciation: a model analysis, Climate of the Past, 7, 591–602, doi:https://doi.org/10.5194/cp-7-591-2011, URL https://www.clim-past.net/7/591/2011/, publisher: Copernicus GmbH, 2011.

Romé, Y. M., Ivanovic, R. F., Gregoire, L. J., Sherriff-Tadano, S., and Valdes, P. J.: Millennial-Scale Climate Oscillations Triggered by Deglacial Meltwater Discharge in Last Glacial Maximum Simulations, Paleoceanography and Paleoclimatology, 37, e2022PA004 451, doi:10.1029/2022PA004451, URL https://onlinelibrary.wiley.com/doi/abs/10.1029/2022PA004451, 2022.

Ruddiman, W.: Earth's Climate: Past and Future, W. H. Freeman, URL https://books.google.co.uk/books?id=93oNqF_tPoEC, 2001.

Ruddiman, W. F.: Late Quaternary deposition of ice-rafted sand in the subpolar North Atlantic (lat 40° to 65°N), GSA Bulletin, 88, 1813–1827, doi:10.1130/0016-7606(1977)88⟨1813:LQDOIS⟩2.0.CO;2, URL https://pubs.geoscienceworld.org/gsabulletin/article/88/12/1813/189749/Late-Quaternary-deposition-of-ice-rafted-sand-in, 1977.

Sayol, J.-M., Dijkstra, H., and Katsman, C.: Seasonal and regional variations of sinking in the subpolar North Atlantic from a high-resolution ocean model, Ocean Science, 15, 1033–1053, doi:10.5194/os-15-1033-2019, URL https://os.copernicus.org/articles/15/1033/2019/, publisher: Copernicus GmbH, 2019.

Schilt, A., Baumgartner, M., Schwander, J., Buiron, D., Capron, E., Chappellaz, J., Loulergue, L., Schüpbach, S., Spahni, R., Fischer, H., and Stocker, T. F.: Atmospheric nitrous oxide during the last 140,000years, Earth and Planetary Science Letters, 300, 33–43, doi:10.1016/j.epsl.2010.09.027, URL http://www.sciencedirect.com/science/article/pii/S0012821X10006023, 2010.

Schmittner, A., Yoshimori, M., and Weaver, A. J.: Instability of Glacial Climate in a Model of the Ocean- Atmosphere-Cryosphere System, Science, 295, 1489–1493, doi:10.1126/science.1066174, URL https://science.sciencemag.org/content/295/5559/1489, publisher: American Association for the Advancement of Science Section: Research Article, 2002.

Schmittner, A., Chiang, J. C. H., and Hemming, S. R.: Ocean Circulation: Mechanisms and Impacts – Past and Future Changes of Meridional Overturning | Wiley, URL https://www.wiley.com/en-us/Ocean+Circulation%3A+Mechanisms+and+Impacts+Past+and+Future+Changes+of+Meridional+Overturning-p-9780875904382, 2007.

Schouten, S., Hopmans, E. C., Schefuß, E., and Sinninghe Damsté, J. S.: Distributional variations in marine crenarchaeotal membrane lipids: a new tool for reconstructing ancient sea water temperatures?, Earth and Planetary Science Letters, 204, 265–274, doi:

10.1016/S0012-821X(02)00979-2, URL https://www.sciencedirect.com/science/article/pii/S0012821X02009792, 2002.

Schulz, M.: On the 1470-year pacing of Dansgaard-Oeschger warm events, Paleoceanography, 17, 4–1–4–9, doi:10.1029/2000PA000571, URL https://onlinelibrary.wiley.com/doi/abs/10.1029/2000PA000571, 2002.

Schulz, M., Paul, A., and Timmermann, A.: Relaxation oscillators in concert: A framework for climate change at millennial timescales during the late Pleistocene, Geophysical Research Letters, 29, 46–1–46–4, doi:10.1029/2002GL016144, URL https://agupubs.onlinelibrary.wiley.com/doi/abs/10.1029/2002GL016144, 2002.

Scourse, J. D., Haapaniemi, A. I., Colmenero-Hidalgo, E., Peck, V. L., Hall, I. R., Austin, W. E. N., Knutz, P. C., and Zahn, R.: Growth, dynamics and deglaciation of the last British–Irish ice sheet: the deep-sea ice-rafted detritus record, Quaternary Science Reviews, 28, 3066–3084, doi:10.1016/j.quascirev.2009.08.009, URL http://www.sciencedirect.com/science/article/pii/S0277379109002753, 2009.

Seager, R., Battisti, D. S., Yin, J., Gordon, N., Naik, N., Clement, A. C., and Cane, M. A.: Is the Gulf Stream responsible for Europe's mild winters?, Quarterly Journal of the Royal Meteorological Society, 128, 2563–2586, doi:10.1256/qj.01.128, URL https://onlinelibrary.wiley.com/doi/abs/10.1256/qj.01.128, 2002.

Severinghaus, J. P. and Brook, E. J.: Abrupt Climate Change at the End of the Last Glacial Period Inferred from Trapped Air in Polar Ice, Science, 286, 930–934, doi:10.1126/science.286.5441.930, URL https://science.sciencemag.org/content/286/5441/930, publisher: American Association for the Advancement of Science Section: Report, 1999.

Severinghaus, J. P., Sowers, T., Brook, E. J., Alley, R. B., and Bender, M. L.: Timing of abrupt climate change at the end of the Younger Dryas interval from thermally fractionated gases in polar ice, Nature, 391, 141–146, doi:10.1038/34346, URL https://www.nature.com/articles/34346, number: 6663 Publisher: Nature Publishing Group, 1998.

Shackleton, N.: Oxygen Isotope Analyses and Pleistocene Temperatures Re-assessed, Nature, 215, 15–17, doi:10.1038/215015a0, URL https://www.nature.com/articles/215015a0, number: 5096 Publisher: Nature Publishing Group, 1967.

Shackleton, N. J., Hall, M. A., and Vincent, E.: Phase relationships between millennial-scale events 64,000–24,000 years ago, Paleoceanography, 15, 565–569, doi:10.1029/2000PA000513, URL https://agupubs.onlinelibrary.wiley.com/doi/abs/10.1029/2000PA000513, 2000.

Shakun, J. D., Clark, P. U., He, F., Marcott, S. A., Mix, A. C., Liu, Z., Otto-

Bliesner, B., Schmittner, A., and Bard, E.: Global warming preceded by increasing carbon dioxide concentrations during the last deglaciation, Nature, 484, 49–54, doi:10.1038/nature10915, URL https://www.nature.com/articles/nature10915, number: 7392 Publisher: Nature Publishing Group, 2012.

Sherriff-Tadano, S. and Abe-Ouchi, A.: Roles of Sea Ice–Surface Wind Feedback in Maintaining the Glacial Atlantic Meridional Overturning Circulation and Climate, Journal of Climate, 33, 3001–3018, doi:10.1175/JCLI-D-19-0431.1, URL https://journals.ametsoc.org/view/journals/clim/33/8/jcli-d-19-0431.1.xml, publisher: American Meteorological Society Section: Journal of Climate, 2020.

Sherriff-Tadano, S., Abe-Ouchi, A., Yoshimori, M., Oka, A., and Chan, W.-L.: Influence of glacial ice sheets on the Atlantic meridional overturning circulation through surface wind change, Climate Dynamics, 50, 2881–2903, doi:10.1007/s00382-017-3780-0, URL https://doi.org/10.1007/s00382-017-3780-0, 2018.

Sherriff-Tadano, S., Abe-Ouchi, A., and Oka, A.: Impact of mid-glacial ice sheets on deep ocean circulation and global climate, Climate of the Past, 17, 95–110, doi:10.5194/cp-17-95-2021, URL https://cp.copernicus.org/articles/17/95/2021/, publisher: Copernicus GmbH, 2021.

Sherriff-Tadano, S., Ivanovic, R., Gregoire, L., Lang, C., Gandy, N., Gregory, J., Edwards, T. L., Pollard, O., and Smith, R. S.: Large ensemble simulations of the North American and Greenland ice sheets at the Last Glacial Maximum with a coupled atmospheric general circulation-ice sheet model, EGUsphere, pp. 1–30, doi:10.5194/egusphere-2023-2082, URL https://egusphere.copernicus.org/preprints/2023/egusphere-2023-2082/, publisher: Copernicus GmbH, 2023.

Simms, A. R., Lisiecki, L., Gebbie, G., Whitehouse, P. L., and Clark, J. F.: Balancing the last glacial maximum (LGM) sea-level budget, Quaternary Science Reviews, 205, 143–153, doi:10.1016/j.quascirev.2018.12.018, URL https://www.sciencedirect.com/science/article/pii/S0277379118304074, 2019.

Singarayer, J. S., Valdes, P. J., and Roberts, W. H. G.: Ocean dominated expansion and contraction of the late Quaternary tropical rainbelt, Scientific Reports, 7, 9382, doi:10.1038/s41598-017-09816-8, URL https://www.nature.com/articles/s41598-017-09816-8, 2017.

Smeed, D. A., McCarthy, G. D., Cunningham, S. A., Frajka-Williams, E., Rayner, D., Johns, W. E., Meinen, C. S., Baringer, M. O., Moat, B. I., Duchez, A., and Bryden, H. L.: Observed decline of the Atlantic meridional overturning circulation 2004–2012, Ocean Science, 10, 29–38, doi:https://doi.org/10.5194/os-10-29-2014, URL https://www.ocean-sci.net/10/29/2014/, 2014.

Smith, R. S. and Gregory, J. M.: A study of the sensitivity of ocean overturning circula-

tion and climate to freshwater input in different regions of the North Atlantic, Geophysical Research Letters, 36, doi:10.1029/2009GL038607, URL https://onlinelibrary.wiley.com/doi/abs/10.1029/2009GL038607, 2009.

Snoll, B., Ivanovic, R. F., Valdes, P. J., Maycock, A. C., and Gregoire, L. J.: Effect of orographic gravity wave drag on Northern Hemisphere climate in transient simulations of the last deglaciation, Climate Dynamics, doi:10.1007/s00382-022-06196-2, URL https://doi.org/10.1007/s00382-022-06196-2, 2022.

Snoll, B., Ivanovic, R., Gregoire, L., Sherriff-Tadano, S., Menviel, L., Obase, T., Abe-Ouchi, A., Bouttes, N., He, C., He, F., Kapsch, M., Mikolajewicz, U., Muglia, J., and Valdes, P.: A multi-model assessment of the early last deglaciation (PMIP4 LDv1): The meltwater paradox reigns supreme, EGUsphere, pp. 1–45, doi:10.5194/egusphere-2023-1802, URL https://egusphere.copernicus.org/preprints/2023/egusphere-2023-1802/, publisher: Copernicus GmbH, 2023.

Stanford, J. D., Rohling, E. J., Bacon, S., Roberts, A. P., Grousset, F. E., and Bolshaw, M.: A new concept for the paleoceanographic evolution of Heinrich event 1 in the North Atlantic, Quaternary Science Reviews, 30, 1047–1066, doi:10.1016/j.quascirev.2011.02.003, URL http://www.sciencedirect.com/science/article/pii/S0277379111000400, 2011.

Steffensen, J. P., Andersen, K. K., Bigler, M., Clausen, H. B., Dahl-Jensen, D., Fischer, H., Goto-Azuma, K., Hansson, M., Johnsen, S. J., Jouzel, J., Masson-Delmotte, V., Popp, T., Rasmussen, S. O., Röthlisberger, R., Ruth, U., Stauffer, B., Siggaard-Andersen, M.-L., Sveinbjörnsdóttir, A. E., Svensson, A., and White, J. W. C.: High-Resolution Greenland Ice Core Data Show Abrupt Climate Change Happens in Few Years, Science, 321, 680–684, doi:10.1126/science.1157707, URL https://science.sciencemag.org/content/321/5889/680, publisher: American Association for the Advancement of Science Section: Report, 2008.

Stenni, B., Buiron, D., Frezzotti, M., Albani, S., Barbante, C., Bard, E., Barnola, J. M., Baroni, M., Baumgartner, M., Bonazza, M., Capron, E., Castellano, E., Chappellaz, J., Delmonte, B., Falourd, S., Genoni, L., Iacumin, P., Jouzel, J., Kipfstuhl, S., Landais, A., Lemieux-Dudon, B., Maggi, V., Masson-Delmotte, V., Mazzola, C., Minster, B., Montagnat, M., Mulvaney, R., Narcisi, B., Oerter, H., Parrenin, F., Petit, J. R., Ritz, C., Scarchilli, C., Schilt, A., Schüpbach, S., Schwander, J., Selmo, E., Severi, M., Stocker, T. F., and Udisti, R.: Expression of the bipolar see-saw in Antarctic climate records during the last deglaciation, Nature Geoscience, 4, 46–49, doi:10.1038/ngeo1026, URL https://www.nature.com/articles/ngeo1026, number: 1 Publisher: Nature Publishing Group, 2011.

Stern, J. V. and Lisiecki, L. E.: North Atlantic circulation and reservoir age changes over

the past 41,000 years, Geophysical Research Letters, 40, 3693–3697, doi:10.1002/grl.50679, URL https://agupubs.onlinelibrary.wiley.com/doi/full/10.1002/grl.50679, 2013.

Stocker, T. F.: The Seesaw Effect, Science, 282, 61–62, doi:10.1126/science.282.5386.61, URL https://www.science.org/doi/full/10.1126/science.282.5386.61, publisher: American Association for the Advancement of Science, 1998.

Stocker, T. F. and Johnsen, S. J.: A minimum thermodynamic model for the bipolar seesaw, Paleoceanography, 18, doi:10.1029/2003PA000920, URL https://onlinelibrary.wiley.com/doi/abs/10.1029/2003PA000920, 2003.

Stockhecke, M., Timmermann, A., Kipfer, R., Haug, G. H., Kwiecien, O., Friedrich, T., Menviel, L., Litt, T., Pickarski, N., and Anselmetti, F. S.: Millennial to orbital-scale variations of drought intensity in the Eastern Mediterranean, Quaternary Science Reviews, 133, 77–95, doi:10.1016/j.quascirev.2015.12.016, URL https://www.sciencedirect.com/science/article/pii/S0277379115301979, 2016.

Stommel, H.: Thermohaline Convection with Two Stable Regimes of Flow, Tellus, 13, 224–230, doi:10.1111/j.2153-3490.1961.tb00079.x, URL https://onlinelibrary.wiley.com/doi/abs/10.1111/j.2153-3490.1961.tb00079.x, 1961.

Stott, P. A., Tett, S. F. B., Jones, G. S., Allen, M. R., Mitchell, J. F. B., and Jenkins, G. J.: External Control of 20th Century Temperature by Natural and Anthropogenic Forcings, Science, 290, 2133–2137, doi:10.1126/science.290.5499.2133, URL https://www.science.org/doi/10.1126/science.290.5499.2133, publisher: American Association for the Advancement of Science, 2000.

Stouffer, R. J., Yin, J., Gregory, J. M., Dixon, K. W., Spelman, M. J., Hurlin, W., Weaver, A. J., Eby, M., Flato, G. M., Hasumi, H., Hu, A., Jungclaus, J. H., Kamenkovich, I. V., Levermann, A., Montoya, M., Murakami, S., Nawrath, S., Oka, A., Peltier, W. R., Robitaille, D. Y., Sokolov, A., Vettoretti, G., and Weber, S. L.: Investigating the Causes of the Response of the Thermohaline Circulation to Past and Future Climate Changes, Journal of Climate, 19, 1365–1387, doi:10.1175/JCLI3689.1, URL https://journals.ametsoc.org/doi/full/10.1175/JCLI3689.1, 2006.

Strogatz, S.: Nonlinear dynamics and chaos : with applications to physics, biology, chemistry, and engineering, Second edition. Boulder, CO : Westview Press, a member of the Perseus Books Group, [2015], URL https://search.library.wisc.edu/catalog/9910223127702121, 2015.

Svensen, H., Planke, S., Malthe-Sørenssen, A., Jamtveit, B., Myklebust, R., Rasmussen Eidem, T., and Rey, S. S.: Release of methane from a volcanic basin as a mechanism for initial Eocene global warming, Nature, 429, 542–545, doi:10.1038/nature02566, URL

https://www.nature.com/articles/nature02566, number: 6991 Publisher: Nature Publishing Group, 2004.

Svensson, A., Andersen, K. K., Bigler, M., Clausen, H. B., Dahl-Jensen, D., Davies, S. M., Johnsen, S. J., Muscheler, R., Parrenin, F., Rasmussen, S. O., Röthlisberger, R., Seierstad, I., Steffensen, J. P., and Vinther, B. M.: A 60 000 year Greenland stratigraphic ice core chronology, Climate of the Past, 4, 47–57, doi:10.5194/cp-4-47-2008, URL https://cp.copernicus.org/articles/4/47/2008/, publisher: Copernicus GmbH, 2008.

Svensson, A., Dahl-Jensen, D., Steffensen, J. P., Blunier, T., Rasmussen, S. O., Vinther, B. M., Vallelonga, P., Capron, E., Gkinis, V., Cook, E., Kjær, H. A., Muscheler, R., Kipfstuhl, S., Wilhelms, F., Stocker, T. F., Fischer, H., Adolphi, F., Erhardt, T., Sigl, M., Landais, A., Parrenin, F., Buizert, C., McConnell, J. R., Severi, M., Mulvaney, R., and Bigler, M.: Bipolar volcanic synchronization of abrupt climate change in Greenland and Antarctic ice cores during the last glacial period, Climate of the Past, 16, 1565–1580, doi:10.5194/cp-16-1565-2020, URL https://cp.copernicus.org/articles/16/1565/2020/, publisher: Copernicus GmbH, 2020.

Sánchez Goñi, M. F.: Regional impacts of climate change and its relevance to human evolution, Evolutionary Human Sciences, 2, e55, doi:10.1017/ehs.2020.56, URL https://www.cambridge.org/core/journals/evolutionary-human-sciences/article/regional-impacts-of-climate-change-and-its-relevance-to-human-evolution/F48FC5562D7FF05FEB172158E60B8894#, publisher: Cambridge University Press, 2020.

Sánchez Goñi, M. F., Turon, J.-L., Eynaud, F., and Gendreau, S.: European Climatic Response to Millennial-Scale Changes in the Atmosphere–Ocean System during the Last Glacial Period, Quaternary Research, 54, 394–403, doi:10.1006/qres.2000.2176, URL https://www.cambridge.org/core/journals/quaternary-research/article/abs/european-climatic-response-to-millennialscale-changes-in-the-atmosphereocean-system-during576DB6EF96D6923ED701B117C5939CD0#access-block, publisher: Cambridge University Press, 2000.

Tachikawa, K., Athias, V., and Jeandel, C.: Neodymium budget in the modern ocean and paleo-oceanographic implications, Journal of Geophysical Research: Oceans, 108, doi:10.1029/1999JC000285, URL https://onlinelibrary.wiley.com/doi/abs/10.1029/1999JC000285, _eprint: https://onlinelibrary.wiley.com/doi/pdf/10.1029/1999JC000285, 2003.

Talley, L.: Closure of the Global Overturning Circulation Through the Indian, Pacific, and Southern Oceans: Schematics and Transports, Oceanography, 26, 80–97, doi:10.5670/oceanog.2013.07, URL https://tos.org/oceanography/article/

closure-of-the-global-overturning-circulation-through-the-indian-pacific-an, 2013.

Tarasov, L. and Peltier, R. W.: Greenland glacial history and local geodynamic consequences, Geophysical Journal International, 150, 198–229, doi:10.1046/j.1365-246X.2002.01702.x, URL https://academic.oup.com/gji/article/150/1/198/591943, publisher: Oxford Academic, 2002.

Tarasov, L., Dyke, A. S., Neal, R. M., and Peltier, W. R.: A data-calibrated distribution of deglacial chronologies for the North American ice complex from glaciological modeling, Earth and Planetary Science Letters, 315-316, 30–40, doi:10.1016/j.epsl.2011.09.010, URL http://www.sciencedirect.com/science/article/pii/S0012821X11005243, 2012.

Taylor, K. E., Stouffer, R. J., and Meehl, G. A.: An Overview of CMIP5 and the Experiment Design, Bulletin of the American Meteorological Society, 93, 485–498, doi:10.1175/BAMS-D-11-00094.1, URL https://journals.ametsoc.org/view/journals/bams/93/4/bams-d-11-00094.1.xml, publisher: American Meteorological Society Section: Bulletin of the American Meteorological Society, 2012.

Thomas, E. R., Wolff, E. W., Mulvaney, R., Johnsen, S. J., Steffensen, J. P., and Arrowsmith, C.: Anatomy of a Dansgaard-Oeschger warming transition: High-resolution analysis of the North Greenland Ice Core Project ice core, Journal of Geophysical Research: Atmospheres, 114, doi:https://doi.org/10.1029/2008JD011215, URL https://agupubs.onlinelibrary.wiley.com/doi/abs/10.1029/2008JD011215, 2009.

Thompson, A. F., Hines, S. K., and Adkins, J. F.: A Southern Ocean Mechanism for the Interhemispheric Coupling and Phasing of the Bipolar Seesaw, Journal of Climate, 32, 4347–4365, doi:10.1175/JCLI-D-18-0621.1, URL https://journals.ametsoc.org/view/journals/clim/32/14/jcli-d-18-0621.1.xml, 2019.

Thompson, E. L. and Smith, L. A.: Escape from model-land, Economics, 13, doi:10.5018/economics-ejournal.ja.2019-40, URL https://www.degruyter.com/document/doi/10.5018/economics-ejournal.ja.2019-40/html, publisher: De Gruyter Open Access, 2019.

Thornalley, D. J. R., Oppo, D. W., Ortega, P., Robson, J. I., Brierley, C. M., Davis, R., Hall, I. R., Moffa-Sanchez, P., Rose, N. L., Spooner, P. T., Yashayaev, I., and Keigwin, L. D.: Anomalously weak Labrador Sea convection and Atlantic overturning during the past 150 years, Nature, 556, 227–230, doi:10.1038/s41586-018-0007-4, URL https://www.nature.com/articles/s41586-018-0007-4, medium - Abstract, 2018.

Tierney, J. E., Poulsen, C. J., Montañez, I. P., Bhattacharya, T., Feng, R., Ford, H. L., Hönisch, B., Inglis, G. N., Petersen, S. V., Sagoo, N., Tabor, C. R., Thirumalai, K., Zhu, J., Burls, N. J., Foster, G. L., Goddéris, Y., Huber, B. T., Ivany, L. C.,

Kirtland Turner, S., Lunt, D. J., McElwain, J. C., Mills, B. J. W., Otto-Bliesner, B. L., Ridgwell, A., and Zhang, Y. G.: Past climates inform our future, Science, 370, eaay3701, doi:10.1126/science.aay3701, URL https://www.science.org/doi/10.1126/science.aay3701, publisher: American Association for the Advancement of Science, 2020a.

Tierney, J. E., Zhu, J., King, J., Malevich, S. B., Hakim, G. J., and Poulsen, C. J.: Glacial cooling and climate sensitivity revisited, Nature, 584, 569–573, doi:10.1038/s41586-020-2617-x, URL https://www.nature.com/articles/s41586-020-2617-x, 2020b.

Timmermann, A., Gildor, H., Schulz, M., and Tziperman, E.: Coherent Resonant Millennial-Scale Climate Oscillations Triggered by Massive Meltwater Pulses, Journal of Climate, 16, 2569–2585, doi:10.1175/1520-0442(2003)016⟨2569:CRMCOT⟩2.0.CO;2, URL https://journals.ametsoc.org/doi/full/10.1175/1520-0442%282003%29016%3C2569%3ACRMCOT%3E2.0.CO%3B2, 2003.

Toggweiler, J. R. and Samuels, B.: On the Ocean's Large-Scale Circulation near the Limit of No Vertical Mixing, Journal of Physical Oceanography, 28, 1832–1852, doi:10.1175/1520-0485(1998)028⟨1832:OTOSLS⟩2.0.CO;2, URL https://journals.ametsoc.org/view/journals/phoc/28/9/1520-0485_1998_028_1832_otosls_2.0.co_2.xml, publisher: American Meteorological Society Section: Journal of Physical Oceanography, 1998.

Toucanne, S., Soulet, G., Freslon, N., Silva Jacinto, R., Dennielou, B., Zaragosi, S., Eynaud, F., Bourillet, J.-F., and Bayon, G.: Millennial-scale fluctuations of the European Ice Sheet at the end of the last glacial, and their potential impact on global climate, Quaternary Science Reviews, 123, 113–133, doi:10.1016/j.quascirev.2015.06.010, URL http://www.sciencedirect.com/science/article/pii/S0277379115300196, 2015.

Trenberth, K. E., Zhang, Y., Fasullo, J. T., and Cheng, L.: Observation-Based Estimates of Global and Basin Ocean Meridional Heat Transport Time Series, Journal of Climate, 32, 4567–4583, doi:10.1175/JCLI-D-18-0872.1, URL https://journals.ametsoc.org/view/journals/clim/32/14/jcli-d-18-0872.1.xml, publisher: American Meteorological Society Section: Journal of Climate, 2019.

Ullman, D. J., LeGrande, A. N., Carlson, A. E., Anslow, F. S., and Licciardi, J. M.: Assessing the impact of Laurentide Ice Sheet topography on glacial climate, Climate of the Past, 10, 487–507, doi:10.5194/cp-10-487-2014, URL https://cp.copernicus.org/articles/10/487/2014/, publisher: Copernicus GmbH, 2014.

Valdes, P.: Built for stability, Nature Geoscience, 4, 414–416, doi:10.1038/ngeo1200, URL https://www.nature.com/articles/ngeo1200, important - Read, 2011.

Valdes, P. J., Armstrong, E., Badger, M. P. S., Bradshaw, C. D., Bragg, F., Davies-

Barnard, T., Day, J. J., Farnsworth, A. J., Hopcroft, P. O., Kennedy, A. T., Lord, N. S., Lunt, D. J., Marzocchi, A., Parry, L. M., Roberts, W. H. G., Stone, E. J., Tourte, G. J. L., and Williams, J. H. T.: The BRIDGE HadCM3 family of climate models: HadCM3@Bristol v1.0, Geoscientific Model Development Discussions, doi:10.5194/gmd-2017-16, URL https://research-information.bris.ac.uk/en/publications/the-bridge-hadcm3-family-of-climate-models-hadcm3bristol-v10-2, publisher: Copernicus GmbH, 2017.

Vallis, G. K.: Geophysical fluid dynamics: whence, whither and why?, Proceedings of the Royal Society A: Mathematical, Physical and Engineering Sciences, 472, 20160 140, doi:10.1098/rspa.2016.0140, URL https://royalsocietypublishing.org/doi/10.1098/rspa.2016.0140, publisher: Royal Society, 2016.

Van Meerbeeck, C. J., Renssen, H., and Roche, D. M.: How did Marine Isotope Stage 3 and Last Glacial Maximum climates differ? – Perspectives from equilibrium simulations, Climate of the Past, 5, 33–51, doi:https://doi.org/10.5194/cp-5-33-2009, URL https://cp.copernicus.org/articles/5/33/2009/, publisher: Copernicus GmbH, 2009.

Vellinga, M. and Wood, R. A.: Global Climatic Impacts of a Collapse of the Atlantic Thermohaline Circulation, Climatic Change, 54, 251–267, doi:10.1023/A:1016168827653, URL https://doi.org/10.1023/A:1016168827653, 2002.

Vellinga, M. and Wu, P.: Low-Latitude Freshwater Influence on Centennial Variability of the Atlantic Thermohaline Circulation, Journal of Climate, 17, 4498–4511, doi:10.1175/3219.1, URL https://journals.ametsoc.org/jcli/article/17/23/4498/29935/Low-Latitude-Freshwater-Influence-on-Centennial, high, 2004.

Veres, D., Bazin, L., Landais, A., Toyé Mahamadou Kele, H., Lemieux-Dudon, B., Parrenin, F., Martinerie, P., Blayo, E., Blunier, T., Capron, E., Chappellaz, J., Rasmussen, S. O., Severi, M., Svensson, A., Vinther, B., and Wolff, E. W.: The Antarctic ice core chronology (AICC2012): an optimized multi-parameter and multi-site dating approach for the last 120 thousand years, Climate of the Past, 9, 1733–1748, doi:https://doi.org/10.5194/cp-9-1733-2013, URL https://www.clim-past.net/9/1733/2013/, publisher: Copernicus GmbH, 2013.

Vettoretti, G. and Peltier, W. R.: Thermohaline instability and the formation of glacial North Atlantic super polynyas at the onset of Dansgaard-Oeschger warming events, Geophysical Research Letters, 43, 5336–5344, doi:10.1002/2016GL068891, URL https://onlinelibrary.wiley.com/doi/abs/10.1002/2016GL068891, important - Abstract, 2016.

Vettoretti, G. and Peltier, W. R.: Fast Physics and Slow Physics in the Nonlinear Dansgaard–Oeschger Relaxation Oscillation, Journal of Climate, 31, 3423–3449, doi:

10.1175/JCLI-D-17-0559.1, URL https://journals.ametsoc.org/view/journals/clim/31/9/jcli-d-17-0559.1.xml, important, 2018.

Vettoretti, G., Ditlevsen, P., Jochum, M., and Rasmussen, S. O.: Atmospheric CO2 control of spontaneous millennial-scale ice age climate oscillations, Nature Geoscience, 15, 300–306, doi:10.1038/s41561-022-00920-7, URL https://www.nature.com/articles/s41561-022-00920-7, number: 4 Publisher: Nature Publishing Group, 2022.

Vidal, L., Labeyrie, L., Cortijo, E., Arnold, M., Duplessy, J. C., Michel, E., Becqué, S., and van Weering, T. C. E.: Evidence for changes in the North Atlantic Deep Water linked to meltwater surges during the Heinrich events, Earth and Planetary Science Letters, 146, 13–27, doi:10.1016/S0012-821X(96)00192-6, URL http://www.sciencedirect.com/science/article/pii/S0012821X96001926, 1997.

Voelker, A. H. L.: Global distribution of centennial-scale records for Marine Isotope Stage (MIS) 3: a database, Quaternary Science Reviews, 21, 1185–1212, doi:10.1016/S0277-3791(01)00139-1, URL http://www.sciencedirect.com/science/article/pii/S0277379101001391, 2002.

Voelker, A. H. L. and de Abreu, L.: A Review of Abrupt Climate Change Events in the Northeastern Atlantic Ocean (Iberian Margin): Latitudinal, Longitudinal, and Vertical Gradients, in: Abrupt Climate Change: Mechanisms, Patterns, and Impacts, pp. 15–37, American Geophysical Union (AGU), URL https://onlinelibrary.wiley.com/doi/abs/10.1029/2010GM001021, low - Extract, 2011.

Waelbroeck, C., Labeyrie, L., Michel, E., Duplessy, J. C., McManus, J. F., Lambeck, K., Balbon, E., and Labracherie, M.: Sea-level and deep water temperature changes derived from benthic foraminifera isotopic records, Quaternary Science Reviews, 21, 295–305, doi:10.1016/S0277-3791(01)00101-9, URL https://www.sciencedirect.com/science/article/pii/S0277379101001019, 2002.

Waelbroeck, C., Paul, A., Kucera, M., Rosell-Melé, A., Weinelt, M., Schneider, R., Mix, A. C., Abelmann, A., Armand, L., Bard, E., Barker, S., Barrows, T. T., Benway, H., Cacho, I., Chen, M.-T., Cortijo, E., Crosta, X., de Vernal, A., Dokken, T., Duprat, J., Elderfield, H., Eynaud, F., Gersonde, R., Hayes, A., Henry, M., Hillaire-Marcel, C., Huang, C.-C., Jansen, E., Juggins, S., Kallel, N., Kiefer, T., Kienast, M., Labeyrie, L., Leclaire, H., Londeix, L., Mangin, S., Matthiessen, J., Marret, F., Meland, M., Morey, A. E., Mulitza, S., Pflaumann, U., Pisias, N. G., Radi, T., Rochon, A., Rohling, E. J., Sbaffi, L., Schäfer-Neth, C., Solignac, S., Spero, H., Tachikawa, K., Turon, J.-L., and MARGO Project Members: Constraints on the magnitude and patterns of ocean cooling at the Last Glacial Maximum, Nature Geoscience, 2, 127–132, doi:10.1038/ngeo411, URL https://www.nature.com/articles/ngeo411, number: 2 Publisher: Nature Publishing Group, 2009.

Waelbroeck, C., Skinner, L. C., Labeyrie, L., Duplessy, J.-C., Michel, E., Vazquez Riveiros, N., Gherardi, J.-M., and Dewilde, F.: The timing of deglacial circulation changes in the Atlantic, Paleoceanography, 26, doi:10.1029/2010PA002007, URL https://onlinelibrary.wiley.com/doi/abs/10.1029/2010PA002007, 2011.

Wang, X., Auler, A. S., Edwards, R. L., Cheng, H., Ito, E., Wang, Y., Kong, X., and Solheid, M.: Millennial-scale precipitation changes in southern Brazil over the past 90,000 years, Geophysical Research Letters, 34, doi:10.1029/2007GL031149, URL https://onlinelibrary.wiley.com/doi/abs/10.1029/2007GL031149, 2007.

Wang, Y. J., Cheng, H., Edwards, R. L., An, Z. S., Wu, J. Y., Shen, C.-C., and Dorale, J. A.: A High-Resolution Absolute-Dated Late Pleistocene Monsoon Record from Hulu Cave, China, Science, 294, 2345–2348, doi:10.1126/science.1064618, URL https://www.science.org/doi/10.1126/science.1064618, publisher: American Association for the Advancement of Science, 2001.

Wang, Z. and Mysak, L. A.: Glacial abrupt climate changes and Dansgaard-Oeschger oscillations in a coupled climate model, Paleoceanography, 21, doi:10.1029/2005PA001238, URL https://agupubs.onlinelibrary.wiley.com/doi/abs/10.1029/2005PA001238, 2006.

Wary, M., Eynaud, F., Sabine, M., Zaragosi, S., Rossignol, L., Malaizé, B., Palis, E., Zumaque, J., Caulle, C., Penaud, A., Michel, E., and Charlier, K.: Stratification of surface waters during the last glacial millennial climatic events: a key factor in subsurface and deep-water mass dynamics, Climate of the Past, 11, 1507–1525, doi:10.5194/cp-11-1507-2015, URL https://cp.copernicus.org/articles/11/1507/2015/, publisher: Copernicus GmbH, 2015.

Weber, M. E., Clark, P. U., Kuhn, G., Timmermann, A., Sprenk, D., Gladstone, R., Zhang, X., Lohmann, G., Menviel, L., Chikamoto, M. O., Friedrich, T., and Ohlwein, C.: Millennial-scale variability in Antarctic ice-sheet discharge during the last deglaciation, Nature, 510, 134–138, doi:10.1038/nature13397, URL https://www.nature.com/articles/nature13397, 2014.

Weber, S. L.: The utility of Earth system Models of Intermediate Complexity (EMICs), WIREs Climate Change, 1, 243–252, doi:10.1002/wcc.24, URL https://onlinelibrary.wiley.com/doi/abs/10.1002/wcc.24, 2010.

Weijer, W. and Dijkstra, H. A.: Multiple Oscillatory Modes of the Global Ocean Circulation, Journal of Physical Oceanography, 33, 2197–2213, doi:10.1175/1520-0485(2003)033⟨2197:MOMOTG⟩2.0.CO;2, URL https://journals.ametsoc.org/view/journals/phoc/33/11/1520-0485_2003_033_2197_momotg_2.0.co_2.xml, 2003.

Weijer, W., Cheng, W., Drijfhout, S. S., Fedorov, A. V., Hu, A., Jackson, L. C., Liu, W., McDonagh, E. L., Mecking, J. V., and Zhang, J.: Stability of the Atlantic Meridional

Overturning Circulation: A Review and Synthesis, Journal of Geophysical Research: Oceans, 124, 5336–5375, doi:10.1029/2019JC015083, URL https://onlinelibrary.wiley.com/doi/abs/10.1029/2019JC015083, important - To read, 2019.

Welander, P.: A simple heat-salt oscillator, Dynamics of Atmospheres and Oceans, 6, 233–242, doi:10.1016/0377-0265(82)90030-6, URL https://www.sciencedirect.com/science/article/pii/0377026582900306, 1982.

Wickert, A. D.: Reconstruction of North American drainage basins and river discharge since the Last Glacial Maximum, Earth Surface Dynamics, 4, 831–869, doi:https://doi.org/10.5194/esurf-4-831-2016, URL https://esurf.copernicus.org/articles/4/831/2016/, publisher: Copernicus GmbH, 2016.

Wickert, A. D., Mitrovica, J. X., Williams, C., and Anderson, R. S.: Gradual demise of a thin southern Laurentide ice sheet recorded by Mississippi drainage, Nature, 502, 668–671, doi:10.1038/nature12609, URL https://www.nature.com/articles/nature12609, number: 7473 Publisher: Nature Publishing Group, 2013.

Wickert, A. D., Williams, C., Gregoire, L. J., Callaghan, K. L., Ivanović, R. F., Valdes, P. J., Vetter, L., and Jennings, C. E.: Marine-Calibrated Chronology of Southern Laurentide Ice Sheet Advance and Retreat: ∼2,000-Year Cycles Paced by Meltwater–Climate Feedback, Geophysical Research Letters, 50, e2022GL100391, doi:10.1029/2022GL100391, URL https://onlinelibrary.wiley.com/doi/abs/10.1029/2022GL100391, 2023.

Winton, M.: Deep Decoupling Oscillations of the Oceanic Thermohaline Circulation, in: Ice in the Climate System, edited by Peltier, W. R., NATO ASI Series, pp. 417–432, Springer, Berlin, Heidelberg, doi:10.1007/978-3-642-85016-5_24, 1993.

Wolf, T. C. W. and Thiede, J.: History of terrigenous sedimentation during the past 10 m.y. in the North Atlantic (ODP Legs 104 and 105 and DSDP Leg 81), Marine Geology, 101, 83–102, doi:10.1016/0025-3227(91)90064-B, URL http://www.sciencedirect.com/science/article/pii/002532279190064B, 1991.

Wolff, E. W., Chappellaz, J., Blunier, T., Rasmussen, S. O., and Svensson, A.: Millennial-scale variability during the last glacial: The ice core record, Quaternary Science Reviews, 29, 2828–2838, doi:10.1016/j.quascirev.2009.10.013, URL http://www.sciencedirect.com/science/article/pii/S0277379109003588, 2010.

Wunsch, C.: Abrupt climate change: An alternative view, Quaternary Research, 65, 191–203, doi:10.1016/j.yqres.2005.10.006, URL http://www.sciencedirect.com/science/article/pii/S0033589405001717, 2006.

Wunsch, C.: Towards understanding the Paleocean, Quaternary Science Reviews, 29,

1960–1967, doi:10.1016/j.quascirev.2010.05.020, URL https://www.sciencedirect.com/science/article/pii/S0277379110001563, 2010.

Wunsch, C. and Heimbach, P.: How long to oceanic tracer and proxy equilibrium?, Quaternary Science Reviews, 27, 637–651, doi:10.1016/j.quascirev.2008.01.006, URL https://www.sciencedirect.com/science/article/pii/S0277379108000048, 2008.

Xu, X., Rhines, P. B., and Chassignet, E. P.: On Mapping the Diapycnal Water Mass Transformation of the Upper North Atlantic Ocean, Journal of Physical Oceanography, 48, 2233–2258, doi:10.1175/JPO-D-17-0223.1, URL https://journals.ametsoc.org/view/journals/phoc/48/10/jpo-d-17-0223.1.xml, publisher: American Meteorological Society Section: Journal of Physical Oceanography, 2018.

Yashayaev, I.: Hydrographic changes in the Labrador Sea, 1960–2005, Progress in Oceanography, 73, 242–276, doi:10.1016/j.pocean.2007.04.015, URL http://www.sciencedirect.com/science/article/pii/S0079661107000857, 2007.

You, D., Stein, R., Fahl, K., Williams, M. C., Schmidt, D. N., McCave, I. N., Barker, S., Schefuß, E., Niu, L., Kuhn, G., and Niessen, F.: Last deglacial abrupt climate changes caused by meltwater pulses in the Labrador Sea, Communications Earth & Environment, 4, 1–12, doi:10.1038/s43247-023-00743-3, URL https://www.nature.com/articles/s43247-023-00743-3, number: 1 Publisher: Nature Publishing Group, 2023.

Zaragosi, S., Eynaud, F., Pujol, C., Auffret, G. A., Turon, J. L., and Garlan, T.: Initiation of the European deglaciation as recorded in the northwestern Bay of Biscay slope environments (Meriadzek Terrace and Trevelyan Escarpment): a multi-proxy approach, Earth and Planetary Science Letters, 188, 493–507, doi:10.1016/S0012-821X(01)00332-6, URL http://www.sciencedirect.com/science/article/pii/S0012821X01003326, 2001.

Zhang, R., Delworth, T. L., Rosati, A., Anderson, W. G., Dixon, K. W., Lee, H.-C., and Zeng, F.: Sensitivity of the North Atlantic Ocean Circulation to an abrupt change in the Nordic Sea overflow in a high resolution global coupled climate model, Journal of Geophysical Research: Oceans, 116, doi:10.1029/2011JC007240, URL https://onlinelibrary.wiley.com/doi/abs/10.1029/2011JC007240, 2011.

Zhang, X., Lohmann, G., Knorr, G., and Purcell, C.: Abrupt glacial climate shifts controlled by ice sheet changes, Nature, 512, 290–294, doi:10.1038/nature13592, URL http://www.nature.com/articles/nature13592, 2014.

Zhang, X., Knorr, G., Lohmann, G., and Barker, S.: Abrupt North Atlantic circulation changes in response to gradual CO_2 forcing in a glacial climate state, Nature Geoscience, 10, 518–523, doi:10.1038/ngeo2974, URL https://www.nature.com/articles/ngeo2974, 2017.

Zhang, X., Barker, S., Knorr, G., Lohmann, G., Drysdale, R., Sun, Y., Hodell, D., and Chen, F.: Direct astronomical influence on abrupt climate variability, Nature Geoscience, 14, 819–826, doi:10.1038/s41561-021-00846-6, URL https://www.nature.com/articles/s41561-021-00846-6, number: 11 Publisher: Nature Publishing Group, 2021.